Searching for Hα-selected planetary nebulae in the UWISH2 Galactic plane molecular hydrogen survey

by

Thomas Ferry

A thesis submitted to
The University of Hertfordshire
for the degree of
MASTERS BY RESEARCH

Centre for Astrophysics Research
School of Physics Astronomy and Mathematics
The University of Hertfordshire
December 2014

Abstract

This thesis seeks to analyse and quantify the differences present in 2 different emission mechanisms seen in Planetary Nebulae (PN). These are Hα emission from recombination of ionised hydrogen and H_2 emission from photoexcitation of molecular hydrogen gas.

Firstly, I have gathered images from the UKIRT Widefield Infrared Survey for H_2 (UWISH2), which correspond to PN in the Macquarie/AAO/Strasbourg Hα (MASH) Planetary Nebula Galactic Catalog, which have been compared and contrasted, and the full extent of which will be featured in the appendices of this report.

Secondly, I have gathered images from the UWISH2, which correspond to PN found in the INT/WFC Photometric Hα Survey (IPHAS) of the Northern Galactic plane by Viironen et al. 2009, which have been compared and contrasted and will be featured in the appendices of this report.

The results gained from this work challenge the assumption of Gatley's Rule that molecular hydrogen is a predictor for bipolar emission in PN with more than half of the PN in the MASH sample showing such emission, and approximately 80% of the PN in the IPHAS sample as well.

This work has shown that H_2 emission is a good method of searching for PN and may further be used as a tool to further confirm objects as true PN.

Contents

List of Figures

Chapter 1

Introduction

1.1 Background

1.1.1 What is a Planetary Nebula?

A Planetary Nebula (PN) is produced after a star of main sequence mass of approximately $1M_{\odot}$ to $10M_{\odot}$ (Iben 1995) moves up the Asymptotic Giant Branch (AGB) and begins to eject its outer layers in an enhanced mass loss phase. As the star reaches the tip of the AGB, the mass loss rate drops by several orders of magnitude and the central star evolves to become a white dwarf. The central star emits ultraviolet photons as it evolves to hotter temperatures, and proceeds to ionise the surrounding material, producing the PN we are then able to see.

1.1.2 Internal changes within the star

The star in question would normally have had a phase of core hydrogen burning and core helium burning in order to generate a PN towards the end of its life cycle.

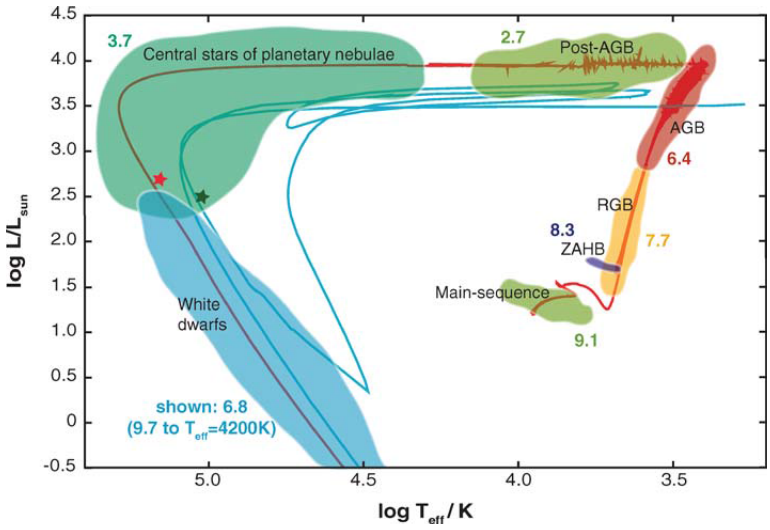

Figure 1.1: A Hertzsprung-Russell diagram of a $2M_{\odot}$ star of Solar metallicity from the main sequence to the white dwarf phase. The red track denotes the main path that a $2M_{\odot}$ takes through the Hertzsprung-Russell diagram. Herwig 2005.

As the star ages, it moves through different regions on the Hertzsprung-Russell (HR) diagram, following a track which is dependent on mass and metallicity of the star. This is demonstrated in Figure 1.1, with the red line being the main evolutionary track of a 2 solar mass star with a solar metallicity, evolving towards a white dwarf.

In the first stage of this evolution the star moves from the main sequence hydrogen core burning phase, where the star is expected to spend a large portion of its life, to the red giant branch. The red giant branch is characterised by energy production via fusion in a hydrogen burning shell around the core. This stage ends when the helium that it has been producing ignites once the core of the star reaches temperatures $\geq 10^8$ Kelvin.

In the early AGB phase the energy output of a star is dominated by a helium burning shell around the core, producing oxygen and carbon, which is then deposited onto the core. The effective temperature of the star decreases during this phase, as seen in Figure 1.1, and this allows the area at which convection can occur to deepen. This produces a mixing of material, called the Second Dredge-Up to occur, which brings material from the hydrogen rich outer layers towards the core, and takes helium rich material away from the core to the outer layers. There is also an enrichment of the outer layers with heavier elements, such as ^{14}N and ^{13}C.

After this mixing has taken place, the helium shell can no longer sustain fusion reactions permanently, and instead the energy output comes to be dominated by a now re-ignited hydrogen shell. As the hydrogen shell burns, it deposits helium onto the helium shell, which in turn, makes the base of the shell slightly degenerate, increasing in temperature, which then causes it to re-ignite. As the helium shell re-ignites, the star becomes larger for a period, and the hydrogen shell cannot sustain a fusion reaction, and so turns off. Once the helium shell has used up all the fuel it can, it stops burning, the star collapses back, and the hydrogen shell takes over as the dominant energy producer in the star. These events are called thermal pulses, and the period between each pulse is determined by stellar mass.

With the sudden increase in energy from the thermal pulsing, a new convective zone occurs between the hydrogen burning shell and the helium burning shell. The outer envelope of the star also increases in convective depth at this point, and now a mixing of material from the zone between the hydrogen shell and helium shell occurs, bringing carbon to the envelope, which may change the composition of the envelope drastically. This event is called the third dredge up, and may occur multiple times during the AGB phase.

1.1.3 External changes in the star

As the internal changes occur as described in section 1.1.2, the star also goes through a number of physical changes externally as well. As the star progresses up the AGB, it experiences a heavy mass loss phase. This removes vast quantities of material from the star, on the order of approximately $10^{-5}M_{\odot}$ to $10^{-6}M_{\odot}$ per year (Iben 1995). In some cases, mass loss may even rise to up to $10^{-4}M_{\odot}$ per year, during the final stages of the AGB phase (Ramos-Larios et al. 2012).

As seen in Figure 1.1, the AGB corresponds to a period in the star's lifetime where apparent luminosity increases, while effective temperature decreases. This drop in surface temperature allows for the production of dust to occur. In stars with large amounts of oxygen near the surface, silicate dust will form . In stars which have experienced a number of third dredge up events, carbon dust will form instead, due to the increased amount of carbon in the envelope. (Ferrarotti and Gail 2006). This production of dust is important for the mass loss phase, as radiation pressure exerted upon the dust grains seems to be a driving factor in powering the mass loss seen in AGB stars. (Winters et al. 2003)

The mass lost in this way produces a circumstellar envelope (CSE), that surrounds the star, and obscures it from view in the optical and the near infrared. The CSE's composition changes as the AGB phase continues. It primarily starts out as hydrogen and helium, but, over time, comes to include oxygen, and in the presence of several third dredge up events, carbon as well.

As the star reaches the peak of the AGB, the mass loss rate drops to a fraction of what it was previously, and the CSE detaches from the star. The dust then becomes optically thin, and the star becomes visible again. What remains of the central star is a core of primarily oxygen and carbon, and possibly neon and magnesium if the initial mass of the star was high enough (Werner et al. 2005), alongside the remaining hydrogen and helium shells around the star.

The CSE continues to expand at this point and the real work of shaping the PN occurs. The mass loss from AGB stars is thought to be mainly spherically symmetric, however, the vast majority of PN do not show spherically symmetric structure at all (Sahai, Morris, Villar 2011). It has been suggested that companion objects such as stars, brown dwarfs or even large planets may have an effect on the final structure of the PN (de Marco, Farihi, Nordhaus 2009)(de Marco & Soker 2011)

The central star begins to evolve towards a white dwarf, with a transition to the left in the HR diagram, reflecting a change in temperature, but a constant luminosity. This can be seen in Figure 1.1. This phase is mass dependent, with higher mass stars taking a shorter amount of time to move through this stage. As a result of this, some PN may not have been seen due to the envelope dissipating before the ionisation of it can take place.

1.1.4 Emission Mechanisms in PN

Hydrogen Recombination emission

The H-alpha (Hα) emission line (656 nm) results from the recombination of electrons and protons in the ionised envelope around the central star once it reaches an effective temperature of approximately T_eff=20,000K. Once this is achieved, the UV flux is sufficient to photodissociate the molecular hydrogen in the envelope, and ionise the hydrogen atoms.

Recombination of electrons and protons results in discrete emission lines with Hα due to transitions between the n=3 and n=2 electronic levels. The Hα line is a widely used diagnostic of ionised gas and has therefore been used to detect PN.

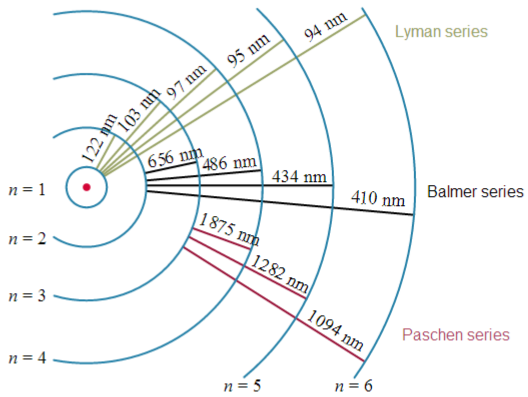

Figure 1.2: A diagram of the energy level transitions of Hydrogen, displaying the Balmer series in black. Source: `en.wikipedia.org/wiki/Hydrogen_spectral_series`

Molecular hydrogen emission

Molecular hydrogen emission can be excited by a variety of mechanisms, the important ones in PN being the photoexcitation of molecular hydrogen by UV photons and shock excitation by fast winds.

UV photons with wavelengths of 100 nm are capable of exciting H_2 to the first electronic state. Subsequent decay to vibrationally bound states of the ground electronic state (See Fig 1.3) results in a cascade of vibrational-rotational lines. The most prominent transition is the 1-0S(1) line at 2.122 μm, resulting from a transition between the ν=1, J=3 and ν=0, J=1 levels of the ground state.

The second source of molecular hydrogen emission is that of collisional excitation. This is present in fast outflows from astronomical objects. These are present in a number of classes of astronomical object (Livio 2000). Jets are thought to be a driving force behind the shaping of PN in the post AGB phase (Huggins et al. 1999)(Sahai 2004)(Sahai et al. 2005).

1.1.5 Morphological classes of PN

PN come in a number of varied shapes and sizes, however, there are a few overarching morphologies present in any large sample of PN. There are 4 morphological classes that are easy to define: Circular, elliptical, bipolar and quadrupolar (Mandchado, Stanghellini, Guerrero 1996). However, not all PN fit these definitions so easily, a large number have abstract or even undefined structures, and as such, classification systems exist on a paper by paper basis (Shaw et

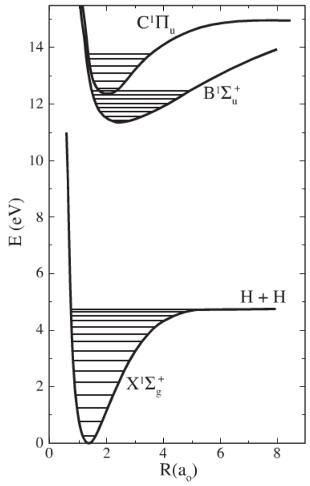

Figure 1.3: A diagram displaying the vibrational energy levels present within the ground and first two excited electronic states in molecular hydrogen. The bottom line to the bottom of the bell curve represents the lower level of the 1-0S(1) transition. Source: Draine, Physics of the Interstellar Medium. Page 40.

al. 2001) (Sahai et al. 2007) (Sahai, Morris, Villar 2011). For this work, I will just be utilising the base 4 morphological classifications, along with a point source classification for any that are too small to measure correctly, and classifying objects that do not fit into these categories as irregular.

1.1.6 Prior research into molecular hydrogen emission from PN

Molecular Hydrogen emission in PN has been an area of study for over 3 decades now (Beckwith, Persson, Gatley 1978), and has been expanded recently with the usage of sensitive, large format, near infrared detector arrays (Kastner et al. 1994).

Work has been focused on linking molecular hydrogen emission with morphological properties of PN (Kastner et al. 1996), and from this an empirical rule was formulated. Based on the data in Zuckerman & Gatley (1988), molecular hydrogen emission is suggested as a marker for bipolar features in PN. This was later expanded upon (Kastner et al 1992)(Kastner et al. 1994)(Kastner et al. 1996)(Kastner et al. 1998) and has been named 'Gatley's Rule'.

1.2 Prior Surveys and UWISH2

1.2.1 Prior Surveys for PN

Many of the surveys used in the search for PN are focused on star formation, and as such, look at the Galactic plane. The discovery of PN is a secondary goal for a lot of these, and as such, the majority of PN finds are within the Galactic plane. As mentioned previously, Hα emission is expected in PN due to the central star producing UV photons with a high enough energy to ionise hydrogen in the surrounding envelope. PN therefore appear in Hα surveys and this has been a principal tool for their detection.

Another tracer of PN is forbidden line emission, most notably [OII] and [OIII] that originates when atoms are excited to a higher energy state, but cannot decay in a preferred way and instead have to take a normally forbidden transition. This occurs in low density gases and plasmas, which are present in PN and therefore are another marker for PN.

Initial Hα surveys (Kouhoutek & Perek 1967), have been expanded upon during the last 2 decades (Acker et al. 1992; Kohoutek 2001; Parker et al. 2008; Viironen et al. 2009), and have vastly expanded the number of PN found. However, there is an issue with Hα, being that it does not penetrate very deeply through the optically thick Galactic plane. This means that there could be a large number of PN undiscovered, just obscured by optically thick dust in the Galactic plane.

1.2.2 UWISH2

The UKIRT (United Kingdom Infrared Telescope) Widefield Infrared Survey for H_2 (UWISH2) is a survey of the H_2 in the first quadrant of the galactic plane ($6 < l < 65; -1.5 < b < +1.5$). This region overlaps spatially with the J, H and K bands being surveyed already by the UKIRT Infrared Deep Sky Survey (UKIDSS) Galactic Plane Survey (GPS), and several mid-IR wavelengths (3.6, 4.5, 5.8, 8.0 μm) already being surveyed by Spitzer as part of Galactic Legacy Infrared Mid-Plane Survey Extraordinaire (GLIMPSE).

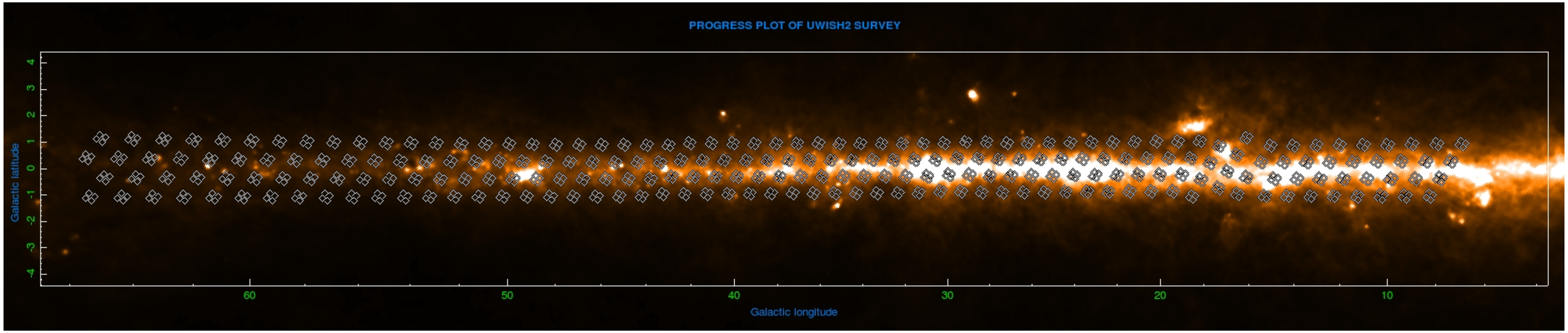

Figure 1.4: The layout of the UWISH2 survey overlaid across a 100μ m IRAS image of the galactic plane. In reality, there are no gaps between the tiles as displayed in this image. Source: `http://astro.kent.ac.uk/uwish2/images/UWISH2-progress-01Sep11.jpg`

The UWISH2 survey uses the UKIRT (United Kingdom Infrared Telescope), and the Wide-Field Camera (WFCAM). The WFCAM is composed of four Rockwell Hawaii II (HgCdTe 2048x2048) arrays (Froebrich et al, 2010). The gaps between the 4 arrays are 94% of the width of an array, and as such, full coverage is a possibility with this set up by mosaicking. The camera has a pixel scale of 0.4 arc seconds per pixel, but, with the usage of a micro-stepping pattern to correct for image artifacts, bad pixels and to fully sample the point spread function, the pixel scale reduces to 0.2 arc seconds per pixel.

The images are acquired through a narrowband filter ($\Delta\lambda = 0.021\ \mu m$) centered on the 1-0 S(1) line of molecular hydrogen at $2.122\mu m$. The exposure time is 60s, but the total per pixel integration time is 720s, after image stacking to form a complete tile.

Each image is 1/16th of a tile, as shown in Figure 1.5. The 4 cameras work in unison to produce a mosaic of the targeted area. The red dot is the position of the 'pointing' for the tile, and the images are taken in reference to this. The first images taken are the green tiles, and then the telescope is stepped around to fully image the area and takes an image at each of the different coloured tiles.

K band images were taken by the UKIDSS GPS, and these can be subtracted from the H_2 images by the use of an appropriate algorithm (Jae-Joon et al. 2014), aligning the images by the use of the astrometric calibration parameters in the file headers to provide a continuum subtraction. The flux scaling between H_2 and K band is calculated for each star individually.

UWISH2 should be a useful tool for finding PN. As mentioned in section 1.2.1, the usage of Hα has meant that PN have only been found in areas of low dust concentrations along the Galactic plane, and there may be undiscovered PN lying at higher optical depths than Hα detections can be made at. This is where H_2 can prove useful, as it allows for the detection of PN in the near-IR at higher optical depths. However, this is not the focus of the project, which will be explained in the next chapter.

Another area where UWISH2 can be useful is the detection of younger PN, which may only just be developing a photo ionized region. As mentioned in section 1.1.3, the CSE is detectable in H_2 before it is detectable in Hα due to the time taken for the central star to start giving off photons with a high enough energy to ionise the envelope.

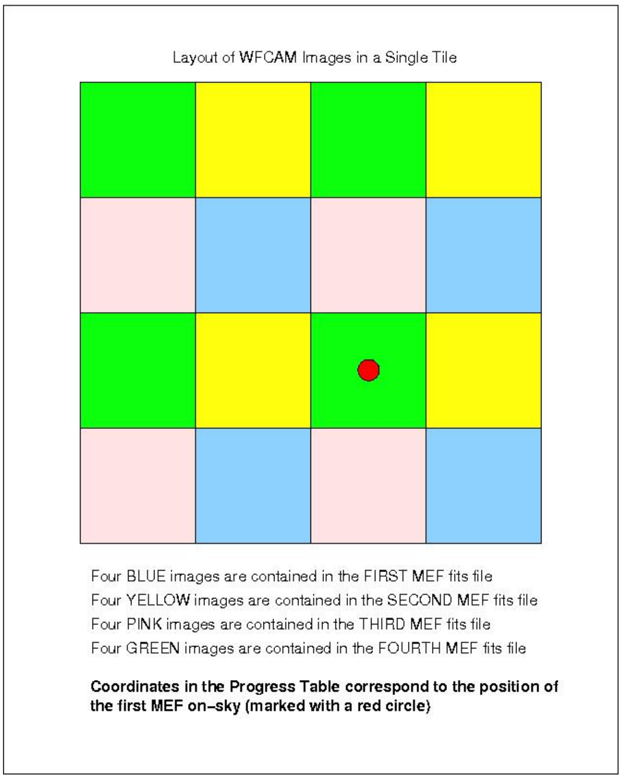

Figure 1.5: The structure of each UWISH2 tile. The red dot corresponds to the original pointing for the tile, and each colour corresponds to a different position which allows for full coverage of the selected area.

1.3 Project Details

1.3.1 Project Work and Goals

The project is focused on the detection of H_2 components of PN with a definite Hα component, and intercomparing emission features. Target selection is based on 2 surveys that have major overlap with the field for UWISH2. These two surveys are IPHAS and MASH.

IPHAS is the Isacc Newton Telescope (INT) Photometric Hα Survey of the Northern Galactic Plane (Drew et al. 2005). It looks at the Northern Galactic Plane between 29 and 215 degrees longitude and latitudes between +5 and -5 degrees. The survey was taken with the wide field camera (WFC) focused around Hα. The survey is a very good resource for this study. A catalogue of PN candidates has been created by Viironen et al. with approximately 1000 candidate PN, and is the main resource for comparison for this project. (Viironen et al. 2009).

MASH 1&2 are the Macquarie/AAO/Strasbourg Hα Planetary Nebula Catalogue 1&2 (Parker et al. 2006)(Miszalski et al. 2008). These look at the Southern Galactic Plane, and have some overlap with UWISH2. The survey itself was based on the Anglo-Australian Observatory UK

Schmidt Telescope (AAO/UKST)Hα survey (Parker et al. 2005) of the Southern Galactic Plane. The survey was then visually inspected, and the MASH list was compiled over the course of several years, with removals of H II areas from the list and other similar objects. This catalogue is of PN candidates, with spectroscopic confirmation, and has approximately 1200 PN present within it.

The principal goal of this work is to identify the fraction of Hα detected PN visible in H_2 to ascertain the viability of molecular hydrogen emission as a tool for finding PN.

Goals for the project

1. Identify and catalogue the H_2 components of the Hα PN from MASH and IPHAS within the UWISH2 surveys area, as mentioned previously.

2. Determine the fraction of Hα detected PN also detected in H_2. Ascertain from image comparisons the morphological classification of these PN. See if features are comparable, or if different features appear altogether.

3. Determine the fraction of Hα detected PN not detected in H_2. Ascertain why this may be the case and check for the validity of empirical rules found in previous research.

Chapter 2

Methodology and Data Collection

2.1 Initial Work

2.1.1 Initial UWISH2 PN detection

The project requires data collection from a number of sources. As mentioned previously, the Hα PN selection uses two surveys, MASH and IPHAS to compare and contrast PN against their H_2 emission.

The first piece of work was to become familiar with the Graphical Astronomy and Image Analysis (GAIA) tool, and also with the UWISH2 database. This was done through the use of a list of PN already found serendipitously by researchers looking for H_2 associated with star formation.

2.2 MASH

The MASH survey (Parker et al. 2006; Miszalski et al. 2008) has over 1200 new confirmed and possible PN that need to be examined.

To cross match targets in the MASH surveys with those in the UWISH2 survey, I used the program Topcat. Topcat is a piece of software that allows for the manipulation of data tables from astronomical surveys by applying constraints based on any feature that is noted in the data table. For example, the usage of Right Ascension and Declination to constrain a data set. However, on applying these constraints using Right Ascension and Declination of the area of the UWISH2 survey, Topcat gave many false matches for targets lying on the edge of the UWISH2 area by not taking into account the staggered nature of the tiles in UWISH2, due to the tiles being aligned via Right Ascension and Declination, and not being aligned parallel to the Galactic plane.

A Python program was then developed that set out each UWISH2 tile as a square in Right Ascension and Declination, and matched the MASH PN coordinates to tiles, and allowed for the elimination of false positives that may have appeared while using Topcat. This narrowed the 1200 MASH objects down to 30 within the UWISH2 area. The code for this program will be included within the appendices.

The MASH images in Hα have a certain size, 357 x 357 pixels, with a pixel to arcsecond ratio of 0.67 arcseconds per pixel (Hambly et al 2001). This gives the images an arcsecond size of 235.62 arcseconds, or 3.927 arcminutes. UWISH2 has an arcsecond to pixel ratio of 0.2, which means that to have an image with the same field of view the image would have to be 1176 by 1176 pixels. We extract images from the UWISH2 survey to have the same field of view as the MASH images, to facilitate intercomparison.

2.3 IPHAS

IPHAS is a very large survey, however Viironen et al. (2009) have acquired a large number (1000) of candidate PN from this. We use the python program detailed in Section 2.2 to match IPHAS PN candidates to UWISH2 fields and find that within UWISH2 the reduced number of PN from IPHAS is approximately 140.

The IPHAS PN images were obtained via a web tool (`http://apm3.ast.cam.ac.uk/iphas_finder.html`). The IPHAS images have a pixel to arcsecond ratio of 0.33. To have the same field of view as the MASH images, 235.62 arcseconds, these images need to be 714x714 pixels.

2.4 Other Surveys

Other surveys of the Galactic plane in other wavelengths have played a role as well. To identify if the object in question is indeed a PN, SIMBAD has been used to cross reference the object with other observations, and determine if the object is likely to be a true PN. This involves checking for ultraviolet and radio components to the object, as these emissions would be normal for a PN.

2.5 Methodology

We have developed a Python program which outputs a list of the co-ordinates of the first centring of the UWISH2 tile, as seen in Figure 1.5, the designation of the UWISH2 tile, and the co-ordinate of the PN that is present in that tile. However, the program sometimes finds PN that are just off the edge of tiles, or not on the survey. These are discarded as they cannot be analysed.

The method used to extract these UWISH2 images was a simple process:

1. Identify where the PN was using the UWISH2 web interface and download the corresponding tile section.

2. Open the image using GAIA and identify the central pixel for the object and note it's X and Y value.

3. Put these pixel values into an excel spreadsheet to give the pixel range for the cut out image. (The pixel range was found by adding 588 to the east direction, taking 588 in west, and repeating the same for north and south, to give an image that was 1176 pixels on each axis in total).

4. Convert the file from .fits to .sdf using the Starlink fits2ndf command.

5. Confirm that the origin pixel value for the source image was [1,1].

6. Use the ndfcopy command to extract the cut out image, using the pixel range gained from inputting the pixel values into the excel sheet.

7. Rename file to desired name and check that the process has worked by opening the file in GAIA.

To make sure that the UWISH2 image was of the same field as the Hα image, I would use the catalogue overlay tool present in GAIA. I would use the 2MASS survey for this, and identify the prominent stars in the UWISH2 field which matched up to the same stars in the other (IPHAS/MASH) field. This provided me with a large degree of certainty that the Hα and H_2 fields were the same, and that in the cases of non-detection in H_2 fields, that this was indeed the same field. See Figure 2.1 and 2.2.

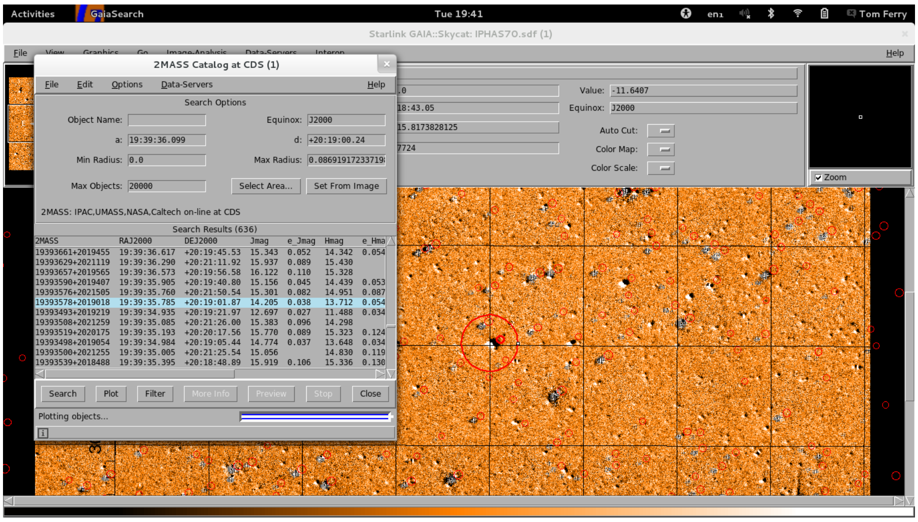

Figure 2.1: An image of the 2MASS overlay showing the stars nearby to a PN from UWISH2. Highlighted in the search box is the star used to show that the next image is of the same field in space.

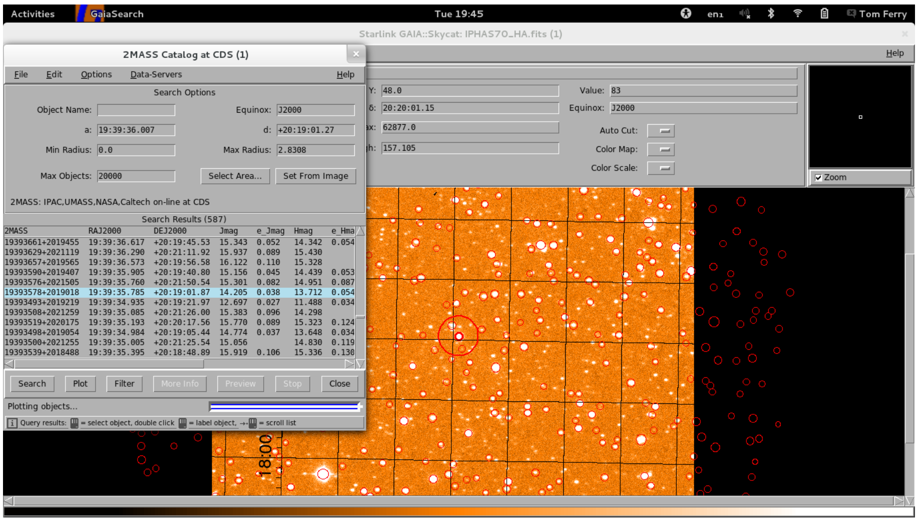

Figure 2.2: An image of the same PN as displayed above, this time in IPHAS. Highlighted in the search box is the same star as before, showing that this is the same field in space.

Chapter 3

Result Tables

The tables shown here are the result of utilising the GAIA software's analysis tools to individually look at each candidate PN found in the IPHAS and MASH surveys which overlaps with UWISH2.

The tool specifically used for this was the photometric apeture tool present in GAIA. This was utilised because of the ability to draw ellipses rather than circles around objects. This allows for the accurate measurement of angular size in pixels of the object, position angle and eccentricity of the ellipse.

The headers of each column are as follows:

- Column 1 is the given name of the PN. As MASH PN are spectroscopically verified PN, they have a PNG identifier, IPHAS are not always verified PN and as such, do not all have PNG identifiers
- Column 2 is a simple check of yes or no for H_2 detection of an object.
- Column 3 is a list of features that the Hα detected object displays.
- Column 4 is a list of features that the H_2 detected object displays.
- Column 5 is a morphological classification type for Hα detected objects.
- Column 6 is a morphological classification type for H_2 detected objects.
- Column 7-9 are the angular size of the Hα object, inclination of the ellipse used to measure it, and the eccentricity of the ellipse.
- Column 10-12 are the angular size of the H_2 object, inclination of the ellipse used to measure it, and the eccentricity of the ellipse.

All these items together give a good analysis of what the object is, and compares it to its counterpart in the other survey.

The images themselves are in the appendices of this document.

3.0.1 IPHAS tables

Name Given	Molecular Hydrogen detection?	H-Alpha Features	Molecular Hydrogen features	Morphology H-Alpha	Morphology Molecular Hydrogen
IPHAS 1	Y	Point Source	Point Source	Point Source	Point Source
IPHAS 2	Y	Point Source	Point Source	Point Source	Point Source
IPHAS 3	N	Point Source	N/A	Point Source	N/A
IPHAS 4	Y	Point Source	Small ellipse	Point Source	Elliptical
IPHAS 5	Y	Point Source	Point Source	Point Source	Point Source
IPHAS 6	Y	Point Source	Point Source	Point Source	Point Source
IPHAS 7	Y	Outer ring of material, gap at N end, connected at S end, large area of emitting material to N and S	No emission from S, small amount of emission from N, sides very visible	Irregular	Irregular
IPHAS 8	Y	Object with connected offshoots at E and W, E extends northwards, diffuse emission in between	Emission less defined than in H-Alpha, similar structure however	Irregular	Irregular
IPHAS 9	Y	Point Source	Point Source	Point Source	Point Source
IPHAS 10	Y	Point Source	Point Source	Point Source	Point Source
IPHAS 11	Y	Point Source	Point Source	Point Source	Point Source
IPHAS 12	N	Small ellipse	N/A	Point Source	N/A
IPHAS 13	Y	Point Source	Point Source	Point Source	Point Source
IPHAS 14	Y	Point Source	Point Source	Point Source	Point Source
IPHAS 15	Y	Point Source	Point Source	Point Source	Point Source
IPHAS 16	Y	Point Source	Point Source	Point Source	Point Source
IPHAS 17	Y	Point Source	Point Source	Point Source	Point Source
IPHAS 18	Y	2 sources close together	2 sources close together	Point Source	Point Source
IPHAS 19	Y	Point Source	Point Source	Point Source	Point Source
IPHAS 20	N	Point Source	N/A	Point Source	N/A
IPHAS 21	N	Point Source	N/A	Point Source	N/A
IPHAS 22	Y	Point Source	Point Source	Point Source	Point Source

Angular Size H-Alpha (arcsecs)	Inclination H-Alpha	Ellipticity H-Alpha	Angular Size Molecular Hydrogen (arcsecs)	Inclination Molecular Hydrogen	Ellipticity Molecular Hydrogen
N/A	N/A	N/A	N/A	N/A	N/A
N/A	N/A	N/A	N/A	N/A	N/A
N/A	N/A	N/A	N/A	N/A	N/A
N/A	N/A	N/A	4.242	135	0.813
N/A	N/A	N/A	N/A	N/A	N/A
N/A	N/A	N/A	N/A	N/A	N/A
40.77	119.0	0.731	17.75	123.5	0.155
11.74	106.2	0.548	11.44	34	0.244
N/A	N/A	N/A	N/A	N/A	N/A
N/A	N/A	N/A	N/A	N/A	N/A
N/A	N/A	N/A	N/A	N/A	N/A
3.69	153.5	0.446	N/A	N/A	N/A
N/A	N/A	N/A	N/A	N/A	N/A
N/A	N/A	N/A	N/A	N/A	N/A
N/A	N/A	N/A	N/A	N/A	N/A
N/A	N/A	N/A	N/A	N/A	N/A
N/A	N/A	N/A	N/A	N/A	N/A
N/A	N/A	N/A	N/A	N/A	N/A
N/A	N/A	N/A	N/A	N/A	N/A
N/A	N/A	N/A	N/A	N/A	N/A
N/A	N/A	N/A	N/A	N/A	N/A
N/A	N/A	N/A	N/A	N/A	N/A

Name Given	Molecular Hydrogen detection?	H-Alpha Features	Molecular Hydrogen features	Morphology H-Alpha	Morphology Molecular Hydrogen
IPHAS 23	N	Extended source, middle gap, E emission larger than W, gap at N, connected at S	N/A	Elliptical	N/A
IPHAS 24	Y	Point Source	Point Source	Point Source	Point Source
IPHAS 25	Y	Point Source	Point Source	Point Source	Point Source
IPHAS 26	Y	Point Source	Point Source	Point Source	Point Source
IPHAS 27	Y	Point Source	Possible diffuse emission	Point Source	Irregular
IPHAS 28	Y	Point Source	Point Source	Point Source	Point Source
IPHAS 29	Y	Point Source	Point Source	Point Source	Point Source
IPHAS 30	Y	Point Source	Point Source	Point Source	Point Source
IPHAS 31	Y	Point Source	Point Source	Point Source	Point Source
IPHAS 32	Y	Point Source	Point Source	Point Source	Point Source
IPHAS 33	Y	Point Source	Point Source	Point Source	Point Source
IPHAS 34	Y	Point Source	Point Source	Point Source	Point Source
IPHAS 35	N	Point Source	N/A	Point Source	N/A
IPHAS 36	Y	Elliptical ring in center , N-S orientation, with diffuse emission going out from NW and SE	Elliptical Ring, N-S, orientation, bar going from E to S in a diagonal	Elliptical	Elliptical
IPHAS 37	Y	Ellipse with 2 bright spots at NW and SE	Ellipse, no bright spots at NW and SE	Elliptical	Elliptical
IPHAS 38	N	Elliptical blob	N/A	Elliptical	N/A
IPHAS 39	Y	Point Source	Point Source	Point Source	Point Source
IPHAS 40	Y	Point Source	Point Source	Point Source	Point Source
IPHAS 41	Y	Point Source	Point Source	Point Source	Point Source
IPHAS 42	Y	Point Source	Point Source	Point Source	Point Source
IPHAS 43	Y	Point Source	Point Source	Point Source	Point Source
IPHAS 44	Y	Point Source	Point Source	Point Source	Point Source
IPHAS 45	Y	Point Source	Point Source	Point Source	Point Source
IPHAS 46	Y	Ellipitcal object connected to another object?	Ellipitcal object	Point Source	Point Source

Angular Size H-Alpha (arcsecs)	Inclination H-Alpha	Ellipticity H-Alpha	Angular Size Molecular Hydrogen (arcsecs)	Inclination Molecular Hydrogen	Ellipticity Molecular Hydrogen
9.49	177.5	0.600	N/A	N/A	N/A
N/A	N/A	N/A	N/A	N/A	N/A
N/A	N/A	N/A	N/A	N/A	N/A
N/A	N/A	N/A	N/A	N/A	N/A
N/A	N/A	N/A	84.568	N/A	N/A
N/A	N/A	N/A	N/A	N/A	N/A
N/A	N/A	N/A	N/A	N/A	N/A
N/A	N/A	N/A	N/A	N/A	N/A
N/A	N/A	N/A	N/A	N/A	N/A
N/A	N/A	N/A	N/A	N/A	N/A
N/A	N/A	N/A	N/A	N/A	N/A
N/A	N/A	N/A	N/A	N/A	N/A
N/A	N/A	N/A	N/A	N/A	N/A
23.61	123.0	0.700	26.14	121.8	0.677
9.17	142.2	0.701	8.16	144	0.547
3.86	20.0	0.521	N/A	N/A	N/A
N/A	N/A	N/A	N/A	N/A	N/A
N/A	N/A	N/A	N/A	N/A	N/A
N/A	N/A	N/A	N/A	N/A	N/A
N/A	N/A	N/A	N/A	N/A	N/A
N/A	N/A	N/A	N/A	N/A	N/A
N/A	N/A	N/A	N/A	N/A	N/A
N/A	N/A	N/A	N/A	N/A	N/A
9.08	157.5	0.744	7.4	4	0.619

Name Given	Molecular Hydrogen detection?	H-Alpha Features	Molecular Hydrogen features	Morphology H-Alpha	Morphology Molecular Hydrogen
IPHAS 47	Y	Point Source	Point Source	Point Source	Point Source
IPHAS 48	Y	Small curved bar, tapers off towards E	Thicker and more curved in the center, emission at NE extreme connected?	Irregular	Irregular
IPHAS 49	Y	Point Source	Point Source	Point Source	Point Source
IPHAS 50	Y	Bipolar, small waist, small outer lobes	Bipolar, small waist, small outer lobes	Bipolar	Bipolar
IPHAS 51	Y	Point Source	Point Source	Point Source	Point Source
IPHAS 52	Y	Elliptical object which tapers slightly at SE .	Larger than the H-Alpha, more visible outer edges, inner structure more visible as well	Elliptical	Elliptical
IPHAS 53	Y	Elliptical	Elliptical Ring	Elliptical	Elliptical
IPHAS 54	Y	Point Source	Point Source	Point Source	Point Source
IPHAS 55	Y	Point Source	Point Source	Point Source	Point Source
IPHAS 56	Y	Point Source	Point Source	Point Source	Point Source
IPHAS 57	N	Small ellipse, ends do not join up	N/A	Elliptical	N/A
IPHAS 58	Y	Small Ellipse NE orientation	Small ellipse, NE orientation	Elliptical	Elliptical
IPHAS 59	N	Point Source	N/A	Point Source	N/A
IPHAS 60	Y	Point Source	Point Source	Point Source	Point Source
IPHAS 61	Y	Point Source	Point Source	Point Source	Point Source
IPHAS 62	Y	Point Source	Point Source	Point Source	Point Source
IPHAS 63	Y	Point Source	Point Source	Point Source	Point Source
IPHAS 64	Y	Point Source	Point Source	Point Source	Point Source
IPHAS 65	Y	Point Source	Point Source	Point Source	Point Source
IPHAS 66	Y	Small number of point sources grouped up	Point Source	Point Source	Point Source

Angular Size H-Alpha (arcsecs)	Inclination H-Alpha	Ellipticity H-Alpha	Angular Size Molecular Hydrogen (arcsecs)	Inclination Molecular Hydrogen	Ellipticity Molecular Hydrogen
N/A	N/A	N/A	N/A	N/A	N/A
11.59	171.0	0.837	9.408	2.49	0.929
N/A	N/A	N/A	N/A	N/A	N/A
7.33	8.2	0.771	10.866	5.8	0.832
N/A	N/A	N/A	N/A	N/A	N/A
15.65	27.8	0.267	22.394	107.2	0.694
7.62	86.2	0.759	6.2	90	0.489
N/A	N/A	N/A	N/A	N/A	N/A
N/A	N/A	N/A	N/A	N/A	N/A
N/A	N/A	N/A	N/A	N/A	N/A
6.09	139.5	0.383	N/A	N/A	N/A
3.97	41.8	0.557	4.842	38.2	0.911
N/A	N/A	N/A	N/A	N/A	N/A
N/A	N/A	N/A	N/A	N/A	N/A
N/A	N/A	N/A	N/A	N/A	N/A
N/A	N/A	N/A	N/A	N/A	N/A
N/A	N/A	N/A	N/A	N/A	N/A
N/A	N/A	N/A	N/A	N/A	N/A
N/A	N/A	N/A	N/A	N/A	N/A
N/A	N/A	N/A	N/A	N/A	N/A

Name Given	Molecular Hydrogen detection?	H-Alpha Features	Molecular Hydrogen features	Morphology H-Alpha	Morphology Molecular Hydrogen
IPHAS 67	Y	Diffuse emission starting in W and moving to E	Small patch nearest the center of bright emission in H-Alpha	Irregular	Irregular
IPHAS 68	N	Point Source	N/A	Point Source	N/A
IPHAS 69	Y	Point Source	Point Source	Point Source	Point Source
IPHAS 70	Y	Point Source	Point Source	Point Source	Point Source
IPHAS 71	Y	Point Source	Point Source	Point Source	Point Source
IPHAS 72	Y	Point Source	Point Source	Point Source	Point Source
IPHAS 73	N	Appearance of a tick, area facing N, with a bar from center towards NW, curves towards W	N/A	Irregular	N/A
IPHAS 74	Y	Point Source	Small tail like structure, extending NW	Point Source	Irregular
IPHAS 75	Y	Curved front facing in E direction, connected to possibly larger structure towards NW	Curved front facing east, similar size to H-Alpha	Irregular	Irregular
IPHAS 76	Y	Point Source	Point Source	Point Source	Point Source
IPHAS 77	Y	Point Source	Point Source	Point Source	Point Source
IPHAS 78	Y	Central source with some diffuse emission	Point Source with large band of emitting material behind it, may cover up diffuse emission	Point Source	Point Source
IPHAS 79	Y	Point Source	Point Source	Point Source	Point Source
IPHAS 80	Y	Ellipse	N/A	Elliptical	N/A
IPHAS 81	Y	Point Source	Point Source	Point Source	Point Source
IPHAS 82	N	Point Source	N/A	Point Source	N/A
IPHAS 83	N	Point Source	N/A	Point Source	N/A

Angular Size H-Alpha (arcsecs)	Inclination H-Alpha	Ellipticity H-Alpha	Angular Size Molecular Hydrogen (arcsecs)	Inclination Molecular Hydrogen	Ellipticity Molecular Hydrogen
16.02	32.5	0.193	13.63	146.2	0.343
N/A	N/A	N/A	N/A	N/A	N/A
N/A	N/A	N/A	N/A	N/A	N/A
N/A	N/A	N/A	N/A	N/A	N/A
N/A	N/A	N/A	N/A	N/A	N/A
N/A	N/A	N/A	N/A	N/A	N/A
12.84	162.0	0.775	N/A	N/A	N/A
N/A	N/A	N/A	5.126	110.5	0.42
21.85	105.0	0.614	14.68	101.2	0.804
N/A	N/A	N/A	N/A	N/A	N/A
N/A	N/A	N/A	N/A	N/A	N/A
N/A	N/A	N/A	N/A	N/A	N/A
N/A	N/A	N/A	N/A	N/A	N/A
N/A	N/A	N/A	N/A	N/A	N/A
N/A	N/A	N/A	N/A	N/A	N/A
N/A	N/A	N/A	N/A	N/A	N/A

Name Given	Molecular Hydrogen detection?	H-Alpha Features	Molecular Hydrogen features	Morphology H-Alpha	Morphology Molecular Hydrogen
IPHAS 84	Y	Central source with curve shaped emission on W side	Diffuse emission, mainly N-S oriented, some in NW to SE orientation	Irregular	Irregular
IPHAS 85	Y	Point Source	Point Source	Point Source	Point Source
IPHAS 86	Y	Point Source	Point Source	Point Source	Point Source
IPHAS 87	Y	Bipolar, lobes are faintly visible. Possible reflection? Waist region not clearly defined.	Bipolar, small waist size in comparison with lobe size.	Bipolar	Bipolar
IPHAS 88	Y	Small Ellipse	Small Ellipse	Elliptical	Elliptical
IPHAS 89	Y	Possibly bipolar, waist region clearly visible, lobes not visible at all.	Clearly Bipolar, waist region visible, lobes visible to a reasonable distance	Bipolar	Bipolar
IPHAS 90	Y	Point Source	Point Source	Point Source	Point Source

Angular Size H-Alpha (arcsecs)	Inclination H-Alpha	Ellipticity H-Alpha	Angular Size Molecular Hydrogen (arcsecs)	Inclination Molecular Hydrogen	Ellipticity Molecular Hydrogen
18.16	92.0	0.800	17.14	101.5	0.528
N/A	N/A	N/A	N/A	N/A	N/A
N/A	N/A	N/A	N/A	N/A	N/A
117.74	17.0	0.978	32.84	24.8	0.889
4.76	149.0	0.587	3.394	150.8	0.716
17.76	39.8	0.814	30.894	41.2	0.945
N/A	N/A	N/A	N/A	N/A	N/A

3.0.2 MASH tables

Name Given	Molecular Hydrogen detection?	H-Alpha Features	Molecular Hydrogen features	Morphology H-Alpha	Morphology Molecular Hydrogen
PN G007.2+00.0	Y	Point Source	Point Source	Point Source	Point Source
PN G007.7+01.2	N	Bipolar	N/A	Bipolar	N/A
PN G008.1+01.3	N	Ellipse with 2 bright sources in SE and NW	N/A	Elliptical	N/A
PN G008.6+01.0	N	Small ellipse with bright patch near center	N/A	Elliptical	N/A
PN G009.4-01.2	N	Small ellipse	N/A	Elliptical	N/A
PN G009.7-01.1	N	Small ellipse	N/A	Elliptical	N/A
PN G009.8-01.1	Y	Possibly bipolar, waist thinning, outer areas larger	Bipolar, waist thinner than lobe regions	Bipolar	Bipolar
PN G010.0-01.5	N	Ellipse, orientation, SW-NE	N/A	Elliptical	N/A
PN G010.2+00.3	Y	Ellipse, orientation, SE-NW, diffuse emission from the SW and NE	Small outer ring, orientation SE-NW	Elliptical	Elliptical
PN G011.0+01.4	Y	Round center, diffuse emission from NE	Ellipse, no diffuse emission.	Elliptical	Elliptical
PN G011.5+01.0	Y	Elliptical?	Point Source	Elliptical	Point Source

Angular Size H-Alpha (arcsecs)	Inclination H-Alpha	Eccentricity H-Alpha	Angular Size Molecular Hydrogen (arcsecs)	Eccentricity Molecular Hydrogen	Ellipticity Molecular Hydrogen
N/A	N/A	N/A	N/A	N/A	N/A
81.3186	120.8	0.376	N/A	N/A	N/A
6.5934	123.8	0.693	N/A	N/A	N/A
7.6956	59.03	0.514	N/A	N/A	N/A
10.2696	42.9	0.561	N/A	N/A	N/A
7.1346	127.8	0.537	N/A	N/A	N/A
18.4866	88.8	0.798	27.018	88	0.915
9.7416	26.5	0.765	N/A	N/A	N/A
48.7212	151.8	0.733	25.176	40	0.89
11.5236	19.79	0.525	17.0558	39.2	0.758
4.5738	46.2	0.957	N/A	N/A	N/A

Name Given	Molecular Hydrogen detection?	H-Alpha Features	Molecular Hydrogen features	Morphology H-Alpha	Morphology Molecular Hydrogen
PN G014.6+01.1	Y	Elliptical object, brightness concentrated in a T shape in the middle	Outer edges of an ellipse illuminated at N and S	Elliptical	Elliptical
PN G016.4-00.9	Y	Elliptical, NW to SE orientation	NW and SE most edges illuminated.	Elliptical	Irregular
PN G017.2+01.1	Y	Faint curve	Faint Curve	Irregular	Irregular
PN G021.2+00.9	N	Elliptical object, brighter band around the middle	N/A	Elliptical	N/A
PN G022.0+01.3	Y	Central source with diffuse emission surrounding	3 point sources close together	Elliptical	Point Source
PN G023.4+00.7	Y	Small ellipse, offshoot at E	Ellipse with offshoot at SE	Elliptical	Elliptical
PN G023.5-00.1	N	Faint elliptical ring	N/A	Elliptical	N/A
PN G027.0+01.5	N	Large ellipse	N/A	Elliptical	N/A
PN G027.5+01.0	N	Small ellipse, possible offshoot at N?	N/A	Elliptical	N/A
PN G027.6-00.8	Y	Elliptical, N-S orientation	Elliptical, outer edges faint	Elliptical	Elliptical
PN G027.7-00.6	N	Point Source	N/A	Point Source	N/A
PN G028.8-00.2	Y	Curved bar, with off shoot at W	Curved bar, possible offshoot at W	Irregular	Irregular

Angular Size H-Alpha (arcsecs)	Inclination H-Alpha	Eccentricity H-Alpha	Angular Size Molecular Hydrogen (arcsecs)	Eccentricity Molecular Hydrogen	Ellipticity Molecular Hydrogen
15.8532	2.5	0.662	13.746	8.79	0.643
18.249	122	0.731	14.48	122.5	0.486
20.4996	3.8	0.892	26.37	22.19	0.887
26.54784	130.5	0.399	N/A	N/A	N/A
27.852	140.99	0.611	N/A	N/A	N/A
7.161	47.5	0.137	6.378	136.5	0.571
15.9522	114.5	0.91	N/A	N/A	N/A
19.206	126.5	0.194	N/A	N/A	N/A
6.0852	121	0.359	N/A	N/A	N/A
15.5034	124.5	0.749	10.5	49.8	0.785
N/A	N/A	N/A	N/A	N/A	N/A
26.07	97.2	0.791	28.212	92.5	0.365

Name Given	Molecular Hydrogen detection?	H-Alpha Features	Molecular Hydrogen features	Morphology H-Alpha	Morphology Molecular Hydrogen
PN G029.3-01.2	N	Elliptical with diffuse emission leading N	N/A	Elliptical	N/A
PN G029.8+00.5	N	Elliptical ring	N/A	Elliptical	N/A
PN G030.0+00.0	Y	Near circular Elliptical ring	Elliptical ring with diffuse emission from SW	Elliptical	Elliptical
PN G030.5-00.2	Y	Ellipse	2 outer edges with very little emission in center	Elliptical	Irregular
PN G033.9-00.9	Y	Ellipse	Faint outer edges of ellipse	Elliptical	Elliptical

Angular Size H-Alpha (arcsecs)	Inclination H-Alpha	Eccentricity H-Alpha	Angular Size Molecular Hydrogen (arcsecs)	Eccentricity Molecular Hydrogen	Ellipticity Molecular Hydrogen
32.1816	107.8	0.843	N/A	N/A	N/A
34.452	36.5	0.343	N/A	N/A	N/A
19.8132	30	0.393	21.556	27.04	0.646
16.3944	67.5	0.672	11.574	71.9	0.133
4.8708	122.8	0.963	5.692	62.2	0.656

Chapter 4

Analysis

The analysis of the data presented in Chapter 3 used several approaches. Firstly, graphs were made to compare the frequency of detection of PN in H_2 to that of Hα and to compare the number of morphologies found of each classification set out in section 1.1.5.

Secondly, each image was compared and contrasted to ascertain the degree to which H_2 emissions matched those of Hα, given the differences in emission mechanism. This was then used with the data gained from the usage of GAIA to determine the differences in size and structure between each wavelength.

4.1 Comparison of detection rates of PN in H_2 and Hα emissions

The usage of H_2 to detect PN is a major part of this work, to see if the wavelength is suitable for the detection of PN in comparison with detections from optical surveys.

Each object in the 2 surveys (MASH, IPHAS) has a definite Hα detection. This means that there may or may not be a detection in H_2, and therefore, we can compare to see how useful H_2 is as a detector for PN with optical emission.

As Figure 4.1 and Figure 4.2 show, not all Hα PN show detectable emission from H_2. This is likely due to the excitation characteristics of the nebulae, see Section 1.1.4

There is a difference between the 2 surveys however. MASH shows a 53% detection rate for H_2 in comparison with IPHAS, which shows a 85% detection rate for H_2. This detection rate may be down to the sample sizing of each of the surveys with their overlap (MASH at 28 objects, IPHAS at 90 objects), or down to the nature of the survey, MASH being a survey of true and confirmed PN and IPHAS being a survey of possible PN.

Gatley's rule states that molecular hydrogen emission in PN is a sign of bipolarity. However, there is evidence to suggest that in the cases of PN found in MASH and IPHAS, that molecular

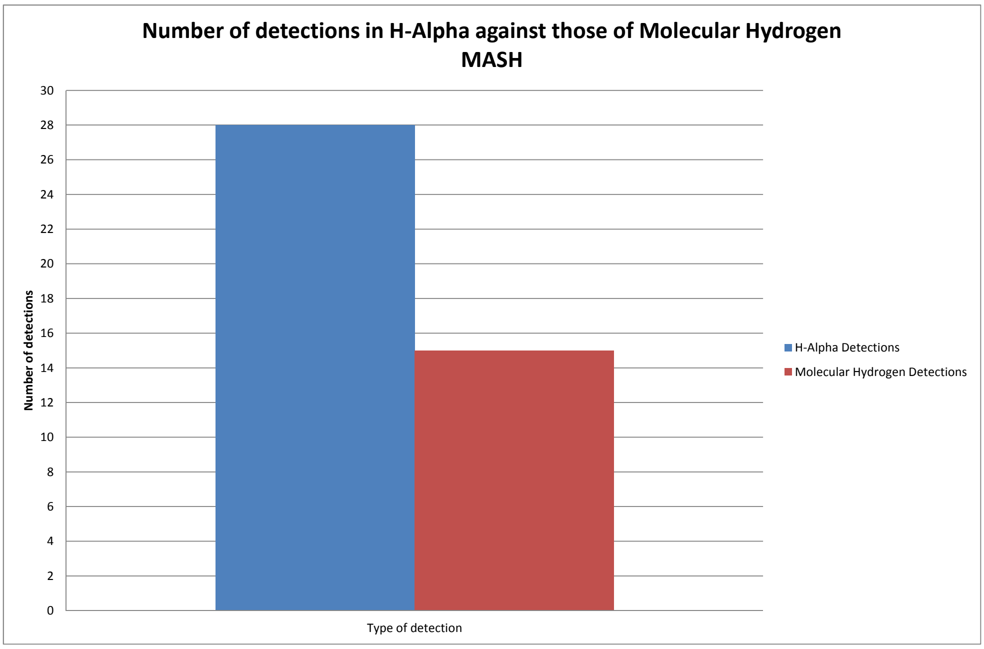

Figure 4.1: A graph showcasing the number of detections in H-Alpha in blue, and the number of H_2 detections in red next to it for the MASH survey.

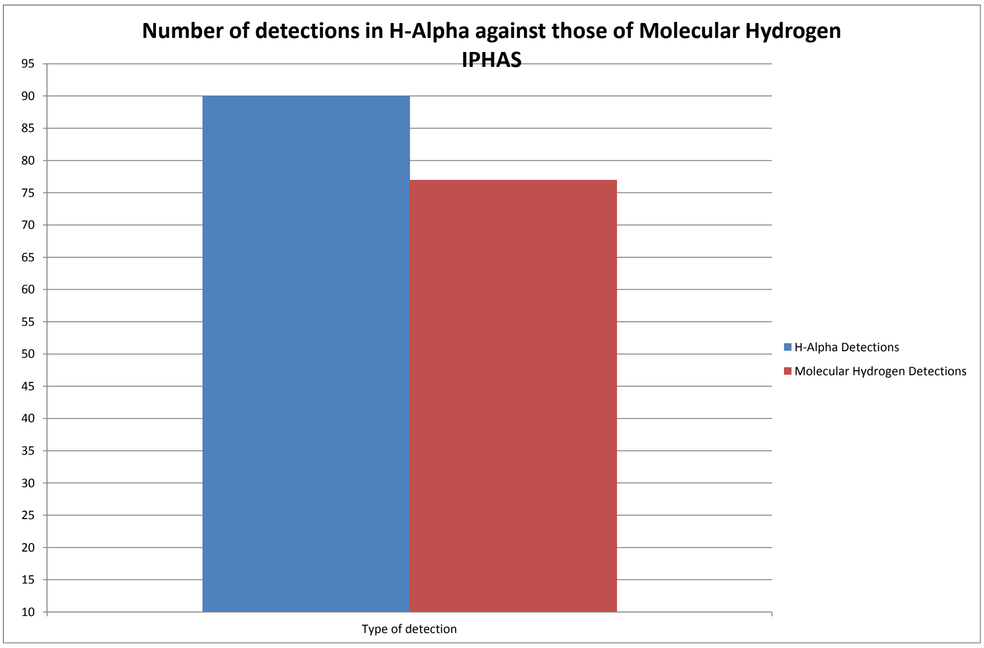

Figure 4.2: A graph showcasing the number of detections in H-Alpha in blue, and the number of H_2 detections in red next to it for the IPHAS survey

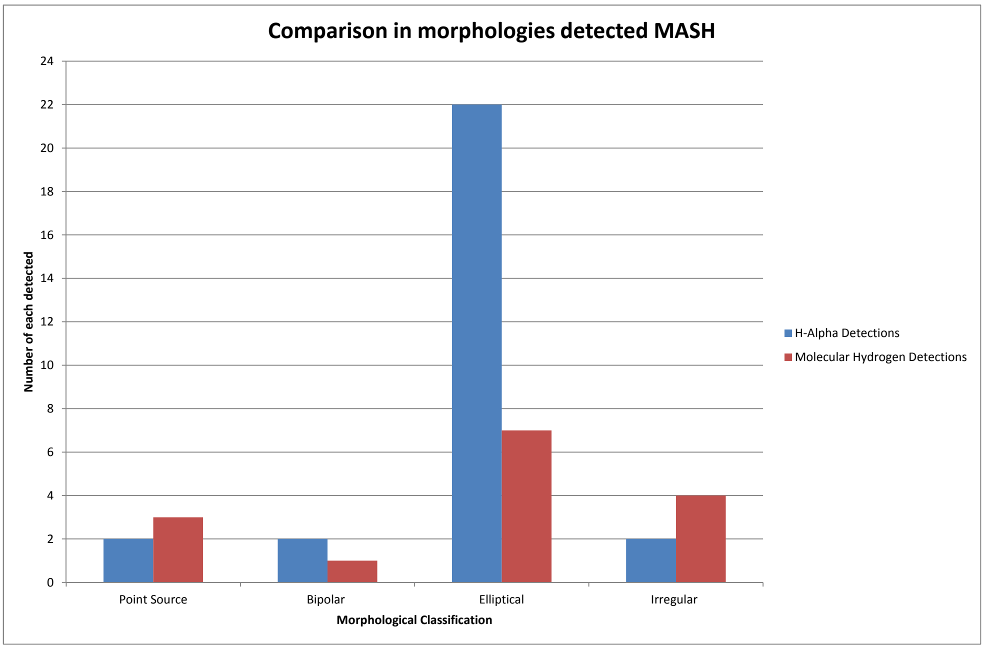

Figure 4.3: A graph showing the number of each morphological type of PN in the MASH survey overlap with the UWISH2 survey, with H-Alpha in blue and H_2 in red.

hydrogen emission is more likely to be due to the phase of evolution that the PN is going through, rather than be linked to a certain morphology. This may also be a cause for the discrepancy in detection rate for PN between the 2 surveys, as elliptical PN could be a morphology that occurs after the PN has had time to expand and evolve (Huarte-Espinosa et al. 2012). There are many more elliptical PN in the MASH survey than in IPHAS, which may contribute to the lower (53%) detection rate in the MASH PN than the IPHAS PN (85%).

As seen in Figure 4.3 and Figure 4.4, bipolar morphologies make up a very small part of the total PN sample. The most common shape in MASH is that of elliptical morphologies, and in IPHAS, it is of Point Sources, where the object is too small to define a structure at all.

Figure 4.5 shows a bipolar PN in the MASH survey, PN G007.7+01.2, that has a definite H-Alpha detection and no H_2 detection. This is not likely linked to the morphology, but more likely to be linked to the evolutionary stage of the PN. The PN on the right is very large (81.3 arcseconds major axis) and this may be an indication that the PN has been active for a long period of time, photo-dissociating the molecular hydrogen present to the point where emission

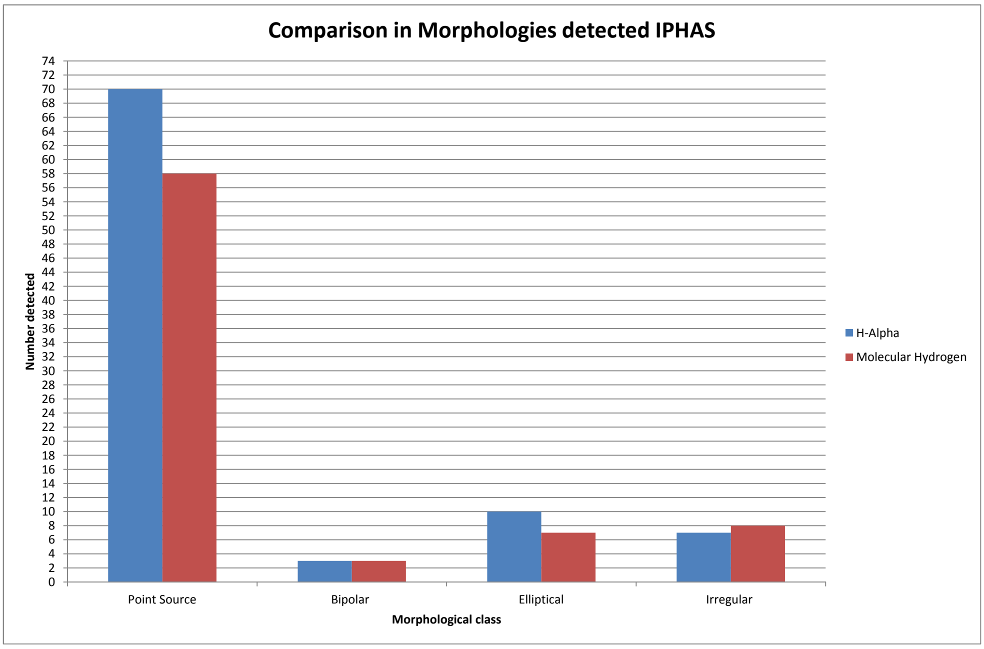

Figure 4.4: A graph showing the number of each morphological type of PN in the IPHAS survey overlap with the UWISH2 survey, with H-Alpha in blue and H_2 in red.

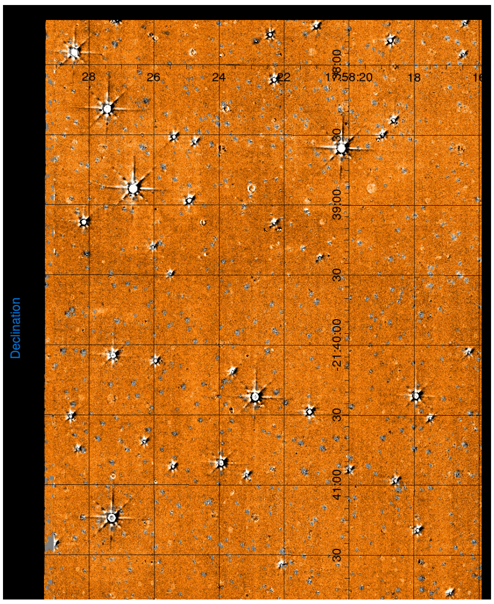

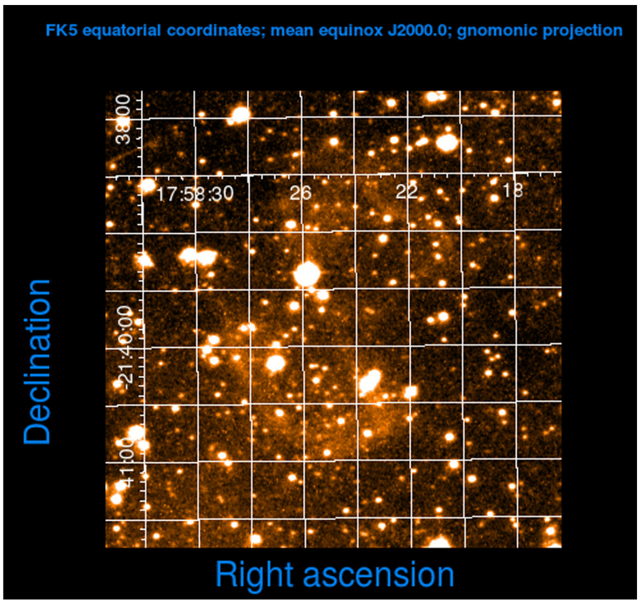

Figure 4.5: A comparison image of PN G007.7+01.2, with H_2 on the left and Hα on the right

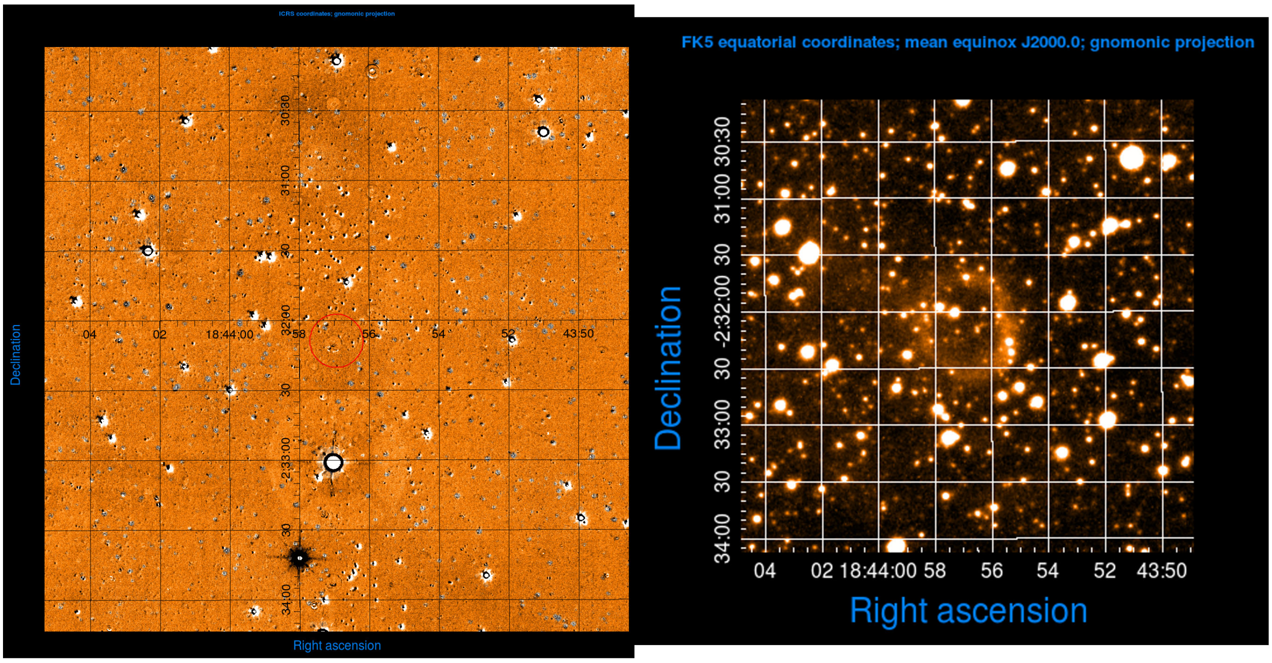

Figure 4.6: A comparison image of PN G0029.8+00.5, with H_2 on the left and Hα on the right

is not detectable.

However, size cannot be a definition of PN age, as distances may not show the true size of a PN, rather its apparent size.

Figure 4.6 shows a smaller PN (34.2 arcseconds) with an extended Hα emission without a corresponding H_2 emission to match. Again, without a measurement of distance, we cannot tell if this PN is very large, however the lack of H_2 emission may provide more of a clue towards its age.

From the emission mechanisms mentioned in section 1.1.4, it may be that H_2 emission is less of a universal marker for PN, but more associated with the age of the PN itself. This is because the photodissociation of molecular hydrogen in the nebula will increase with age. So that H_2 may be prevalent in early PN but dissapate as the PN becomes older and fully ionised.

4.2 Comparison of H_2 emission and Hα emission in the structure of PN

One of the goals outlined in section 1.3.1 is to compare features found in both wavelengths to ascertain if there are major changes.

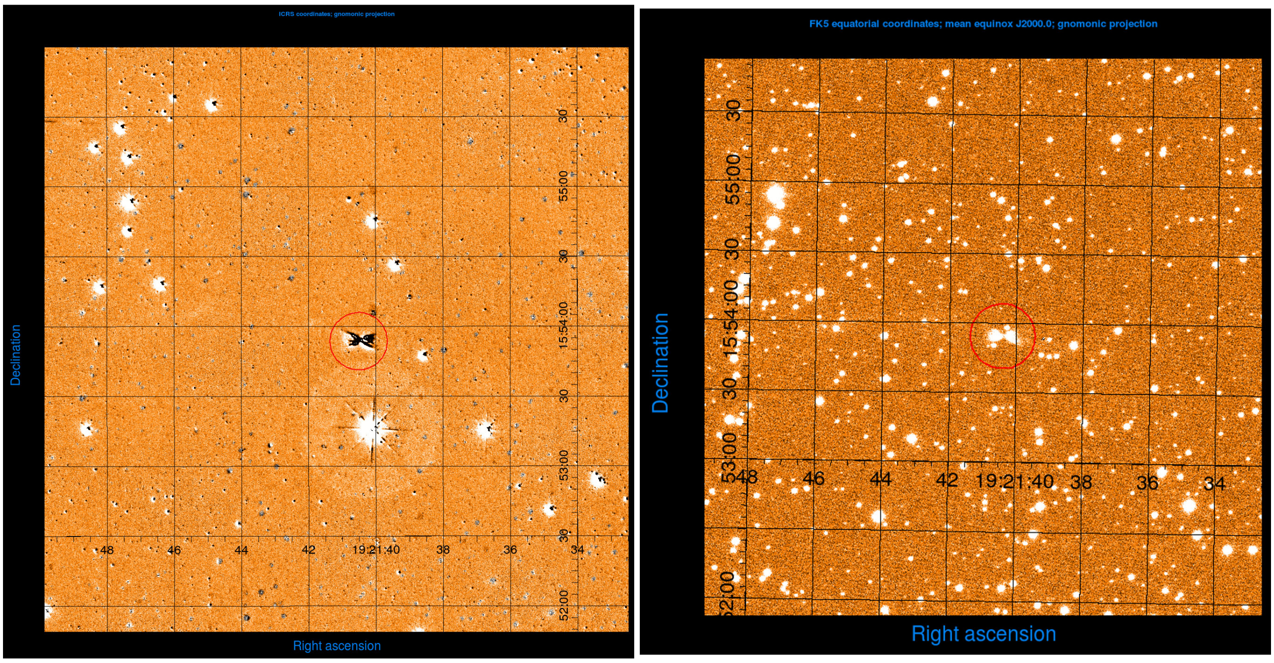

Figure 4.7: A comparison image of IPHAS 50, with H_2 on the left, and Hα on the right

4.2.1 Bipolar PN

There are a very limited number of bipolar PN found in both survey overlaps (MASH and IPHAS), however, these are very interesting due to the previously mentioned Gatley's rule that states that molecular hydrogen emission is a sign of bipolarity.

Overall, there are 3 bipolar PN in IPHAS and 2 in MASH, giving a total of 5 for the whole sample. Of these 5, there is 1 that does not have an H_2 component. This is shown in Figure 4.5. As mentioned in the previous section, this may be down to the PN being older, and therefore having very little non photodissociated molecular hydrogen left.

Of the remaining objects, there are a number of differences present between the two wavelengths.

These PN, IPHAS 50 and PN G009.8-01.1 (Figure 4.7 and 4.8), show large similarities. They show a similar size in both wavelengths, along with a similar structure.

However, these PN show a difference in the structure. Both of the images show a clear difference in size between the wavelengths (IPHAS 89 is 17.76 arcseconds in Hα and 30.89 in H_2), which could be linked to the propagation of the UV photons from the central star, which shows a different stage of evolution. However, the structural changes could also be down to the

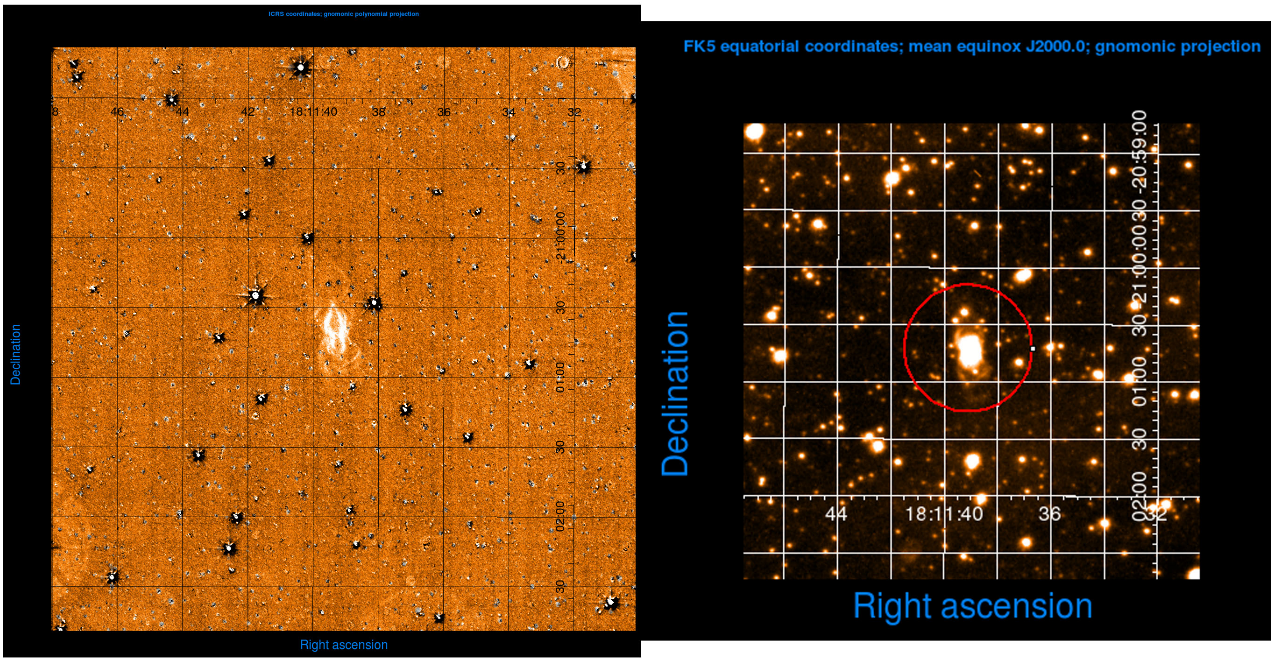

Figure 4.8: A comparison image of PN G009.8-01.1, with H_2 on the left, and Hα on the right

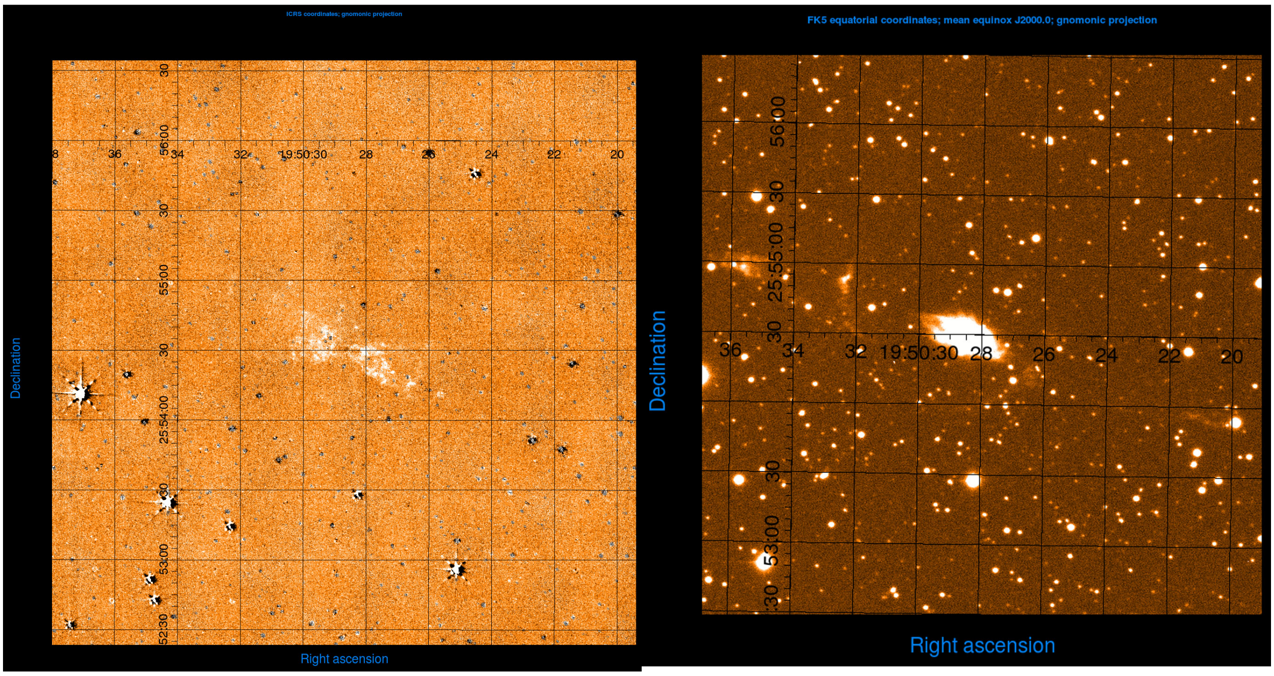

Figure 4.9: A comparison image of IPHAS 87, with H_2 on the left, and Hα on the right

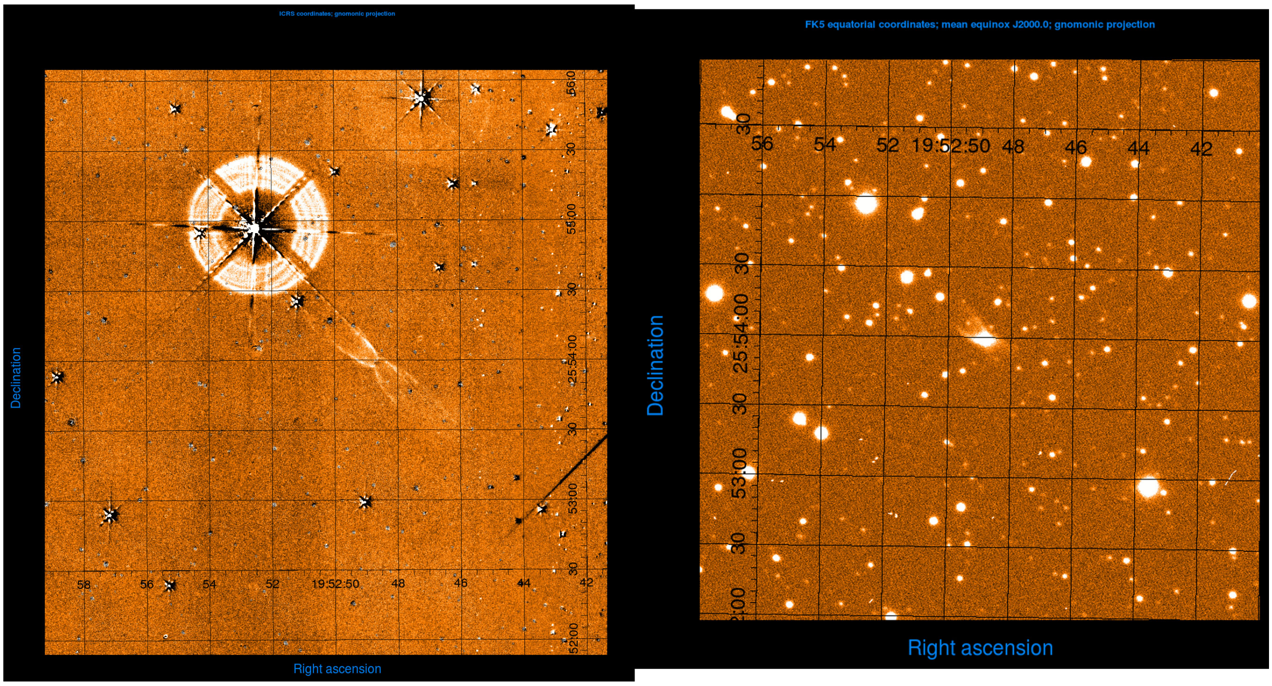

Figure 4.10: A comparison image of IPHAS 89, with H_2 on the left, and Hα on the right

higher resolution of UWISH2 in comparison to IPHAS (0.2 arcseconds/pixel for UWISH2, 0.33 arcseconds/pixel for IPHAS).

Figure 4.9 shows IPHAS 87, where the main waist area of the PN in question is closer to being an elliptical blob in Hα than it is in H_2 where it definitely shows the thin waist, wide lobe characteristics that make it a bipolar PN. However, I would expect that H_2 emission would have a large size than Hα solely due to the emission mechanisms, however, Figure 4.9 shows that this may not be the case.

Figure 4.10 shows IPHAS 89, which has a much more expected emission in both wavelengths. The H_2 emission image displays a larger PN than in Hα, which is expected because of the propagation of the UV photons having not reached as far through the cloud to dissociate it yet, meaning that the Hα is smaller (17.76 arcsecond major axis in comparison with 30.89 arcsecond major axis).

Overall, bipolar PN seem to display similar features in both wavelengths, but, this would have to be clarified with a larger sample size to ascertain if this holds true in general for PN.

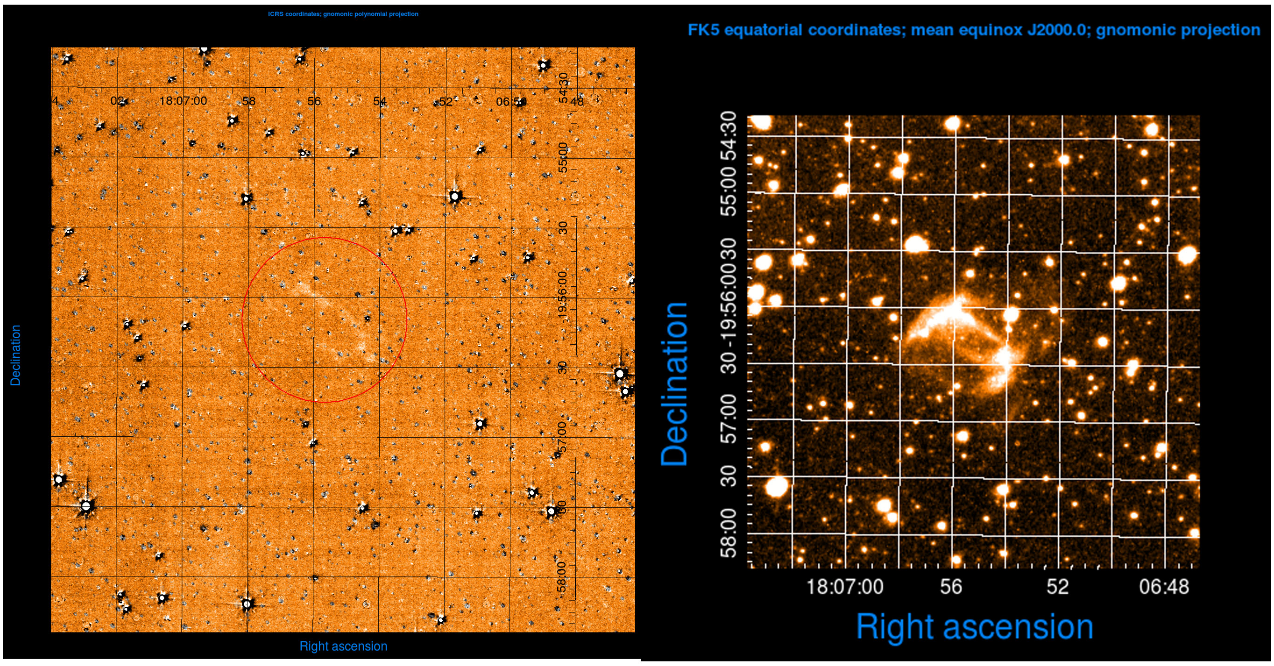

Figure 4.11: A comparison image of PN G010.2+00.3, with H_2 on the left, and Hα on the right

4.2.2 Elliptical PN

Elliptical PN are more prevalent in the MASH sample than they are in the IPHAS sample. As explained in Section 4.1, elliptical PN seem to not show emission in H_2 at all in half of the cases. However, it is still useful to compare and contrast the emissions seen in those that have detections in both wavelengths.

Elliptical PN in the MASH survey which have detections in both wavelengths show a similar trend. Hα emission displays the whole structure of the object, whereas H_2 emission tracks the edges of the object.

In Figure 4.11, the Hα emission shows much more clearly the structure of the object, whereas the H_2 emission seems to only show the outer edge of the bright inner ring of material. As mentioned in the previous section, ellipticals are more likely to be older PN, so Hα should track the material better than the H_2 solely because more time has passed, and the UV propagation can photodissociate more of the molecular hydrogen.

Figure 4.12 shows this, but in a less dramatic example. The overall structure remains the same, but, the middle has substantially less emission in H_2 than in Hα.

However, the differences in resolution between the surveys may contribute to the differences

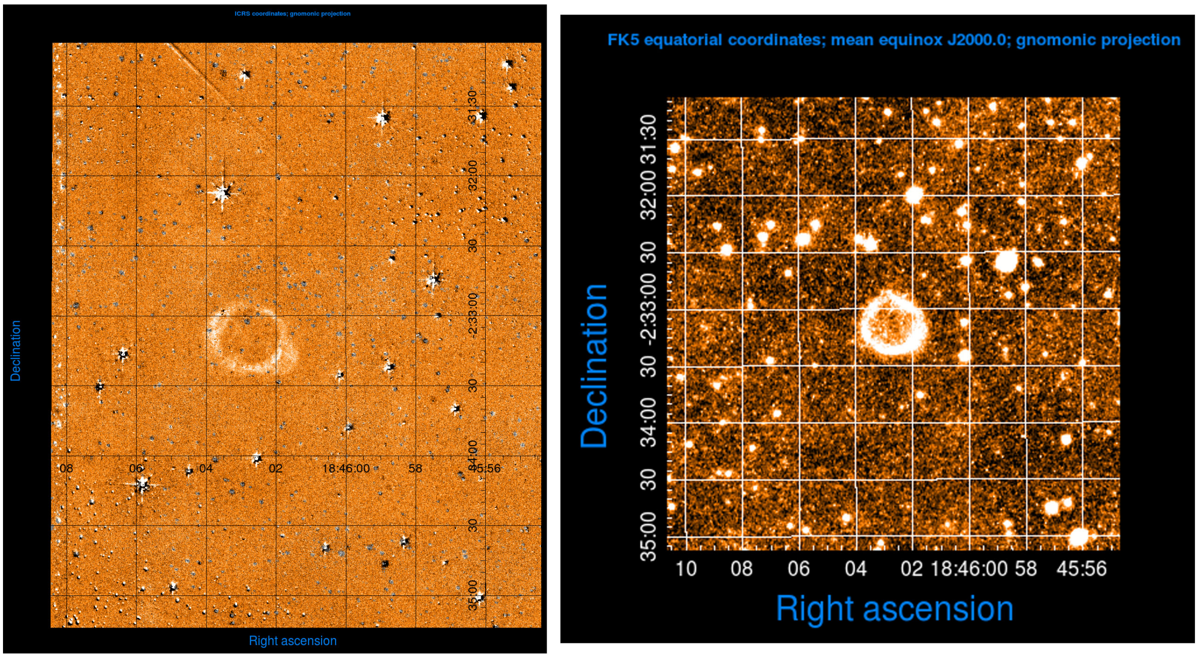

Figure 4.12: A comparison image of PN G030.0+00.0, with H_2 on the left, and Hα on the right

seen between the 2 wavelengths.

Figure 4.13 pictured above shows an example of H_2 emission clearly showing the structure of the object well, with clear morphological similarities between Hα and H_2, whereas Figure 4.14 is more in-line with the previous examples, where the edges of the object are the higher emitting areas of the object in H_2.

4.2.3 Irregular PN

Irregular PN were defined as objects that did not fit any of the normal classifications set out in Section 1.15. Overall, there were 2 Hα detections in MASH of irregular objects, with 4 more being detected in H_2. In IPHAS there are 7 detections of irregular PN in Hα and there are 8 detections in H_2. This does not mean that there are non detections in Hα, this means that the detections in H_2 do not represent the structure of the emission in Hα.

Figure 4.15 shows PN G017.2+01.1. Both wavelengths show a similar structure, in a small arc across the center of the image that has shown up to be very dim. This object does not display the characteristics discussed earlier relating to elliptical PN and the emission mechanisms of Hα, as both images seem to show a similar level of diffuse emissions. This could however, be a central

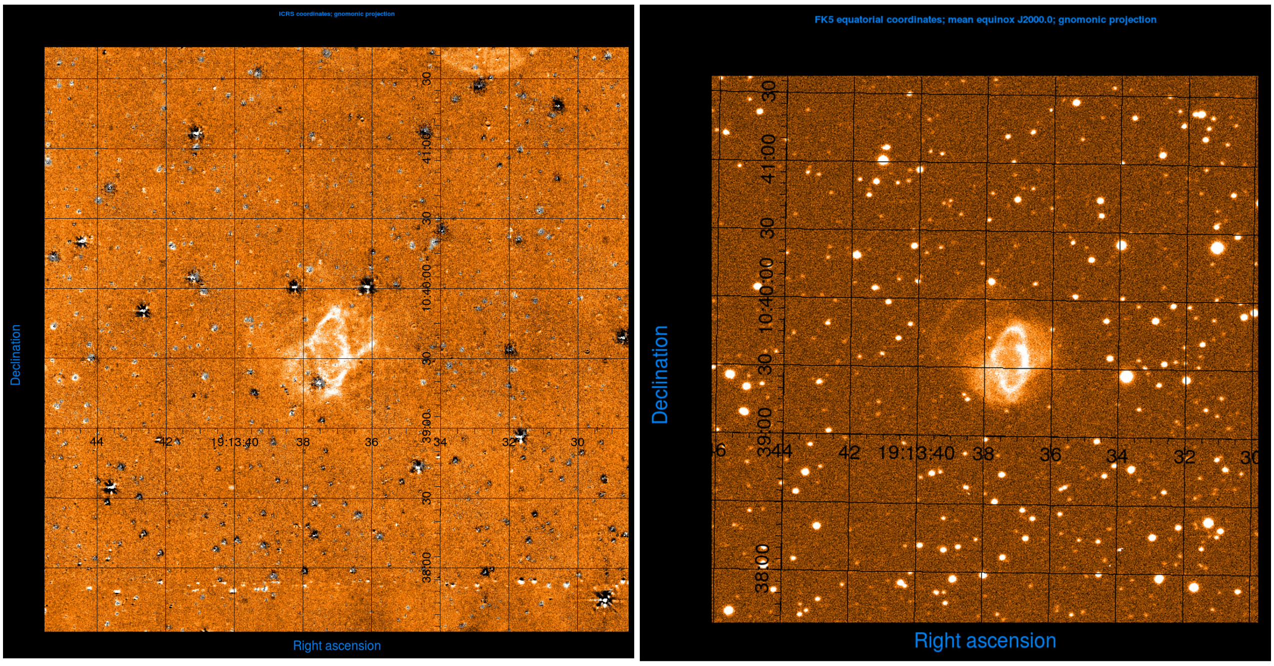

Figure 4.13: A comparison image of IPHAS 36, with H_2 on the left, and Hα on the right

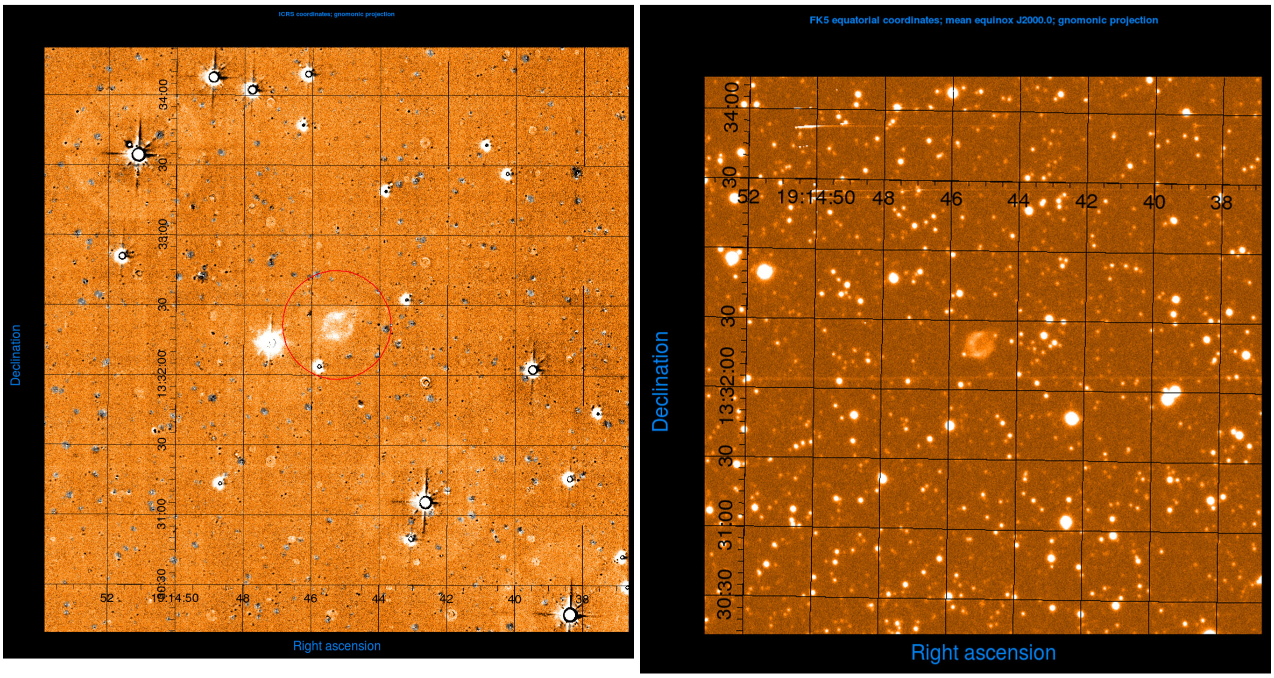

Figure 4.14: A comparison image of IPHAS 37, with H_2 on the left, and Hα on the right

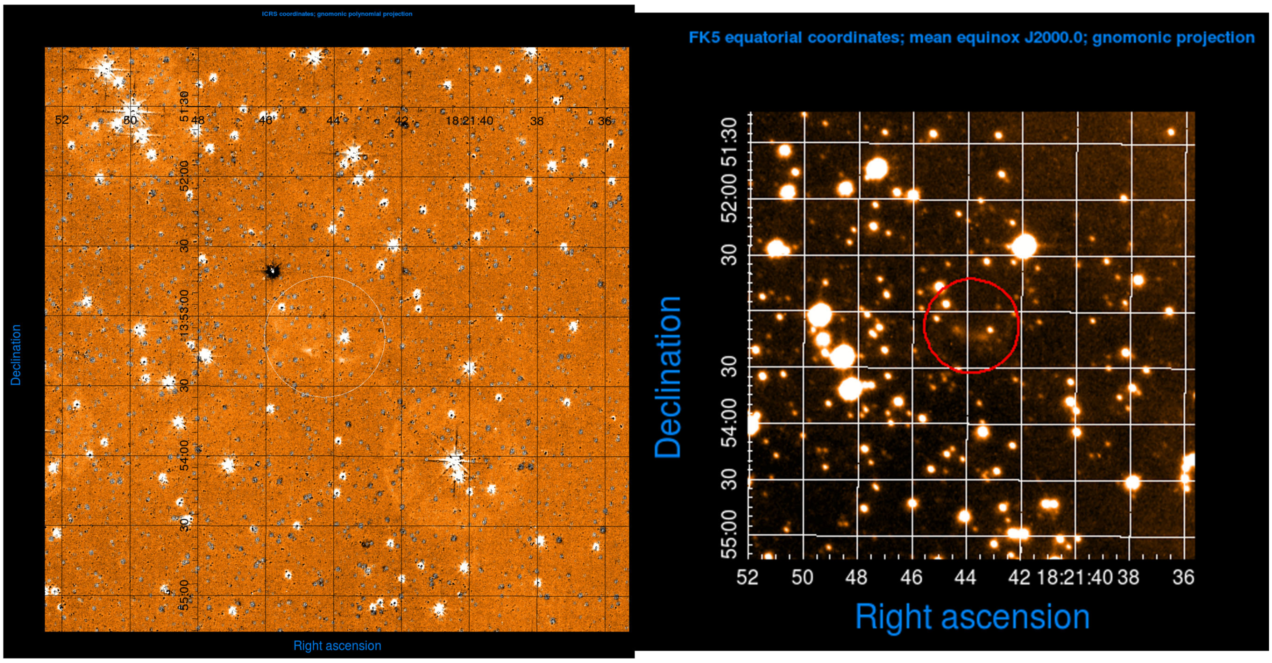

Figure 4.15: A comparison image of PN G017.2+01.1, with H_2 on the left, and Hα on the right

section of a bipolar PN that has

Figure 4.16 shows another possible irregular PN in both wavelengths. However, the density of the emission could be interpreted as bipolar. The orientation contribute to a number of objects being labelled irregular, as from our viewing angle, the PN may appear to have no features of any known PN type, but, in reality may be another morphology.

Overall, H_2 seems to detect irregular PN as the emissions seem to track quite well. However, irregular PN themselves may be another type of PN, at another viewing angle, such as bipolar or elliptical.

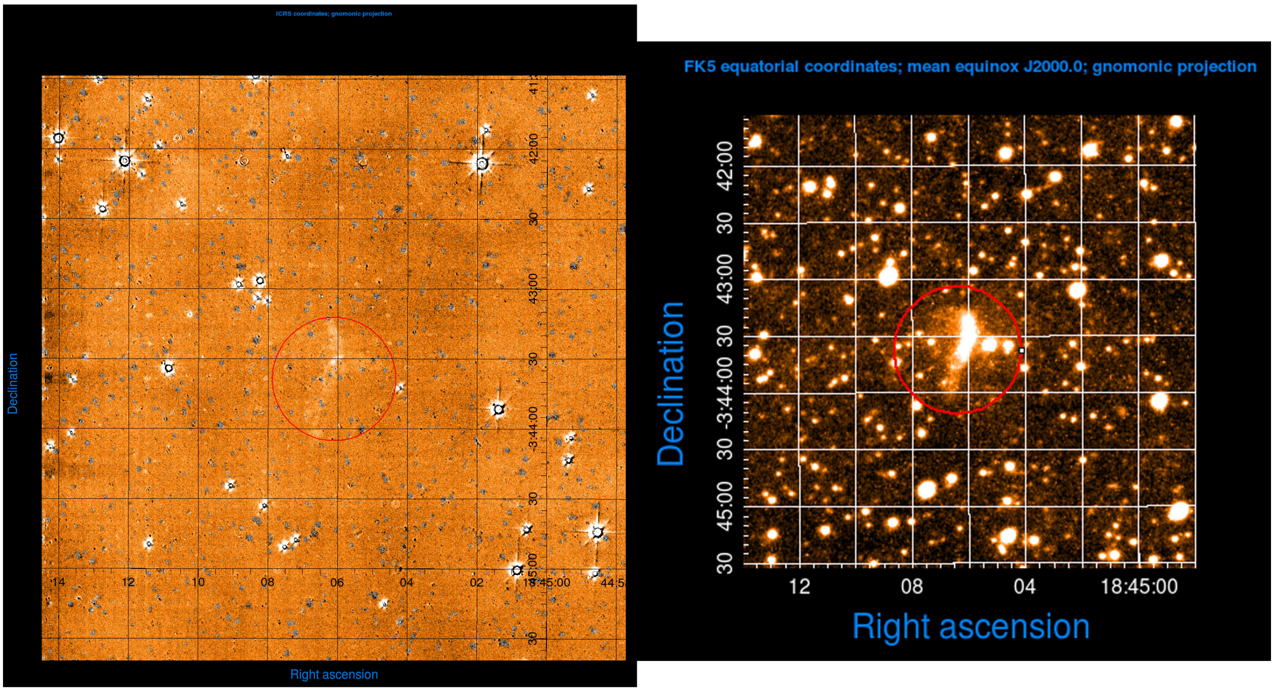

Figure 4.16: A comparison image of PN G028.8-00.2, with H_2 on the left, and Hα on the right

Chapter 5

Conclusions

In conclusion, the work presented here shows a clear trend between H_2 emission and $H\alpha$ emission in PN, with 53% of PN in the MASH sample showing H_2 emission and 83% of the IPHAS sample showing H_2 emission also.

Morphologically, elliptical PN in the MASH sample showed the greatest discrepancy in detection rates, with only 37.5% of them having a corresponding H_2 detection, whereas in IPHAS, there is a 70% detection rate for ellipticals. Bipolars range from 100% with a H_2 detection in IPHAS to 50% in MASH. Irregulars range from 50% in MASH to 87.5% in IPHAS, and point sources range from 82.9% in IPHAS to 66% in MASH. Finally, irregular PN detections in H_2 range from 50% in MASH to 82.8% in IPHAS.

The validity of Gatley's Rule comes into question with these results, as molecular hydrogen emission has been detected across the breadth of PN morphologies, showing that H_2 is not only a sign of bipolarity, but could just be a wavelength that all PN have some emissions in.

Overall, these numbers show that H_2 could be a valuable tool for detecting and confirming PN.

However, with the limited sample size presented here (120 PN), it could be argued that this work does not represent a wide enough subset of PN to really gauge the usefulness of H_2 emission as a tool for finding and confirming PN.

Nevertheless, this work bears further study to see if it still holds true for other surveys of PN, and to see if morphology and other quantifiable elements have an impact upon H_2 emission in a larger sample size of PN.

References

[1] A. Acker, J. Marcout, F. Ochsenbein, B. Stenholm, R. Tylenda, and C. Schohn. The Strasbourg-ESO Catalogue of Galactic Planetary Nebulae. Parts I, II. *The Strasbourg-ESO Catalogue of Galactic Planetary Nebulae. Parts I, II., by Acker, A.; Marcout, J.; Ochsenbein, F.; Stenholm, B.; Tylenda, R.; Schohn, C.. European Southern Observatory, Garching (Germany), 1992, 1047 p., ISBN 3-923524-41-2,*, -1, 1992.

[2] S. Beckwith, I. Gatley, and S. E. Persson. Detection of molecular hydrogen emission from five planetary nebulae. *The Astrophysical Journal*, 219:L33, January 1978.

[3] Orsola De Marco, J Farihi, and J Nordhaus. The WD perspective on the PN binary hypothesis. *Journal of Physics: Conference Series*, 172:012031, June 2009.

[4] Orsola De Marco and Noam Soker. The Role of Planets in Shaping Planetary Nebulae. *Publications of the Astronomical Society of the Pacific*, 123(902):402–411, April 2011.

[5] Janet E. Drew, R. Greimel, M. J. Irwin, A. Aungwerojwit, M. J. Barlow, R. L. M. Corradi, J. J. Drake, B. T. Gansicke, P. Groot, A. Hales, E. C. Hopewell, J. Irwin, C. Knigge, P. Leisy, D. J. Lennon, A. Mampaso, M. R. W. Masheder, M. Matsuura, L. Morales-Rueda, R. A. H. Morris, Q. A. Parker, S. Phillipps, P. Rodriguez-Gil, G. Roelofs, I. Skillen, J. L. Sokoloski, D. Steeghs, Y. C. Unruh, K. Viironen, J. S. Vink, N. A. Walton, A. Witham, N. Wright, A. A. Zijlstra, and A. Zurita. The INT Photometric Halpha Survey of the Northern Galactic Plane (IPHAS). *Monthly Notices of the Royal Astronomical Society*, 362(3):753–776, September 2005.

[6] A S Ferrarotti and H Gail. Composition and quantities of dust produced by AGB-stars and returned to the interstellar medium. *Astronomy & Astrophysics*, 576:553–576, 2006.

[7] D. Froebrich, C. J. Davis, G. Ioannidis, T. M. Gledhill, M. Takami, a. Chrysostomou, J. Drew, J. Eislöffel, a. Gosling, R. Gredel, J. Hatchell, K. W. Hodapp, M. S. N. Kumar,

P. W. Lucas, H. Matthews, M. G. Rawlings, M. D. Smith, B. Stecklum, W. P. Varricatt, H. T. Lee, P. S. Teixeira, C. Aspin, T. Khanzadyan, J. Karr, H.-J. Kim, B.-C. Koo, J. J. Lee, Y.-H. Lee, T. Y. Magakian, T. a. Movsessian, E. H. Nikogossian, T. S. Pyo, and T. Stanke. UWISH2 - the UKIRT Widefield Infrared Survey for H2. *Monthly Notices of the Royal Astronomical Society*, 413(1):480–492, May 2011.

[8] Nigel Hambly, Harvey MacGillivray, Mike Read, Sue Tritton, Eve Thomson, Dennis Kelly, David Morgan, Rob Smith, Simon Driver, John Williamson, Quentin Parker, Mike Hawkins, Perry Williams, and Andy Lawrence. The SuperCOSMOS Sky Survey. Paper I: Introduction and Description. *Monthly Notices of the Royal Astronomical Society*, 326:18, August 2001.

[9] Falk Herwig. Evolution of Asymptotic Giant Branch Stars. *Annual Review of Astronomy and Astrophysics*, 43(1):435–479, September 2005.

[10] M. Huarte-Espinosa, A. Frank, B. Balick, E. G. Blackman, O. De Marco, J. H. Kastner, and R. Sahai. From bipolar to elliptical: simulating the morphological evolution of planetary nebulae. *Monthly Notices of the Royal Astronomical Society*, 424(3):2055–2068, August 2012.

[11] P. J. Huggins, R. Bachiller, T. Forveille, P. Cox, and J. P. Maillard. The Shaping of Planetary Nebulae by Bipolar Outflows or Jets. *American Astronomical Society*, 31, 1999.

[12] I Iben Jr. Planetary nebulae and their central stars ? origin and evolution. *Physics Reports*, 250(1?2):1–94, 1995.

[13] J. H. Kastner, L. Henn, D. A. Weintraub, I. Gatley, and R. Siebenmorgen. Kinematics of Molecular Hydrogen Emission from Bipolar Pre-planetary, Protoplanetary, and Planetary Nebulae. *American Astronomical Society*, 30, 1998.

[14] Joel H. Kastner, I. Gatley, K. M. Merrill, R. Probst, and David A. Weintraub. The Bipolar Symmetry of Ring-Like Planetary Nebulae: H_2 Imaging at 2.122 microns with the Kitt Peak Cryogenic Optical Bench. *American Astronomical Society*, 24, 1992.

[15] Joel H. Kastner, David A. Weintraub, Ian Gately, K. M. Merrill, and Ronald G. Probst. H 2 Emission from Planetary Nebulae: Signpost of Bipolar Structure. *The Astrophysical Journal*, 462:777, May 1996.

[16] L. Kohoutek. Version 2000 of the Catalogue of Galactic Planetary Nebulae. *Astronomy and Astrophysics*, 378(3):843–846, November 2001.

[17] L. Kohoutek. Version 2000 of the Catalogue of Galactic Planetary Nebulae. *Astronomy and Astrophysics*, 378(3):843–846, November 2001.

[18] L. Kohoutek. Version 2000 of the Catalogue of Galactic Planetary Nebulae. *Astronomy and Astrophysics*, 378(3):843–846, November 2001.

[19] J.-J. Lee, B.-C. Koo, Y.-H. Lee, H.-G. Lee, J.-H. Shinn, H.-J. Kim, Y. Kim, T.-S. Pyo, D.-S. Moon, S.-C. Yoon, M.-Y. Chun, D. Froebrich, C. J. Davis, W. P. Varricatt, J. Kyeong, N. Hwang, B.-G. Park, M. G. Lee, H. M. Lee, and M. Ishiguro. UKIRT Widefield Infrared Survey for Fe+. *Monthly Notices of the Royal Astronomical Society*, 443(3):2650–2660, August 2014.

[20] Mario Livio. Jets in Planetary Nebulae. *Asymmetrical Planetary Nebulae II: From Origins to Microstructures*, 199, 2000.

[21] Arturo Manchado, Letizia Stanghellini, and Martín A. Guerrero. Quadrupolar Planetary Nebulae: A New Morphological Class. *The Astrophysical Journal*, 466(2):L95–L98, August 1996.

[22] B. Miszalski, A. Acker, and Q. A. Parker. Central Stars of MASH Planetary Nebulae. *Hydrogen-Deficient Stars ASP Conference Series*, 391, 2008.

[23] Quentin A. Parker, A. Acker, D. J. Frew, M. Hartley, A. E. J. Peyaud, F. Ochsenbein, S. Phillipps, D. Russeil, S. F. Beaulieu, M. Cohen, J. Köppen, B. Miszalski, D. H. Morgan, R. A. H. Morris, M. J. Pierce, and A. E. Vaughan. The Macquarie/AAO/Strasbourg H? Planetary Nebula Catalogue: MASH. *Monthly Notices of the Royal Astronomical Society*, 373(1):79–94, November 2006.

[24] Quentin A. Parker, S. Phillipps, M. J. Pierce, M. Hartley, N. C. Hambly, M. A. Read, H. T. MacGillivray, S. B. Tritton, C. P. Cass, R. D. Cannon, M. Cohen, J. E. Drew, D. J. Frew, E. Hopewell, S. Mader, D. F. Malin, M. R. W. Masheder, D. H. Morgan, R. A. H. Morris, D. Russeil, K. S. Russell, and R. N. F. Walker. The AAO/UKST SuperCOSMOS

Hα survey. *Monthly Notices of the Royal Astronomical Society*, 362(2):689–710, September 2005.

[25] Lubos Perek and Lubos Kohoutek. Catalogue of galactic planetary nebulae. *Prague: Publication House Czechoslovak Academy of Sciences, 1967*, -1, 1967.

[26] G. Ramos-Larios, M. a. Guerrero, O. Suárez, L. F. Miranda, and J. F. Gómez. Searching for heavily obscured post-AGB stars and planetary nebulae. *Astronomy & Astrophysics*, 545:A20, August 2012.

[27] R. Sahai. Sowing the Seeds of Asymmetry: Jet-like Outflows in Proto-Planetary Nebulae and AGB Stars. *Asymmetrical Planetary Nebulae III: Winds*, 313, 2004.

[28] R. Sahai, D. Le Mignant, C. Sánchez Contreras, R. D. Campbell, and F. H. Chaffee. Sculpting a Pre-planetary Nebula with a Precessing Jet: IRAS 16342-3814. *The Astrophysical Journal*, 622(1):L53–L56, March 2005.

[29] Raghvendra Sahai, Mark Morris, Carmen Sánchez Contreras, and Mark Claussen. Preplanetary Nebulae: A Hubble Space Telescope Imaging Survey and a New Morphological Classification System. *The Astronomical Journal*, 134(6):2200–2225, December 2007.

[30] Raghvendra Sahai, Mark R. Morris, and Gregory G. Villar. Young Planetary Nebulae: Hubble Space Telescope Imaging and a New Morphological Classification System. *The Astronomical Journal*, 141(4):134, April 2011.

[31] Richard A. Shaw, Letizia Stanghellini, Max Mutchler, Bruce Balick, and J. Chris Blades. Morphology and Evolution of the Large Magellanic Cloud Planetary Nebulae. *The Astrophysical Journal*, 548(2):727–748, February 2001.

[32] K. Viironen, R. Greimel, R. L. M. Corradi, a. Mampaso, M. Rodríguez, L. Sabin, G. Delgado-Inglada, J. E. Drew, C. Giammanco, E. a. González-Solares, M. J. Irwin, B. Miszalski, Q. a. Parker, E. R. Rodríguez-Flores, and a. Zijlstra. Candidate planetary nebulae in the IPHAS photometric catalogue. *Astronomy and Astrophysics*, 504(1):291–301, September 2009.

[33] K Werner, NJ Hammer, and T Nagel. On Possible Oxygen/Neon White Dwarfs: H1504+65 and the White Dwarf Donors in Ultracompact X-ray Binaries. *arXiv preprint astro-ph/ . . .*, 334:165–170, 2004.

[34] J M Winters, T Le Bertre, K S Jeong, L Nyman, and N Epchtein. Mass-loss from dusty , low outflow-velocity AGB stars I . Wind structure and mass-loss rates. *Astronomy & Astrophysics*, 735:715–735, 2003.

[35] B. Zuckerman and Ian Gatley. Molecular hydrogen maps of extended planetary nebulae - The Dumbbell, the Ring, and NGC 2346. *The Astrophysical Journal*, 324:501, January 1988.

Appendix A

Appendix

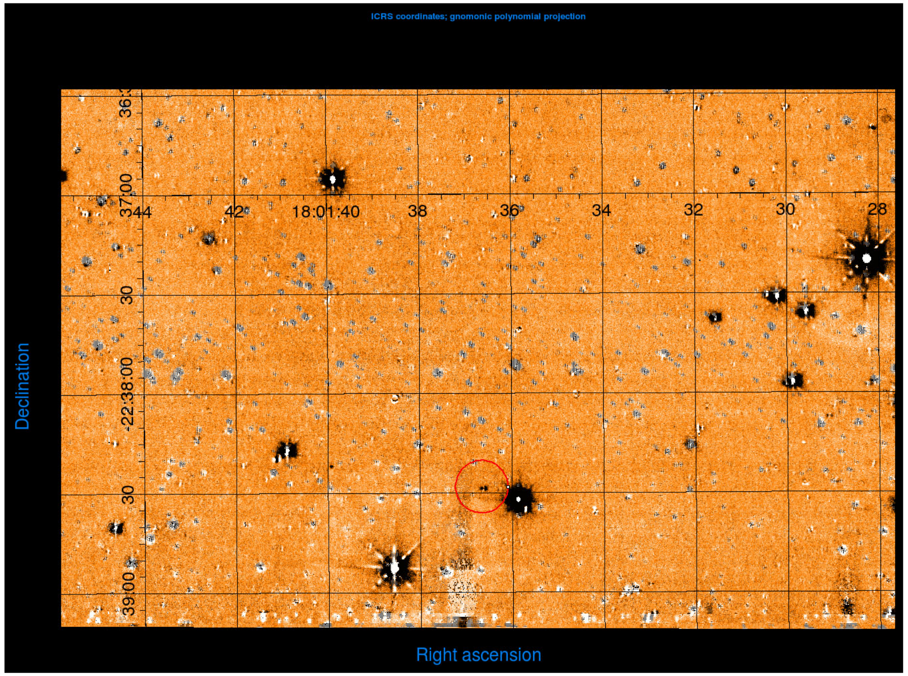

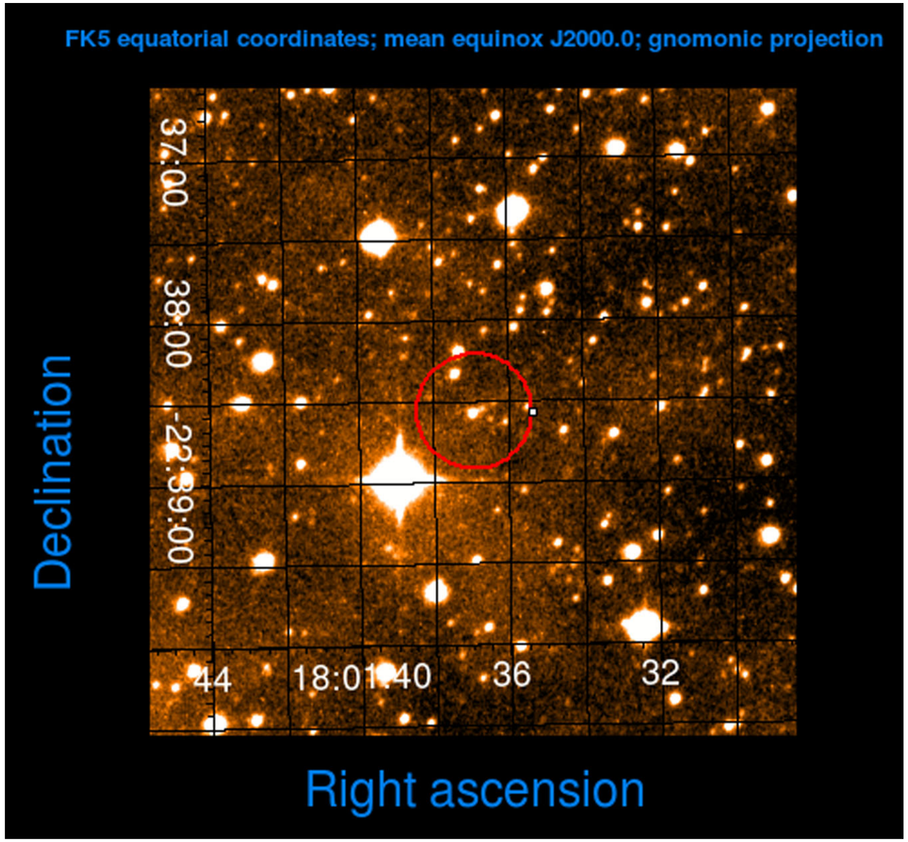

Comparison of PNG007.2+00.0, Hα on the left, H_2 on the right.

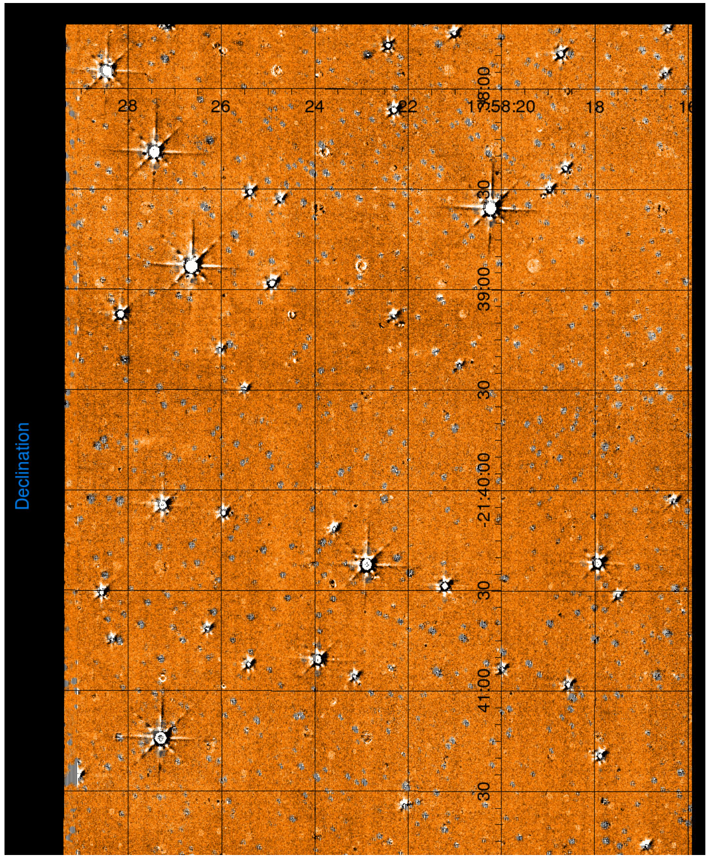

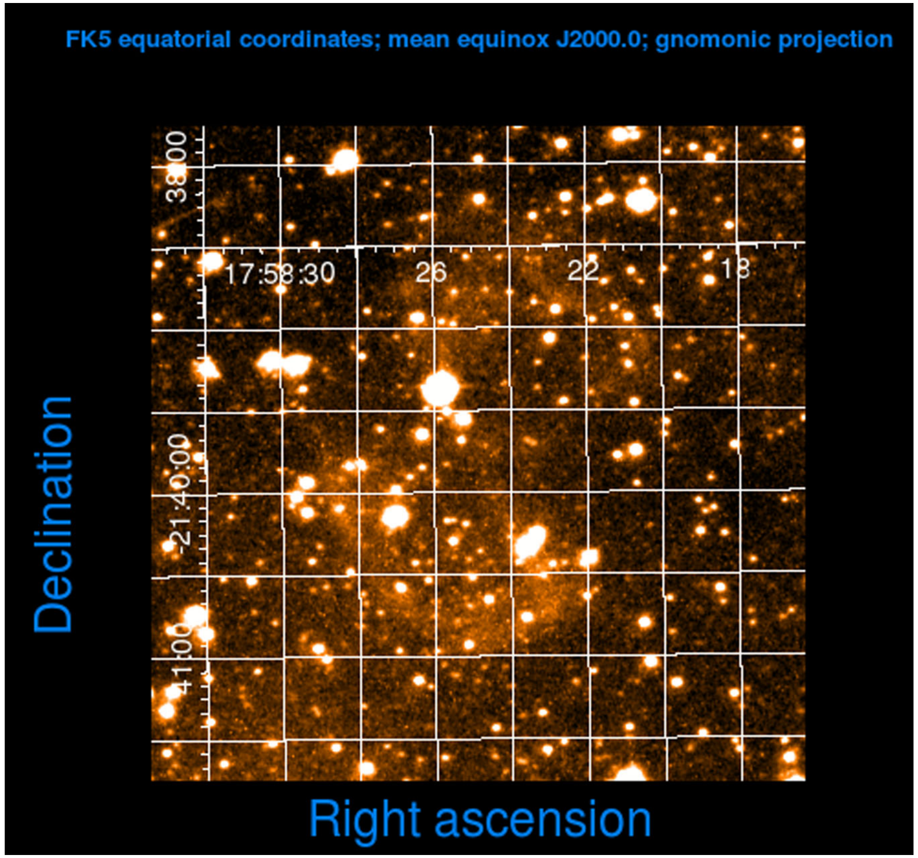

Comparison of PNG007.7+01.2, H_2 on the left, $H\alpha$ on the right

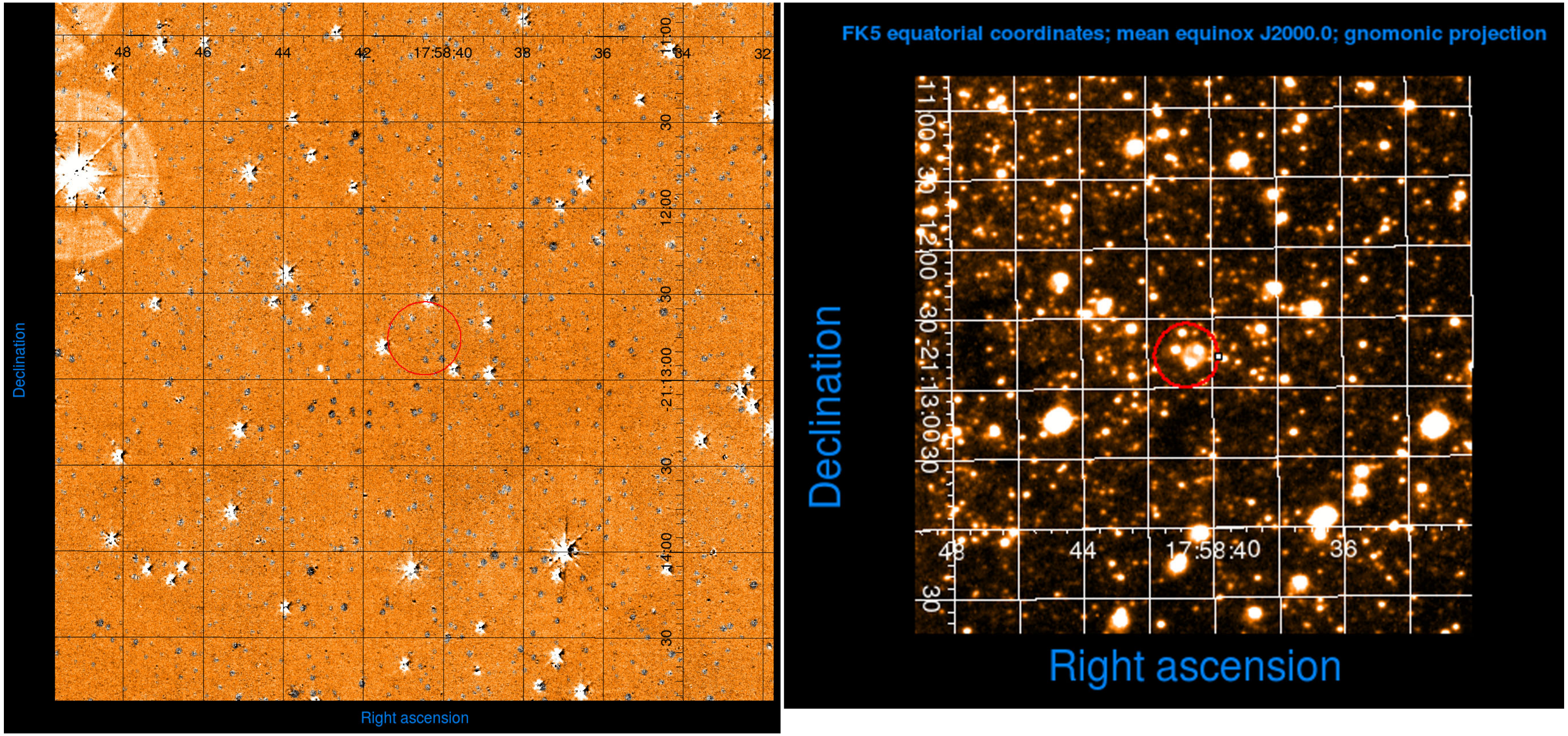

Comparison of PNG008.1+01.3, H_2 on the left, Hα on the right

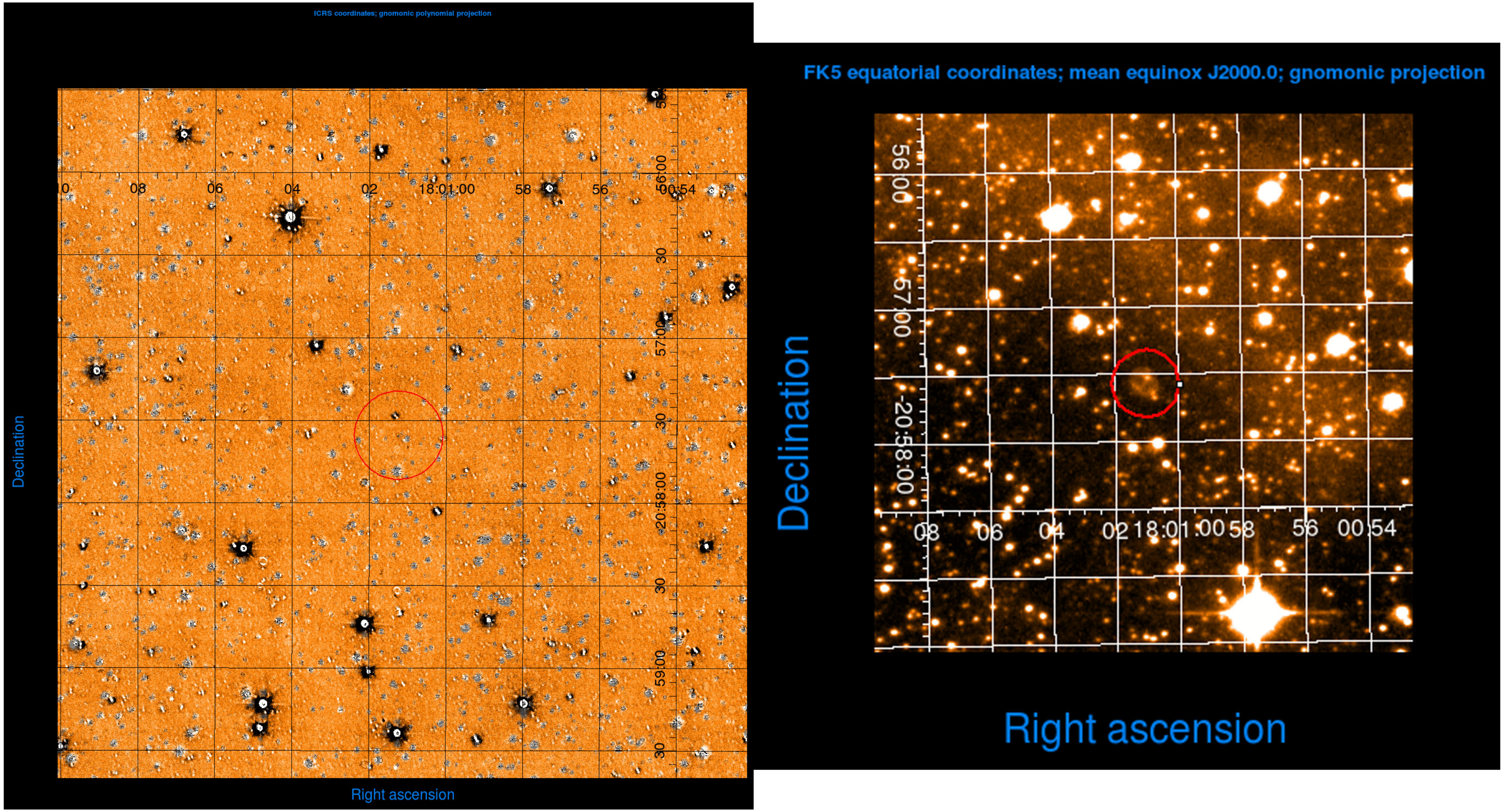

Comparison of PNG008.6+01.0, H_2 on the left, Hα on the right

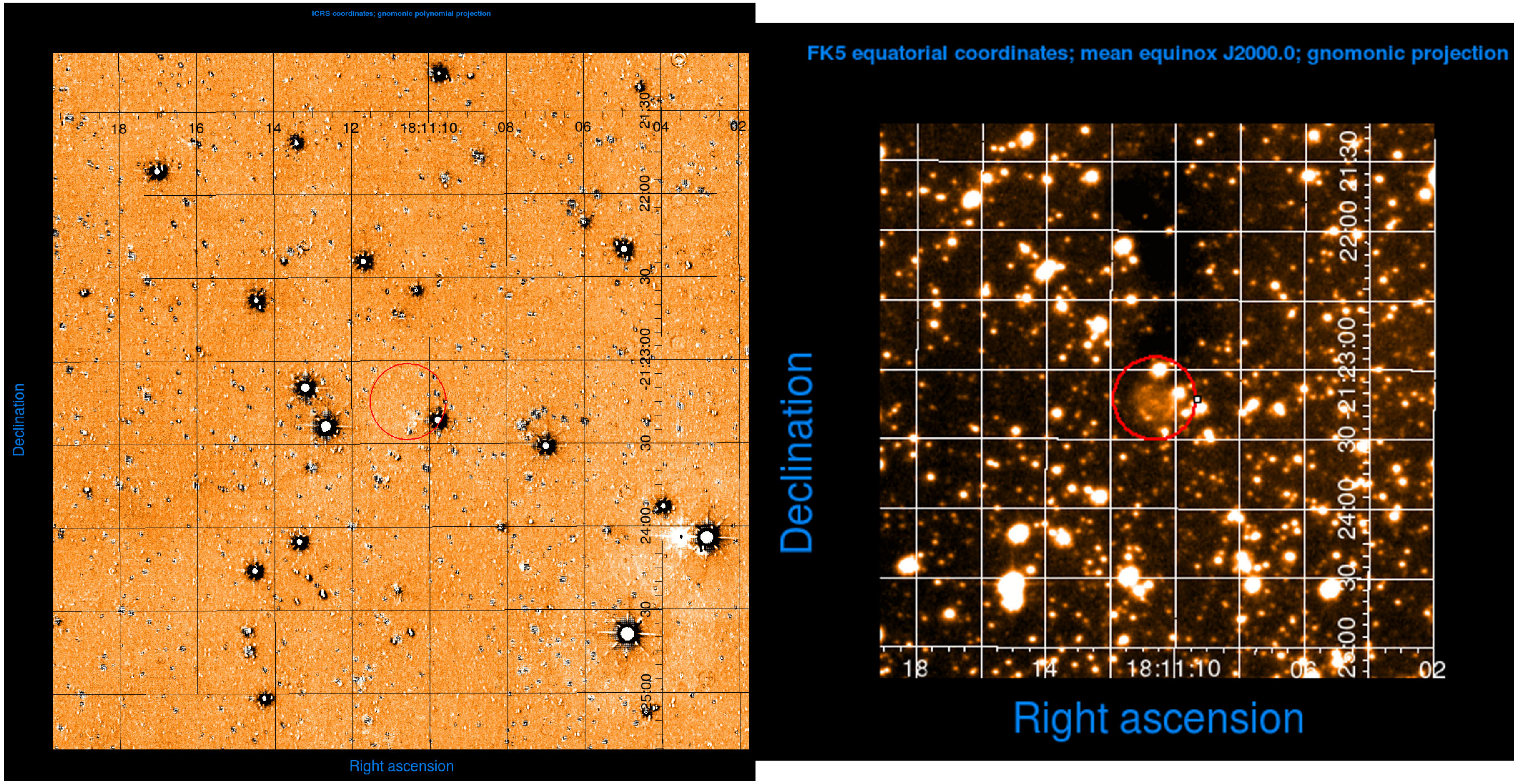

Comparison of PNG009.4-01.2, H_2 on the left, Hα on the right

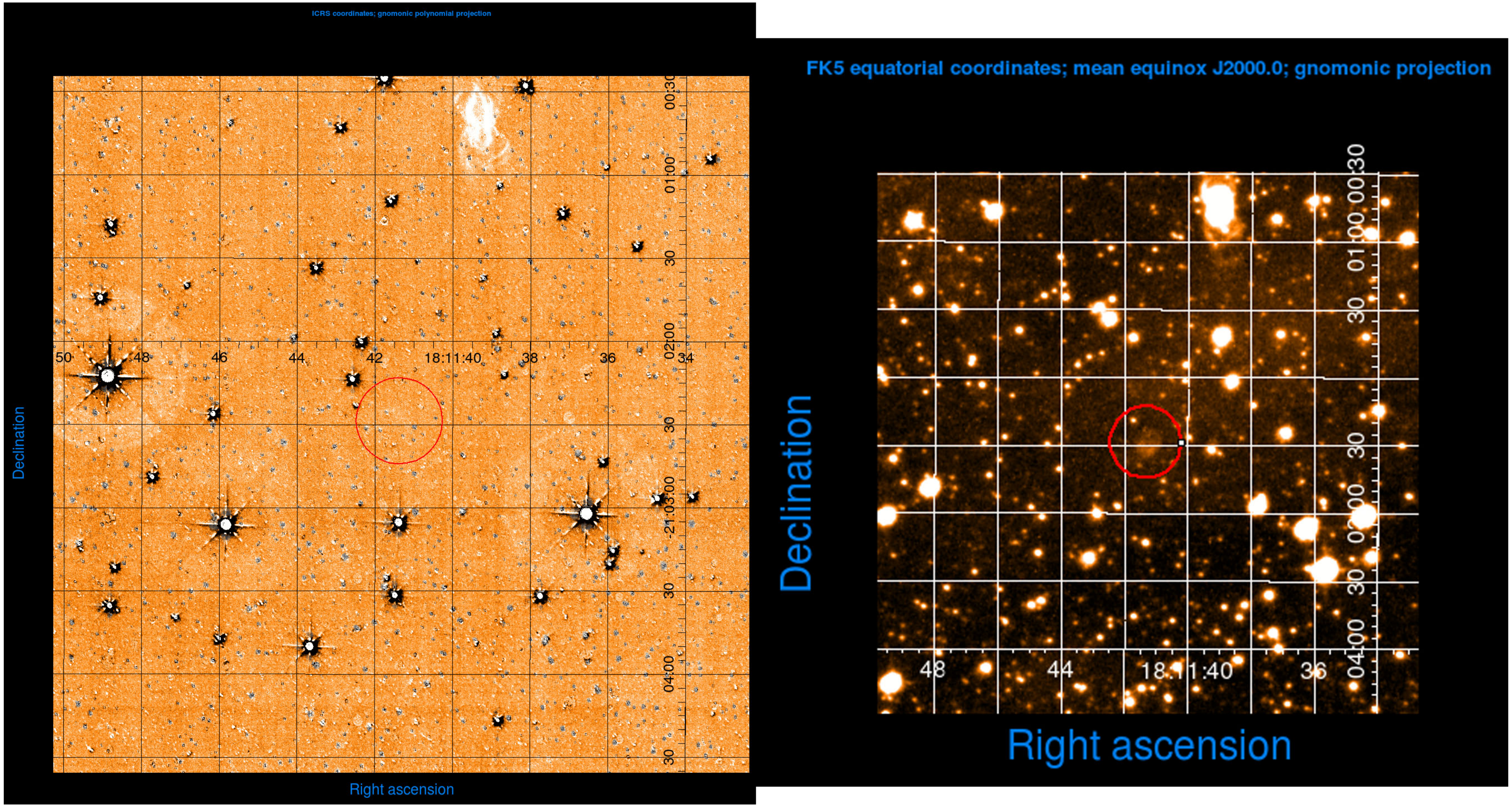

Comparison of PNG009.7-01.1, H_2 on the left, Hα on the right

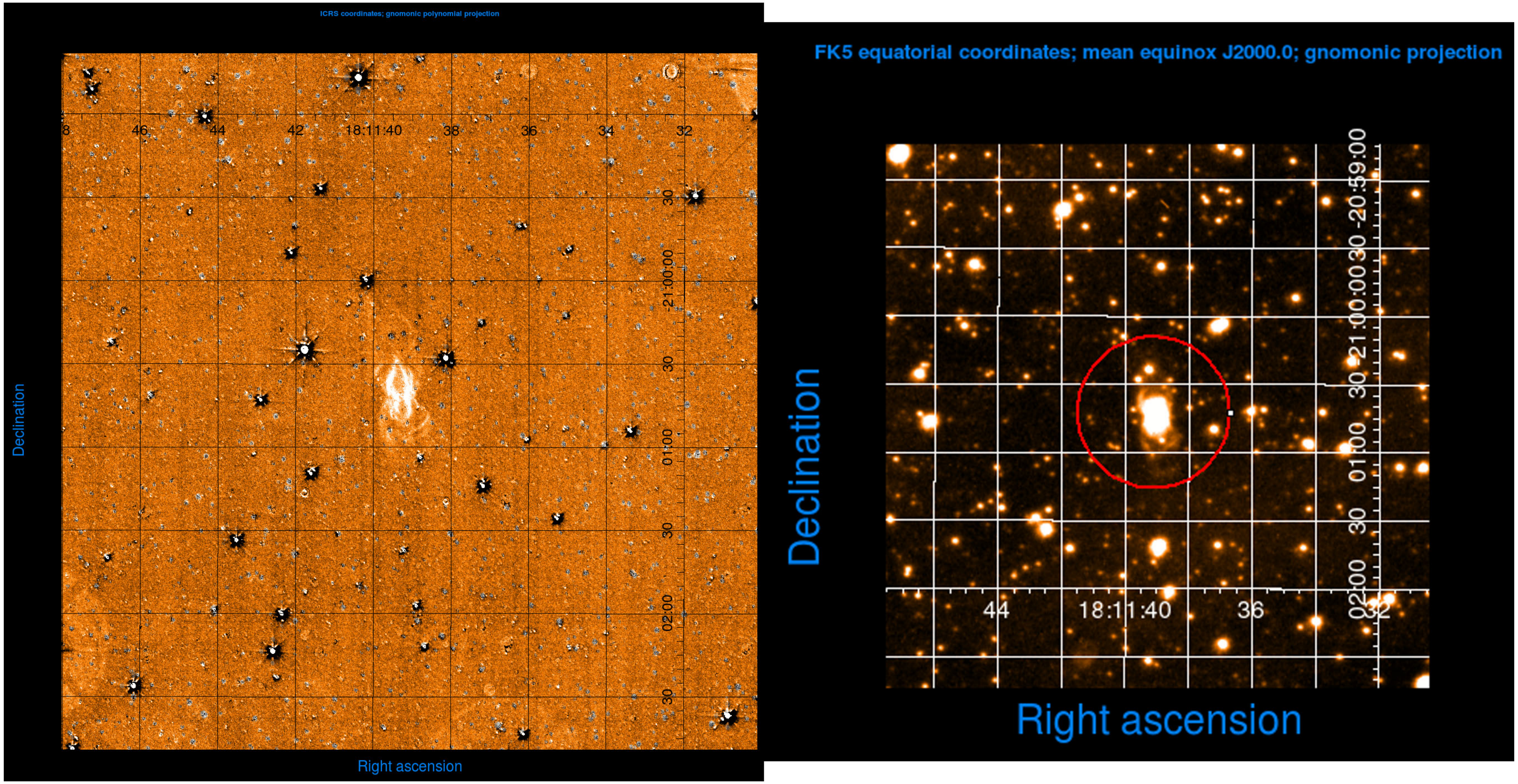

Comparison of PNG009.8-01.1, H_2 on the left, $H\alpha$ on the right

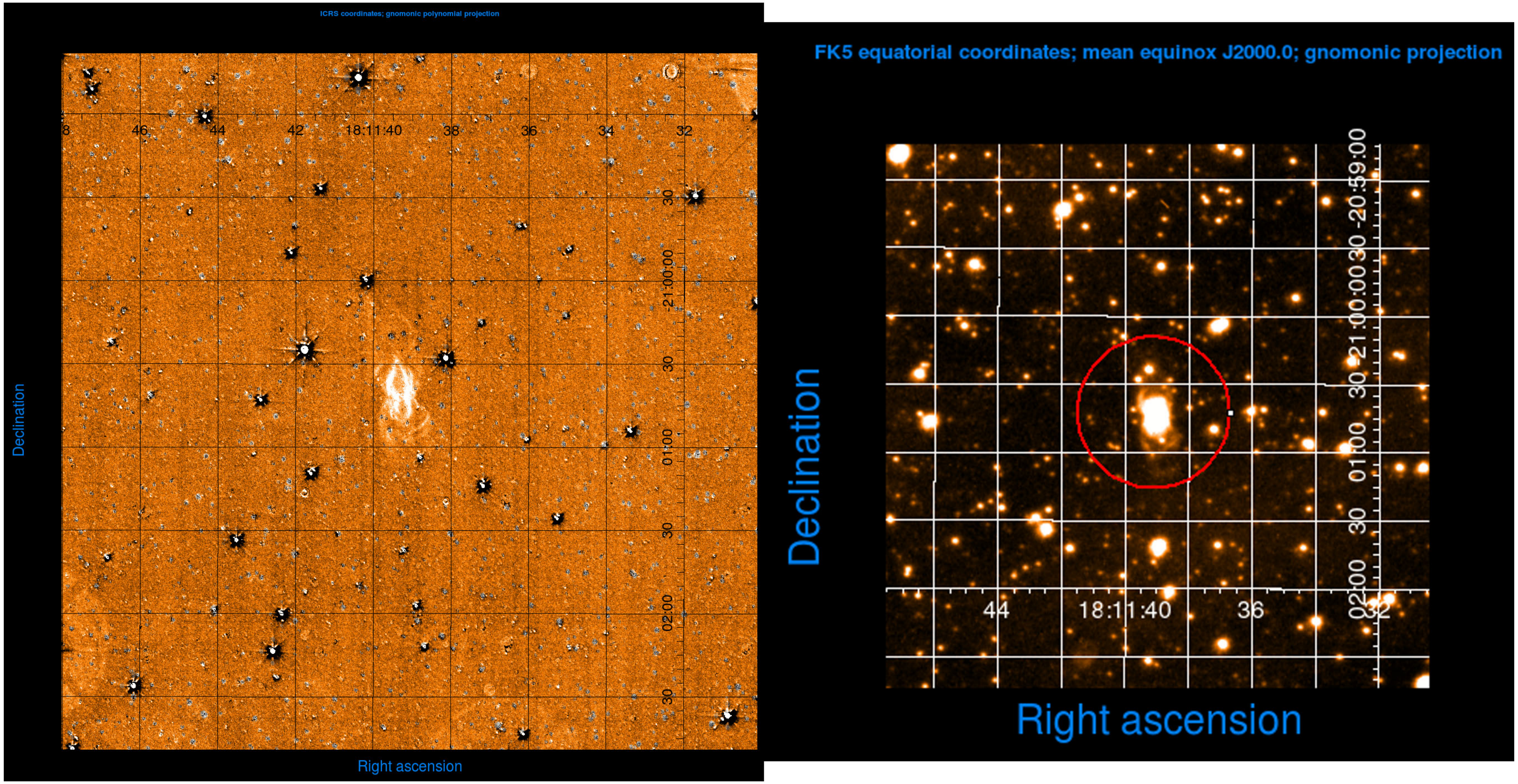

Comparison of PNG009.8-01.1, H_2 on the left, $H\alpha$ on the right

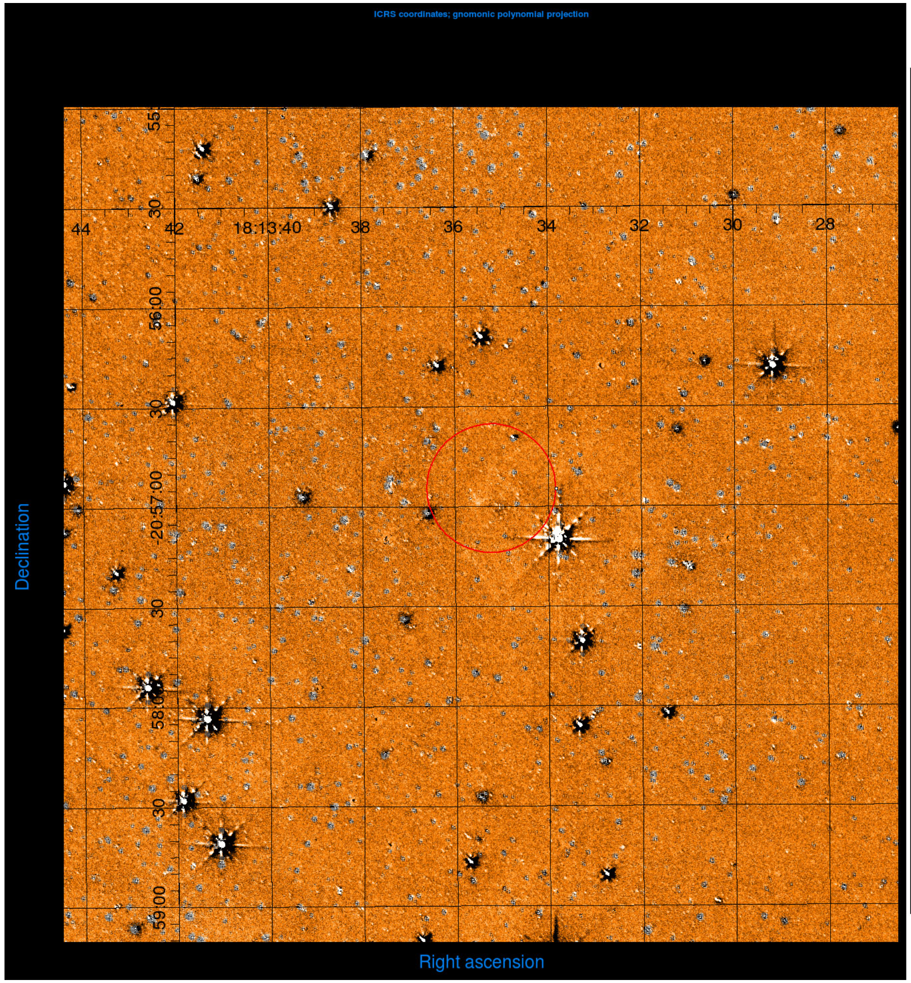

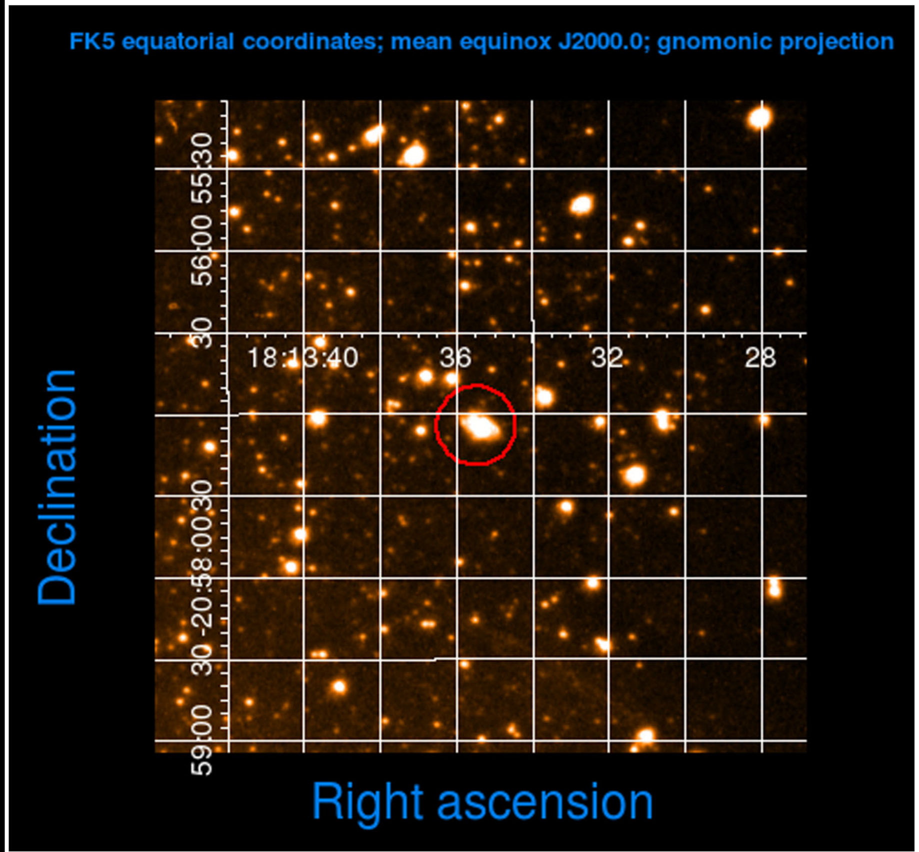

Comparison of PNG010.0-01.5, H_2 on the left, Hα on the right

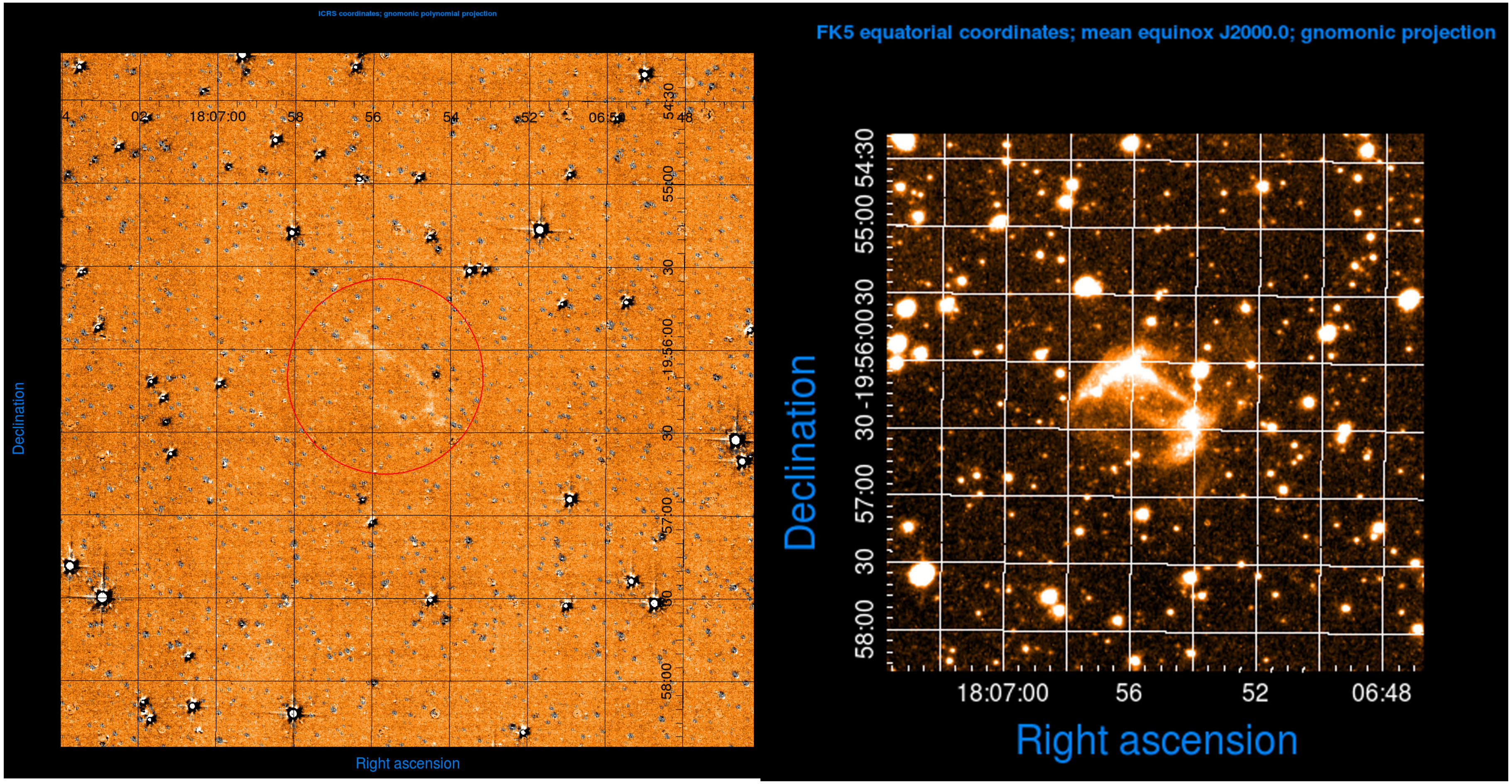

Comparison of PNG010.2+00.3, H_2 on the left, Hα on the right

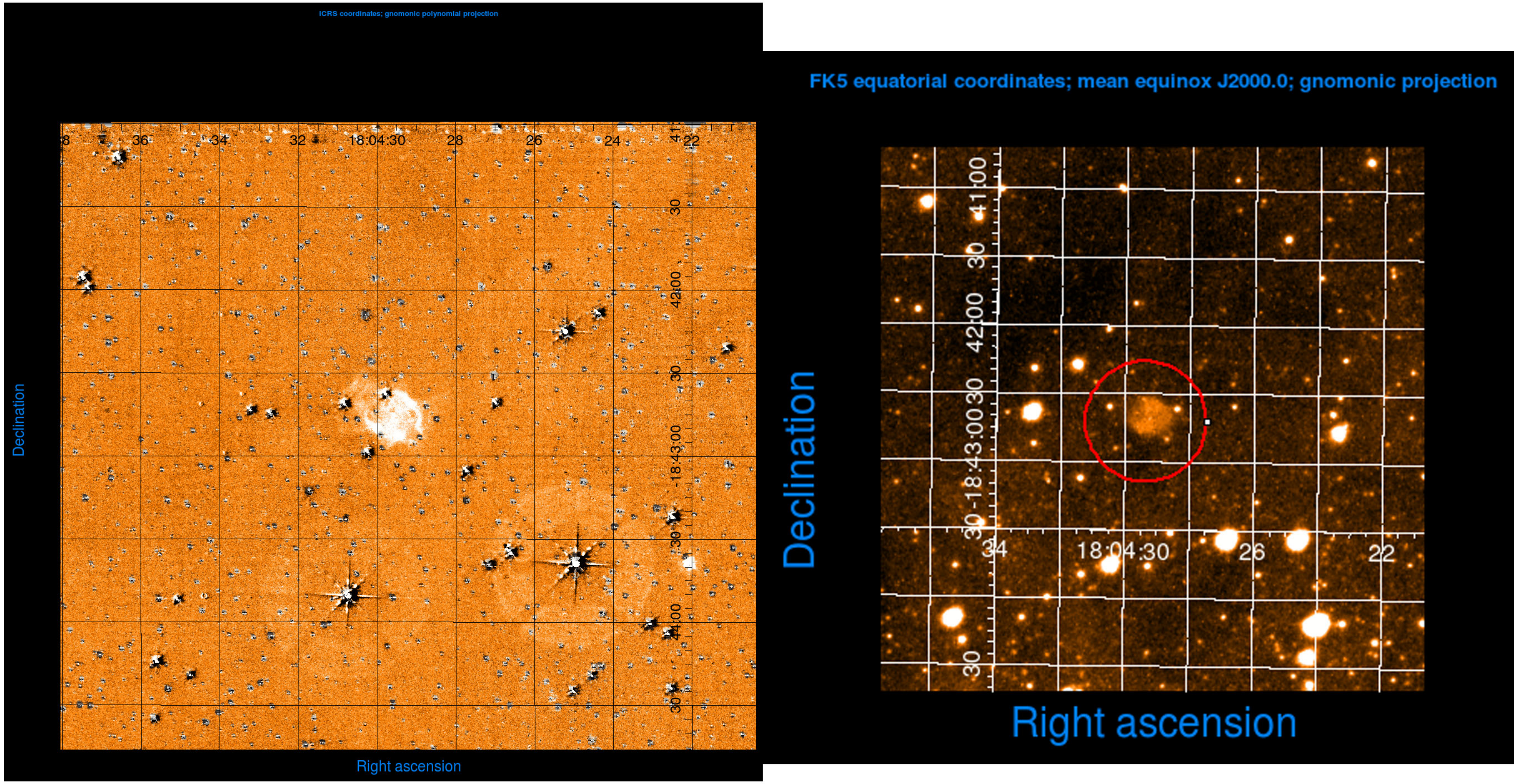

Comparison of PNG011.0+01.4, H_2 on the left, Hα on the right

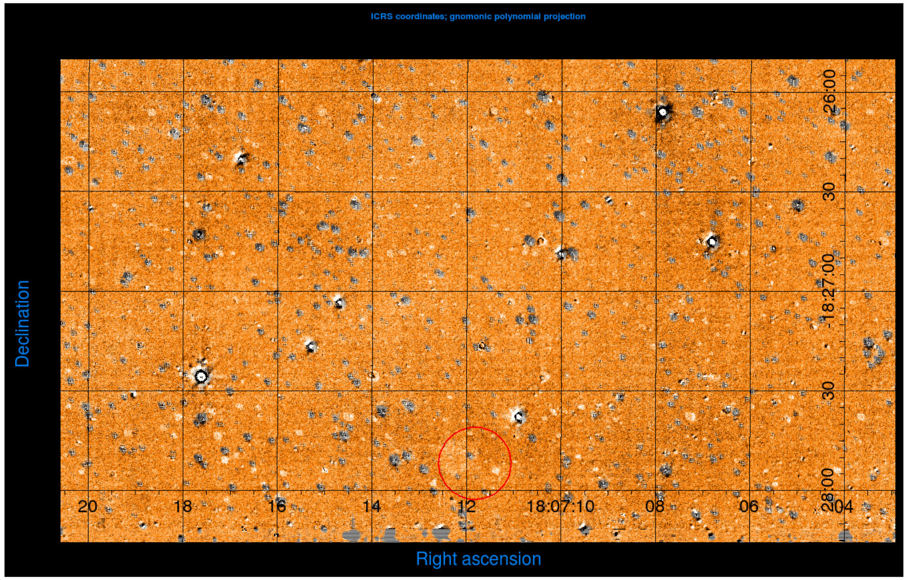

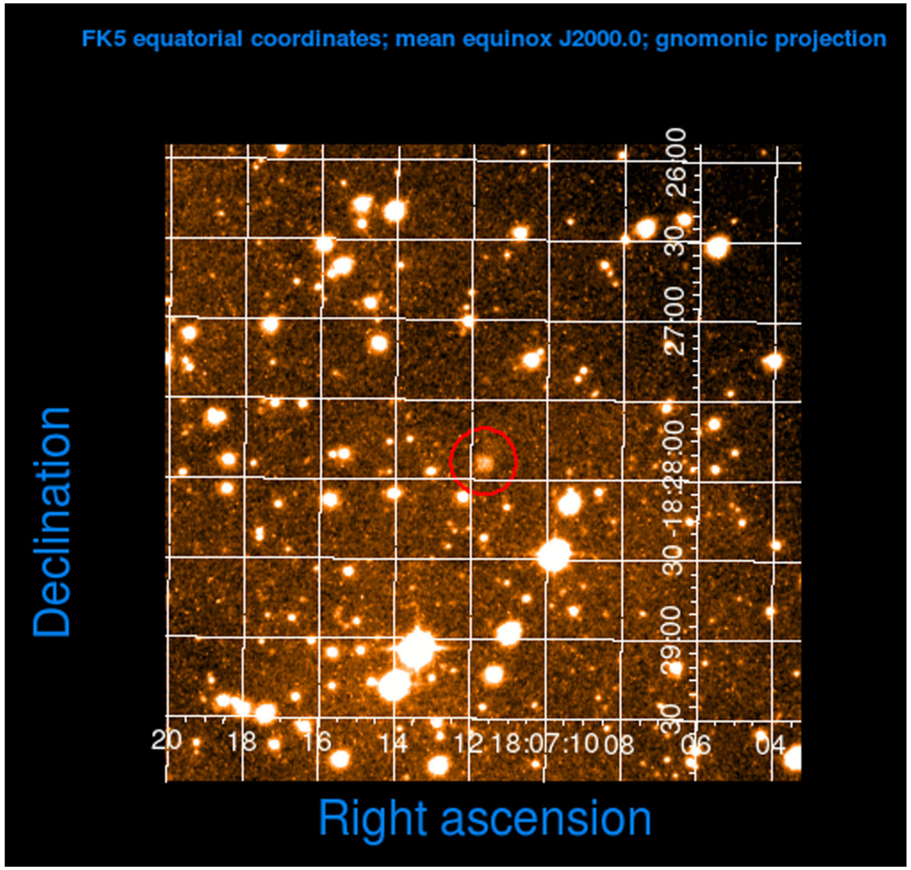

Comparison of PNG011.5+01.0, H_2 on the left, Hα on the right

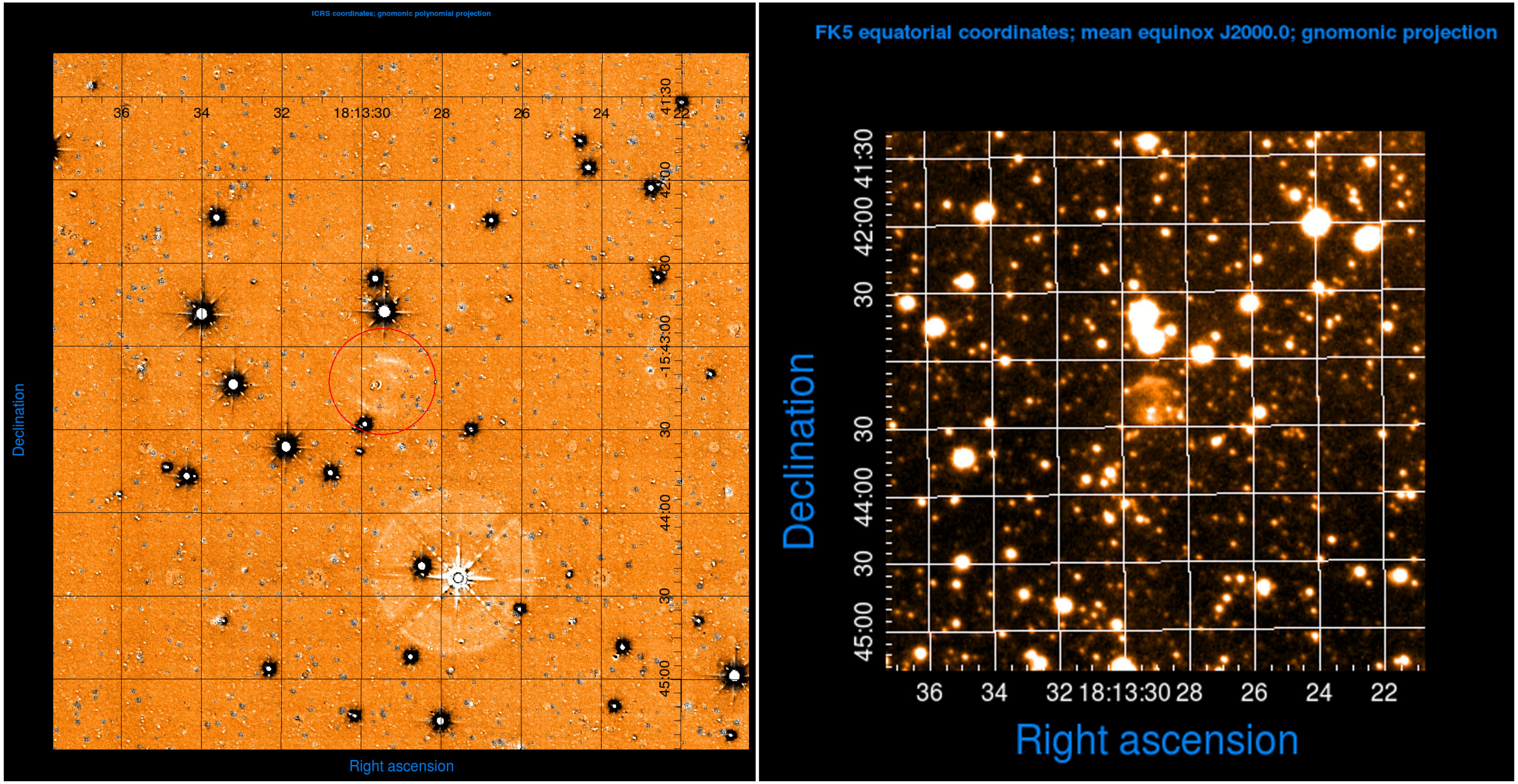

Comparison of PNG014.6+01.0, H_2 on the left, Hα on the right

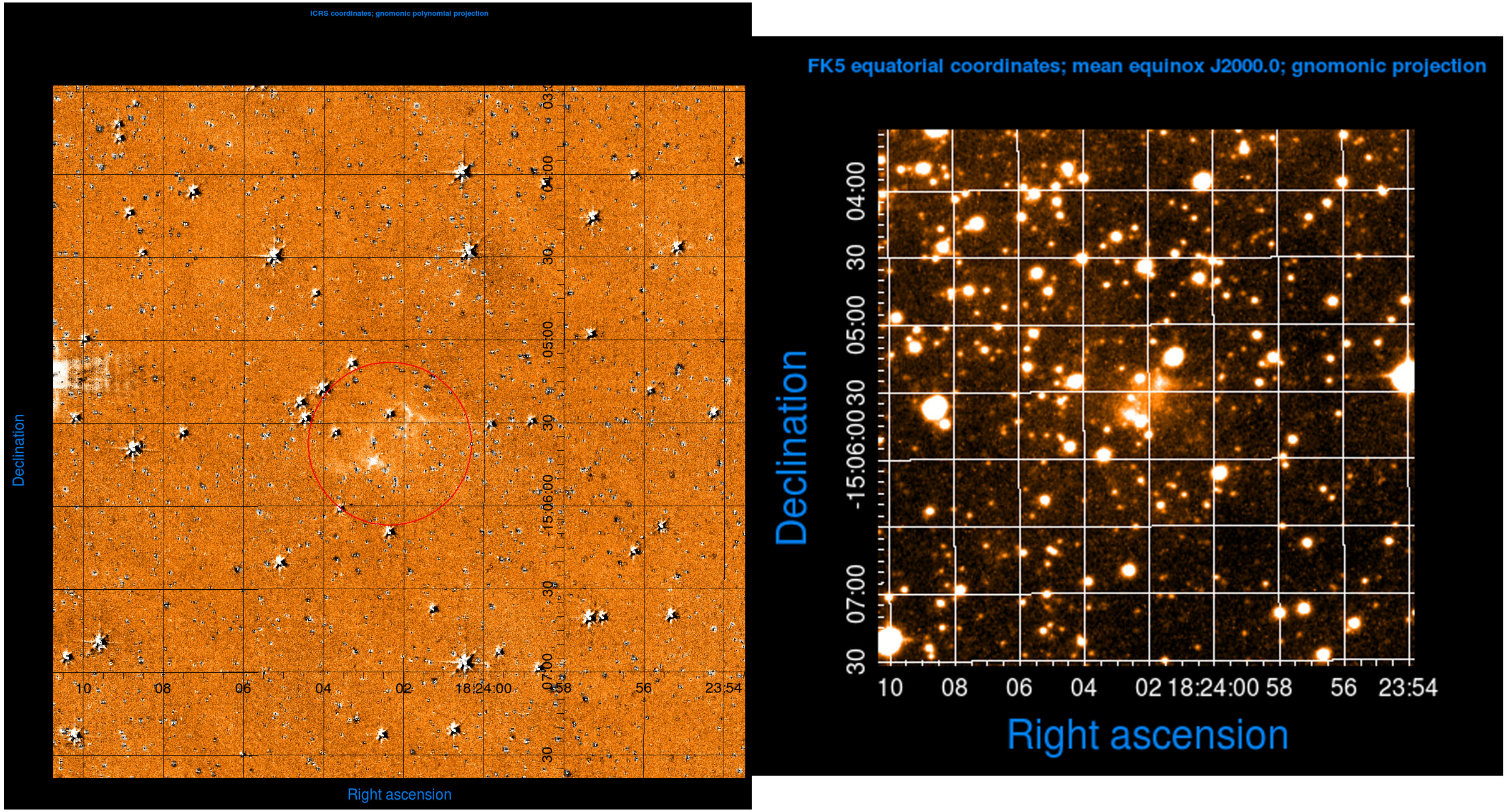

Comparison of PNG016.4-00.9, H_2 on the left, $H\alpha$ on the right

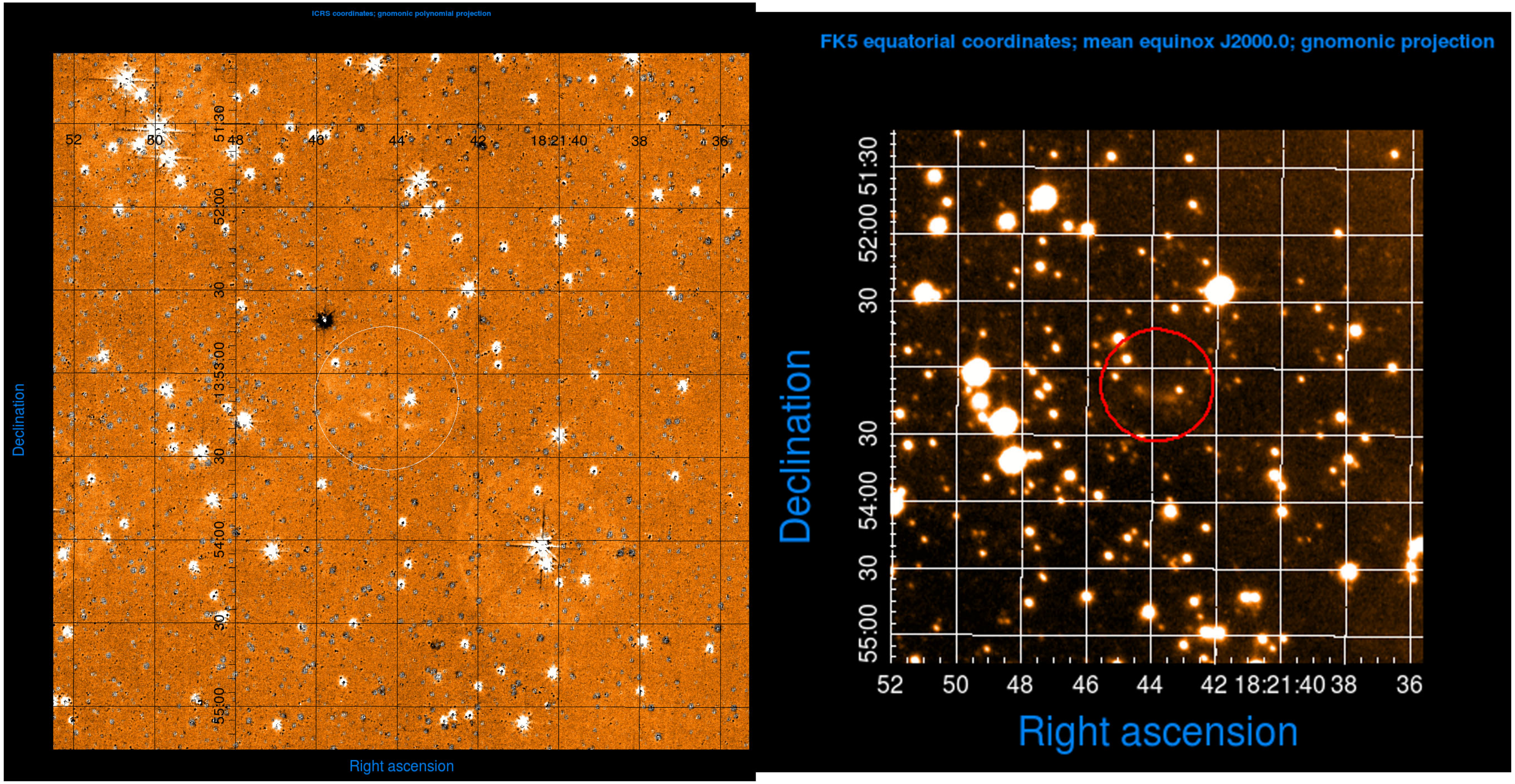

Comparison of PNG017.2+01.1, H_2 on the left, Hα on the right

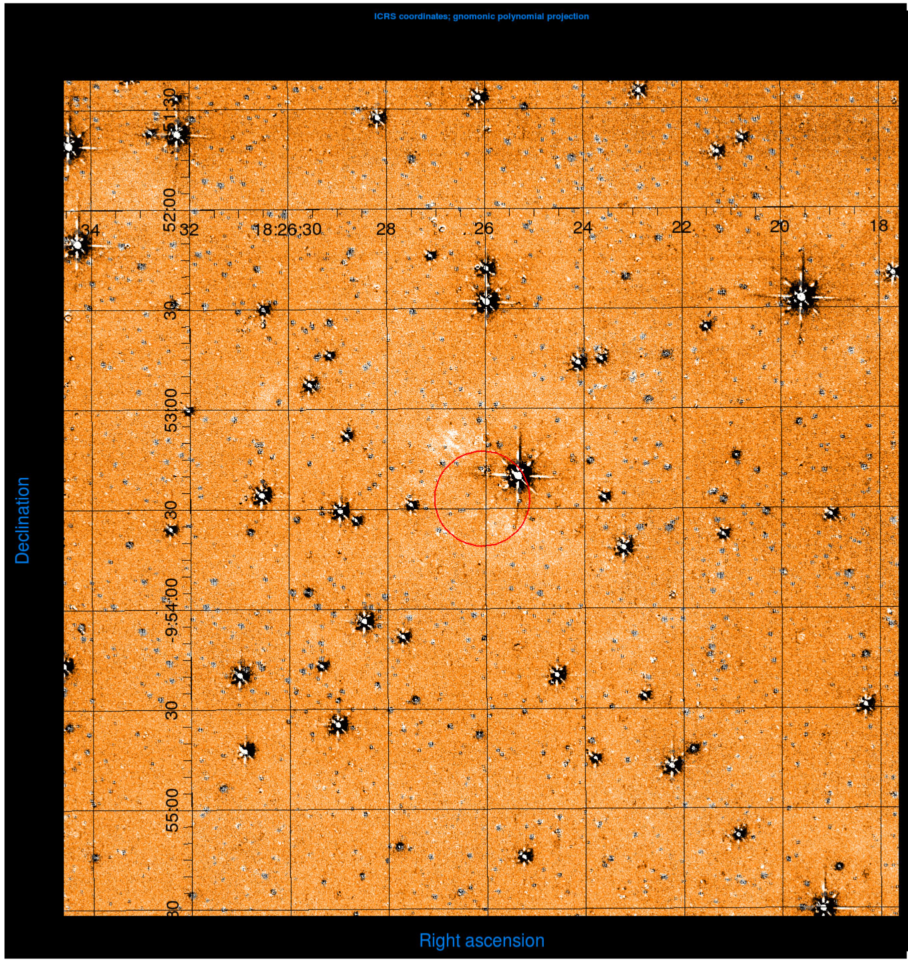

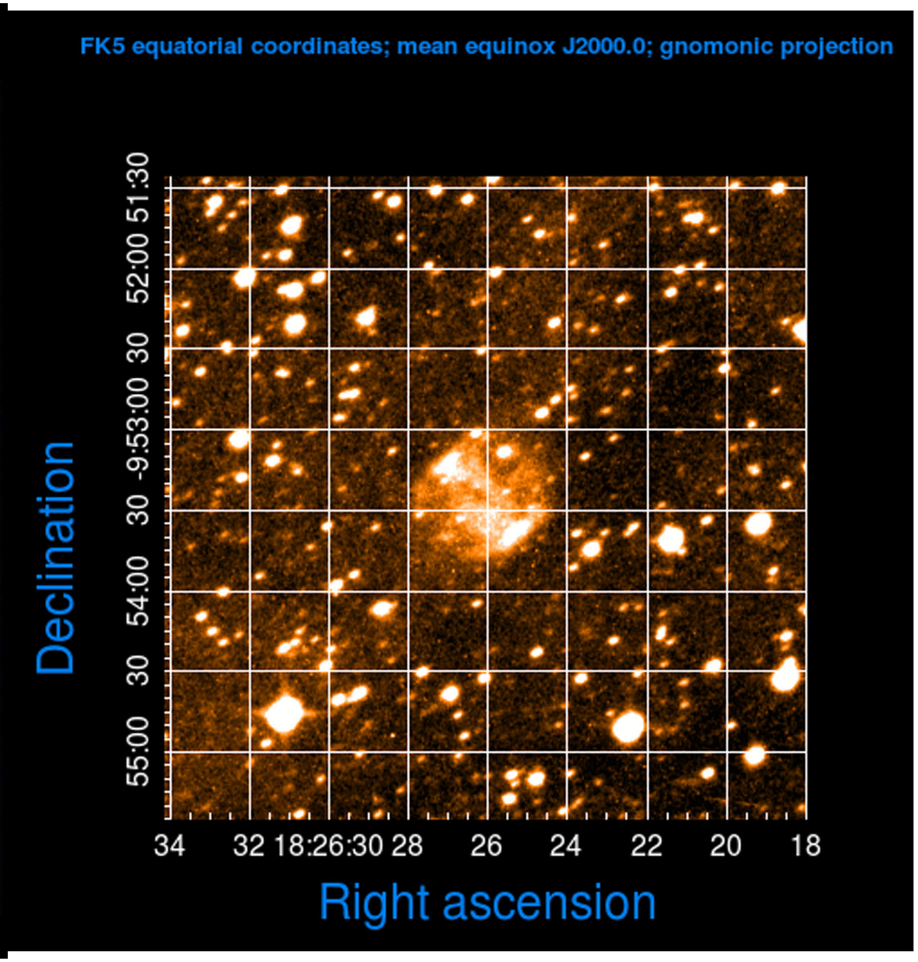

Comparison of PNG021.2+00.9, H_2 on the left, Hα on the right

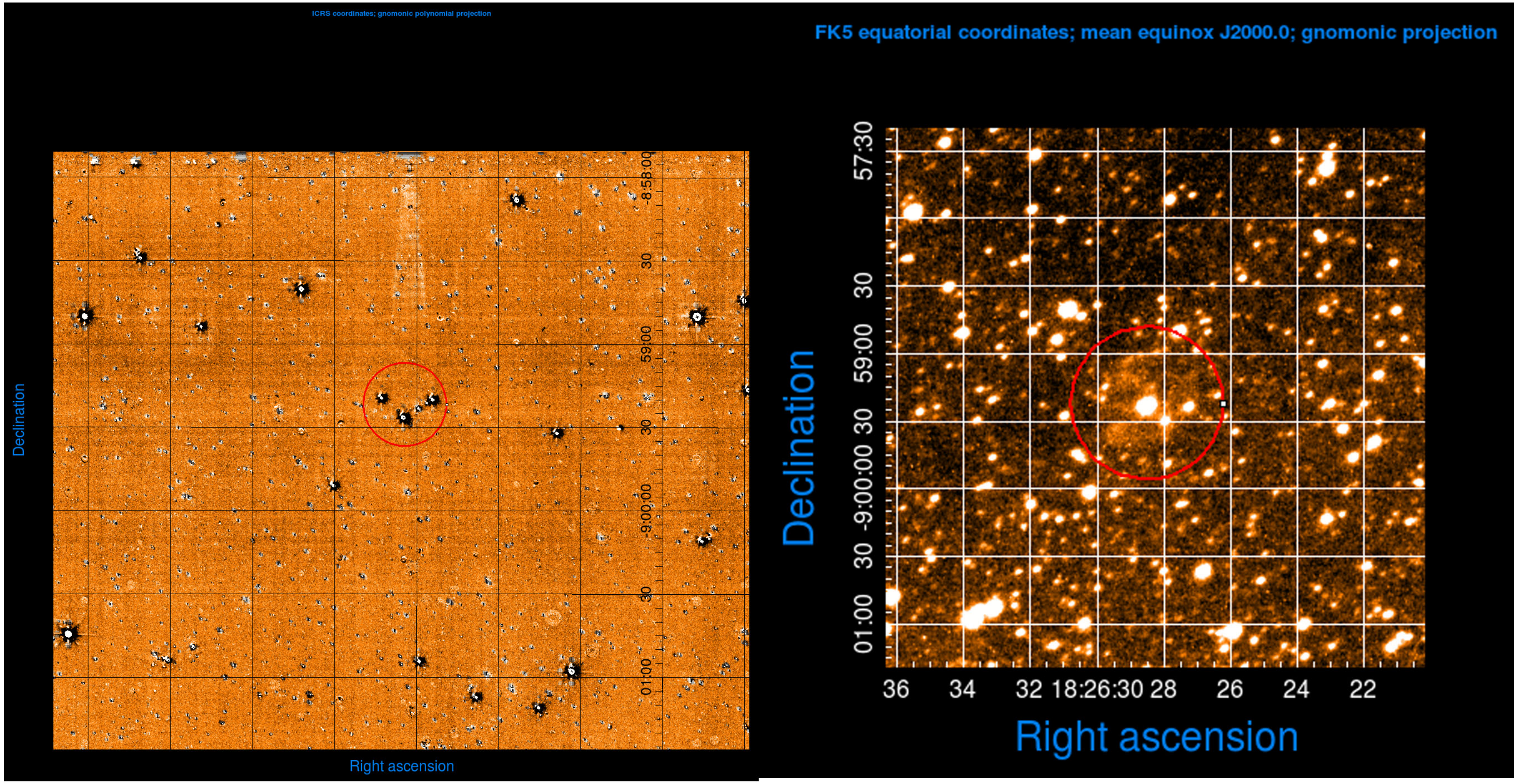

Comparison of PNG022.0+01.3, H_2 on the left, Hα on the right

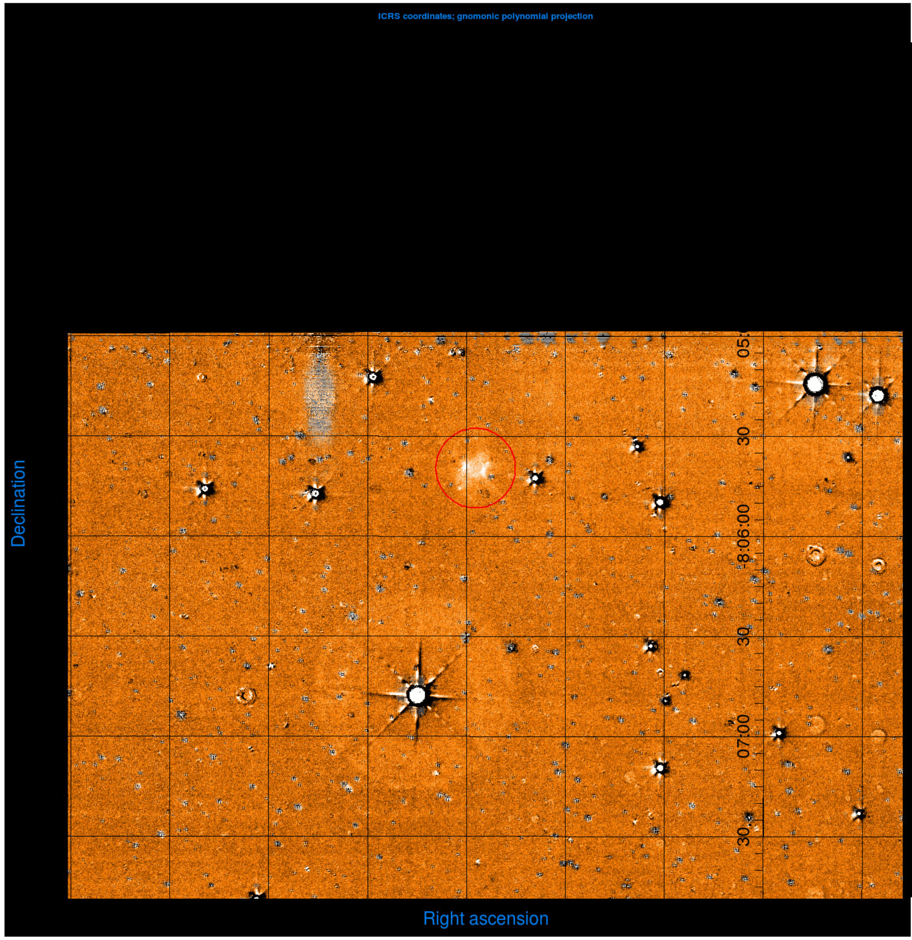

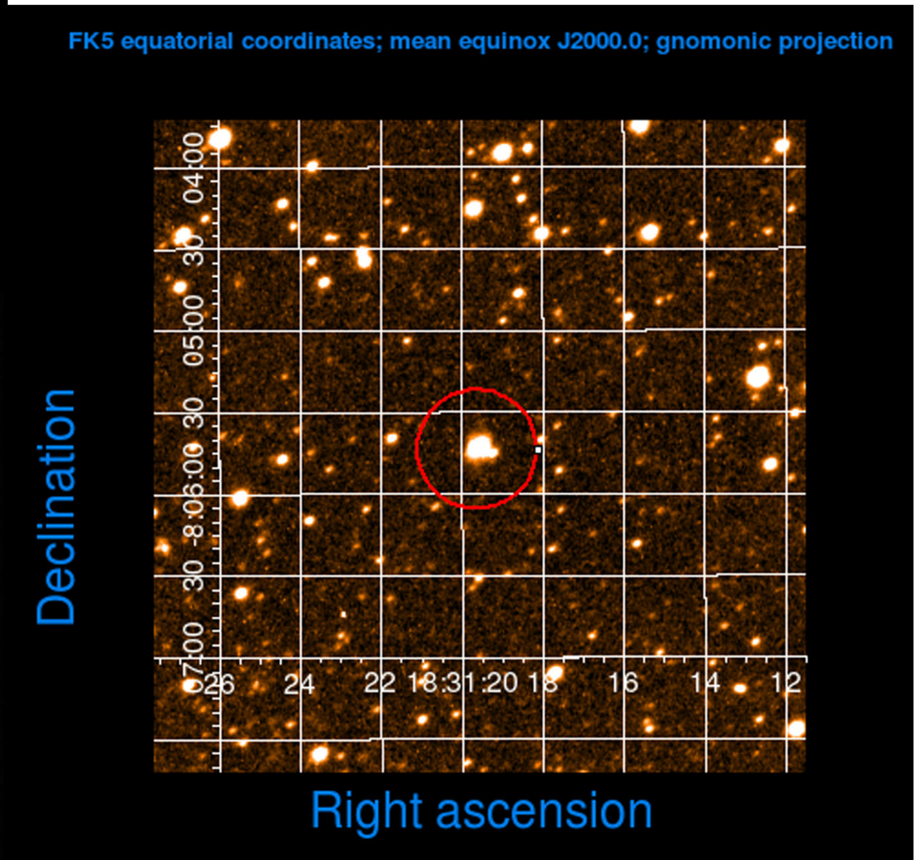

Comparison of PNG023.4+00.7, H_2 on the left, Hα on the right

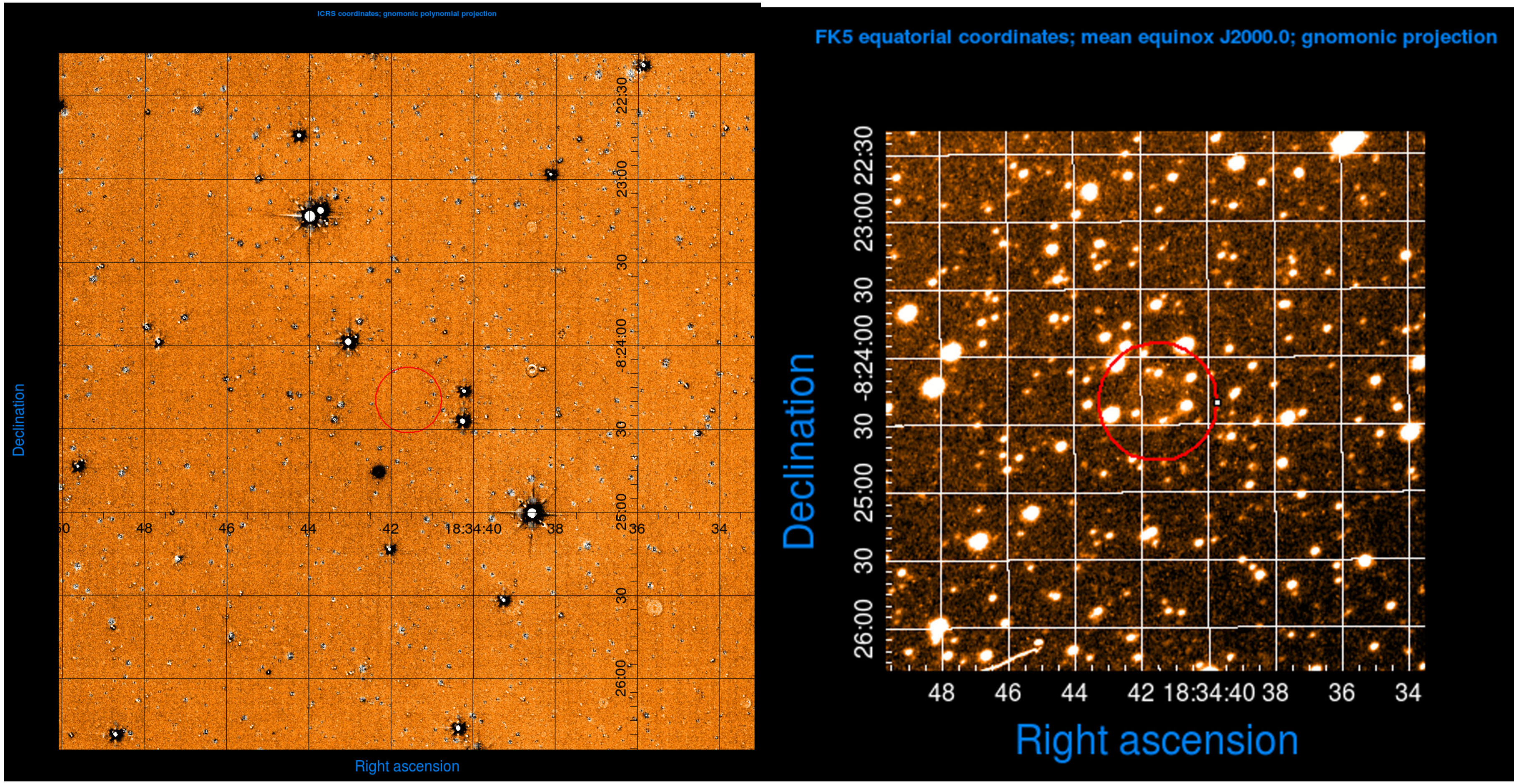

Comparison of PNG023.5-00.1, H_2 on the left, Hα on the right

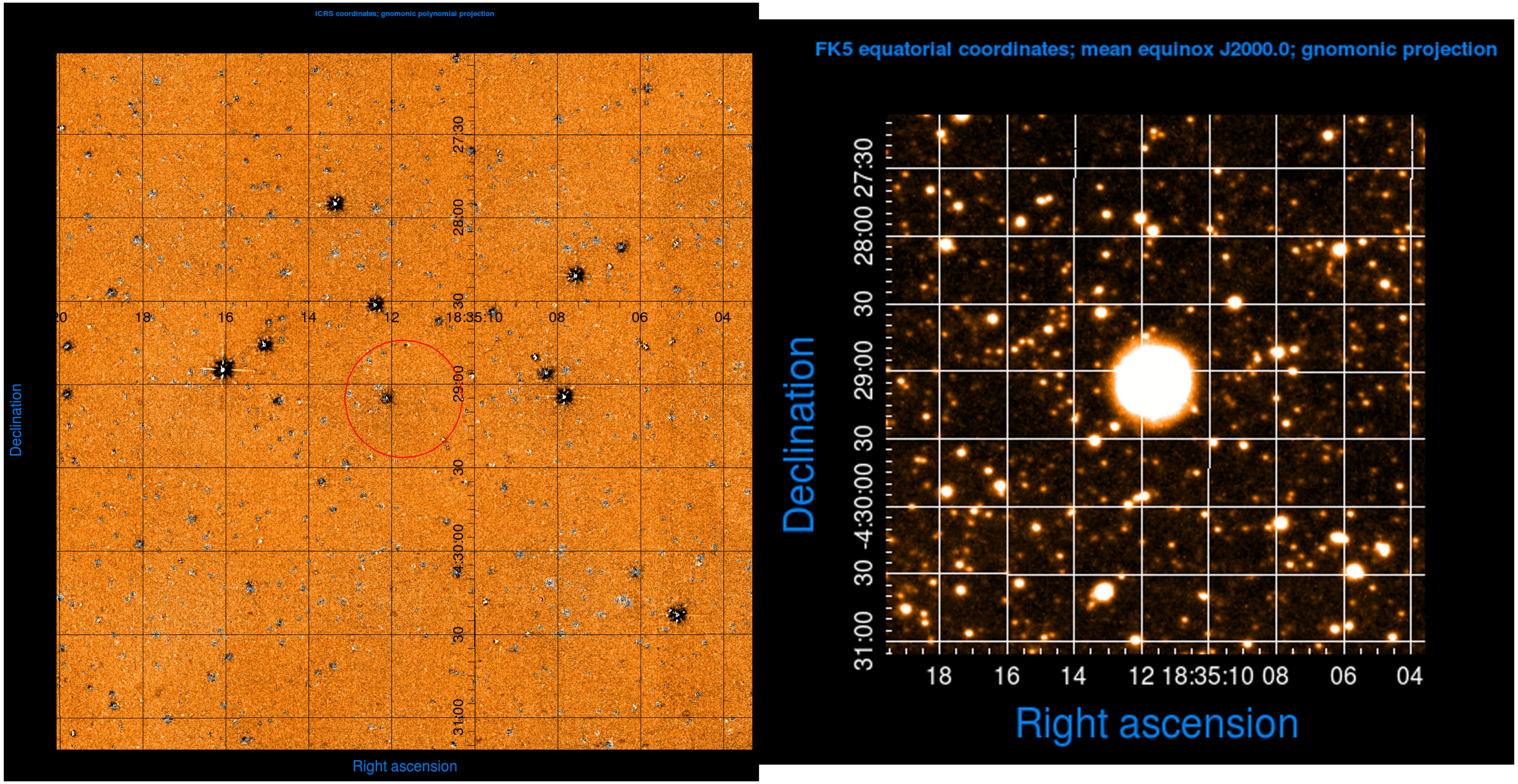

Comparison of PNG027.0+01.5, H_2 on the left, $H\alpha$ on the right

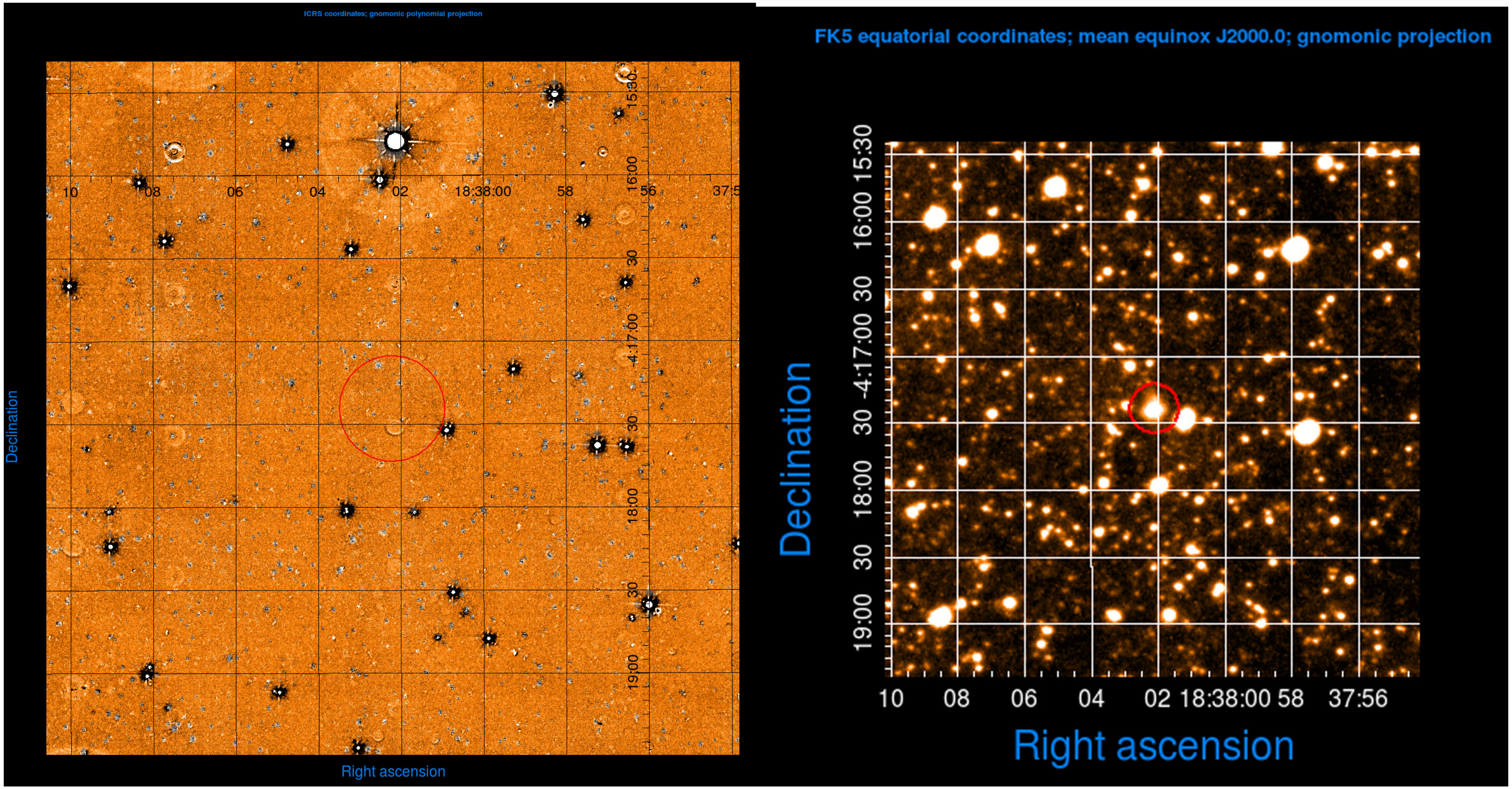

Comparison of PNG027.5+01.0, H_2 on the left, Hα on the right

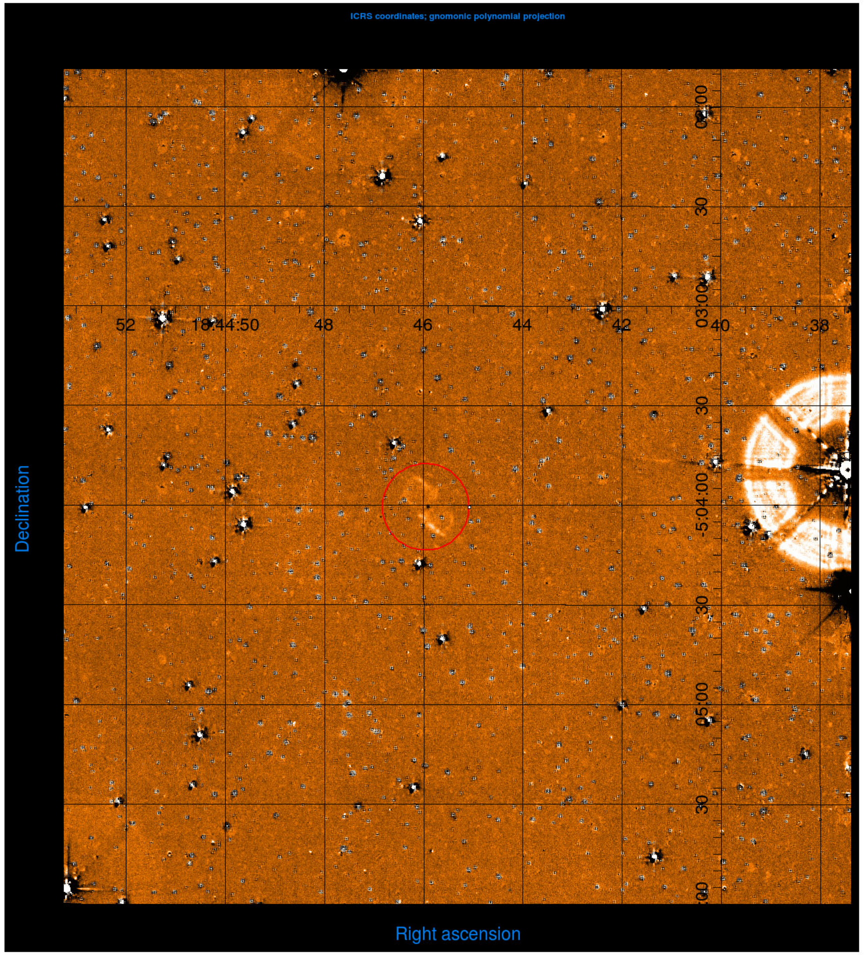

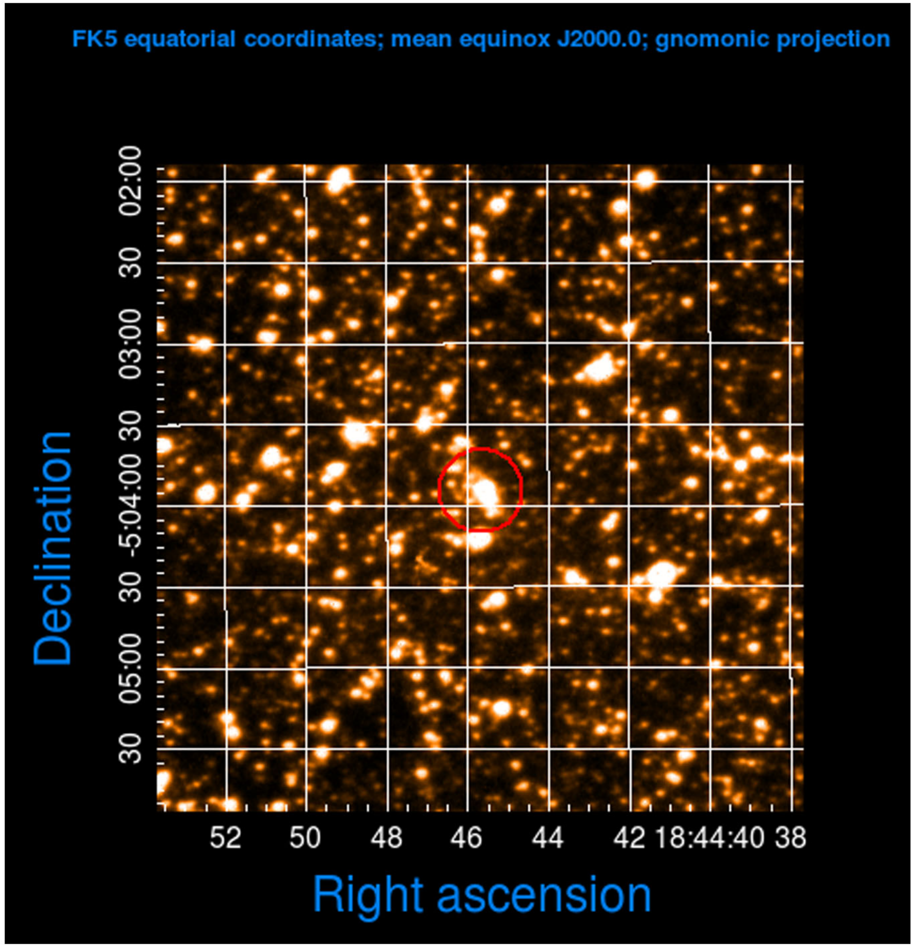

Comparison of PNG027.6-00.8, H_2 on the left, Hα on the right

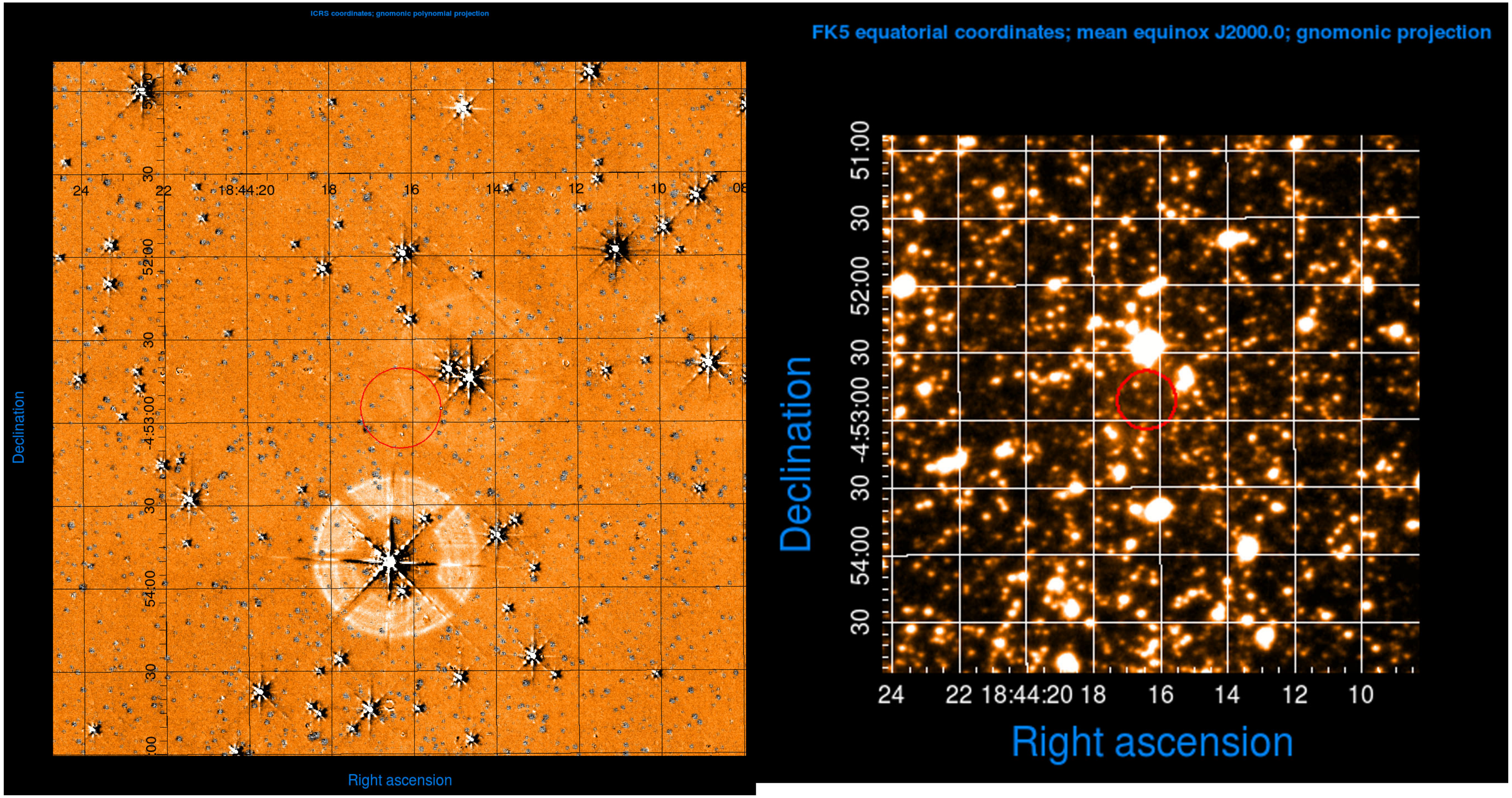

Comparison of PNG027.7-00.6, H_2 on the left, Hα on the right

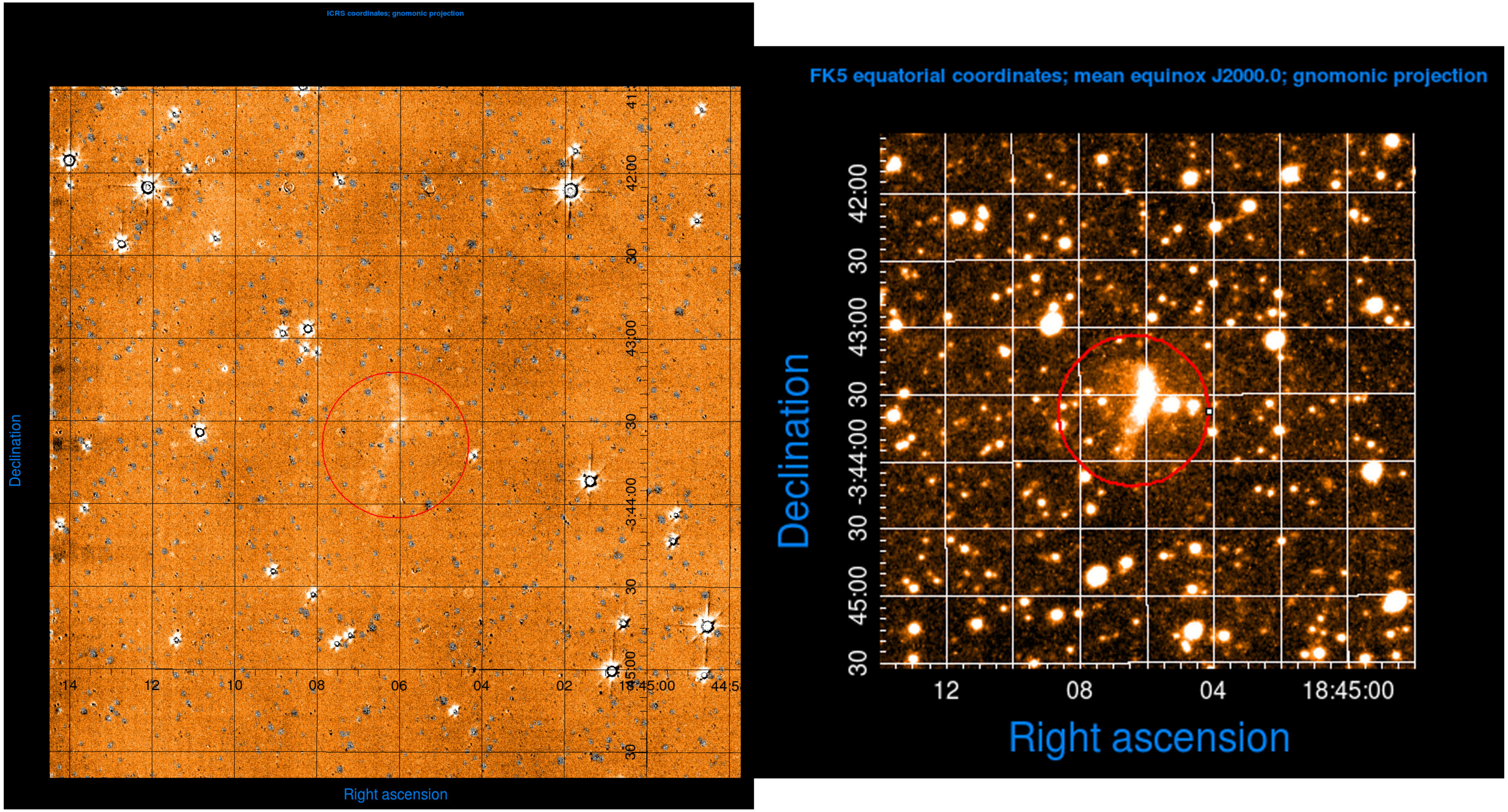

Comparison of PNG028.8-00.2, H_2 on the left, Hα on the right

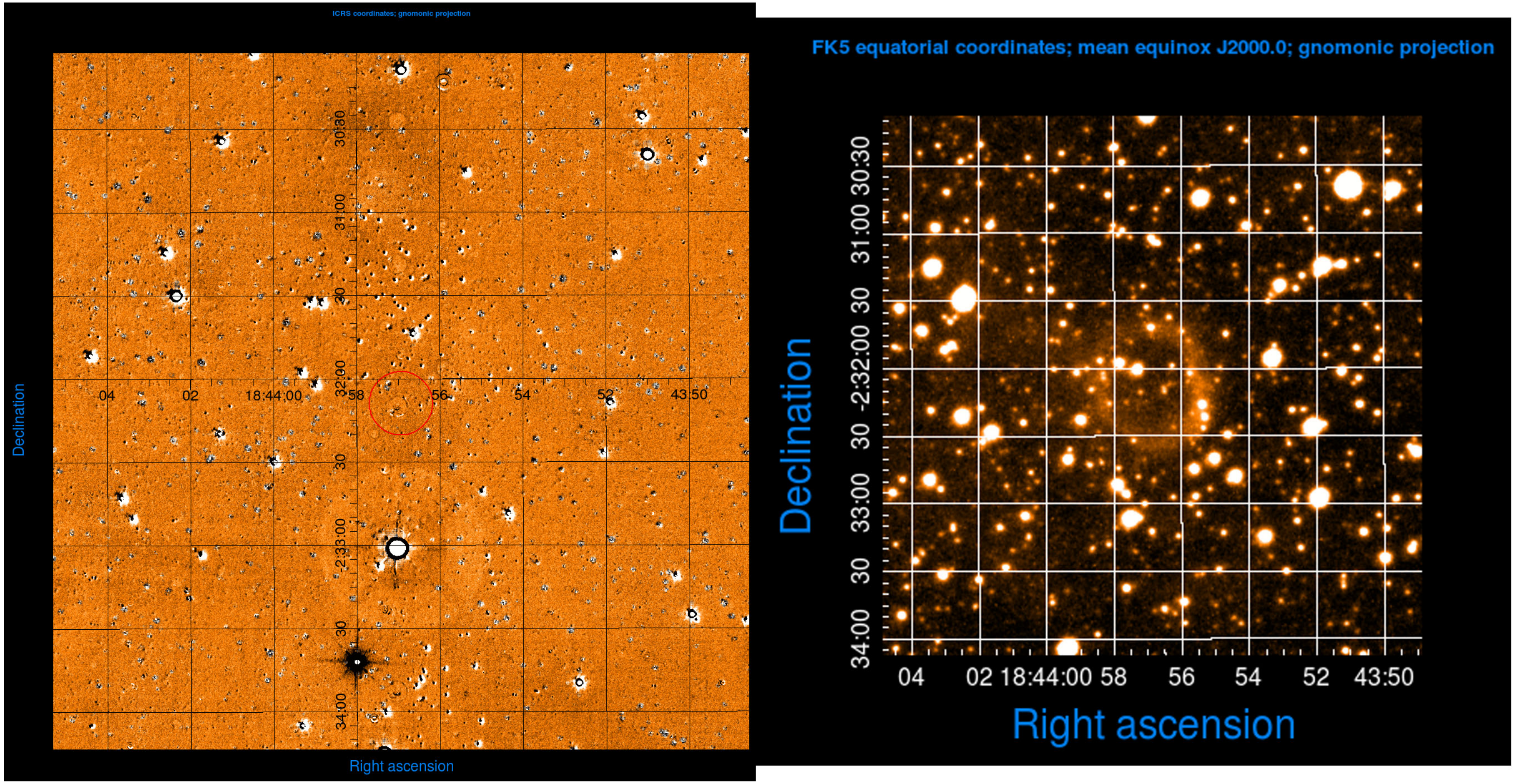

Comparison of PNG029.8+00.5, H_2 on the left, Hα on the right

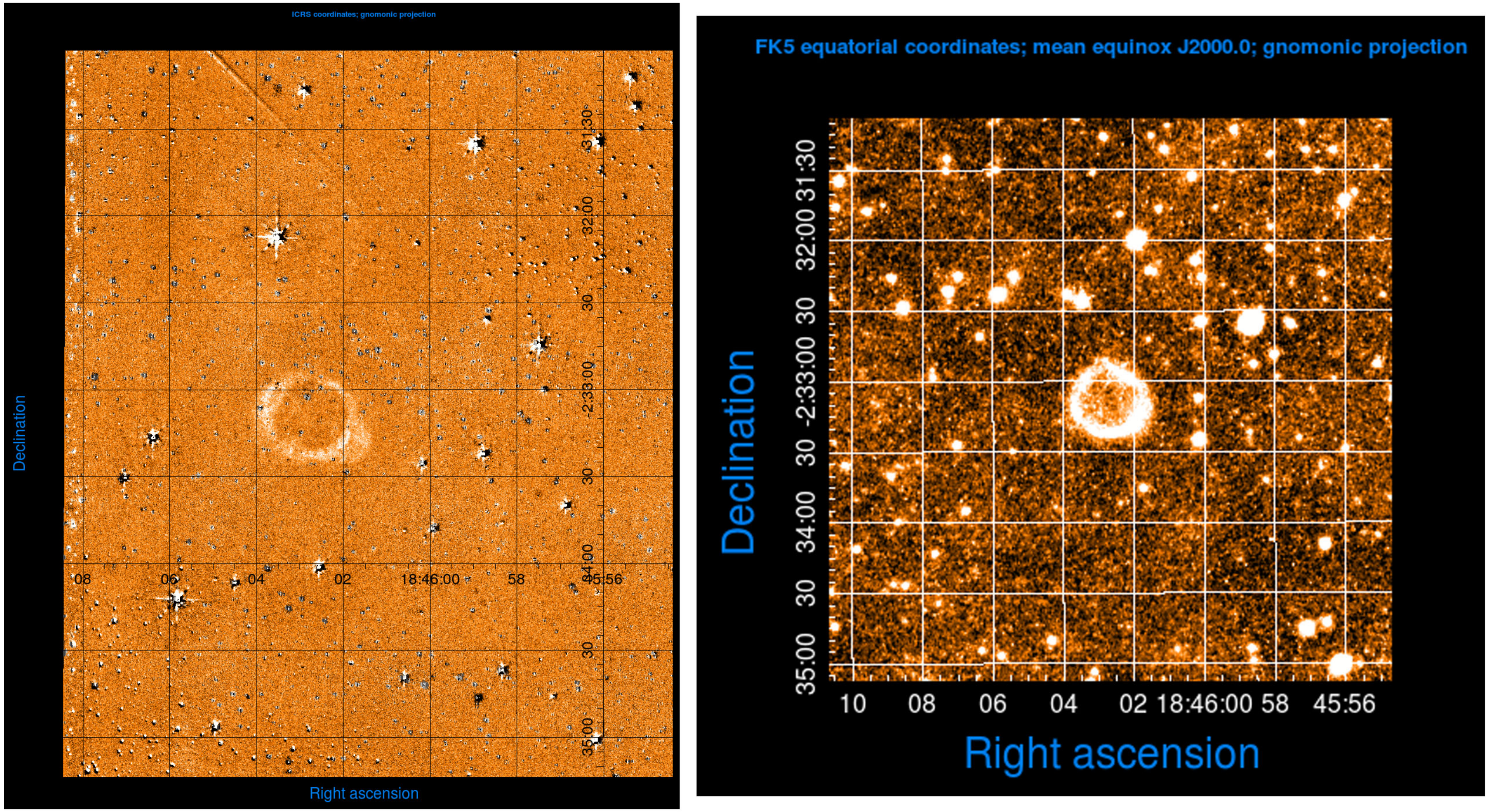

Comparison of PNG030.0+00.0, H_2 on the left, $H\alpha$ on the right

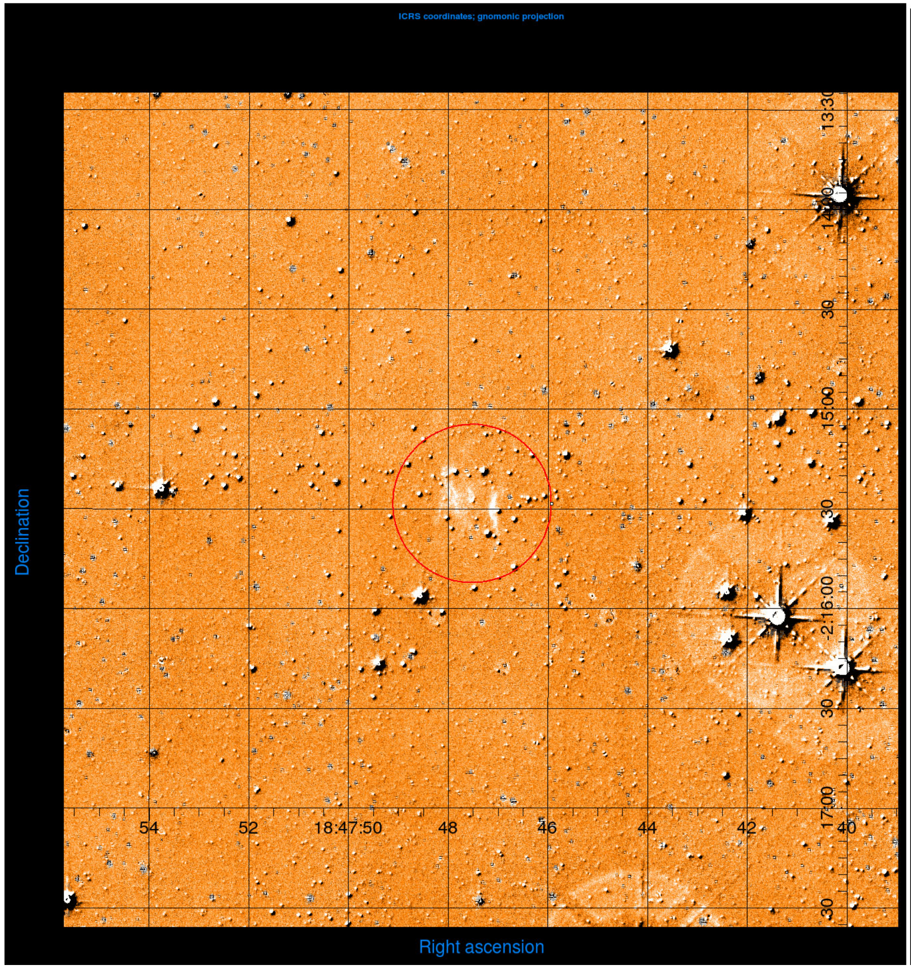

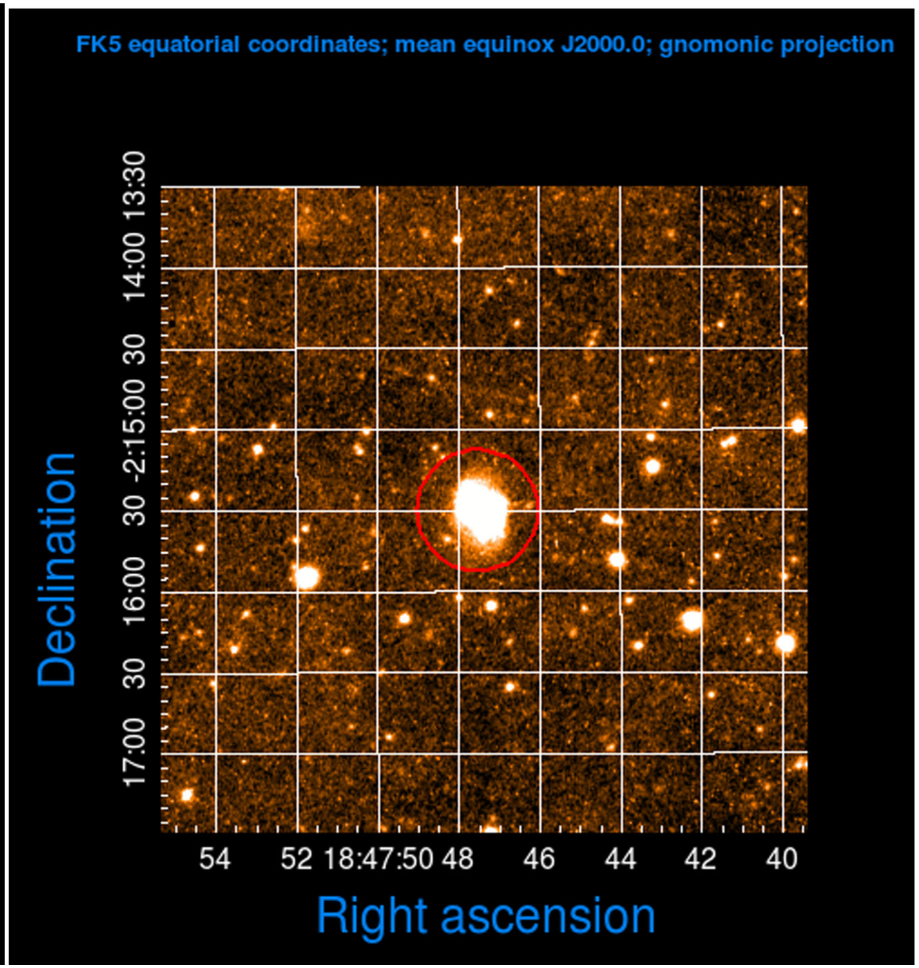

Comparison of PNG030.5-00.2, H_2 on the left, Hα on the right

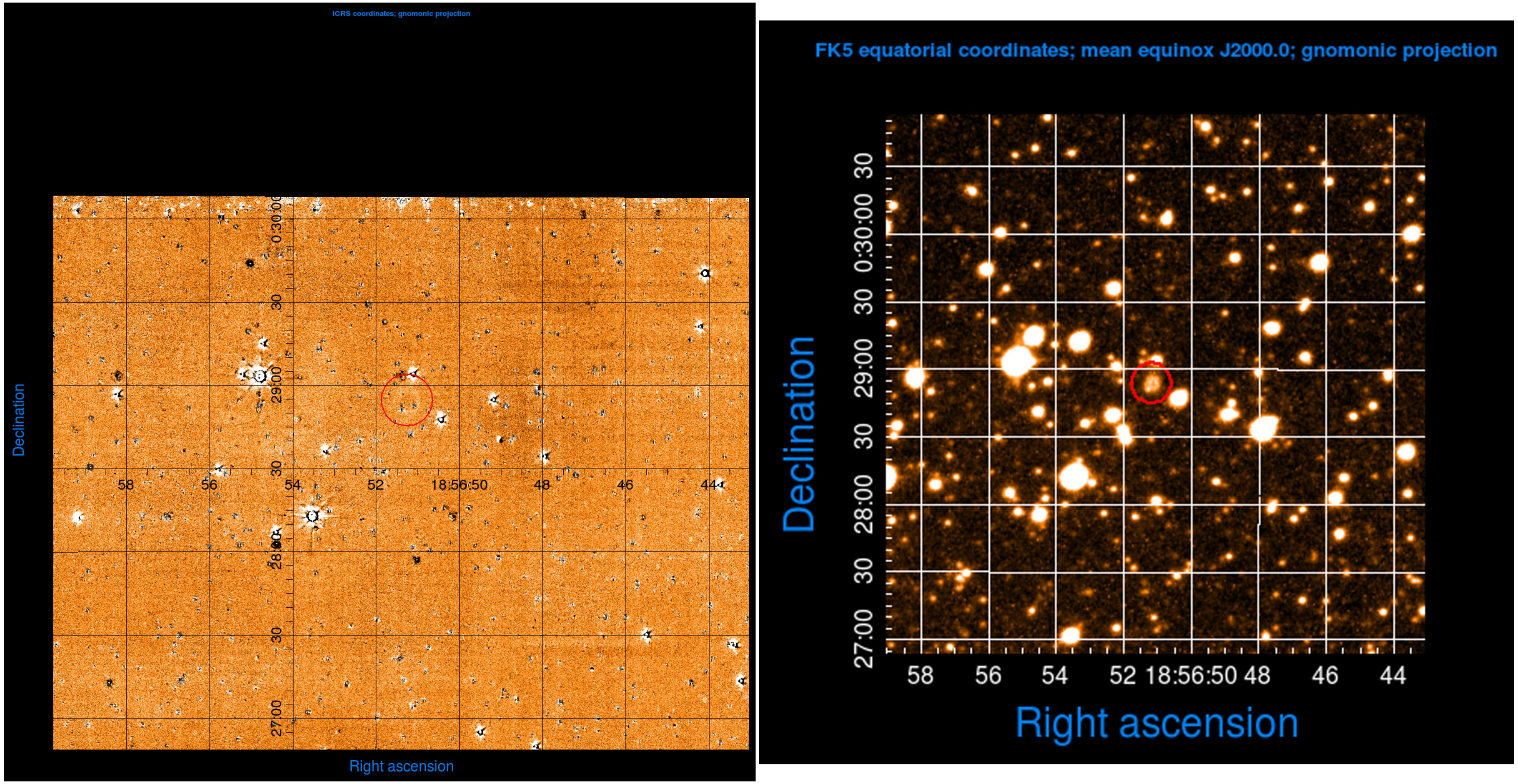

Comparison of PNG033.9-00.9, H_2 on the left, Hα on the right

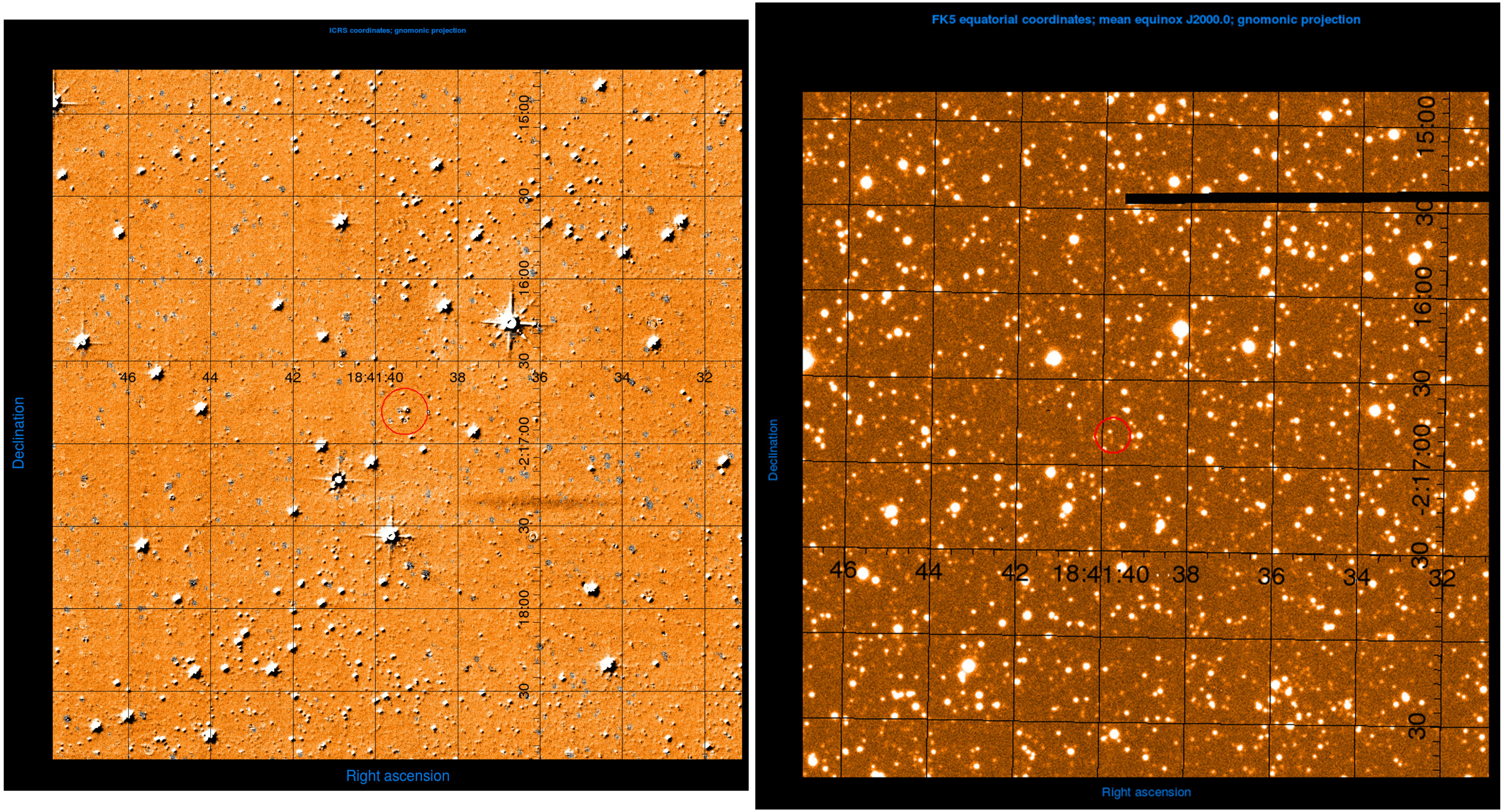

Comparison of IPHAS1, H_2 on the left, $H\alpha$ on the right

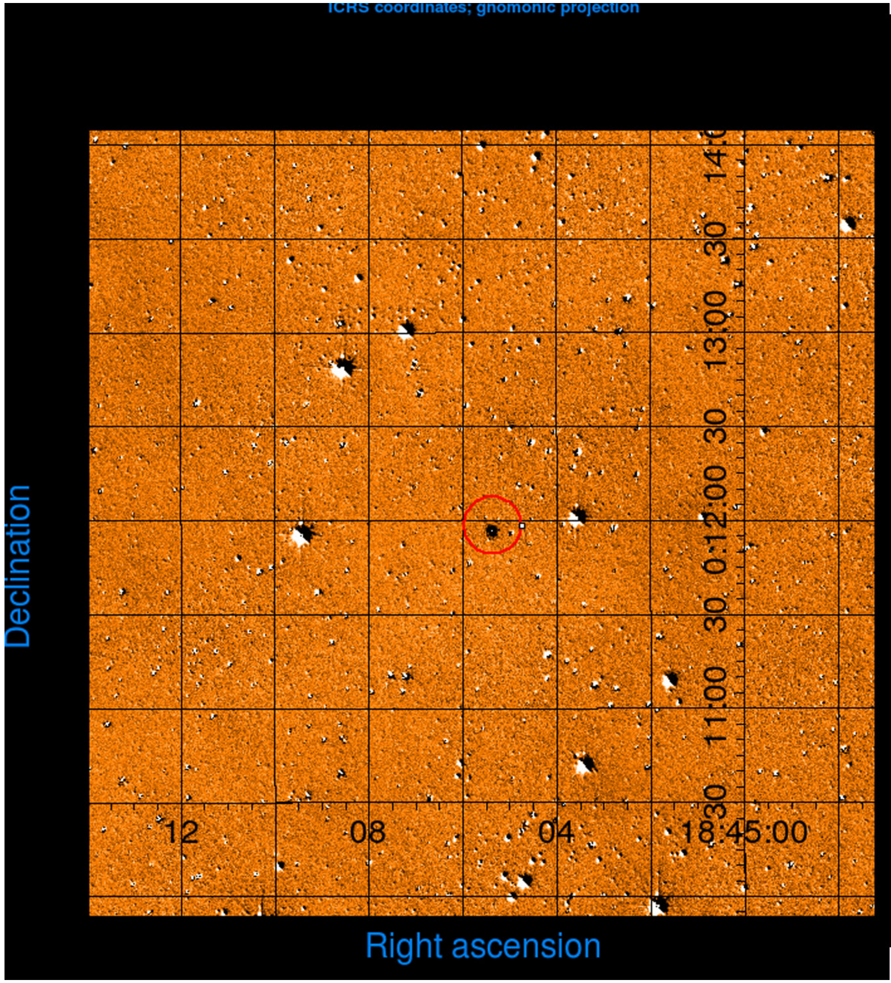

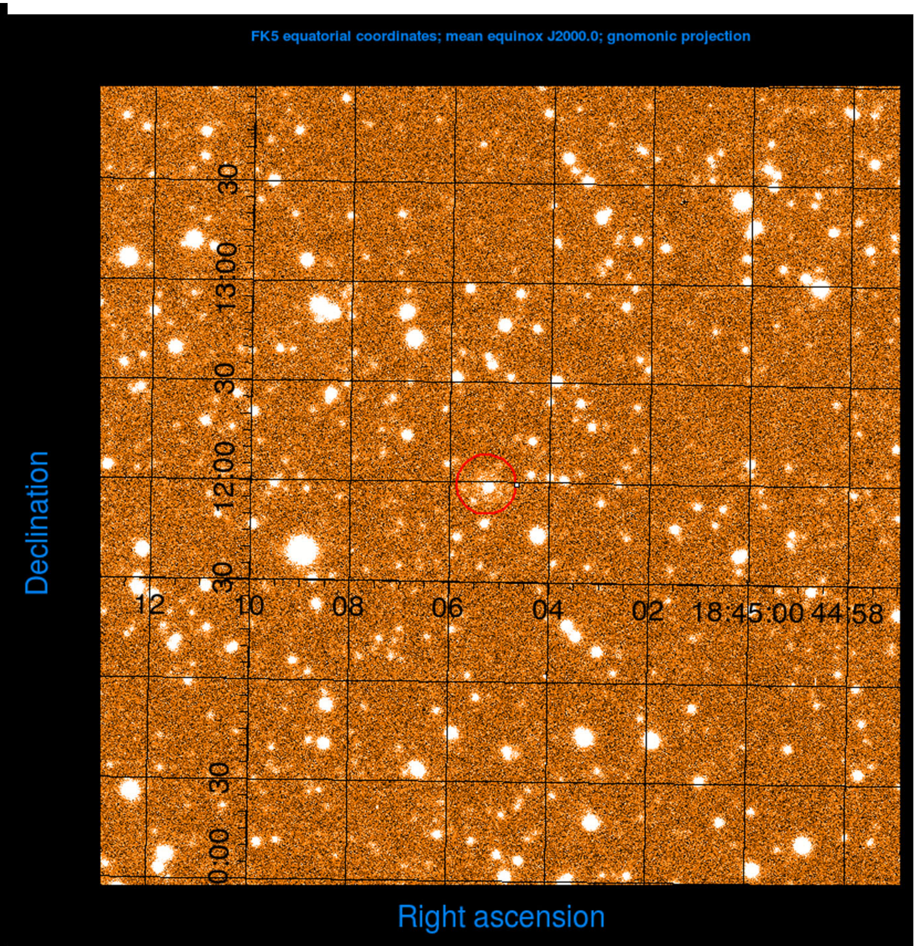

Comparison of IPHAS2, H_2 on the left, Hα on the right

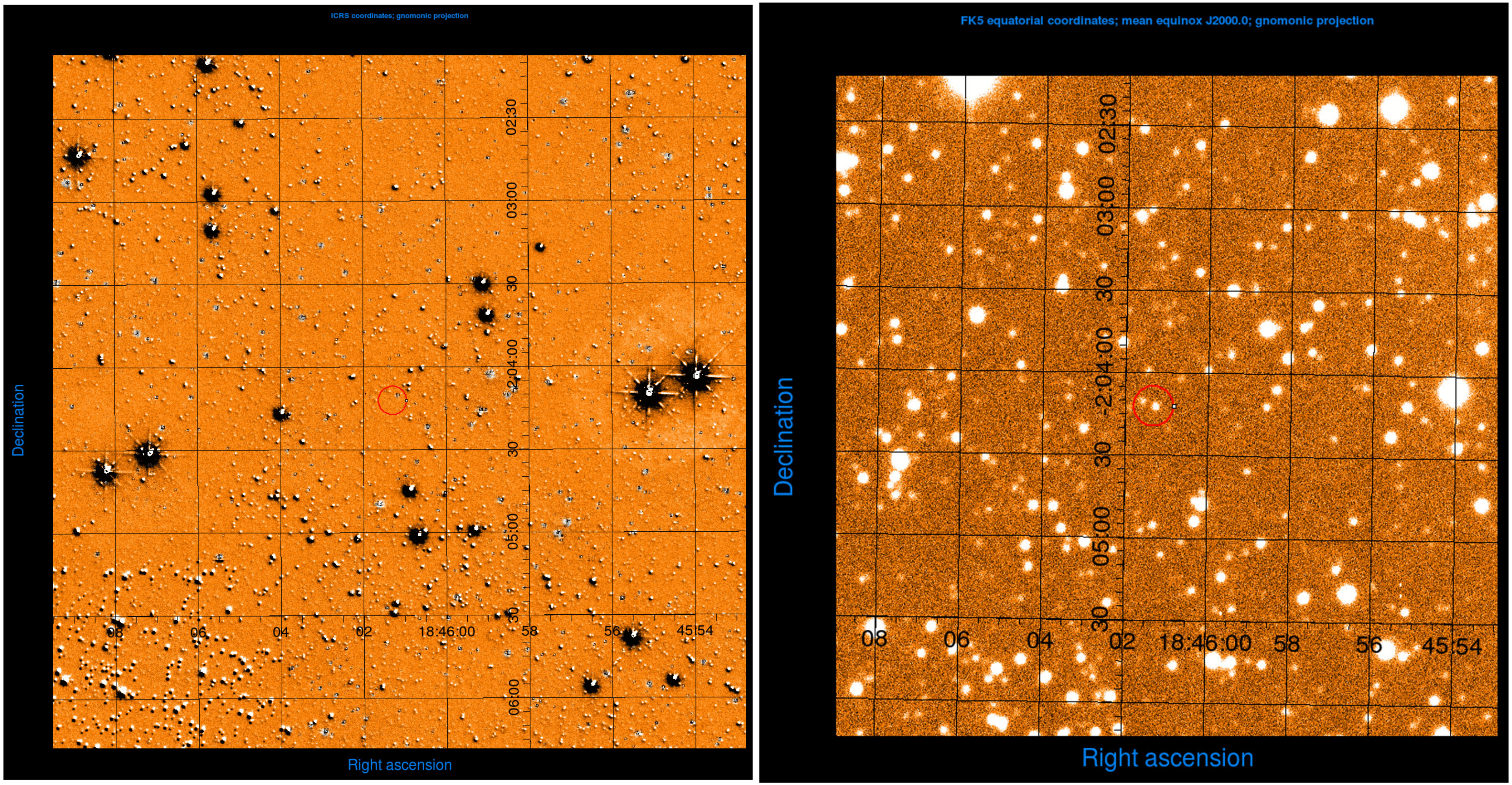

Comparison of IPHAS3, H_2 on the left, $H\alpha$ on the right

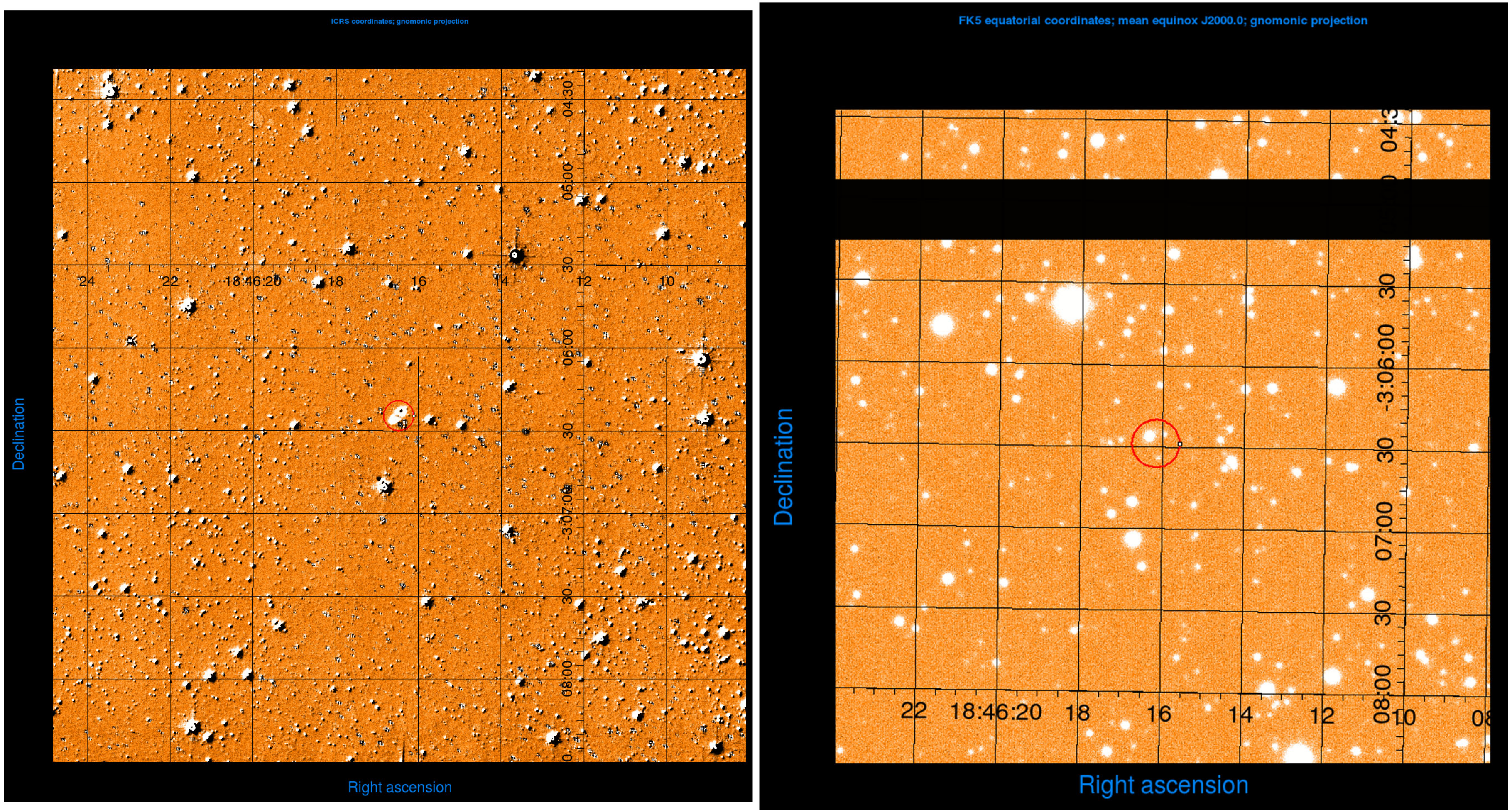

Comparison of IPHAS4, H_2 on the left, $H\alpha$ on the right

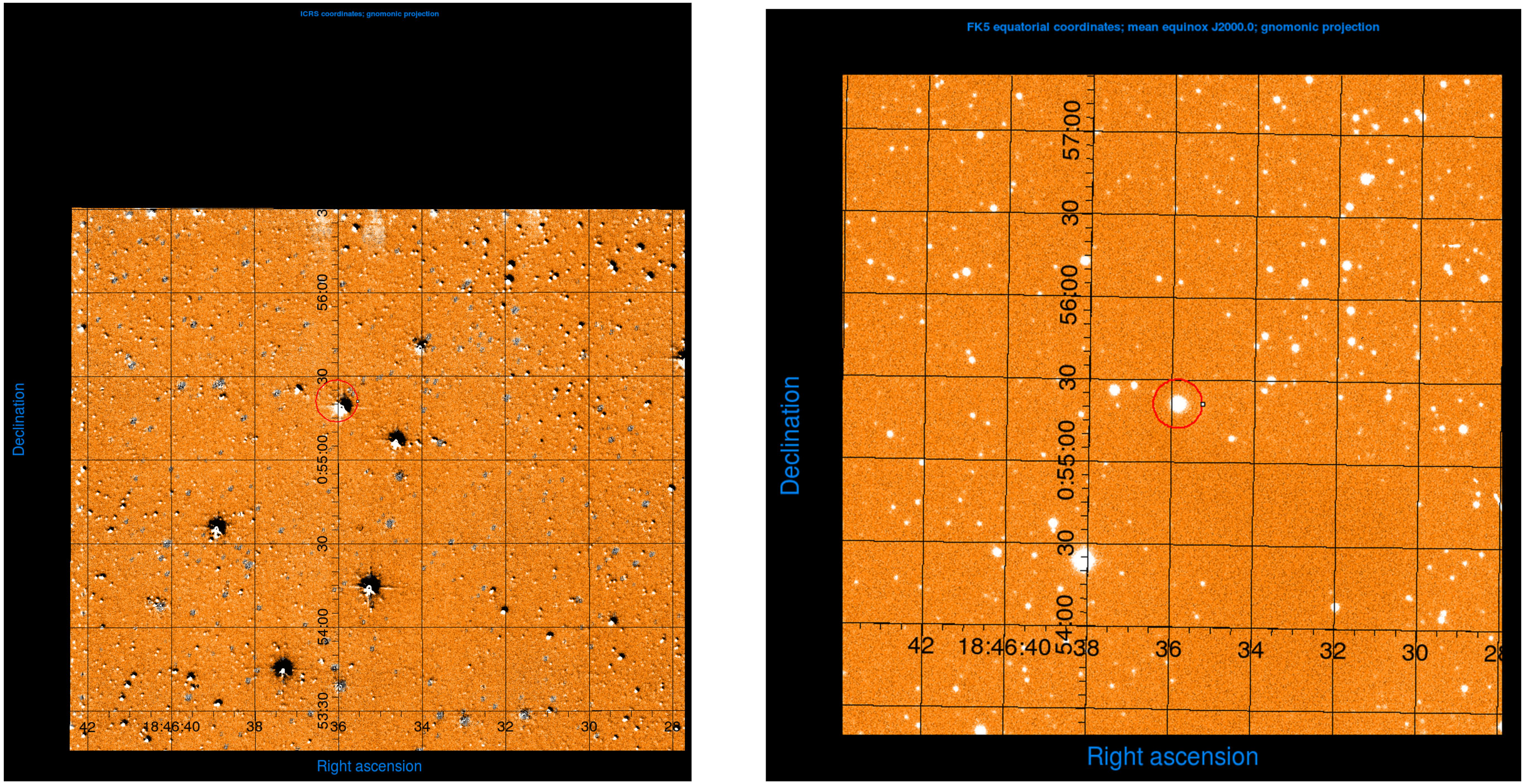

Comparison of IPHAS5, H_2 on the left, Hα on the right

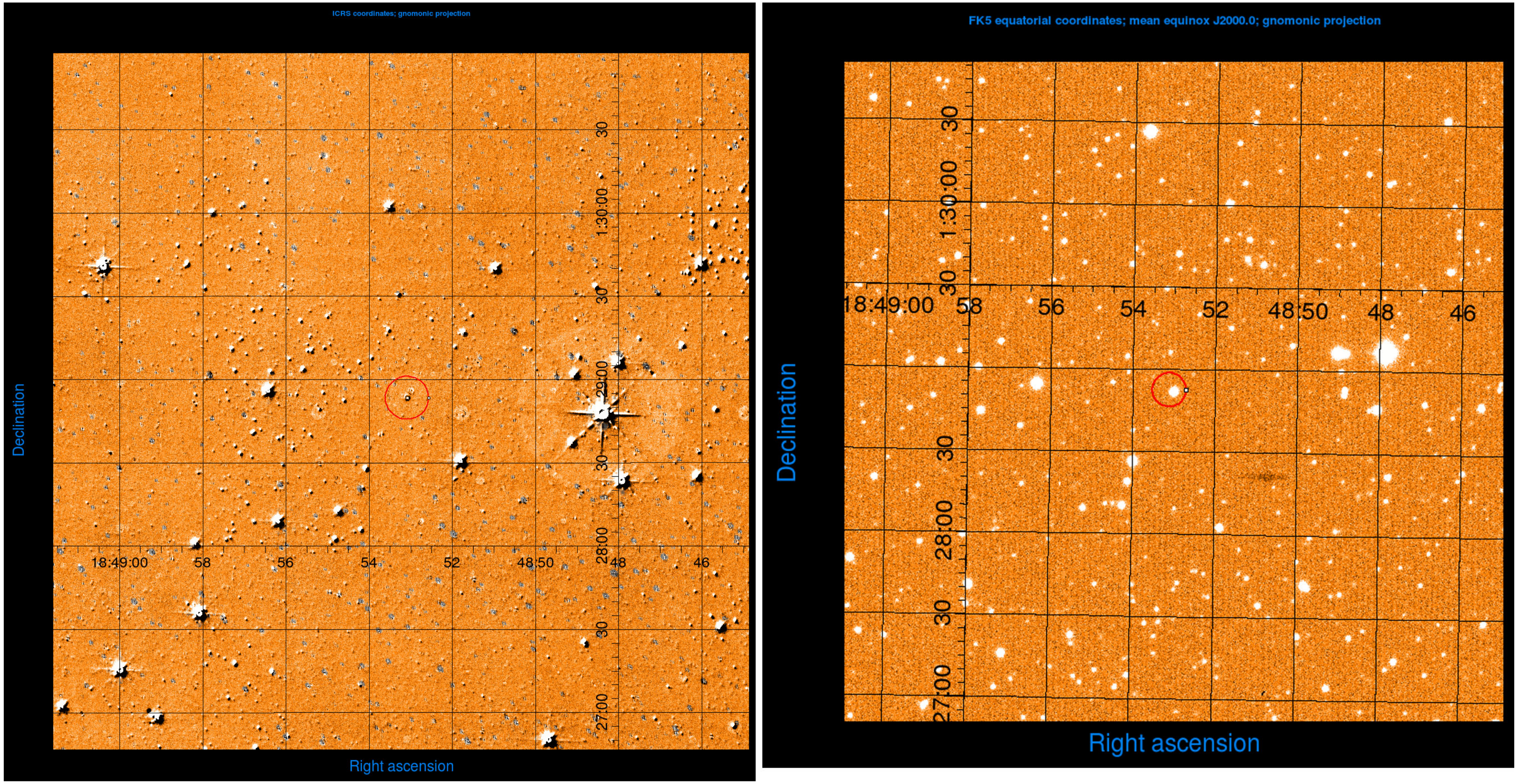

Comparison of IPHAS6, H_2 on the left, $H\alpha$ on the right

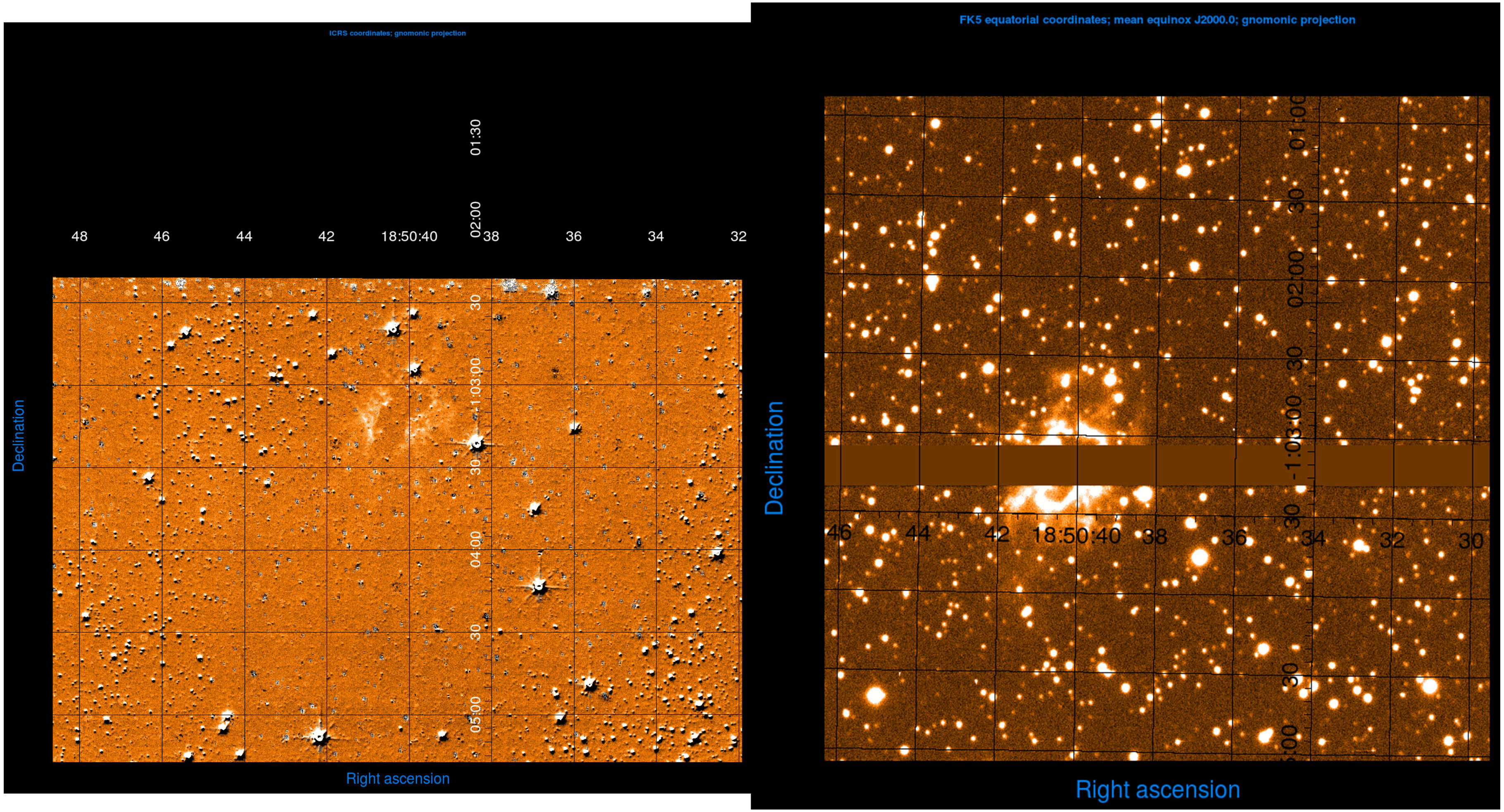

Comparison of IPHAS7, H_2 on the left, $H\alpha$ on the right

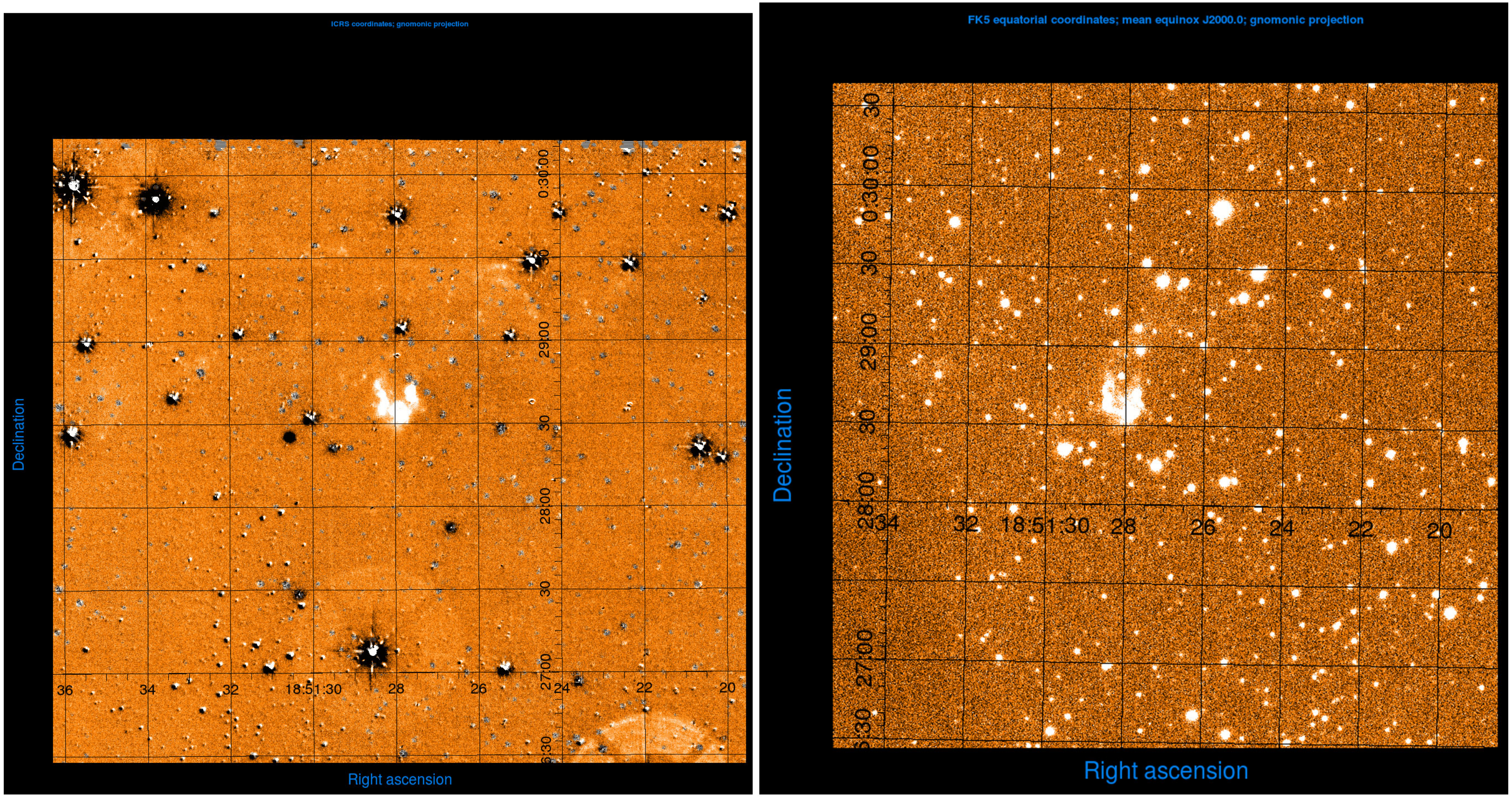

Comparison of IPHAS8, H_2 on the left, $H\alpha$ on the right

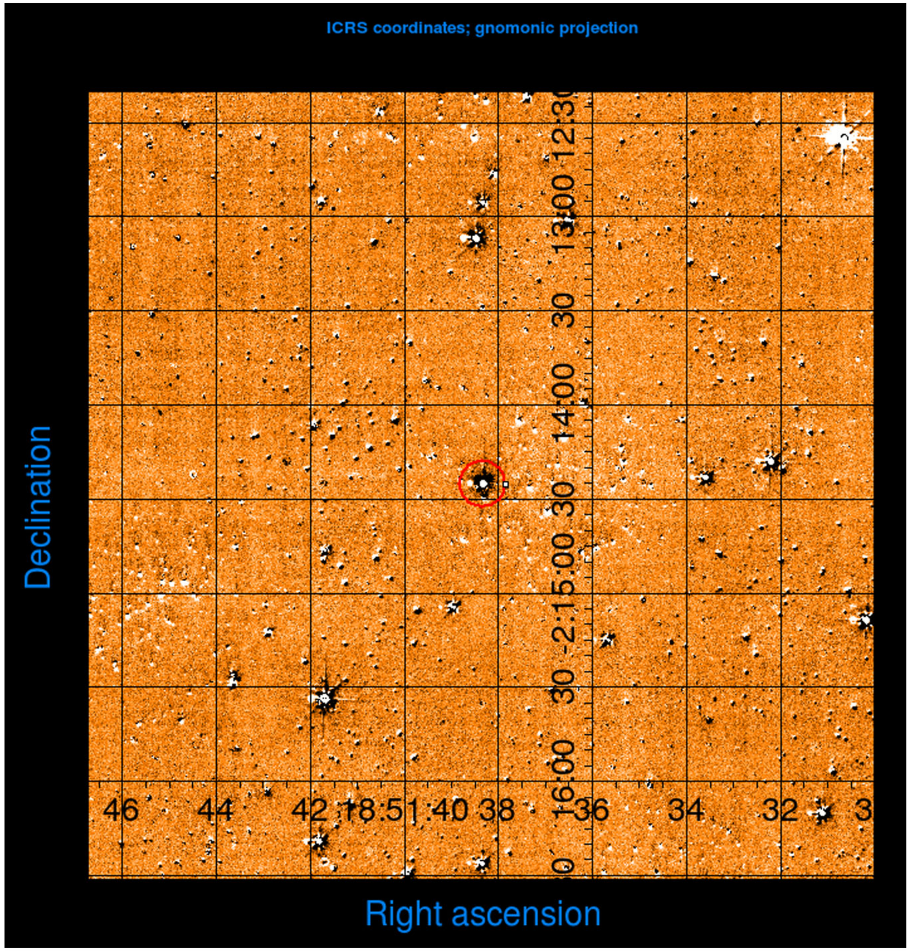

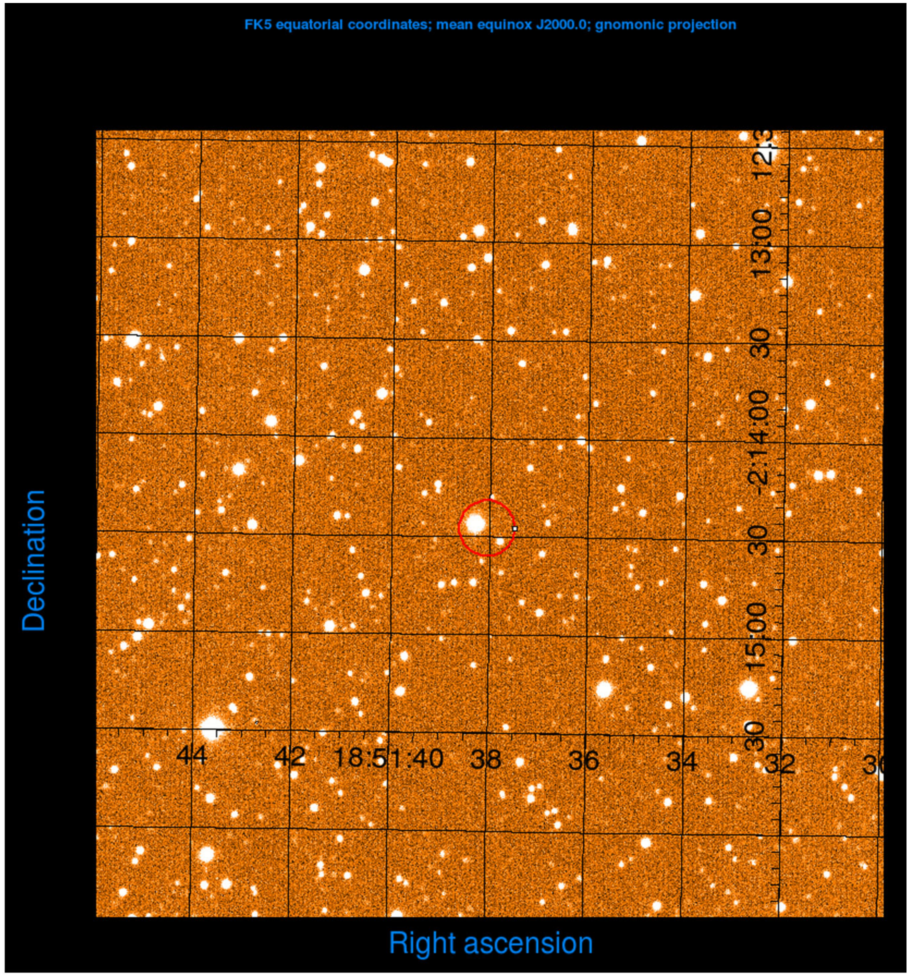

Comparison of IPHAS9, H_2 on the left, $H\alpha$ on the right

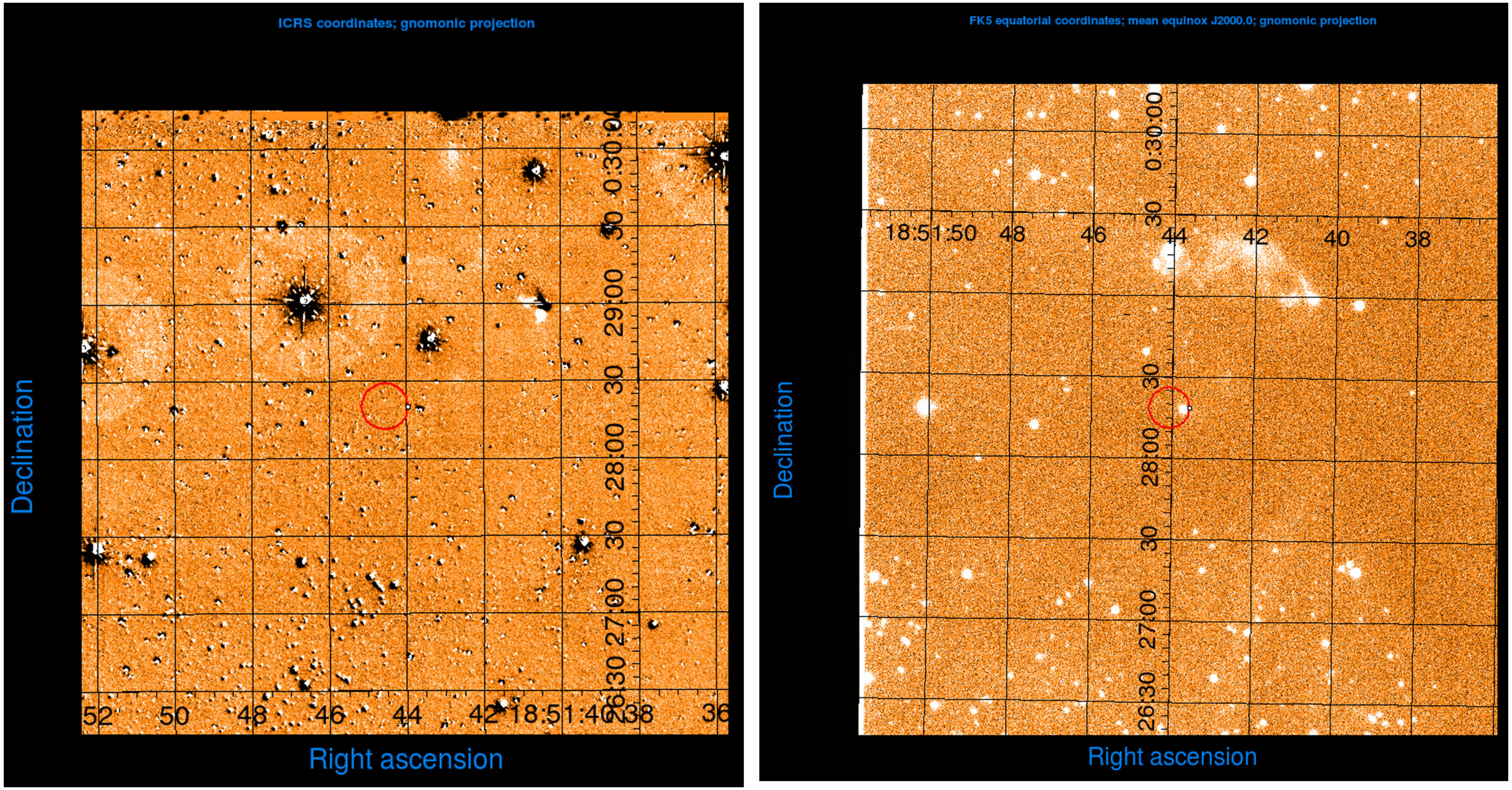

Comparison of IPHAS10, H_2 on the left, $H\alpha$ on the right

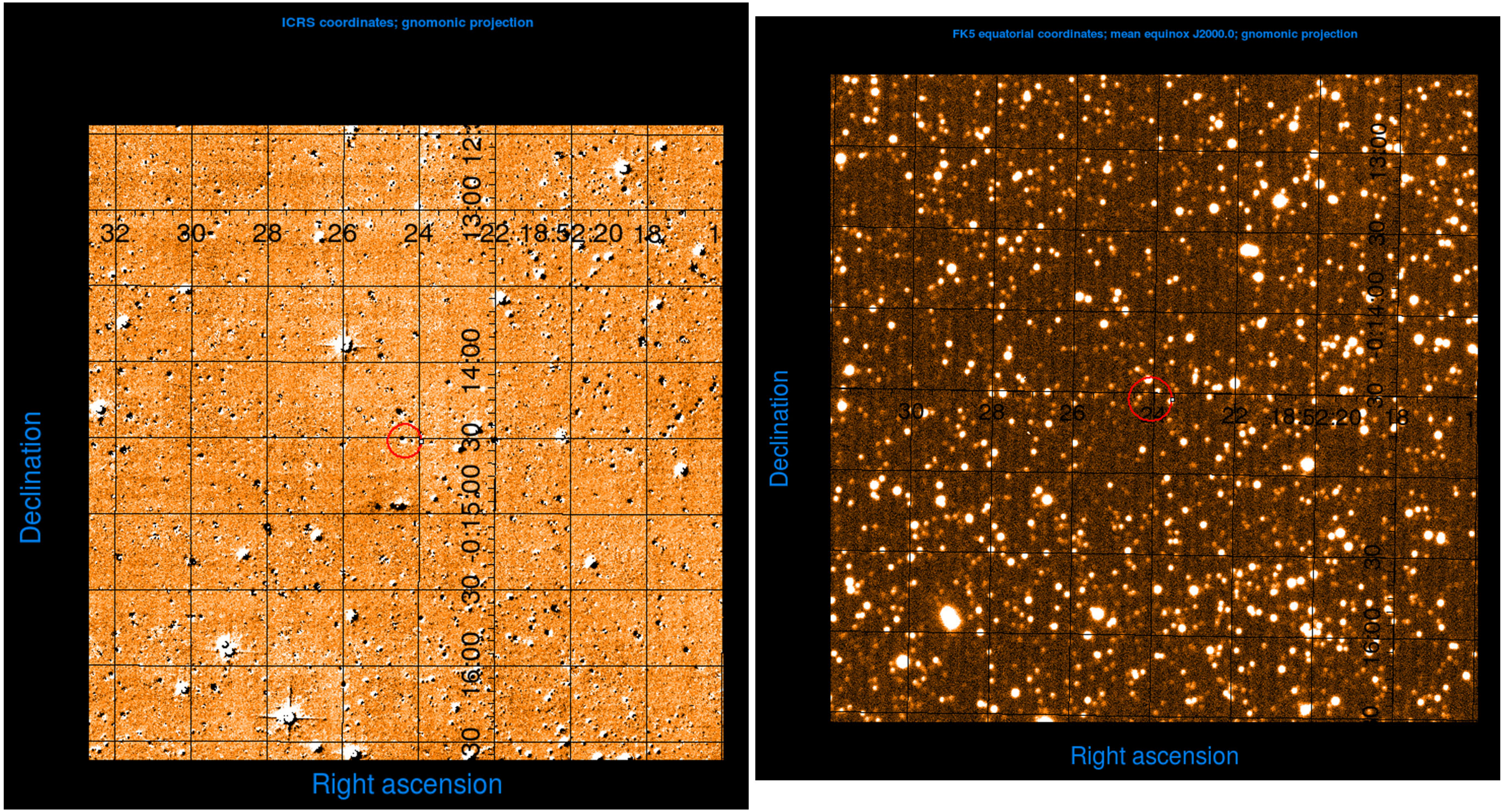

Comparison of IPHAS11, H_2 on the left, Hα on the right

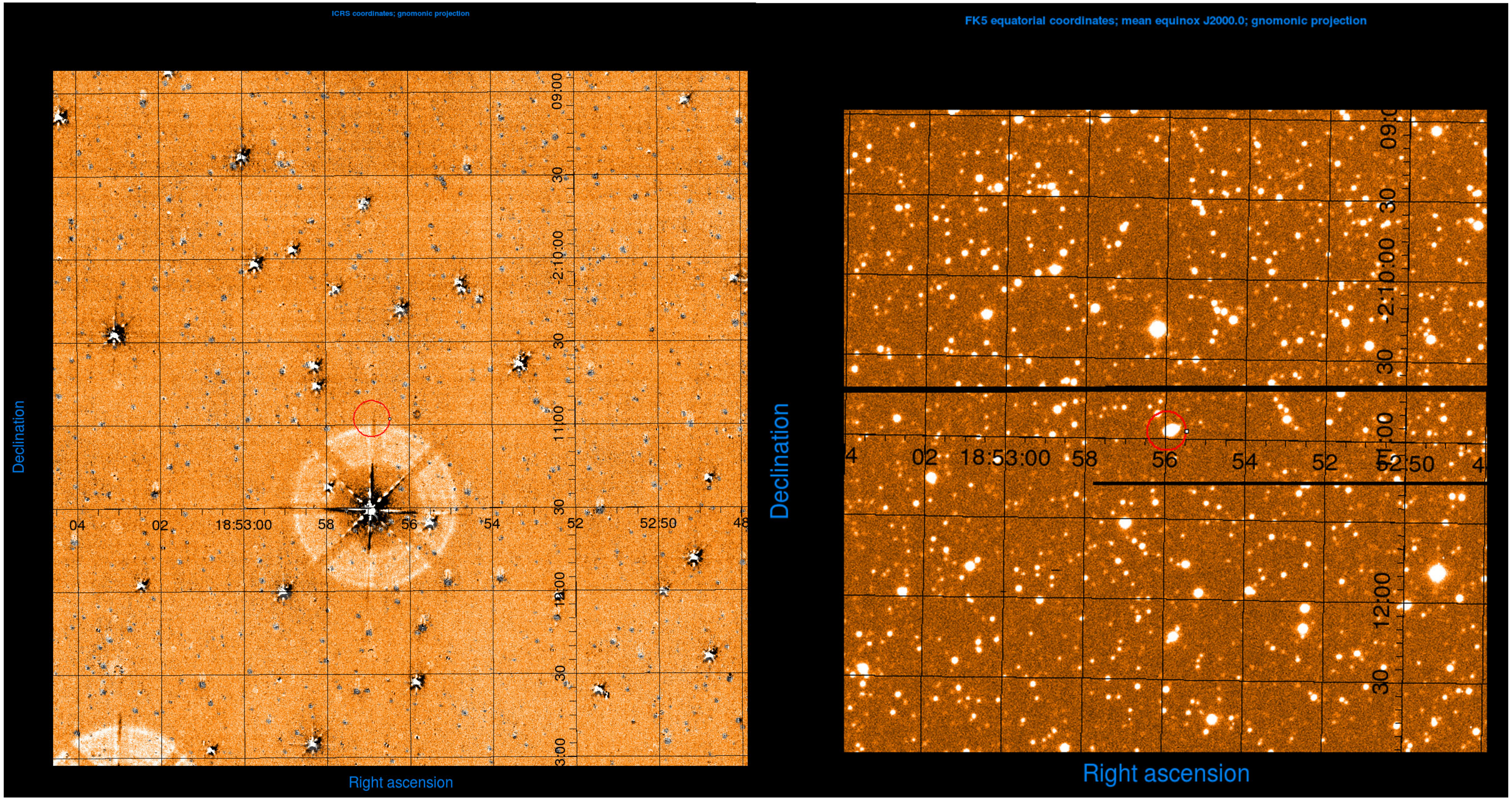

Comparison of IPHAS12, H_2 on the left, Hα on the right

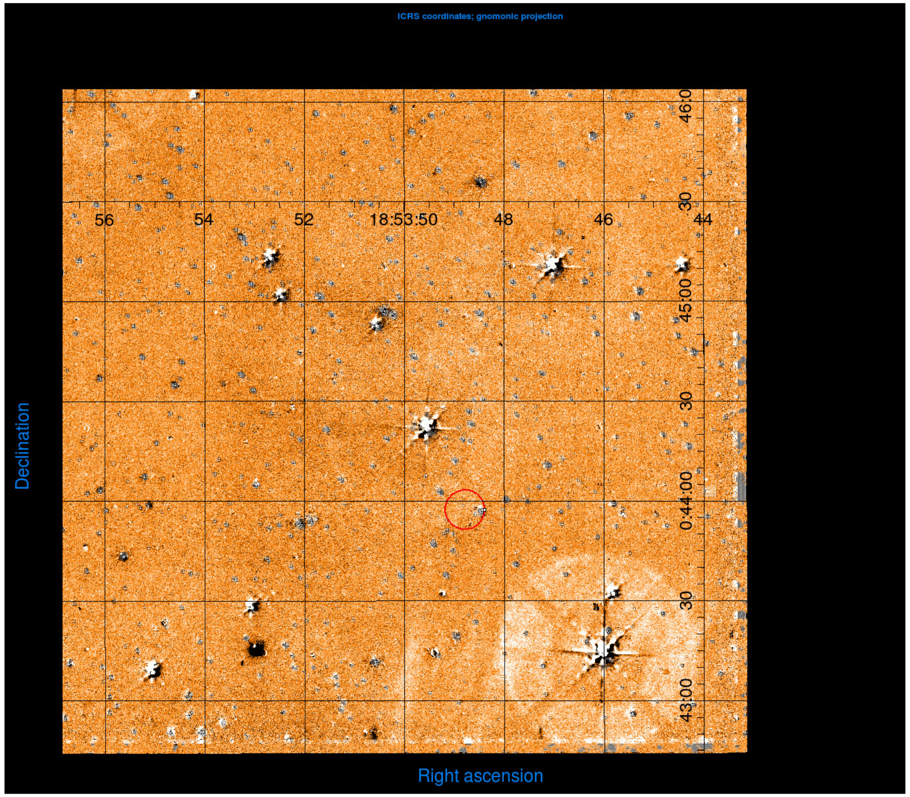

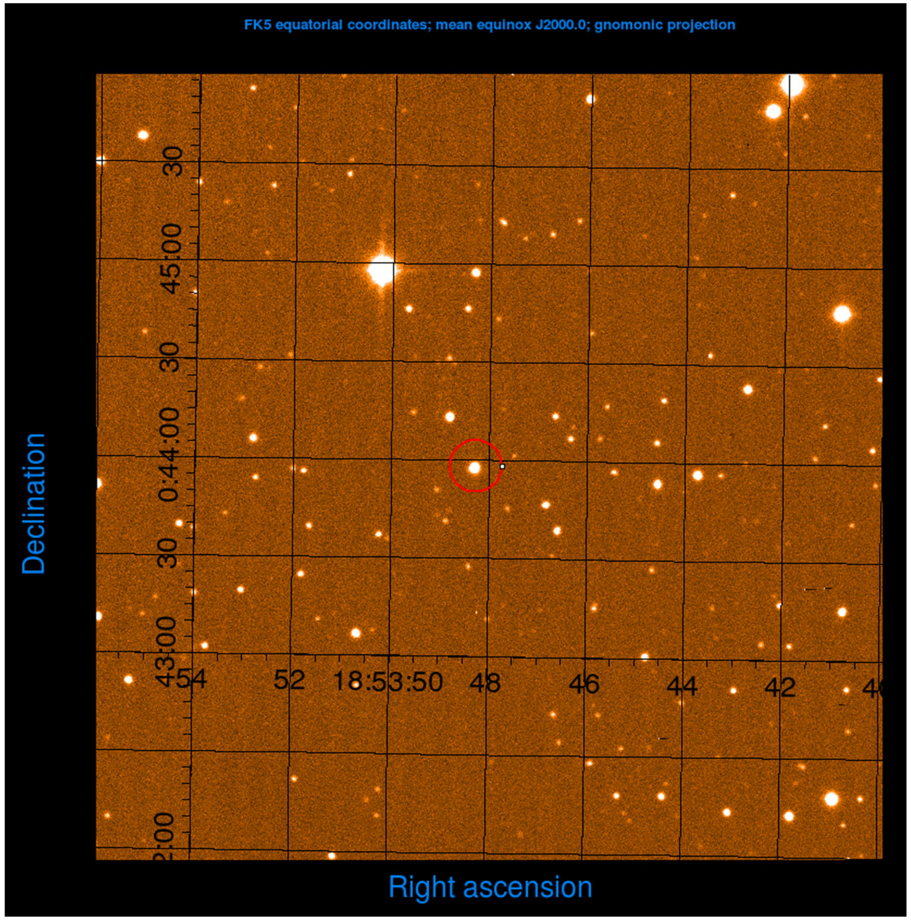

Comparison of IPHAS13, H_2 on the left, Hα on the right

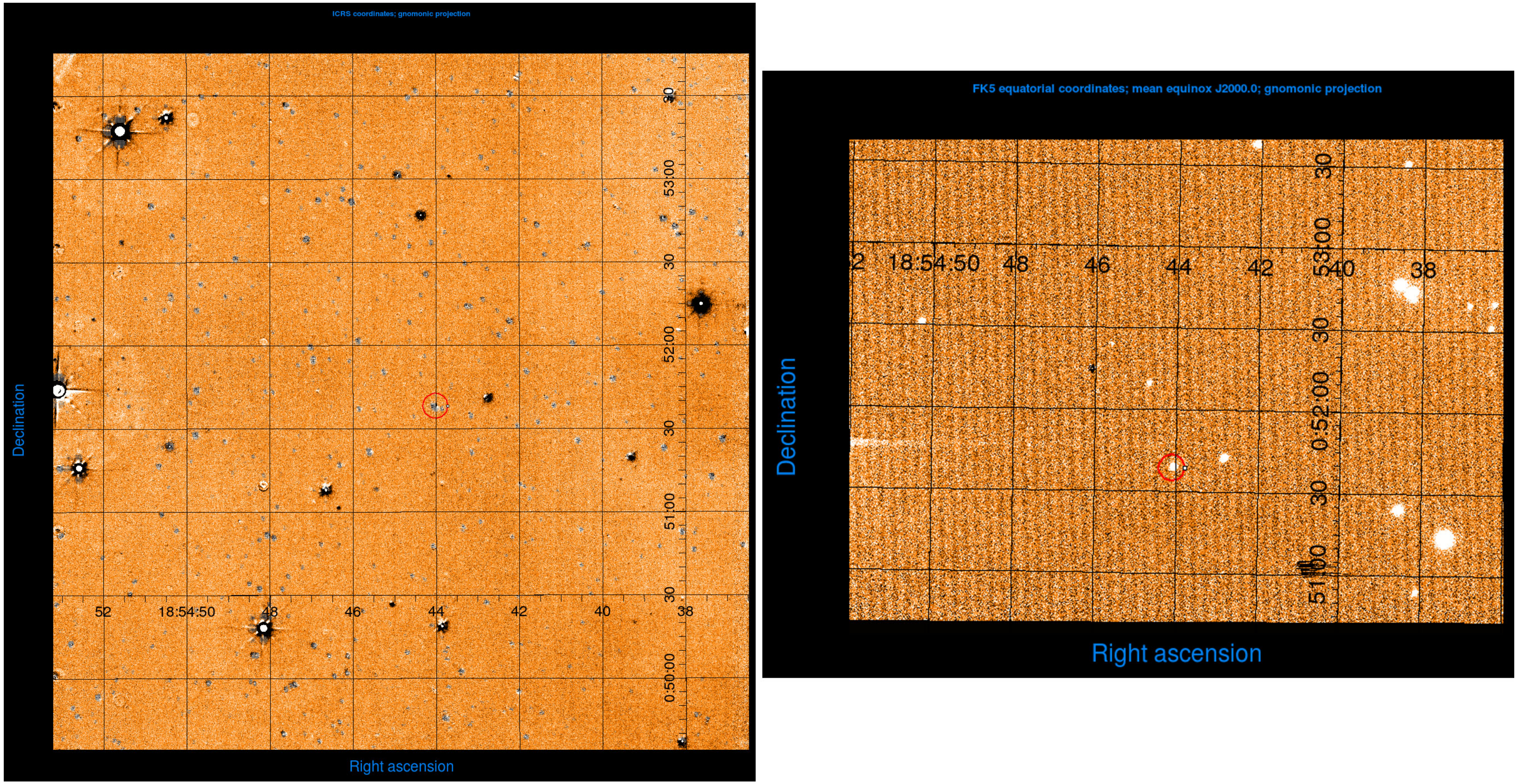

Comparison of IPHAS14, H_2 on the left, Hα on the right

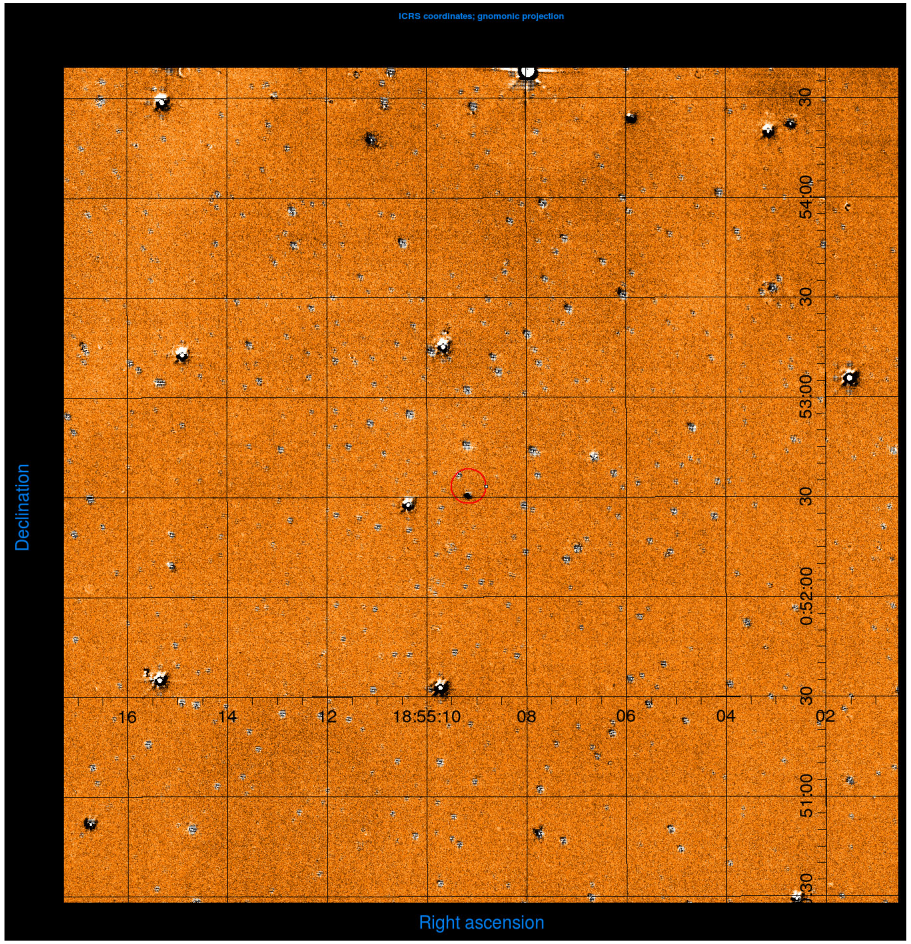

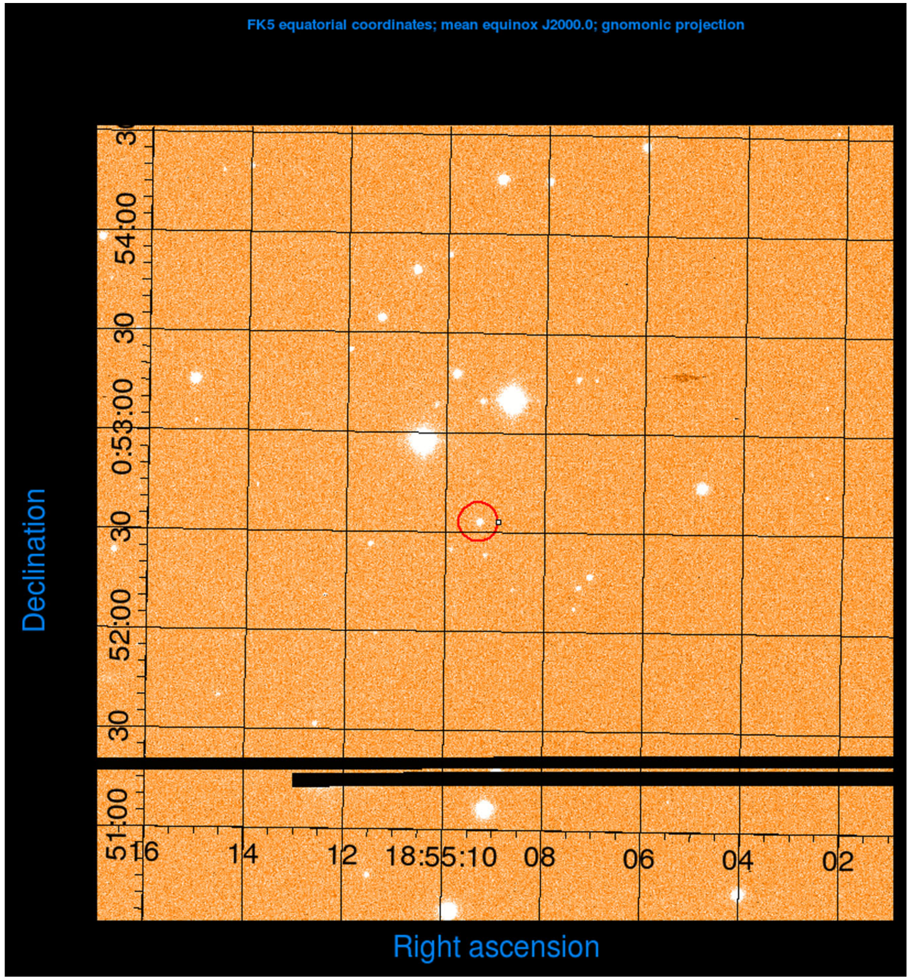

Comparison of IPHAS15, H_2 on the left, Hα on the right

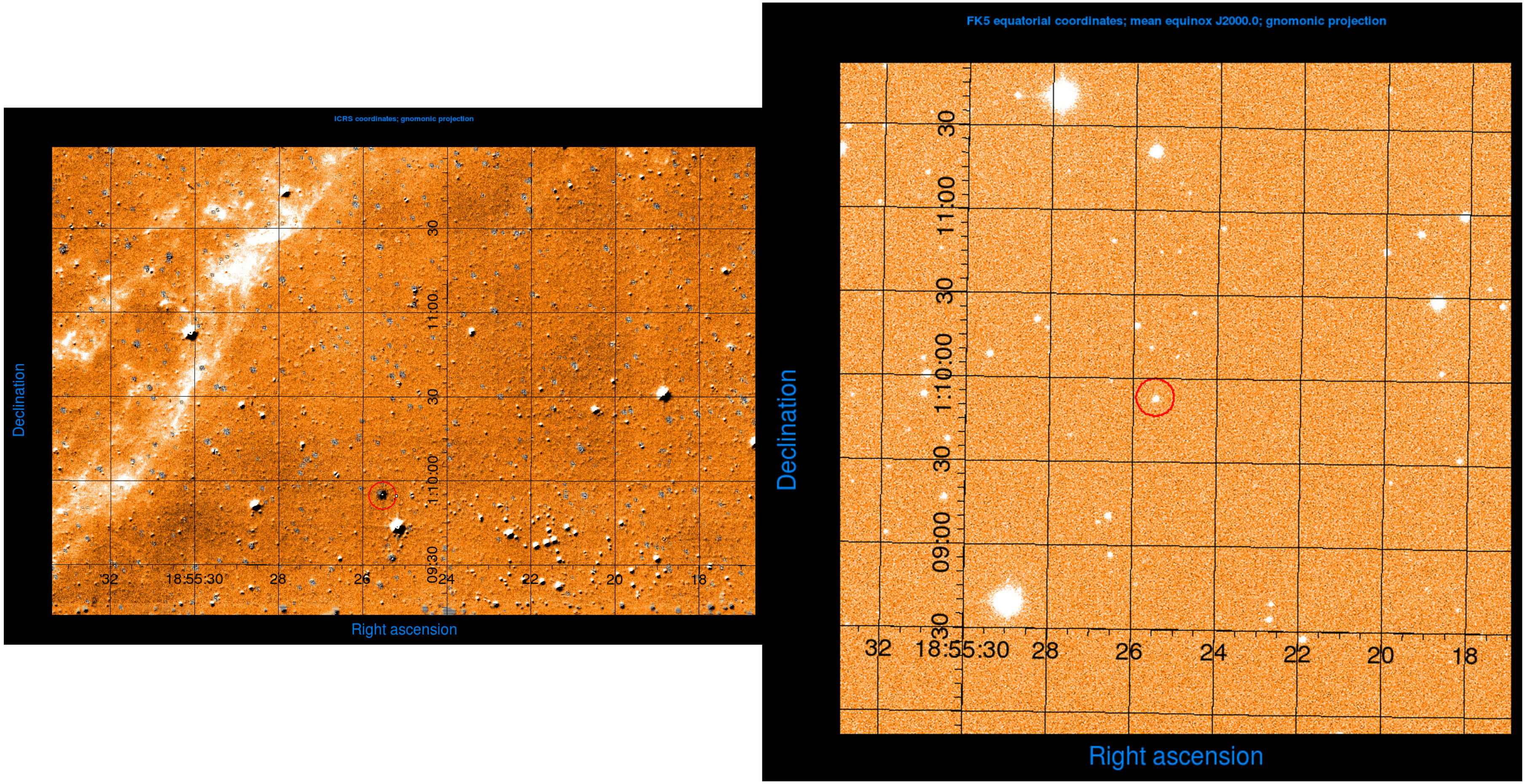

Comparison of IPHAS16, H_2 on the left, $H\alpha$ on the right

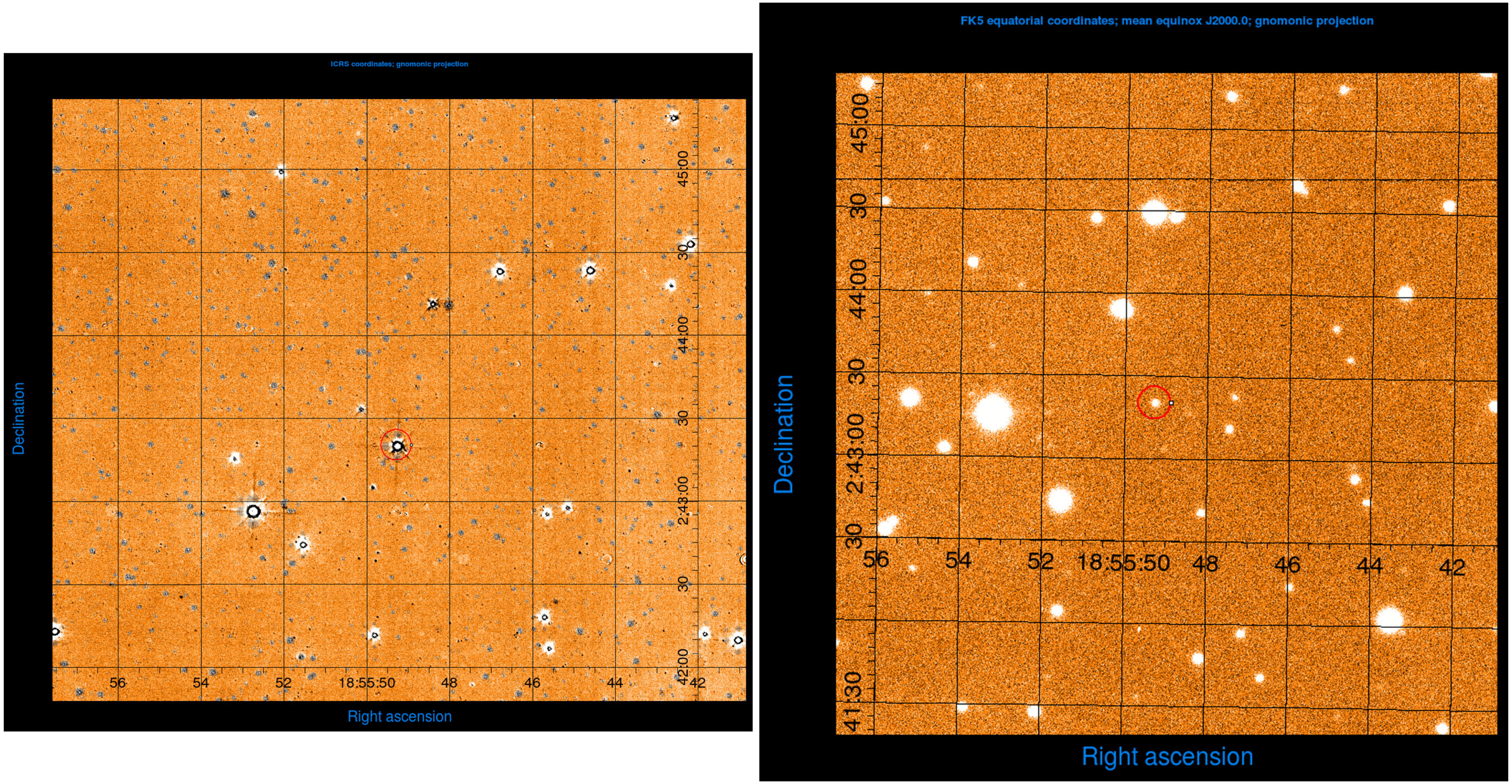

Comparison of IPHAS17, H_2 on the left, $H\alpha$ on the right

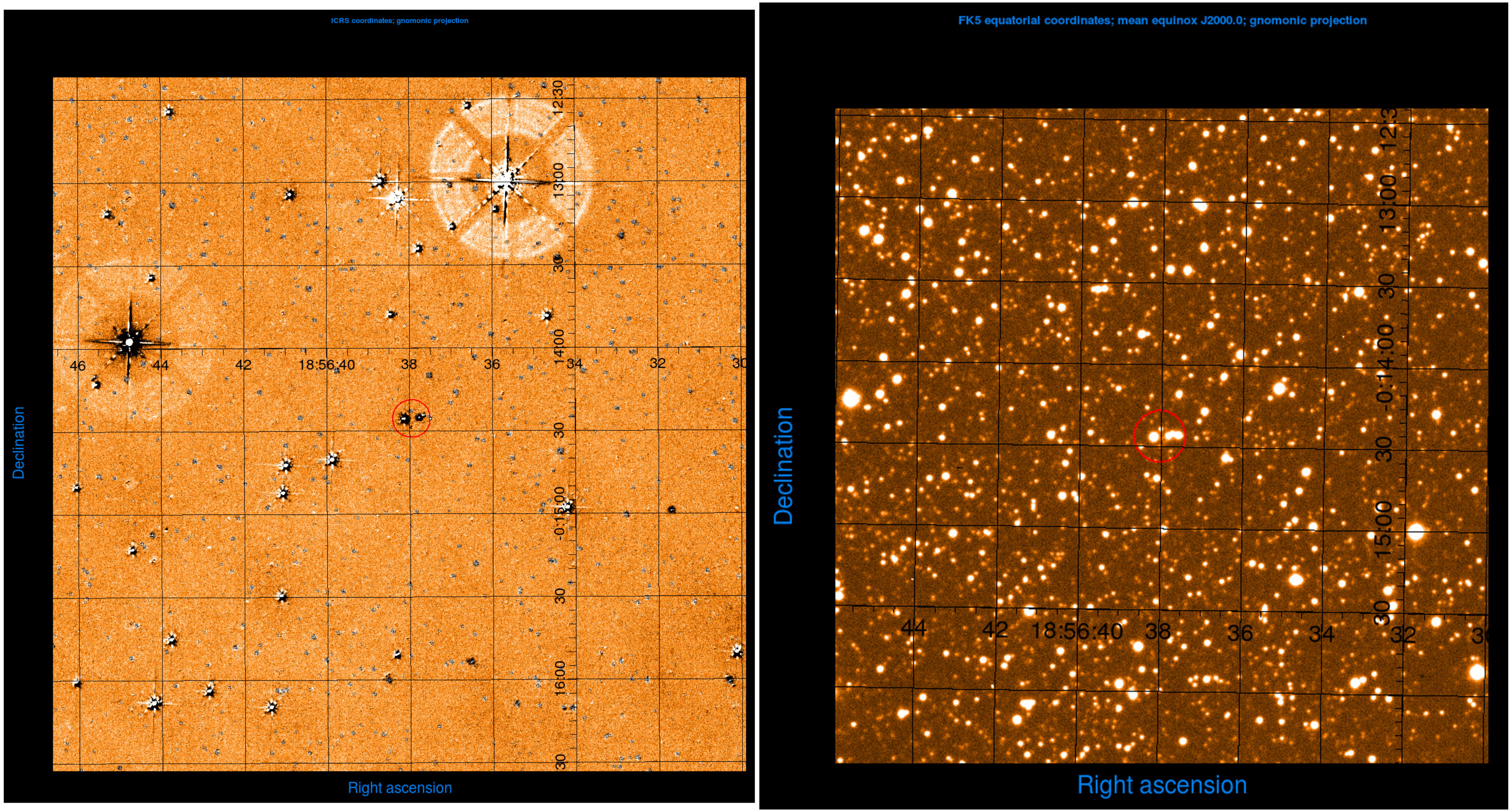

Comparison of IPHAS18, H_2 on the left, Hα on the right

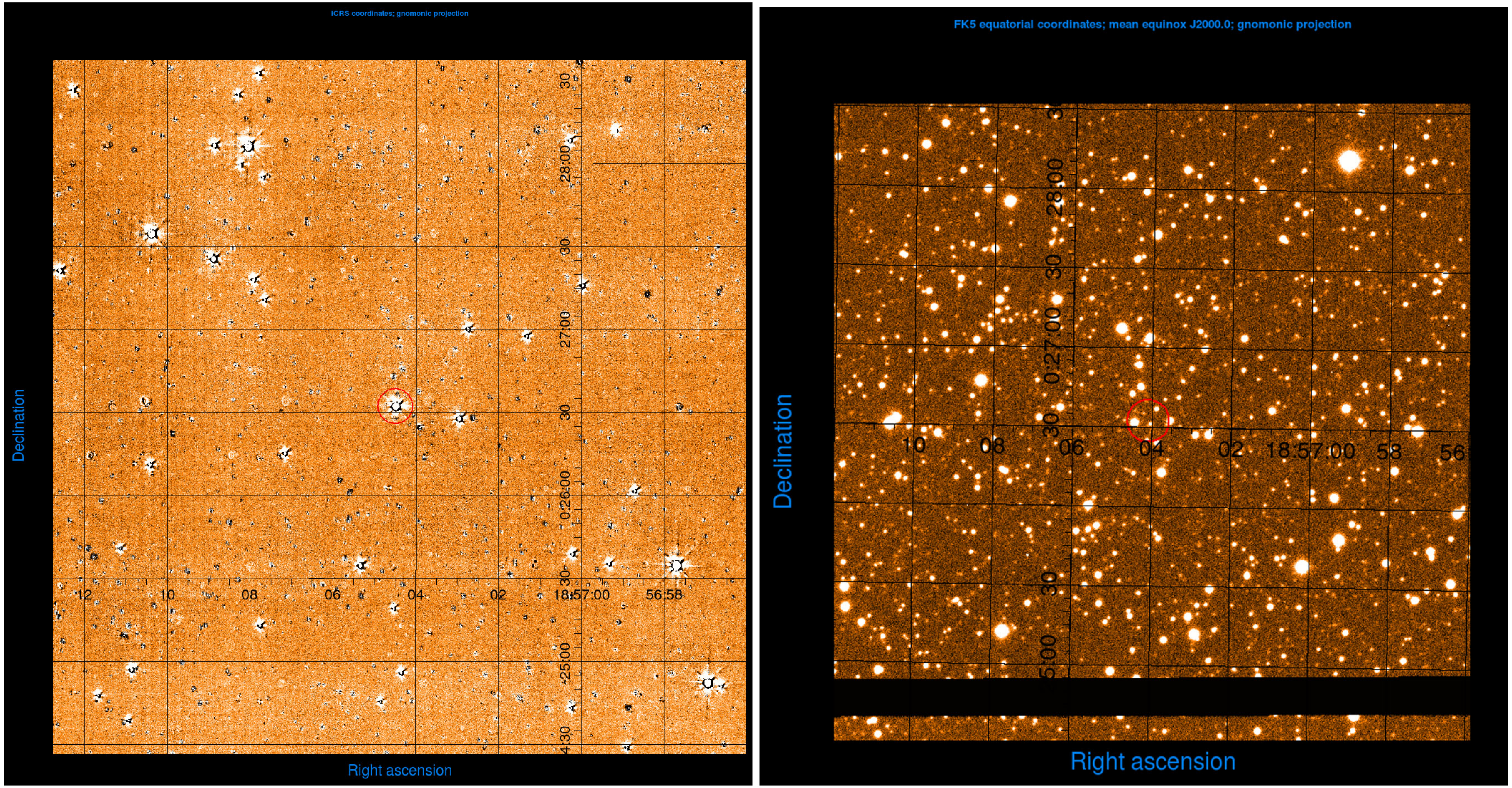

Comparison of IPHAS19, H_2 on the left, Hα on the right

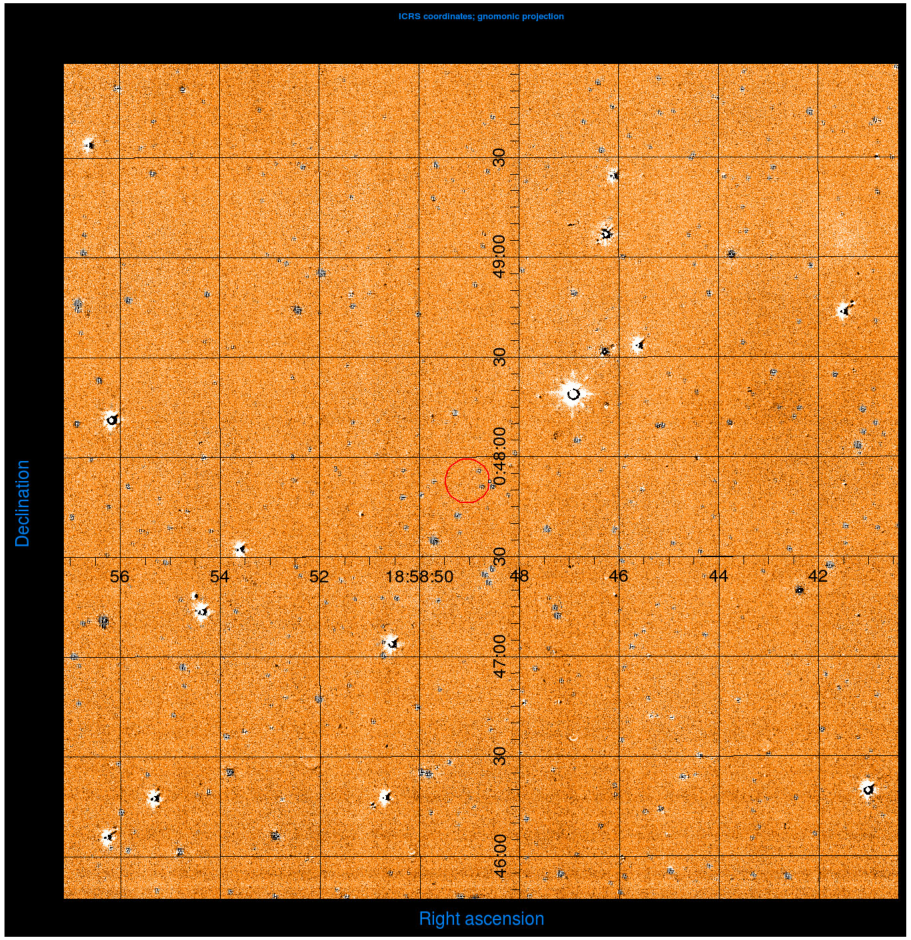

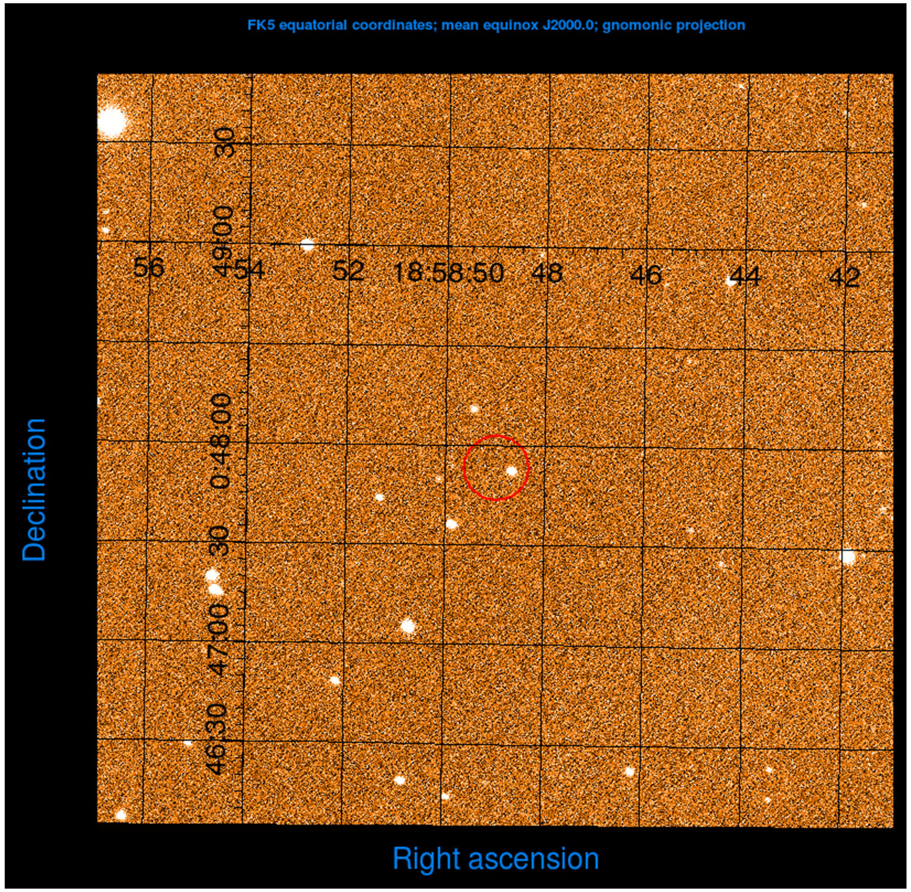

Comparison of IPHAS20, H_2 on the left, $H\alpha$ on the right

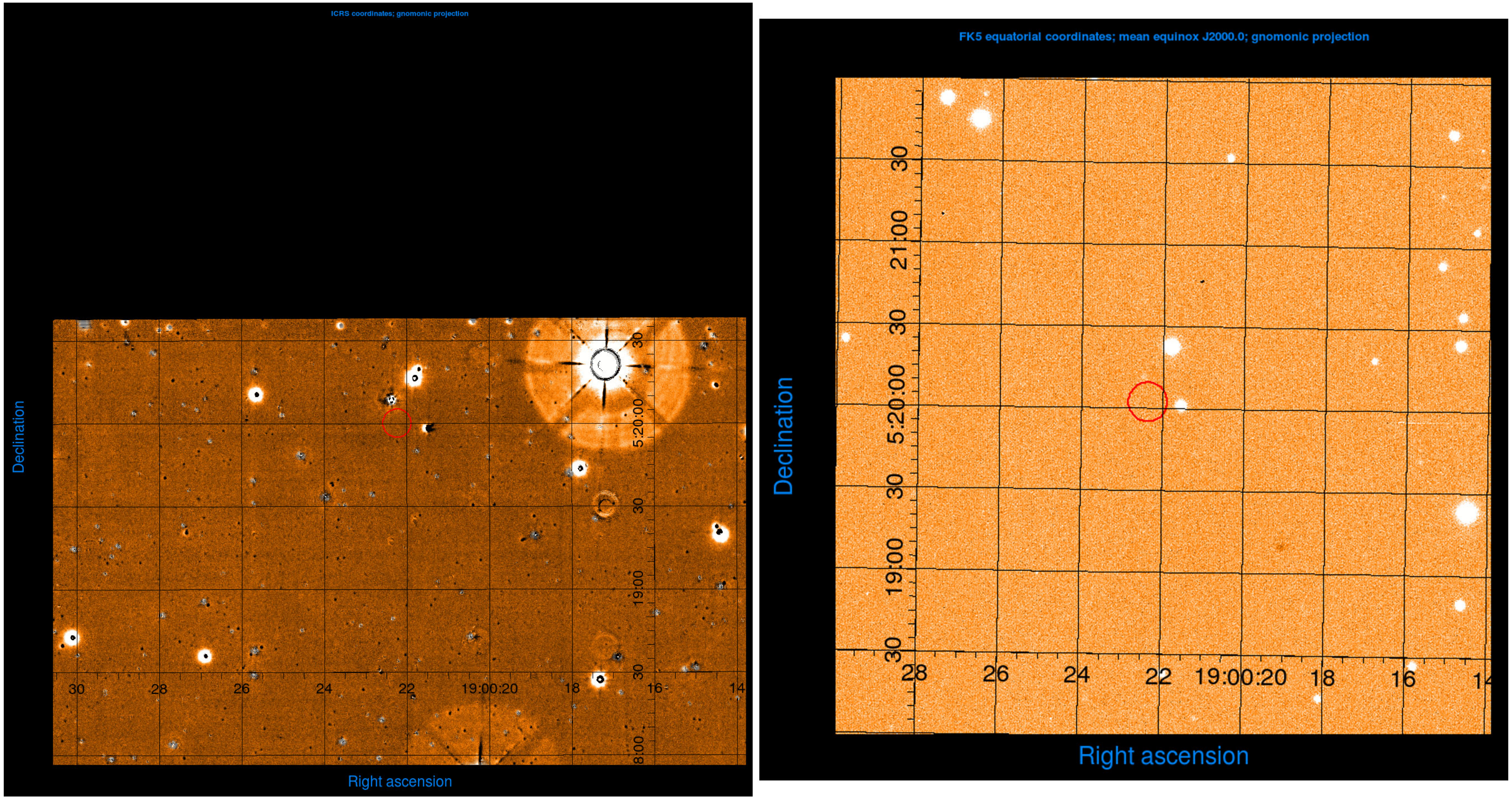

Comparison of IPHAS21, H_2 on the left, $H\alpha$ on the right

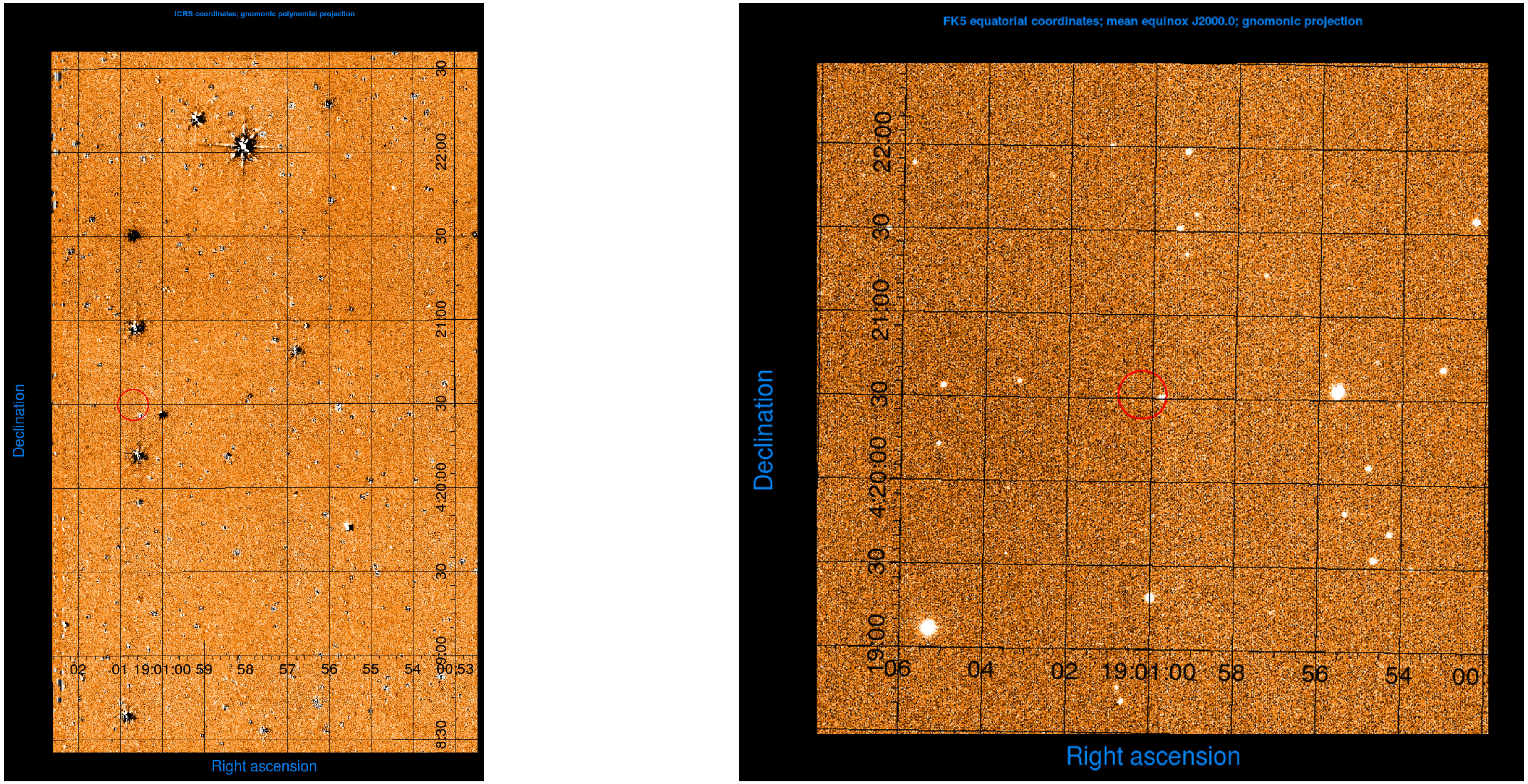

Comparison of IPHAS22, H_2 on the left, Hα on the right

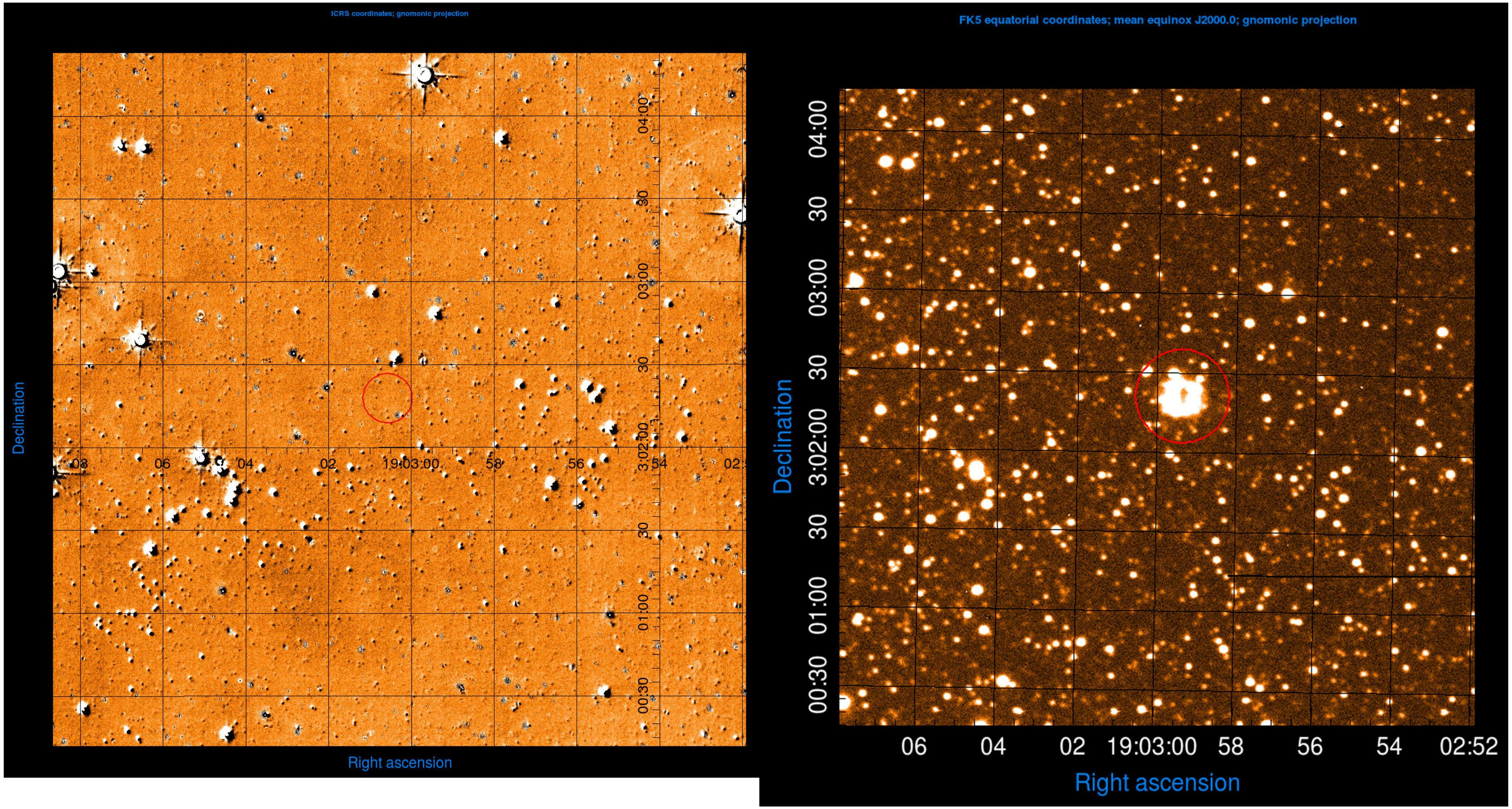

Comparison of IPHAS23, H_2 on the left, Hα on the right

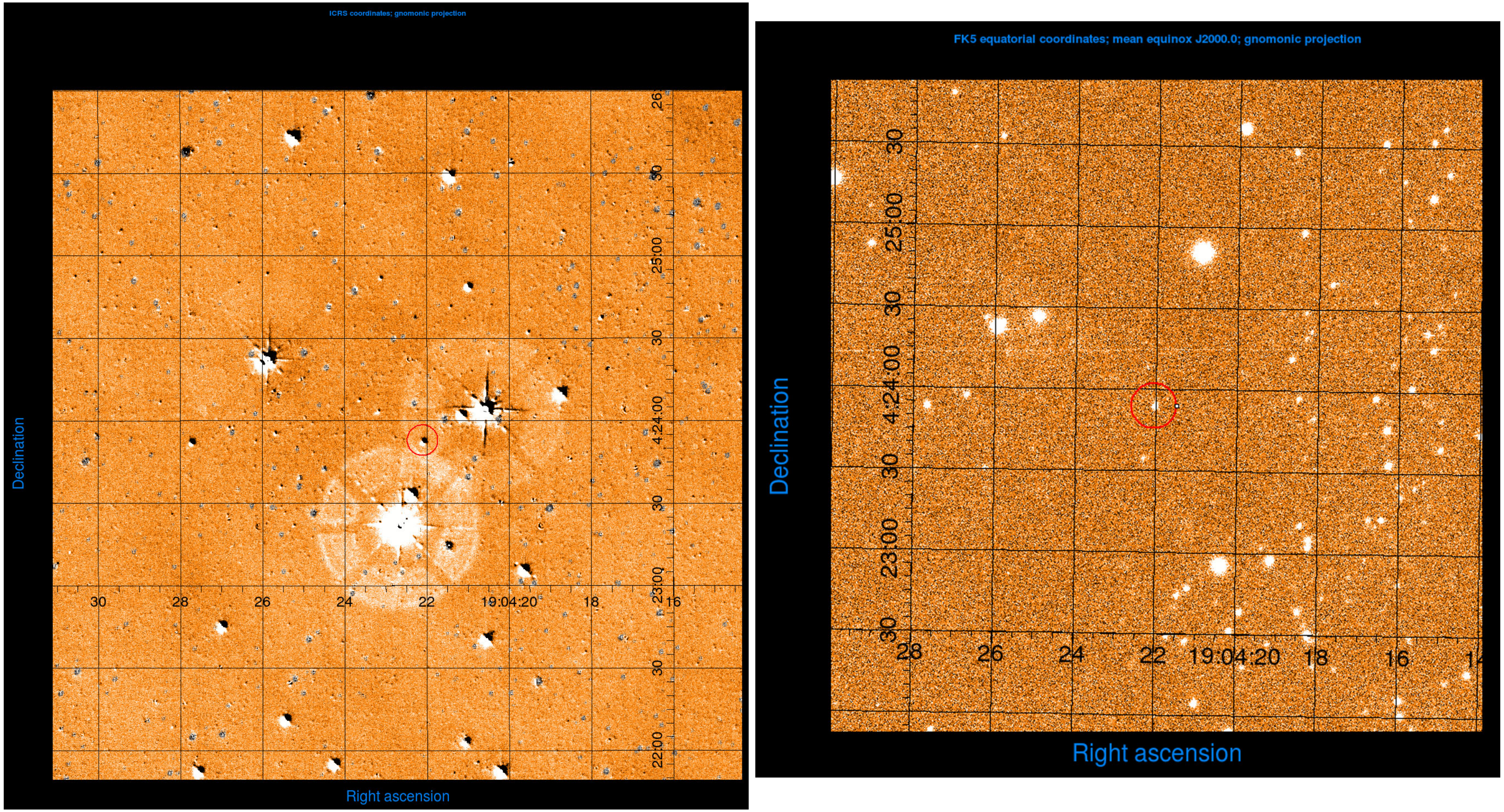

Comparison of IPHAS24, H_2 on the left, $H\alpha$ on the right

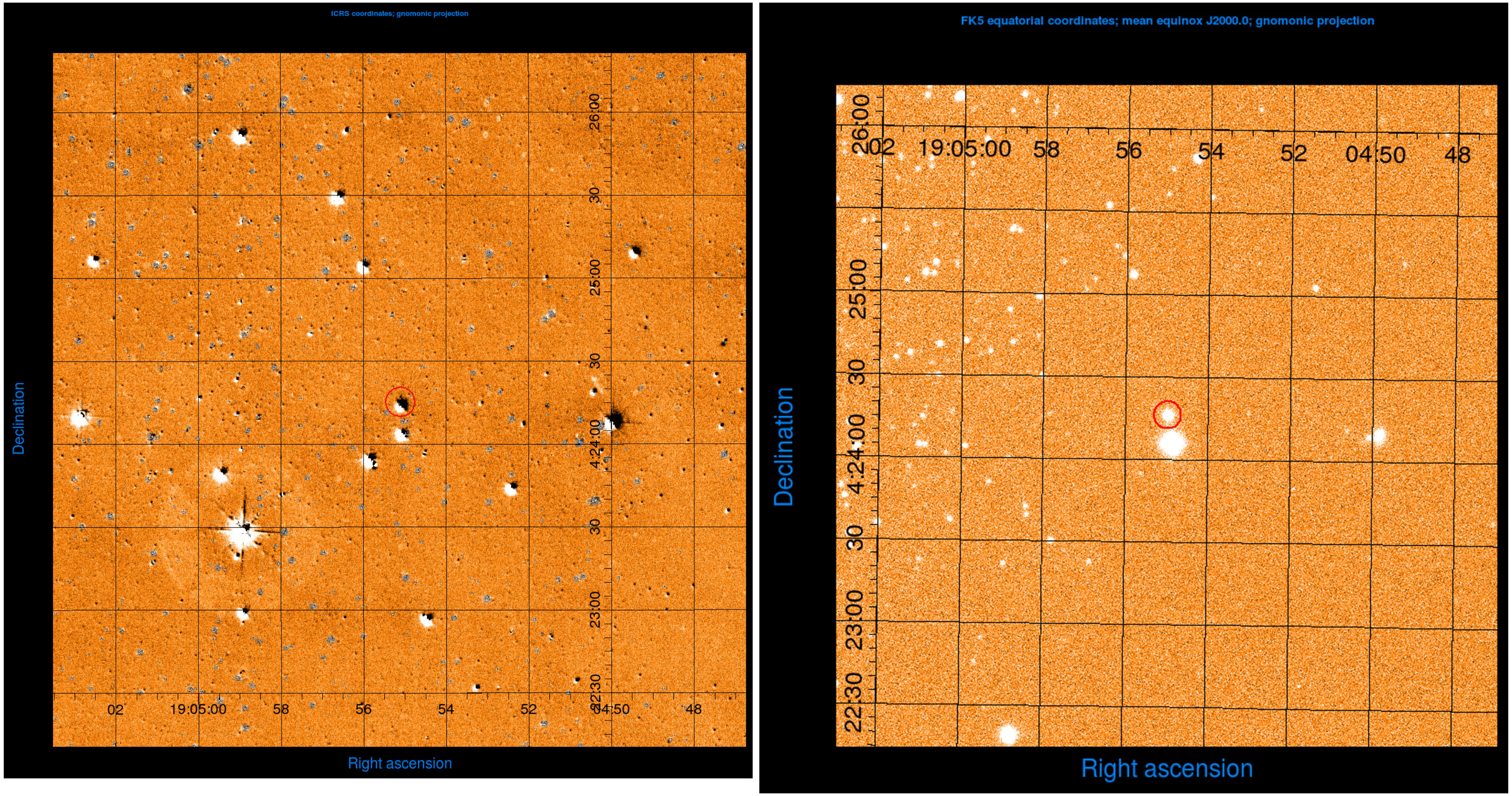

Comparison of IPHAS25, H_2 on the left, Hα on the right

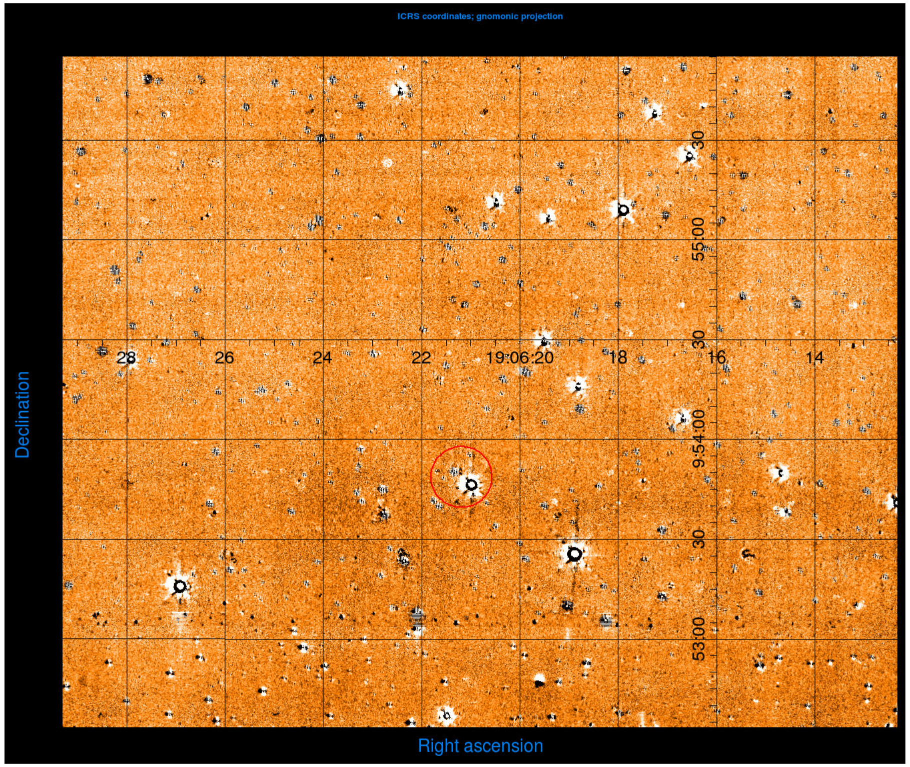

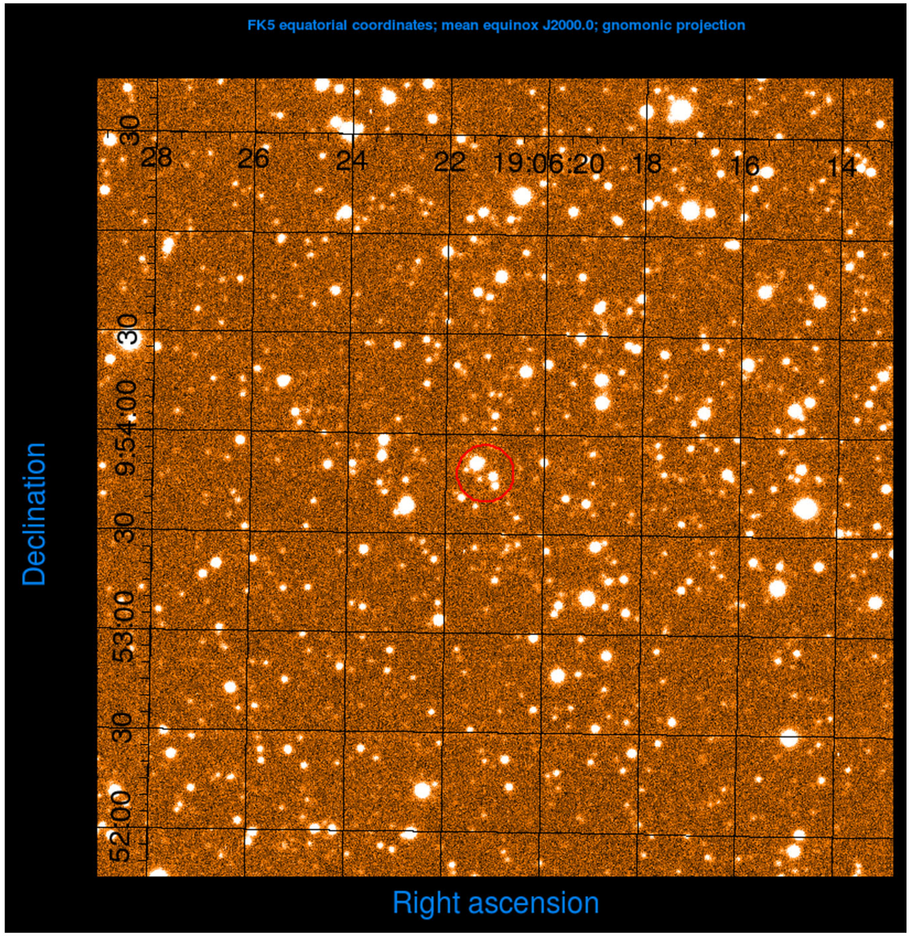

Comparison of IPHAS26, H_2 on the left, Hα on the right

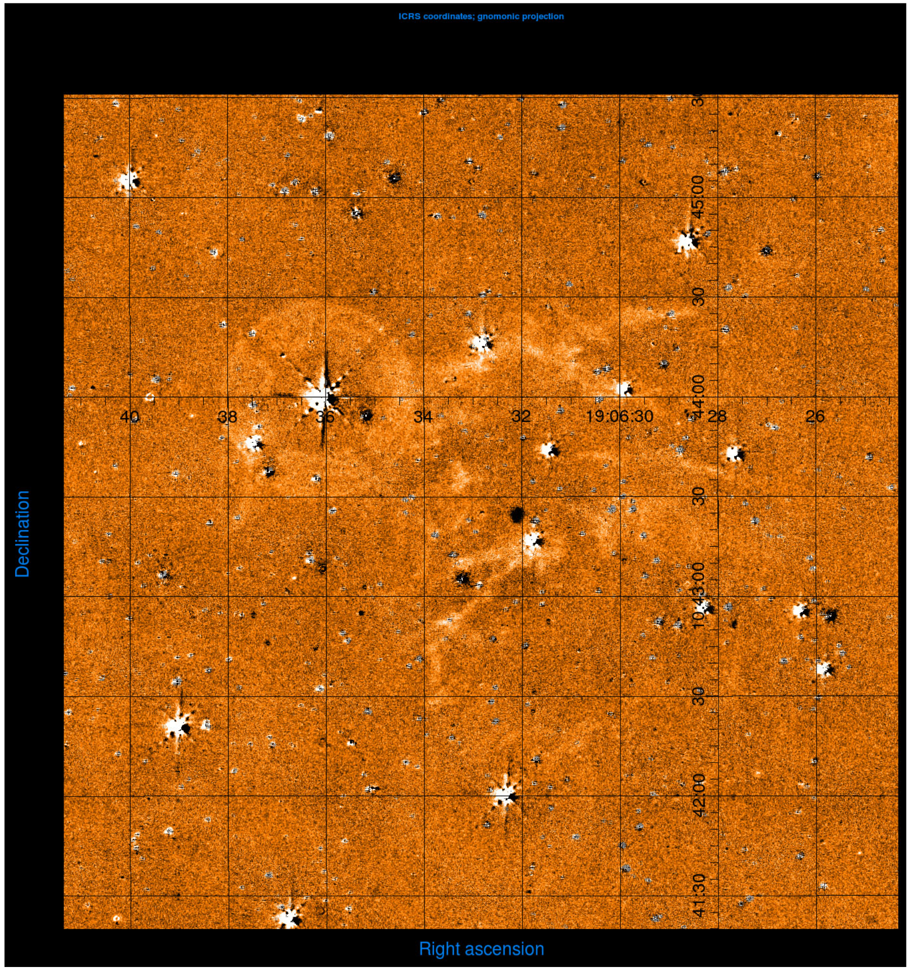

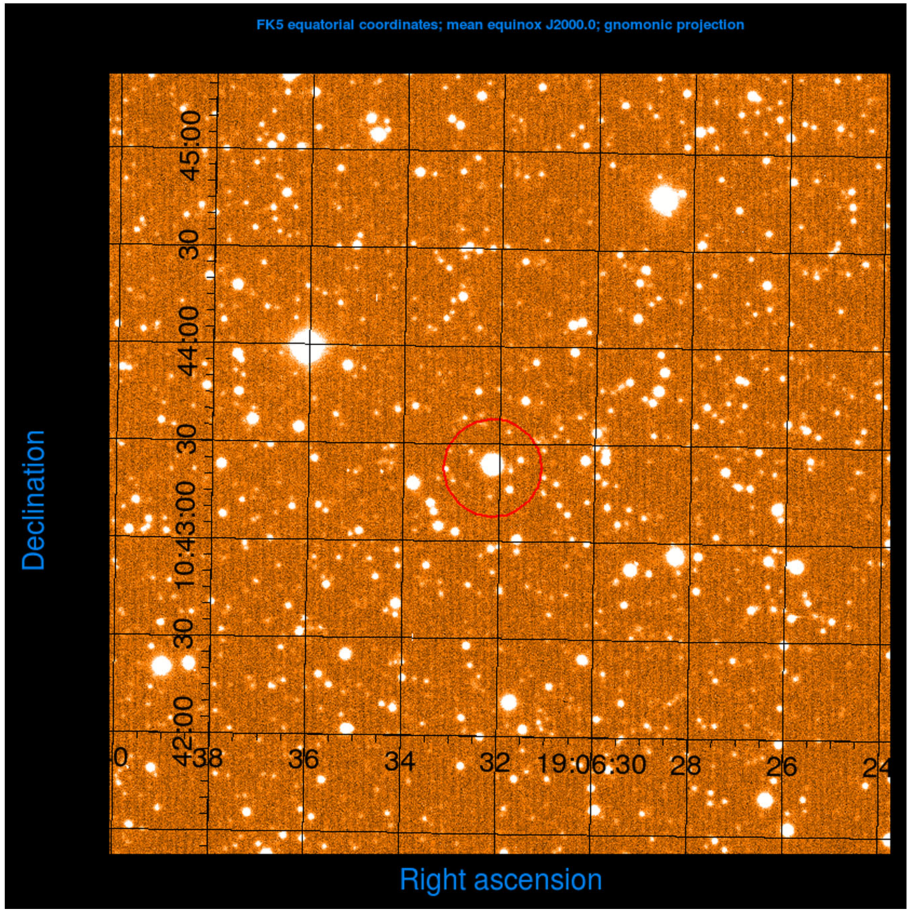

Comparison of IPHAS27, H_2 on the left, Hα on the right

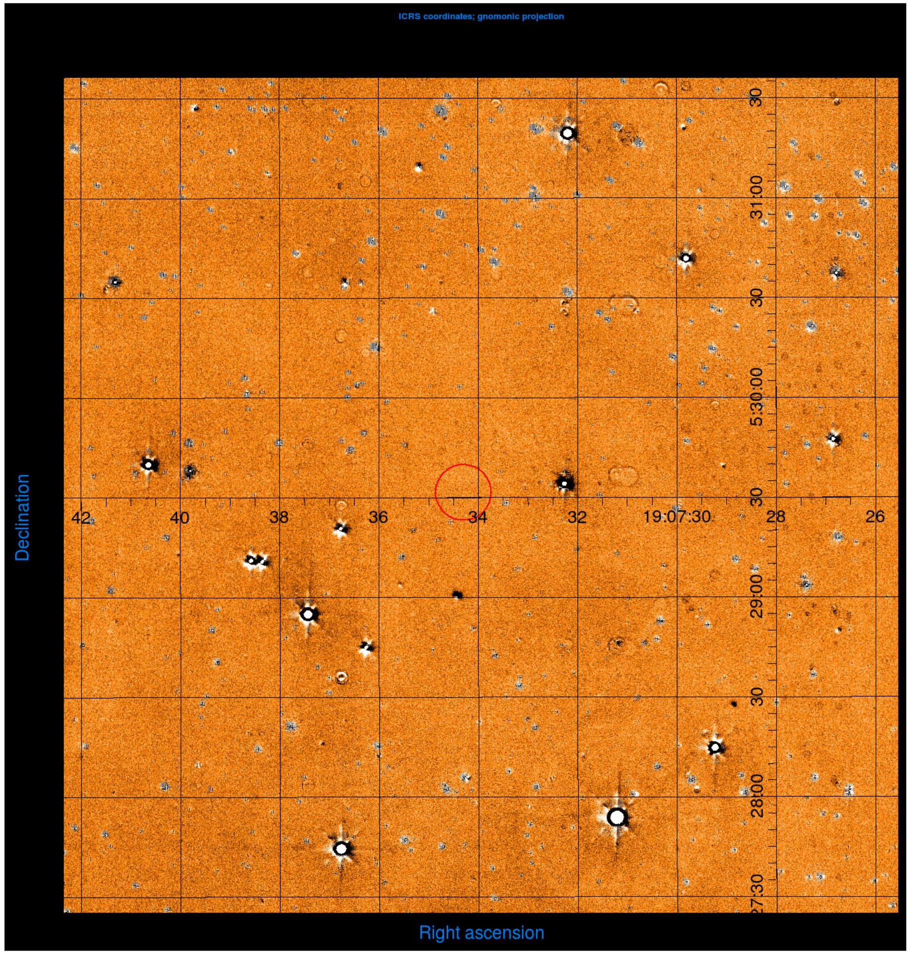

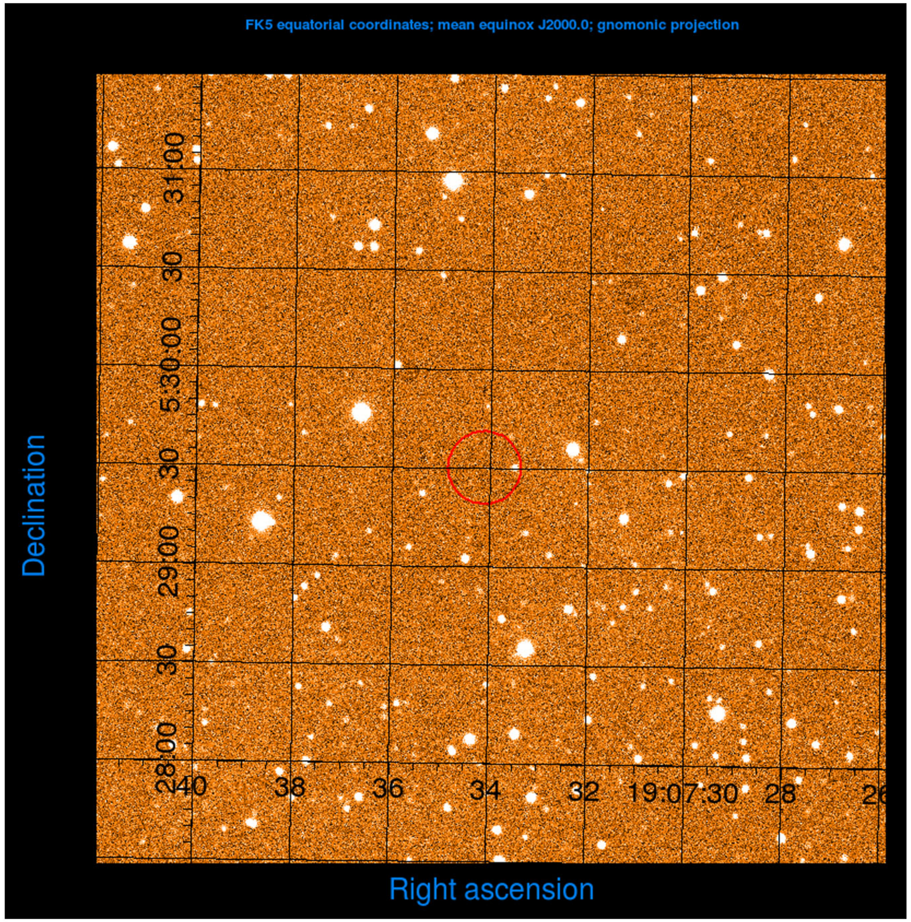

Comparison of IPHAS28, H_2 on the left, Hα on the right

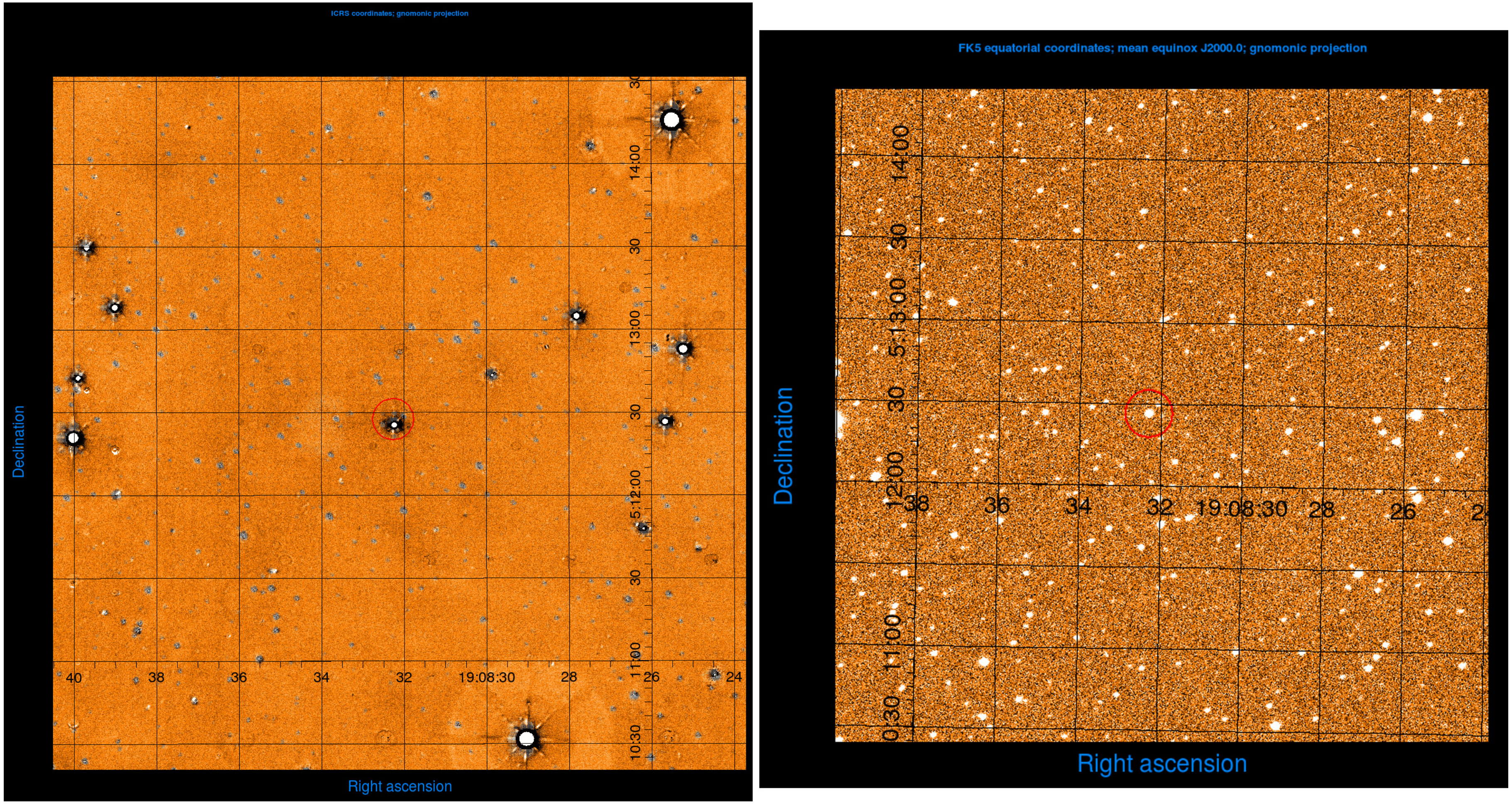

Comparison of IPHAS29, H_2 on the left, Hα on the right

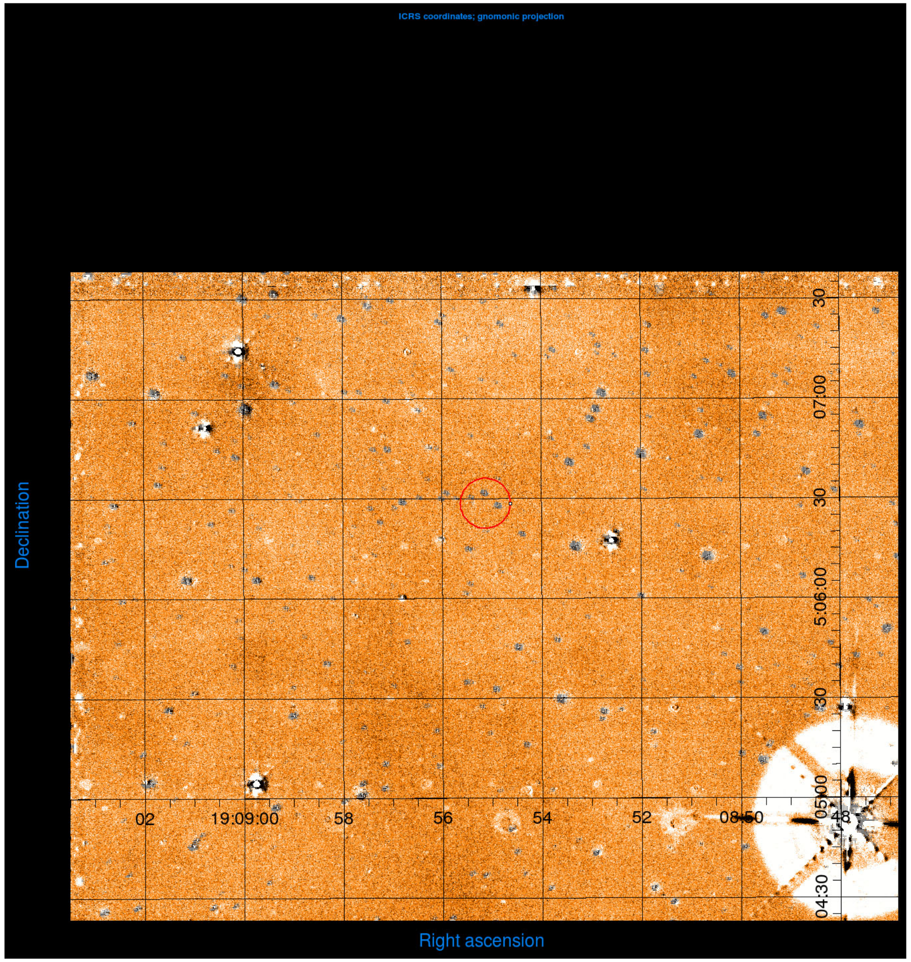

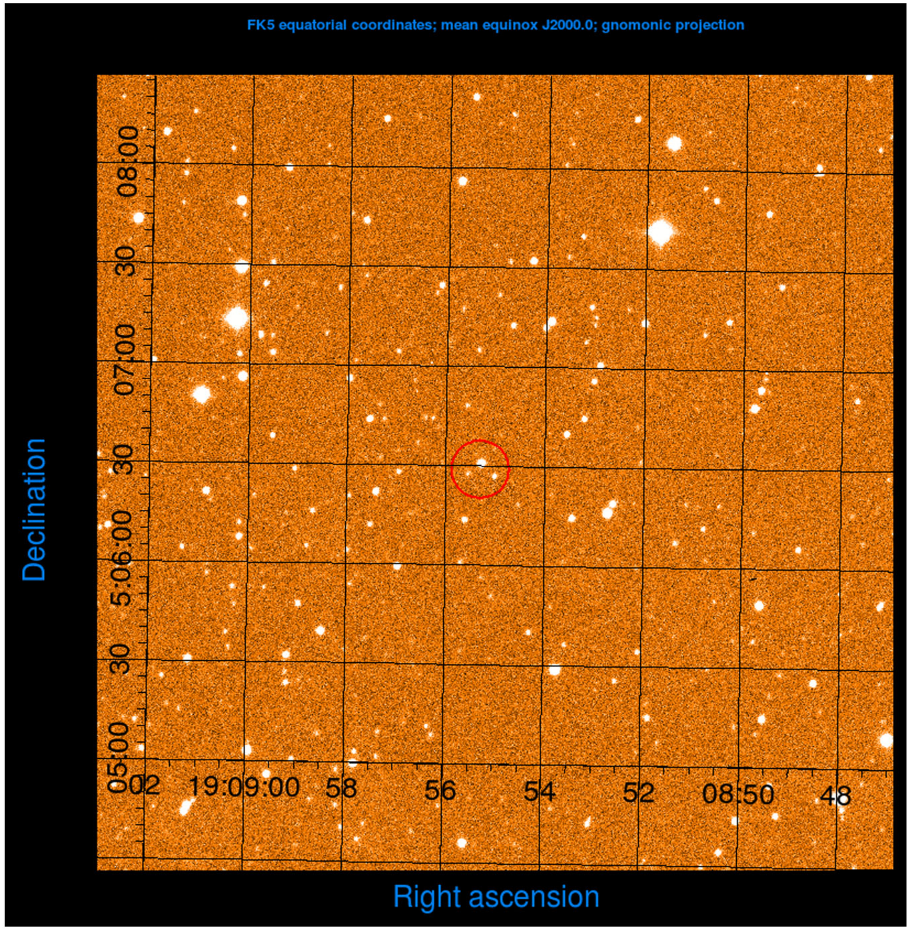

Comparison of IPHAS30, H_2 on the left, Hα on the right

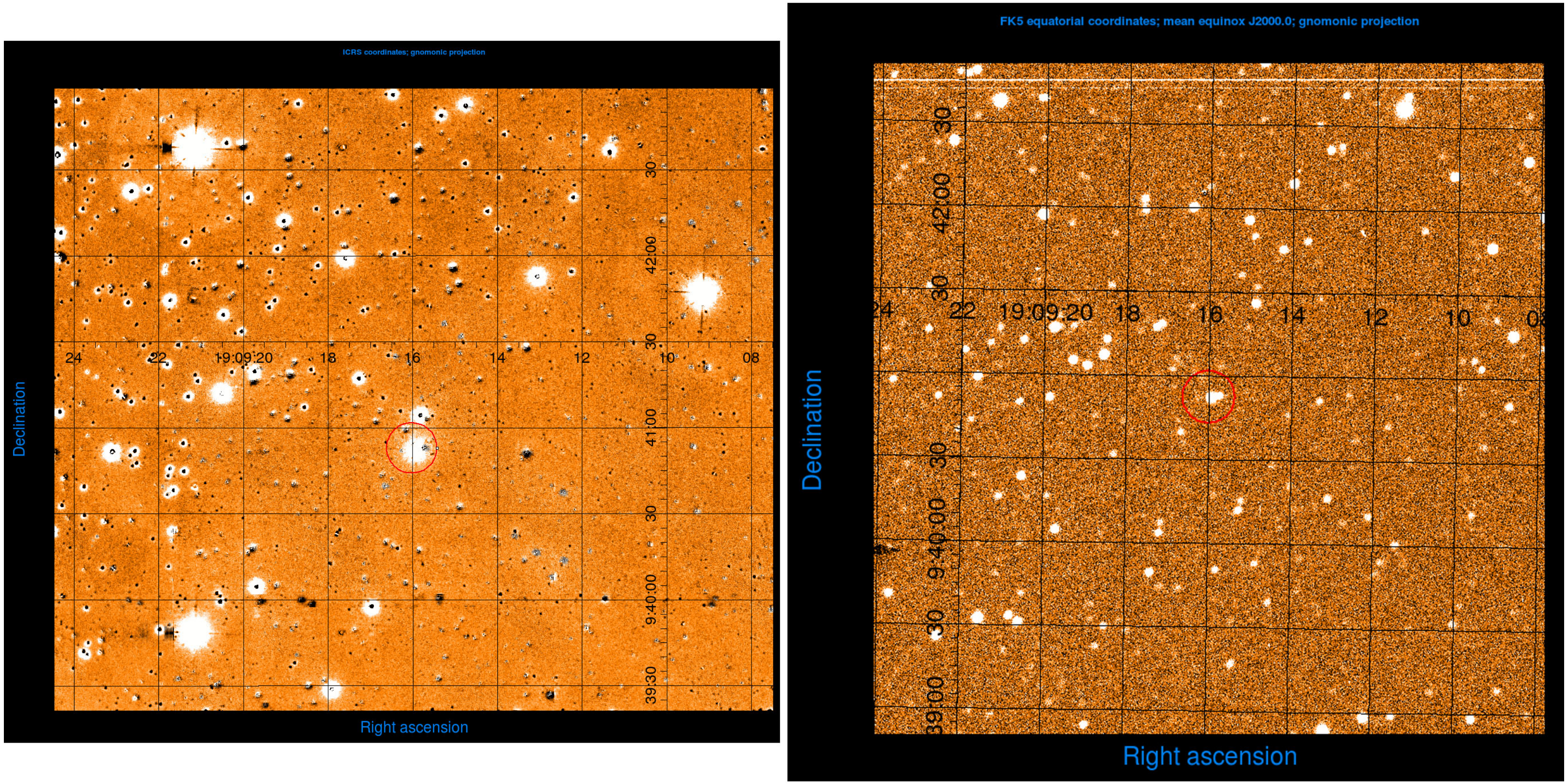

Comparison of IPHAS31, H_2 on the left, Hα on the right

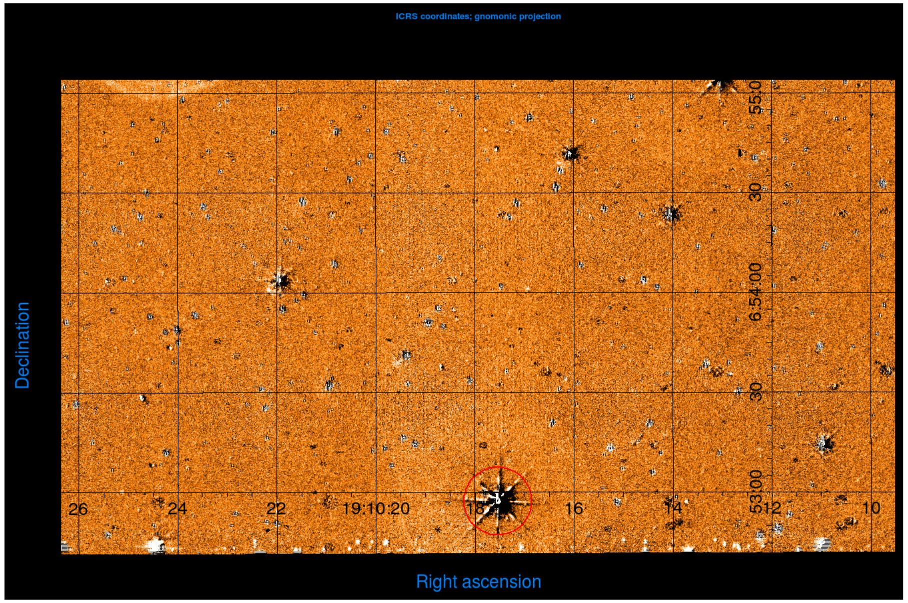

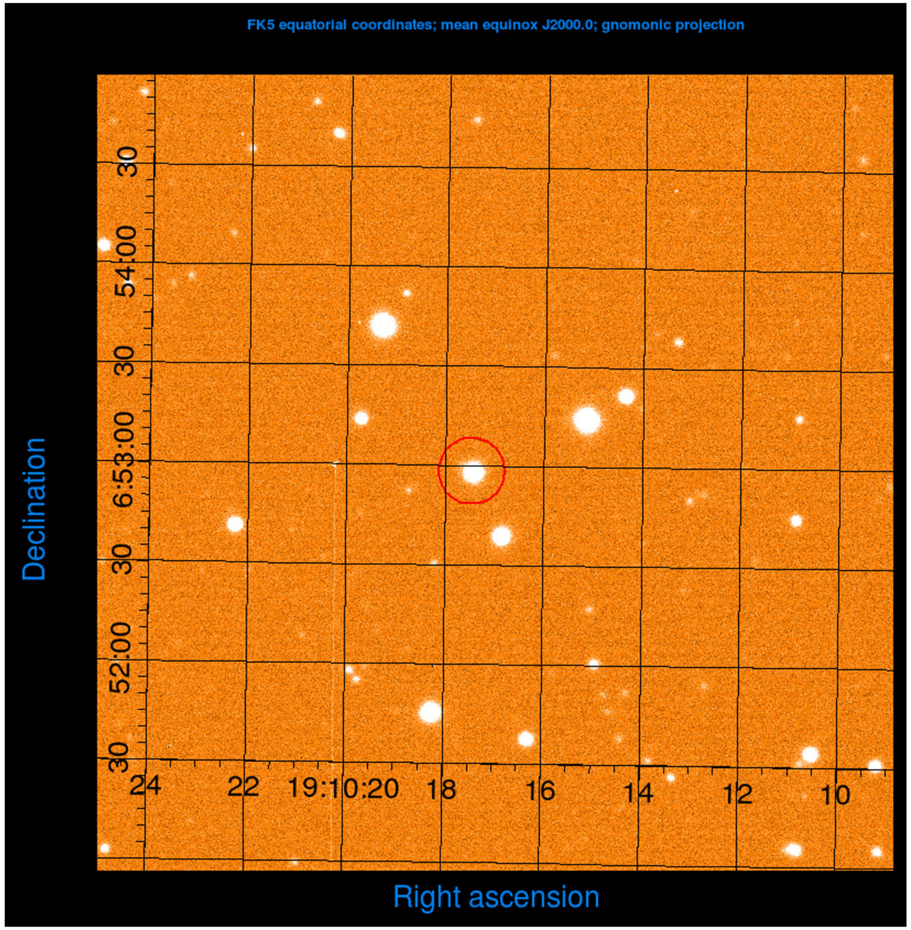

Comparison of IPHAS32, H_2 on the left, Hα on the right

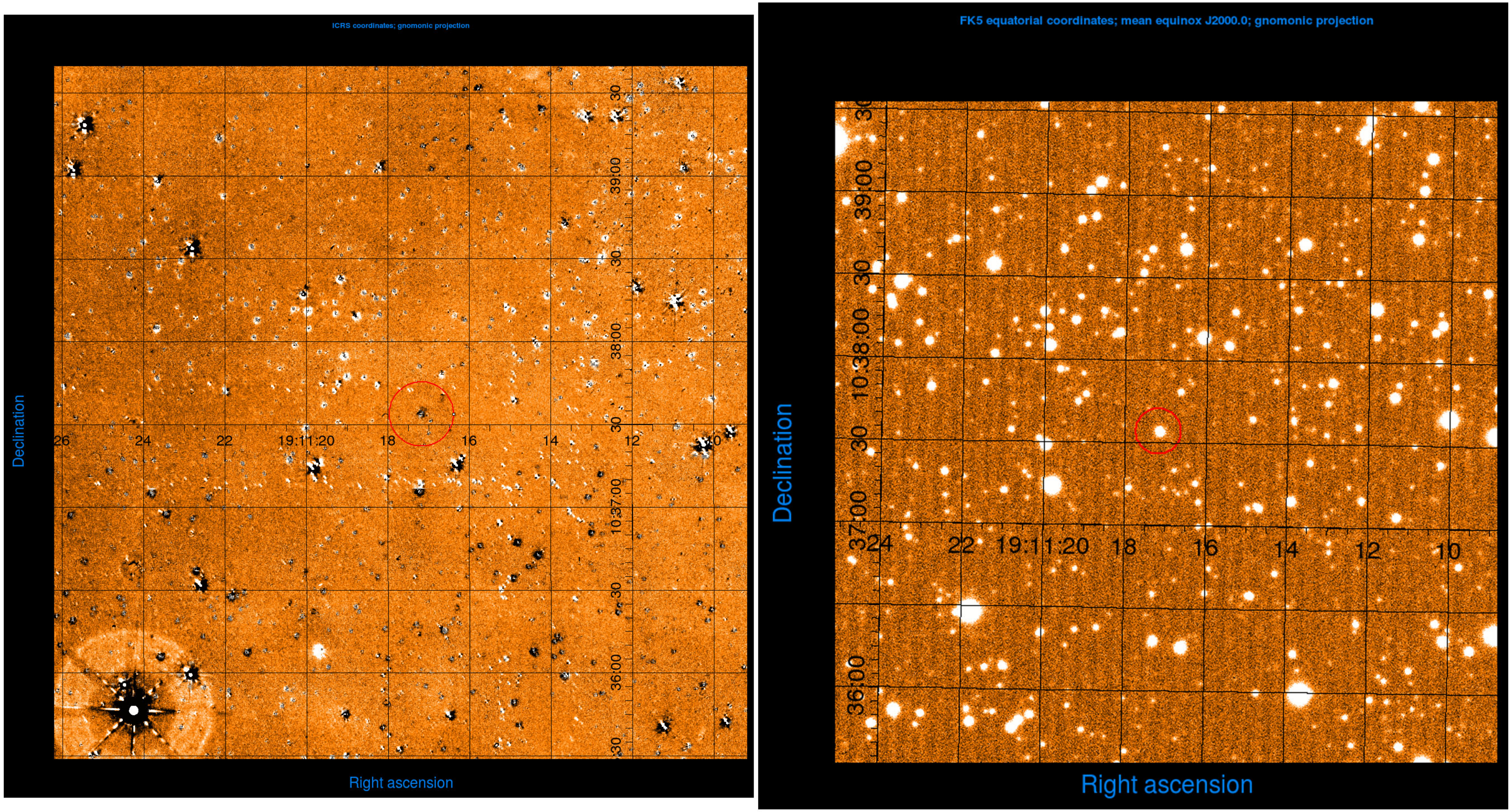

Comparison of IPHAS32, H_2 on the left, Hα on the right

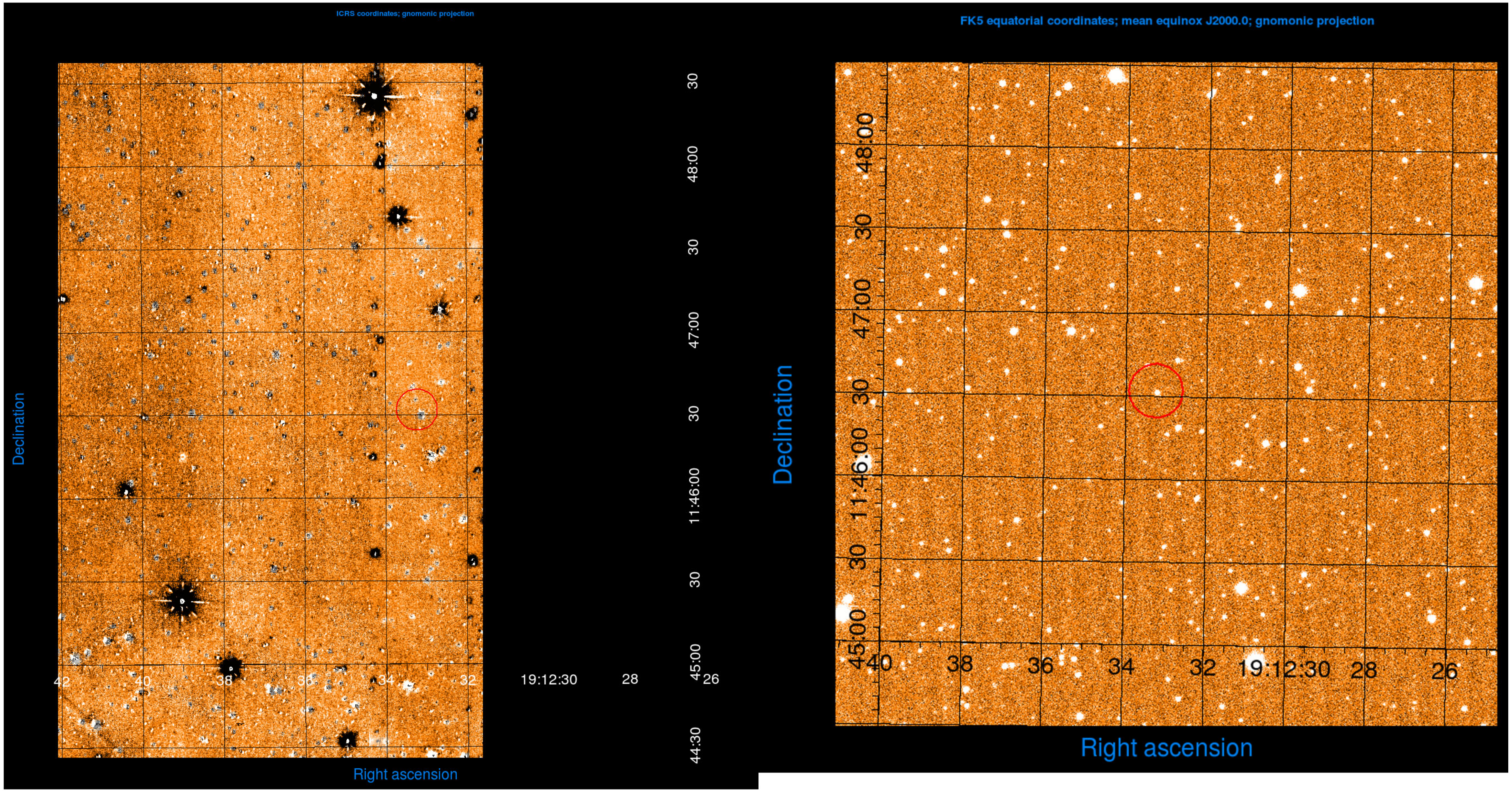

Comparison of IPHAS34, H_2 on the left, Hα on the right

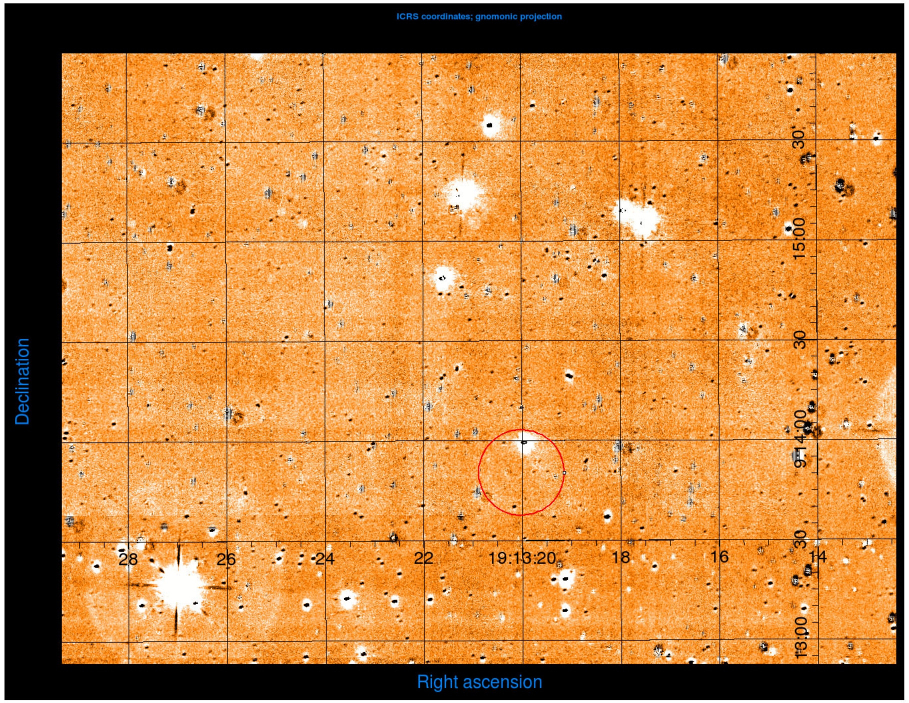

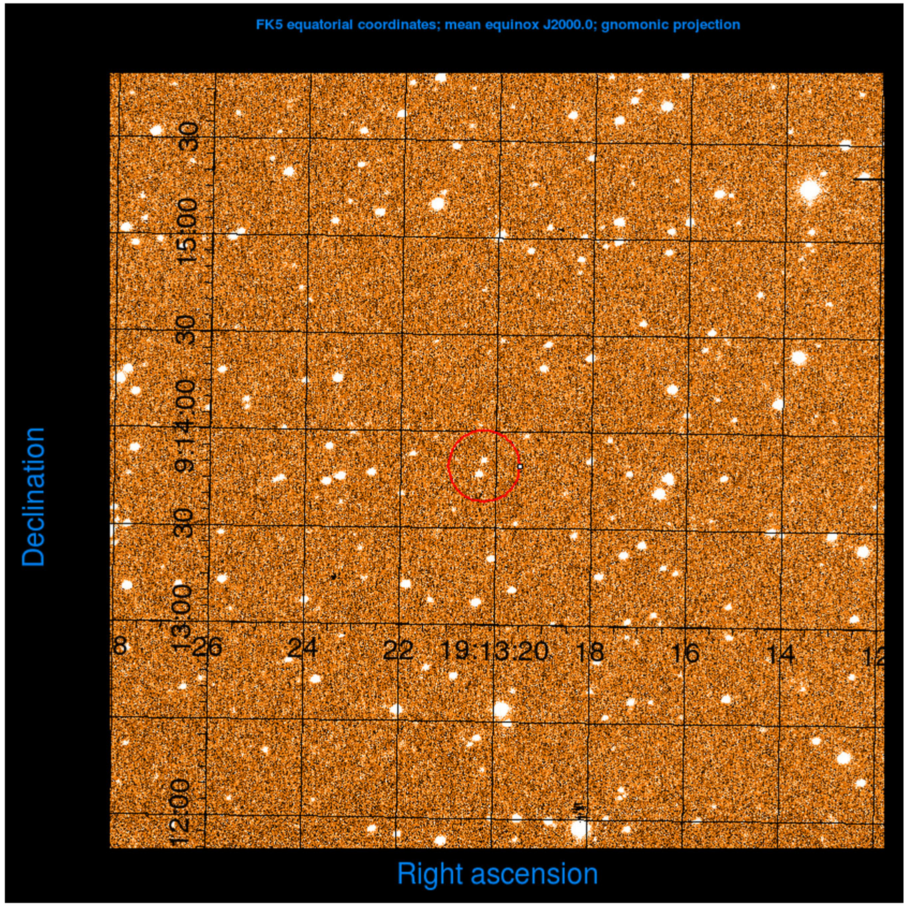

Comparison of IPHAS35, H_2 on the left, Hα on the right

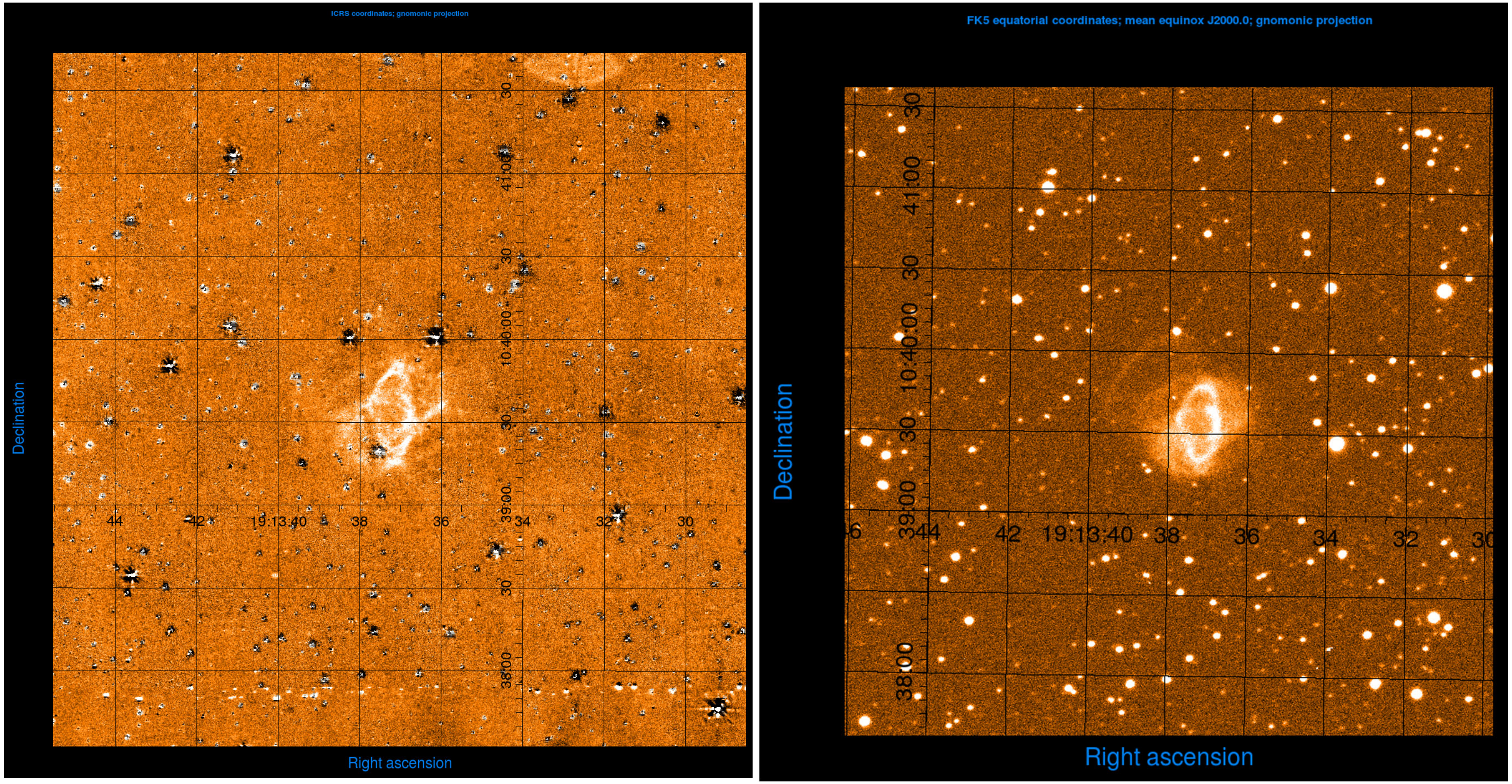

Comparison of IPHAS36, H_2 on the left, Hα on the right

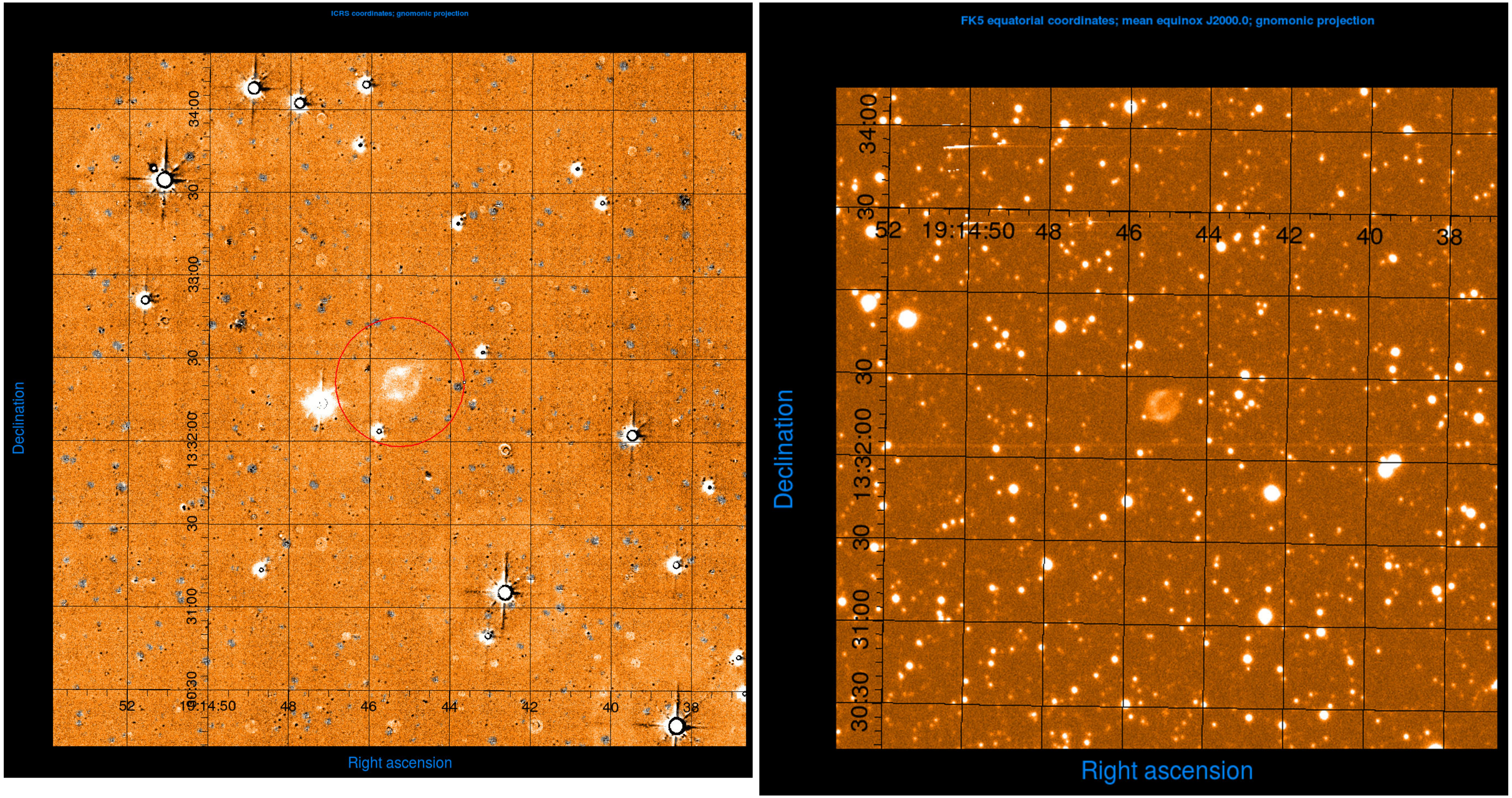

Comparison of IPHAS37, H_2 on the left, Hα on the right

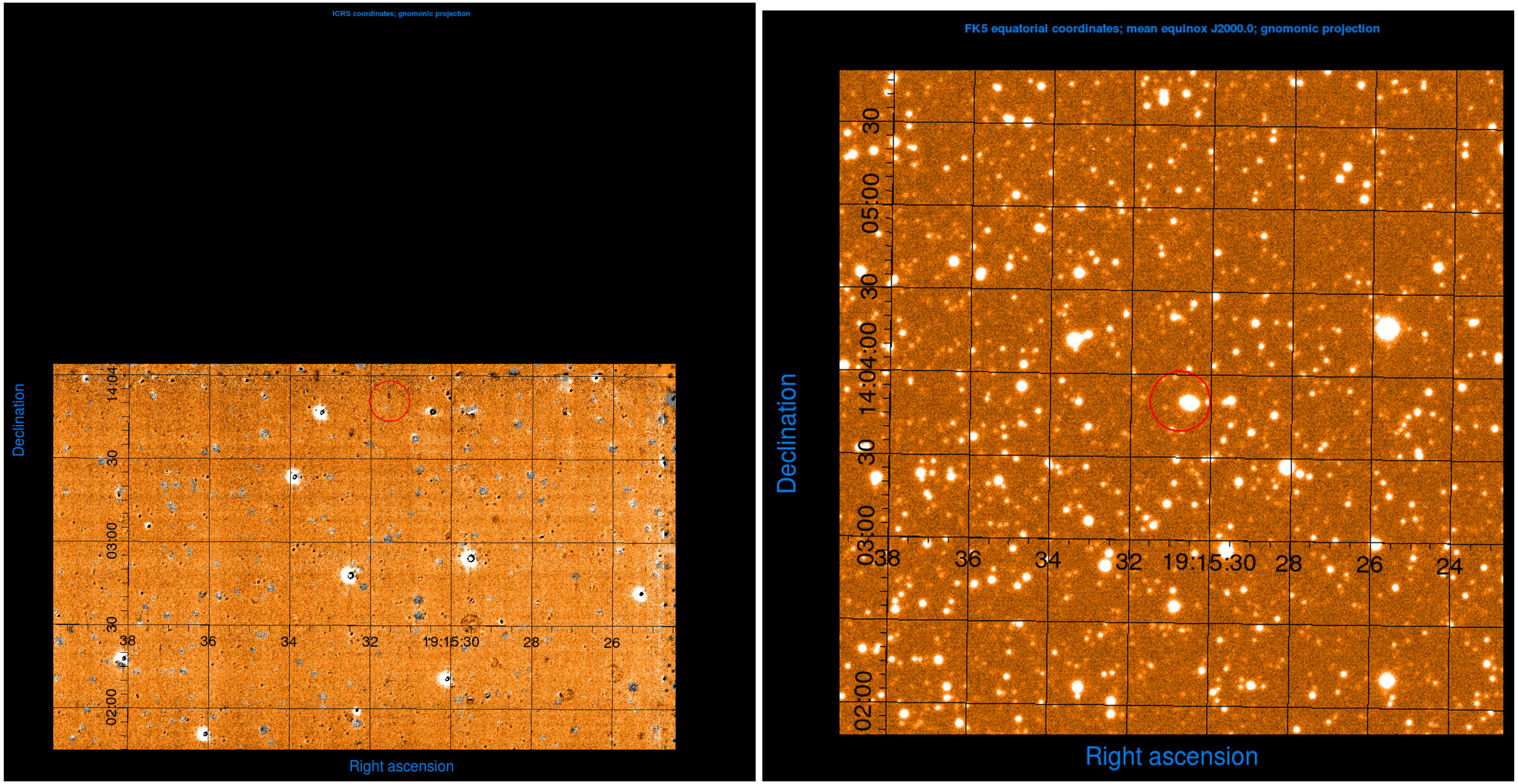

Comparison of IPHAS38, H_2 on the left, Hα on the right

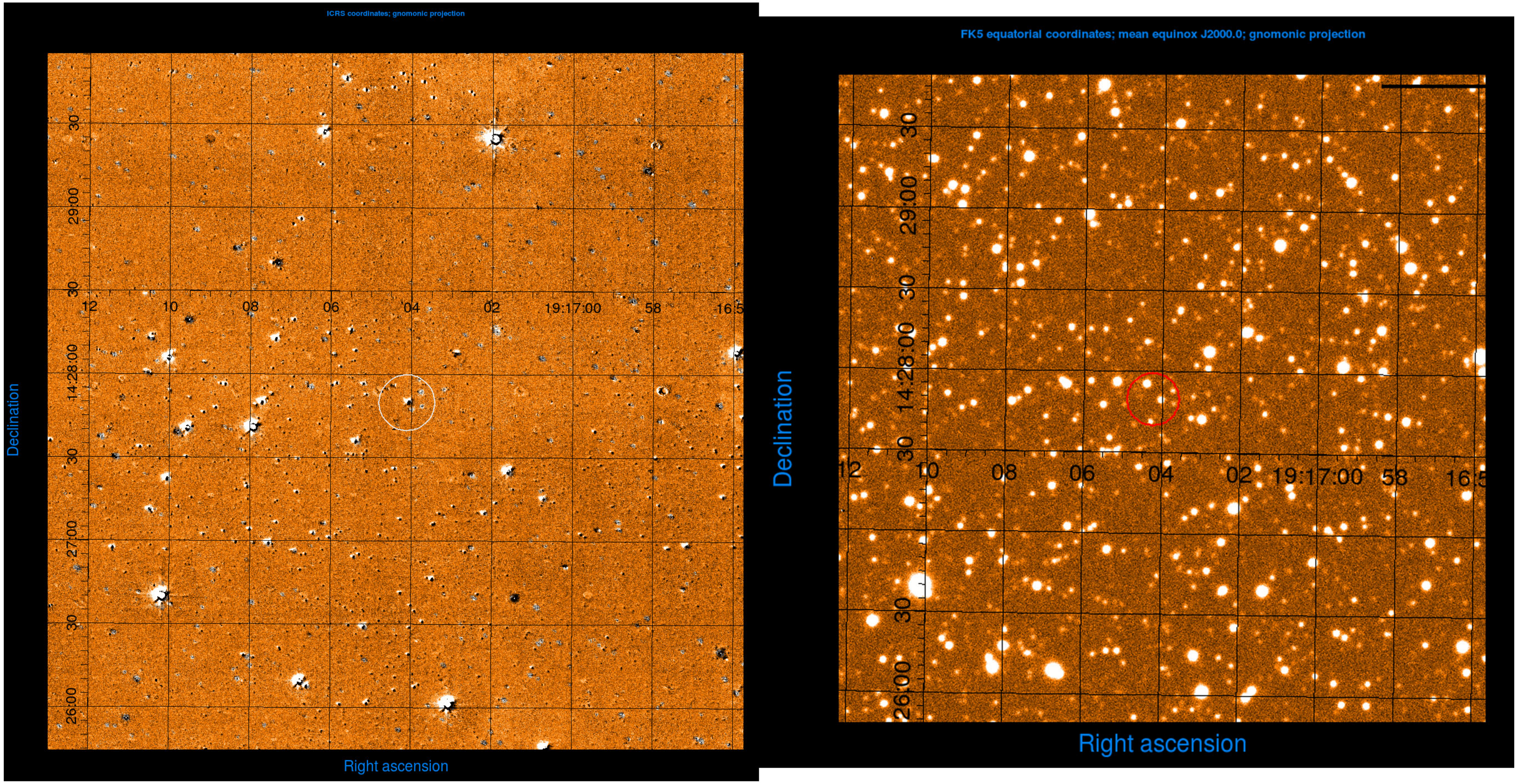

Comparison of IPHAS39, H_2 on the left, Hα on the right

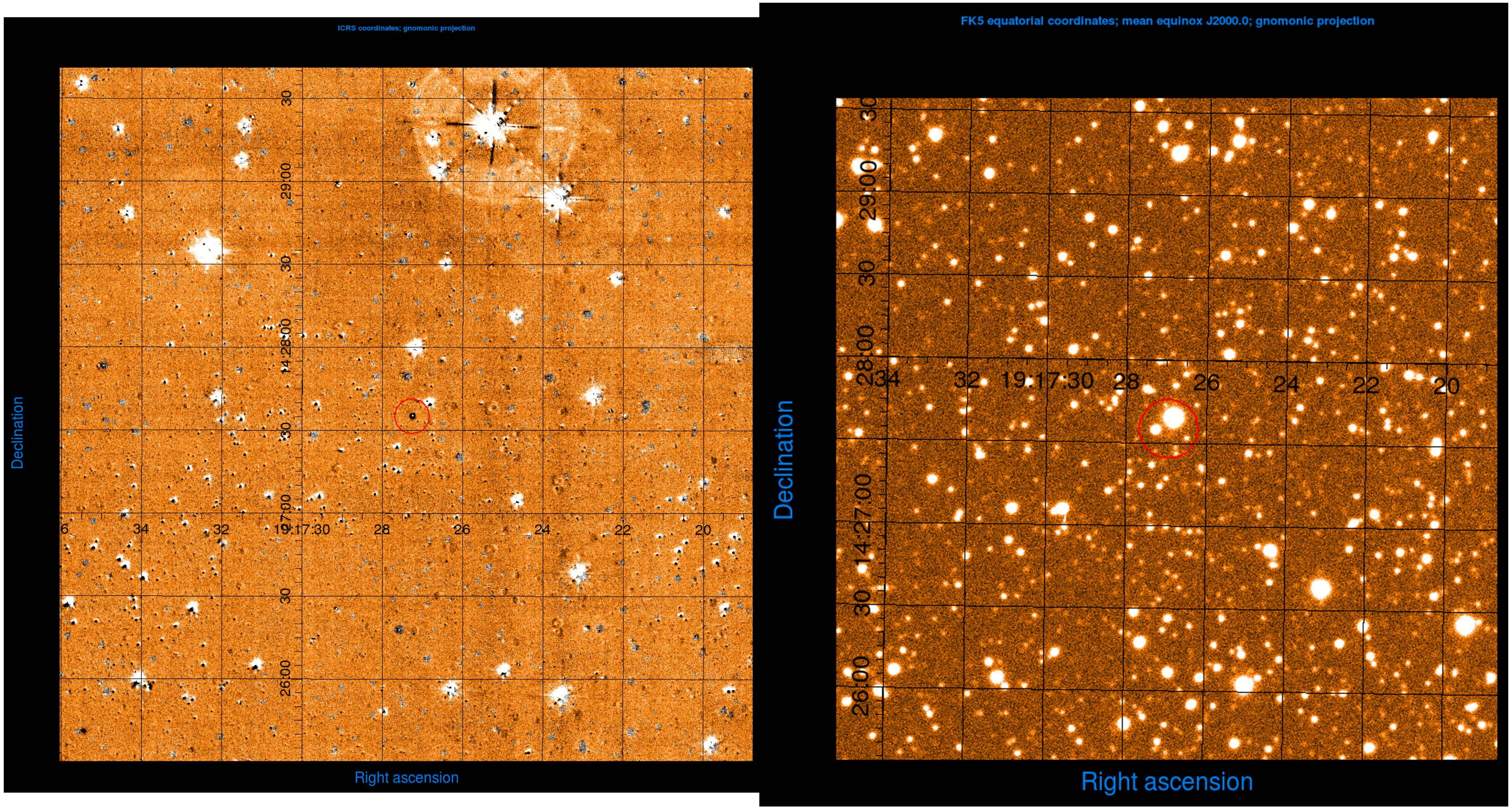

Comparison of IPHAS40, H_2 on the left, Hα on the right

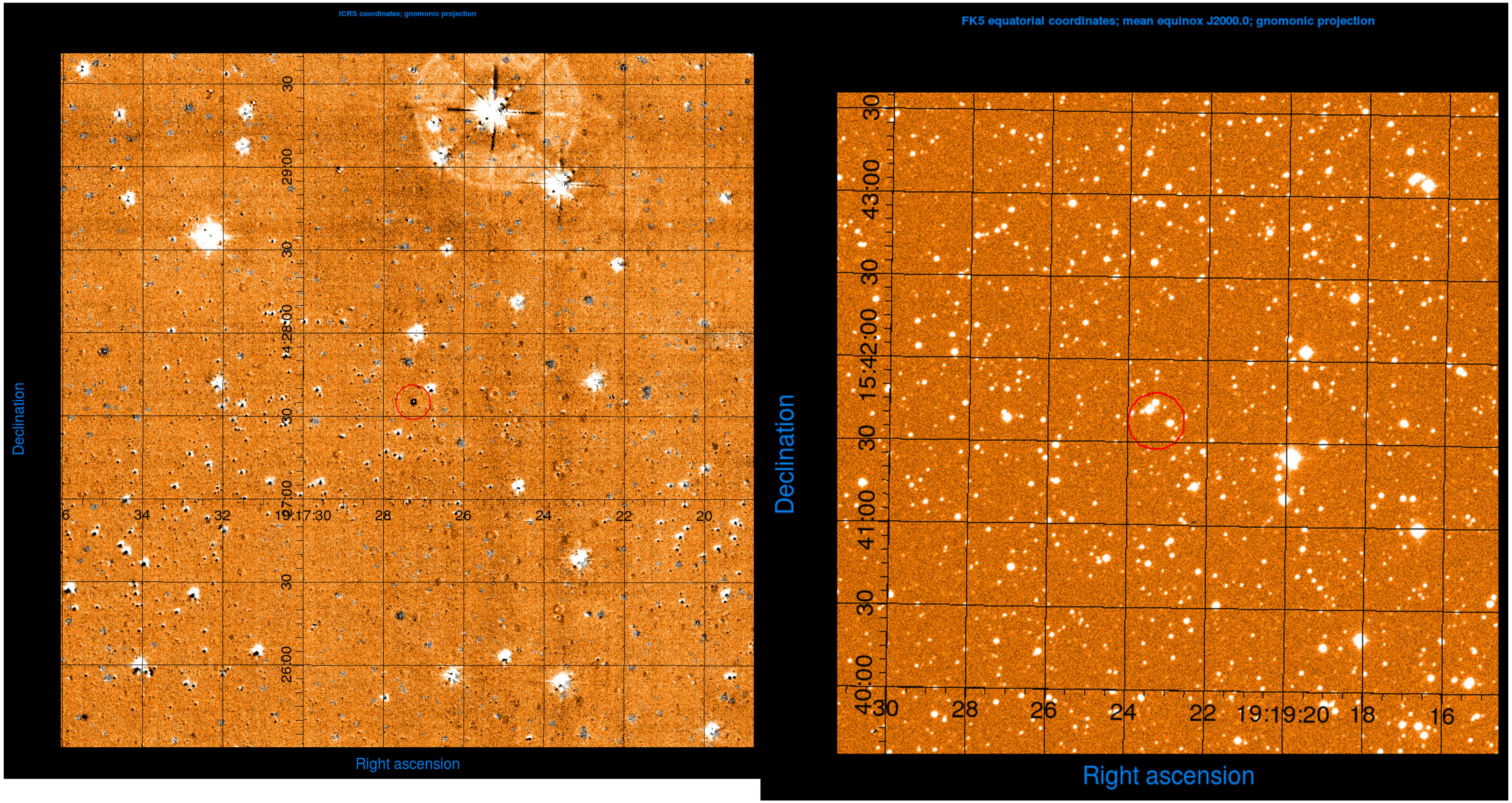

Comparison of IPHAS41, H_2 on the left, Hα on the right

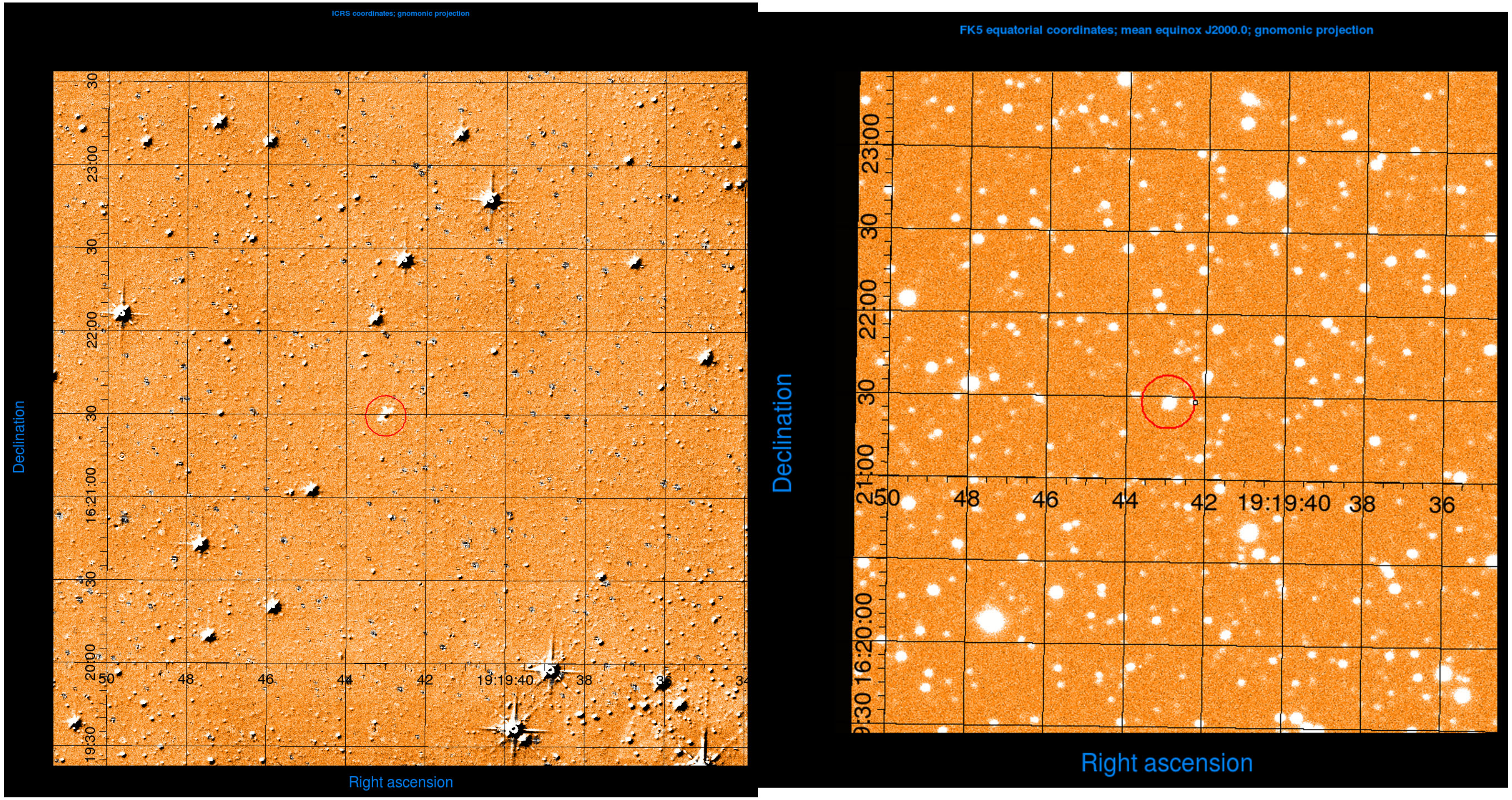

Comparison of IPHAS42, H_2 on the left, $H\alpha$ on the right

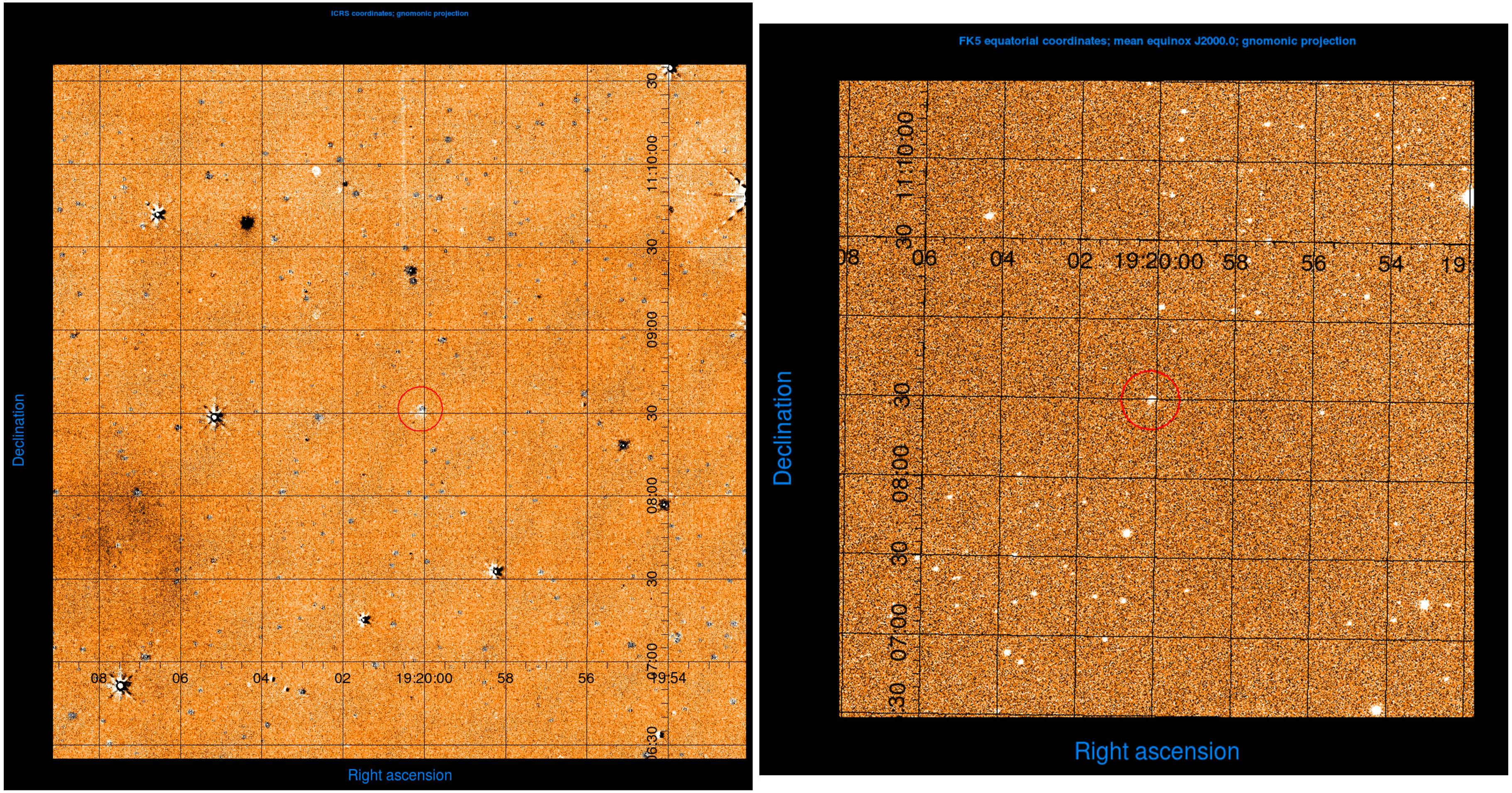

Comparison of IPHAS43, H_2 on the left, Hα on the right

IPHAS44_Comparison.jpg

Comparison of IPHAS44, H_2 on the left, Hα on the right

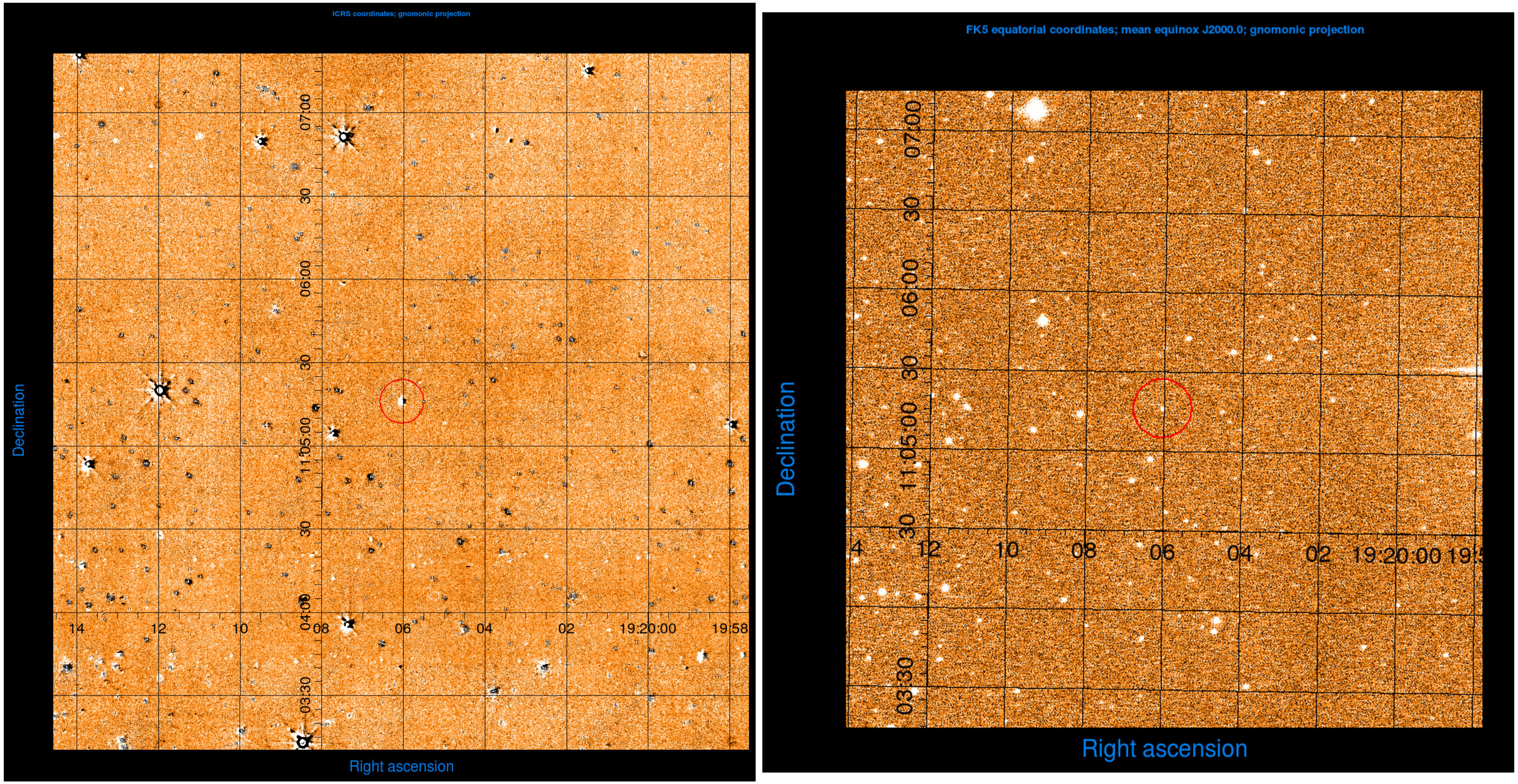

Comparison of IPHAS45, H_2 on the left, $H\alpha$ on the right

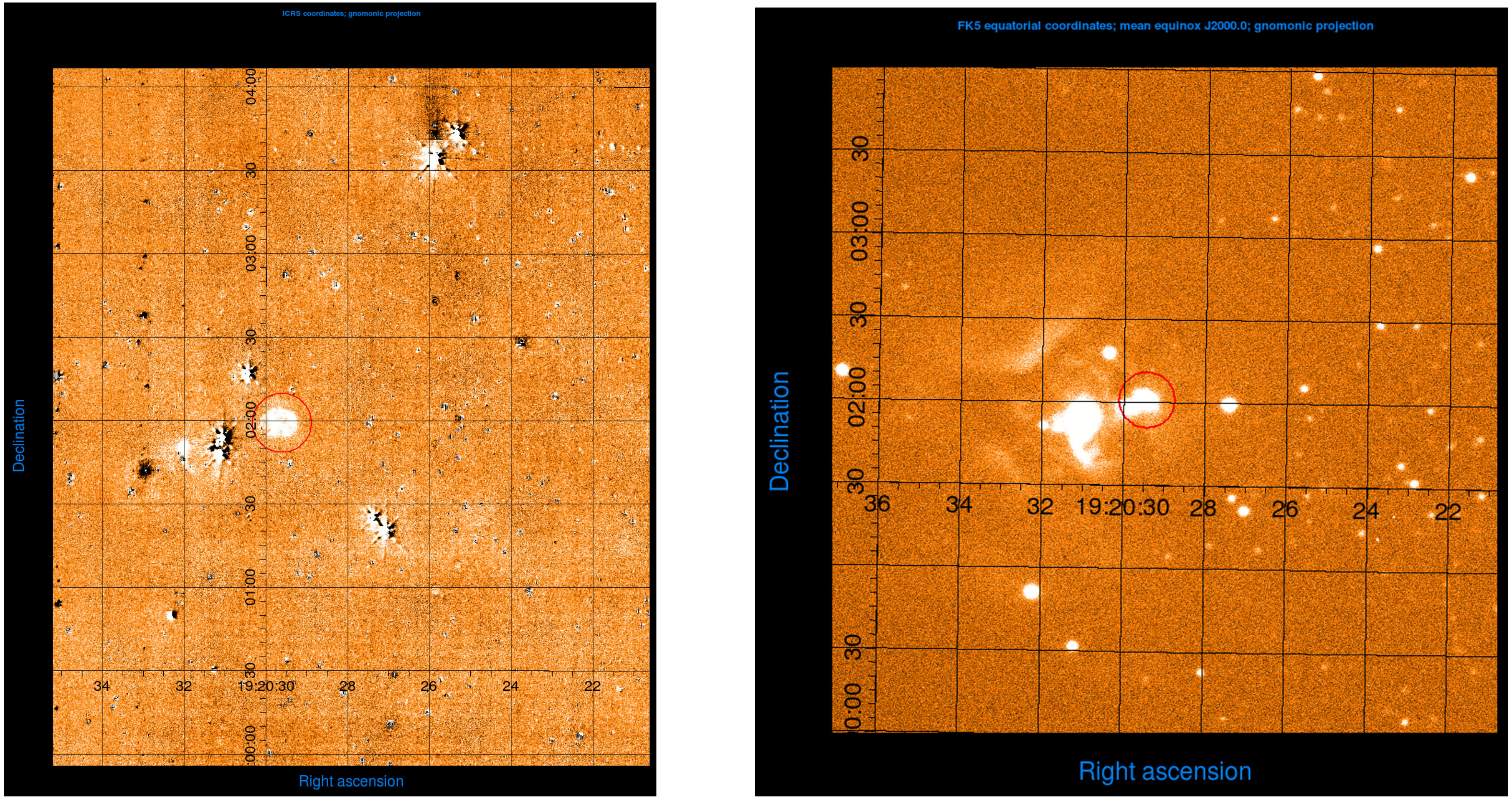

Comparison of IPHAS46, H_2 on the left, Hα on the right

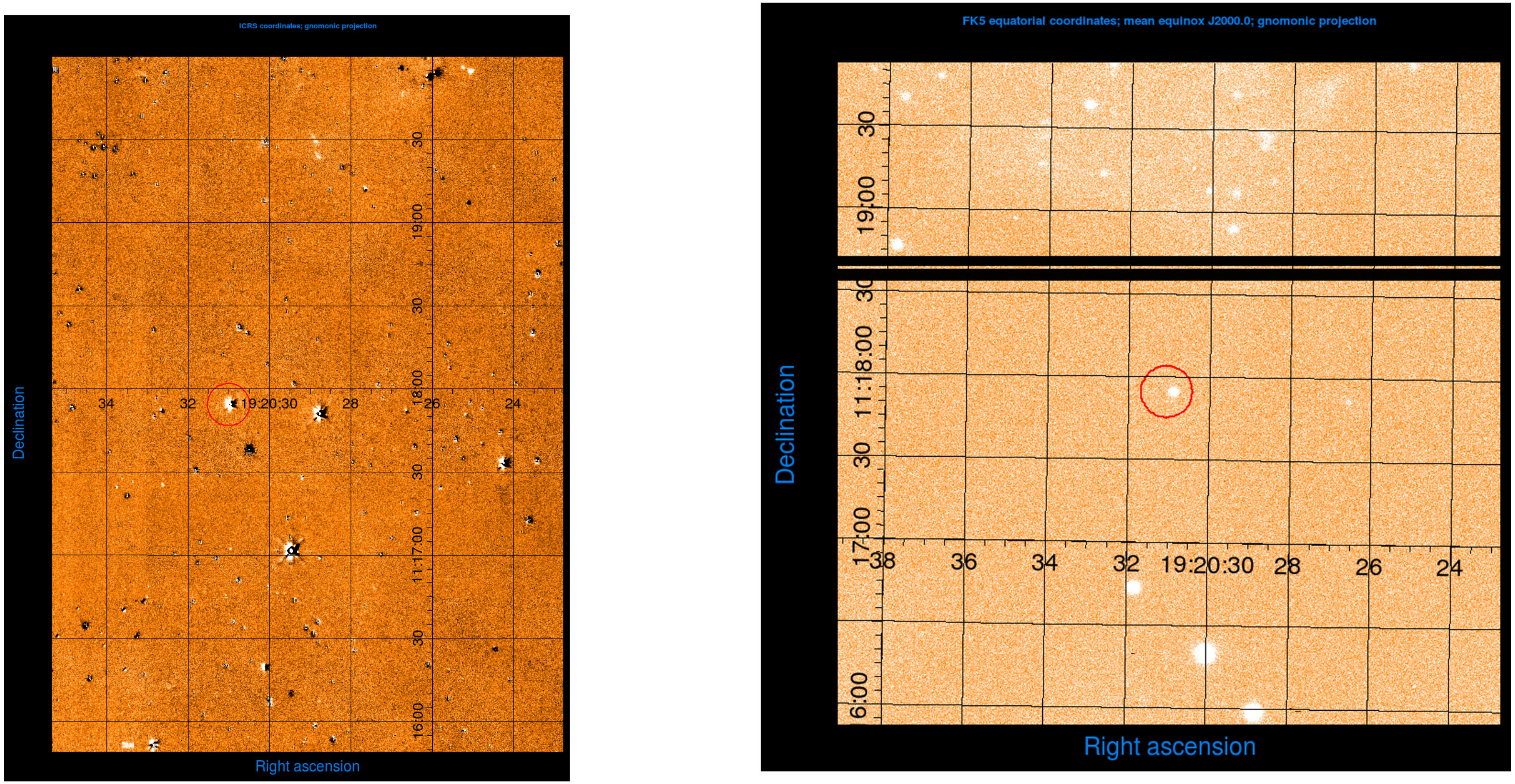

Comparison of IPHAS47, H_2 on the left, Hα on the right

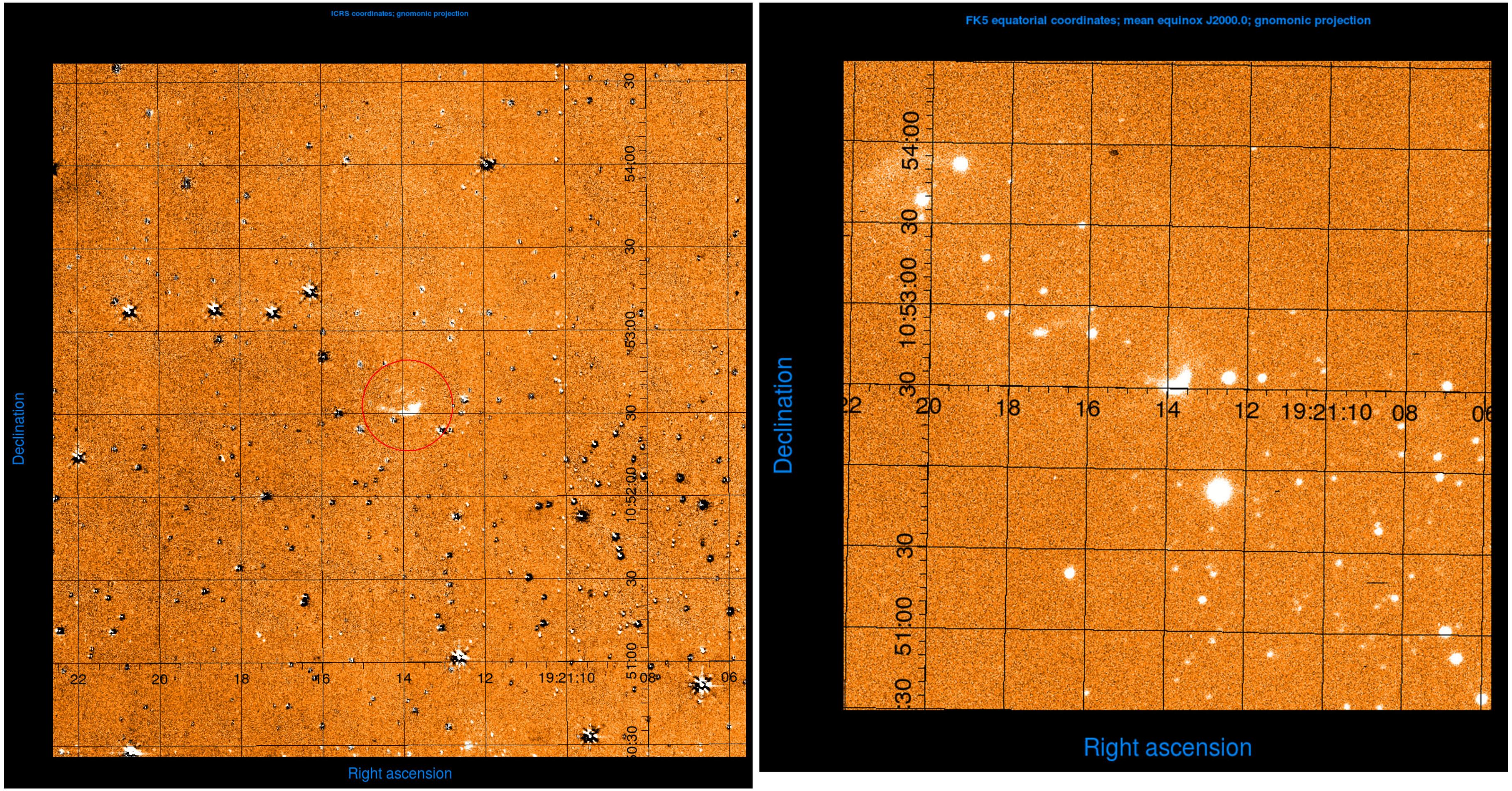

Comparison of IPHAS48, H_2 on the left, $H\alpha$ on the right

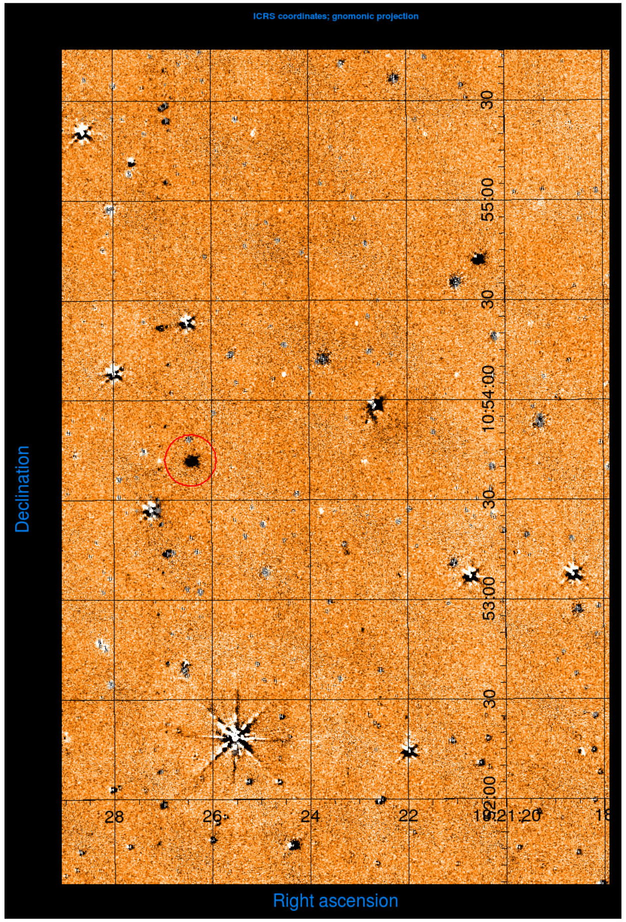

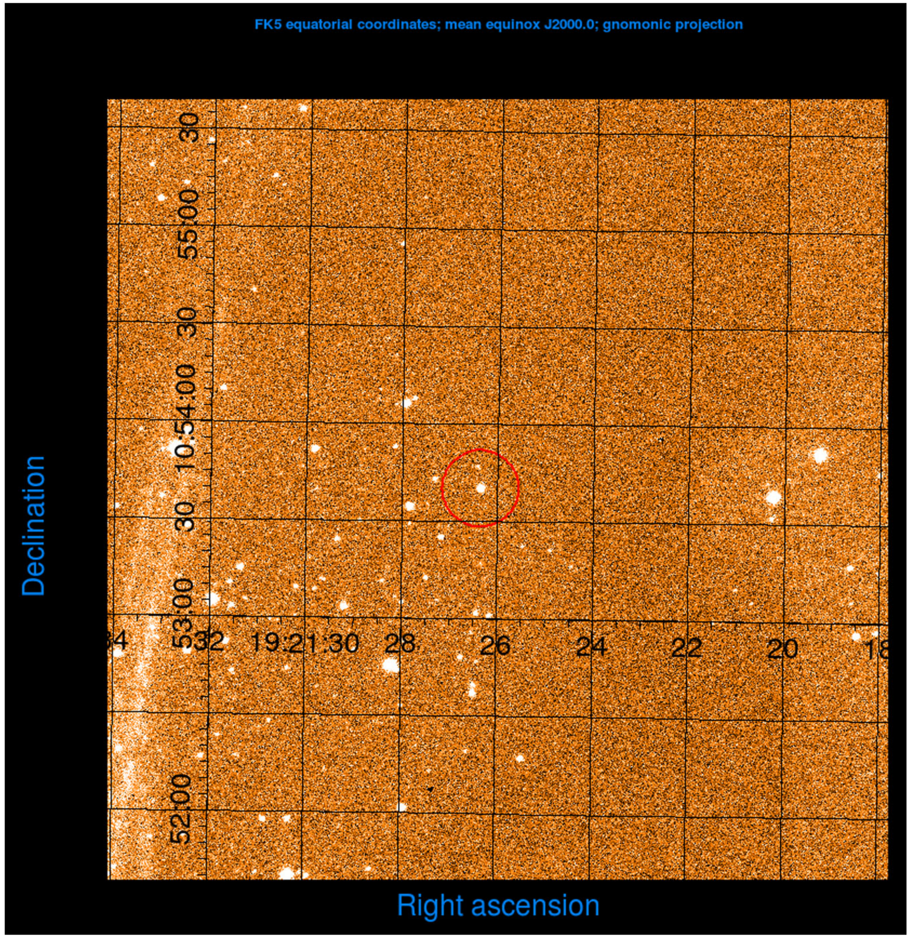

Comparison of IPHAS49, H_2 on the left, Hα on the right

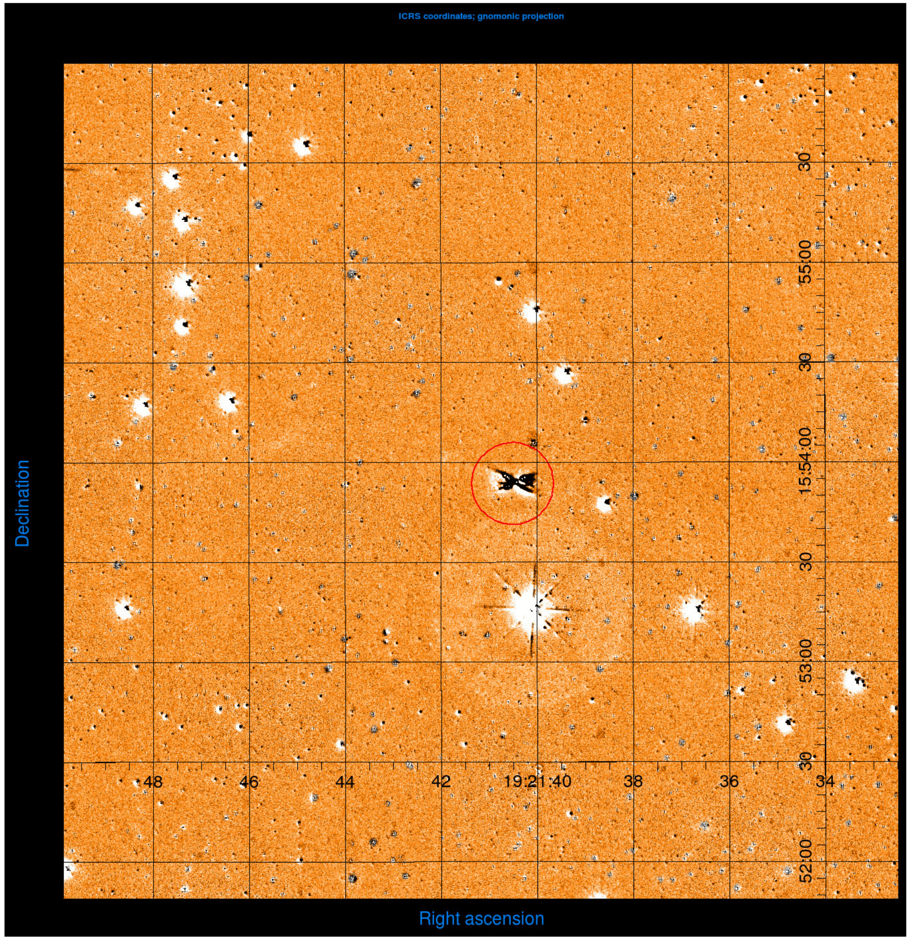

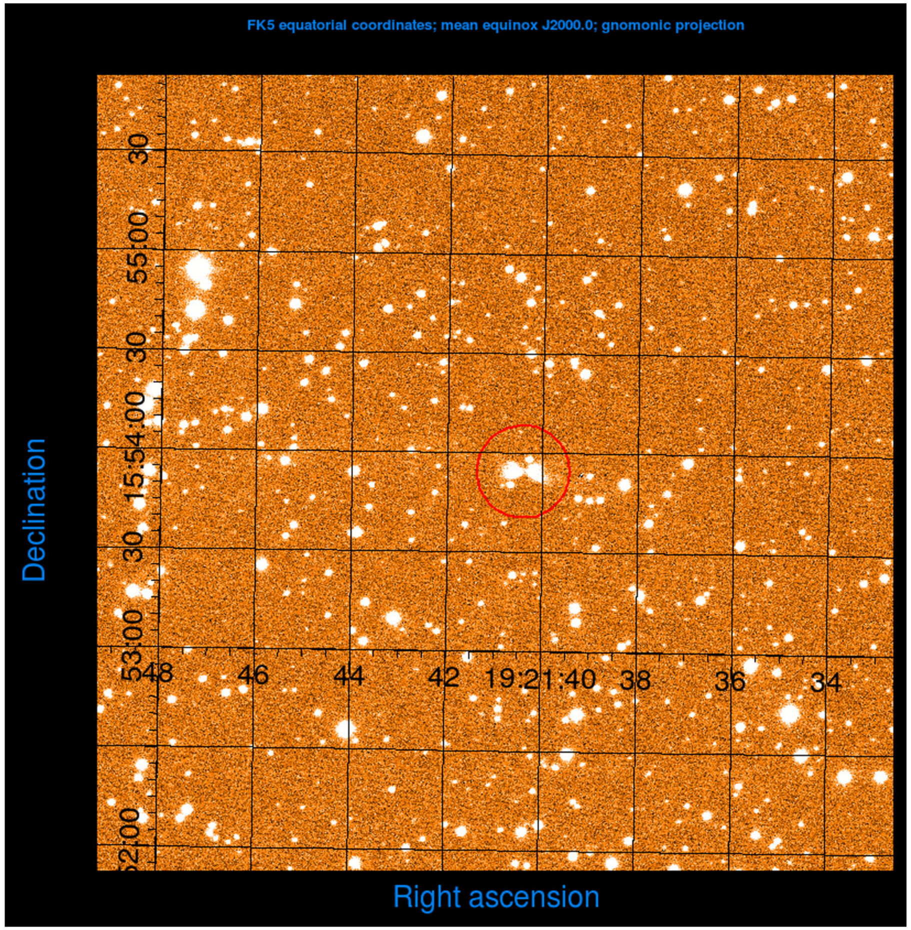

Comparison of IPHAS50, H_2 on the left, $H\alpha$ on the right

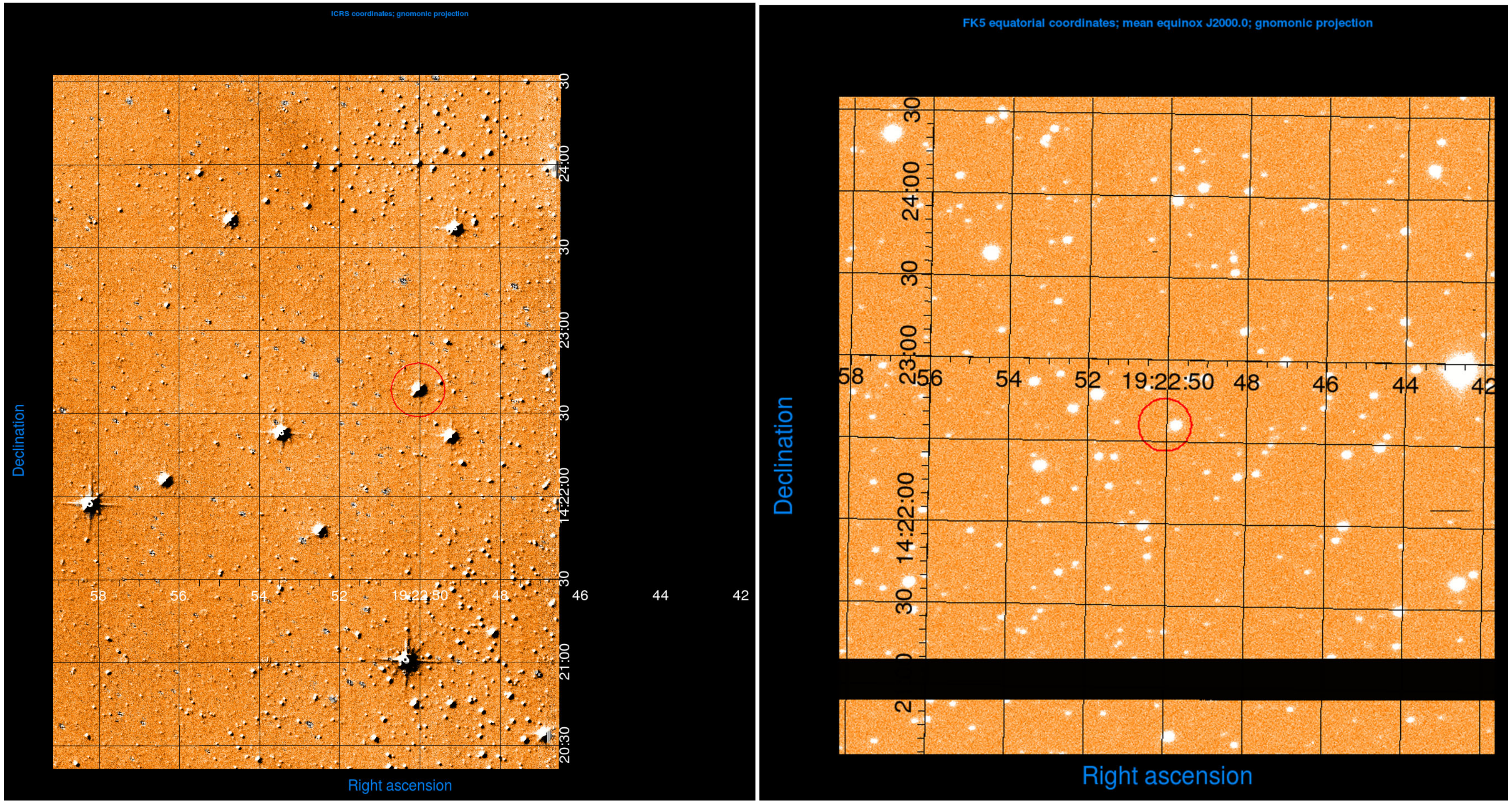

Comparison of IPHAS51, H_2 on the left, $H\alpha$ on the right

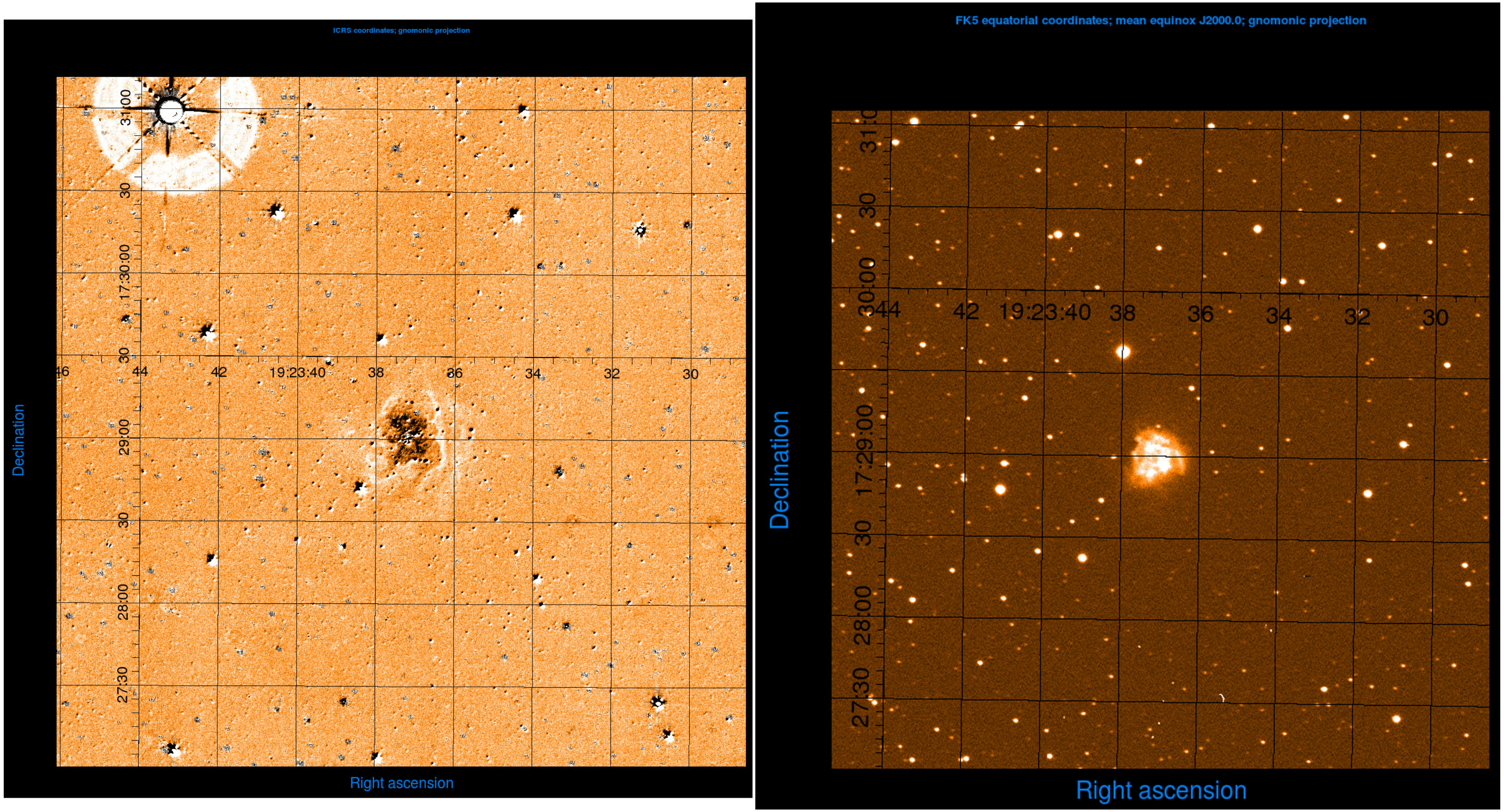

Comparison of IPHAS52, H_2 on the left, Hα on the right

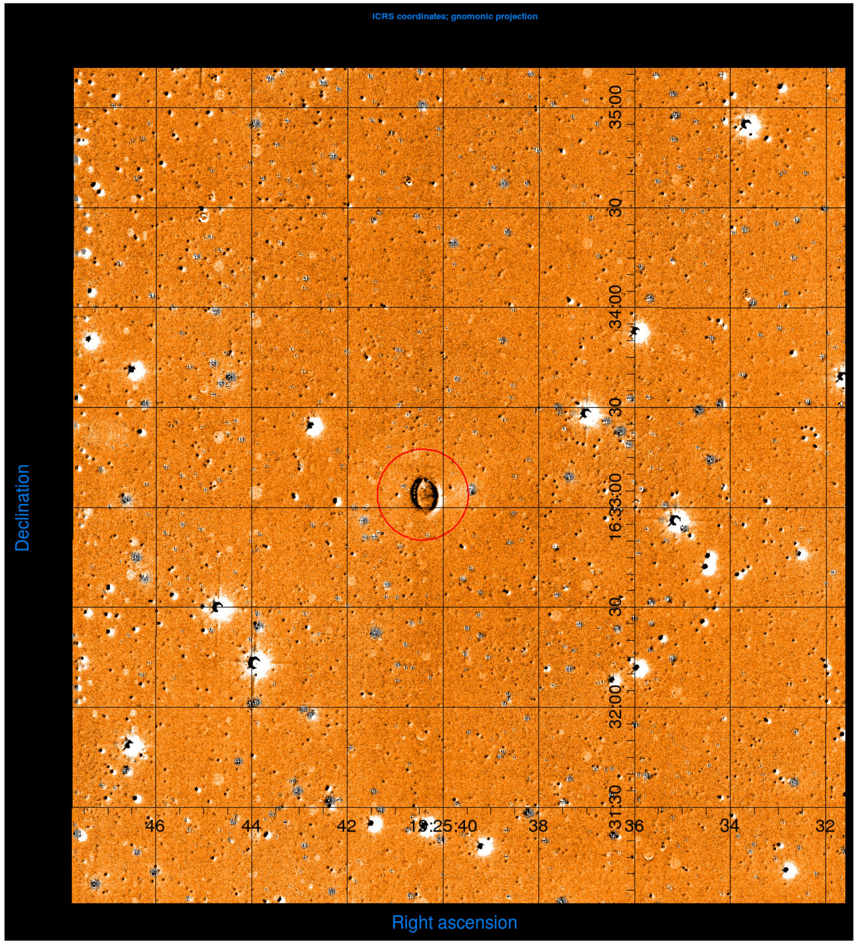

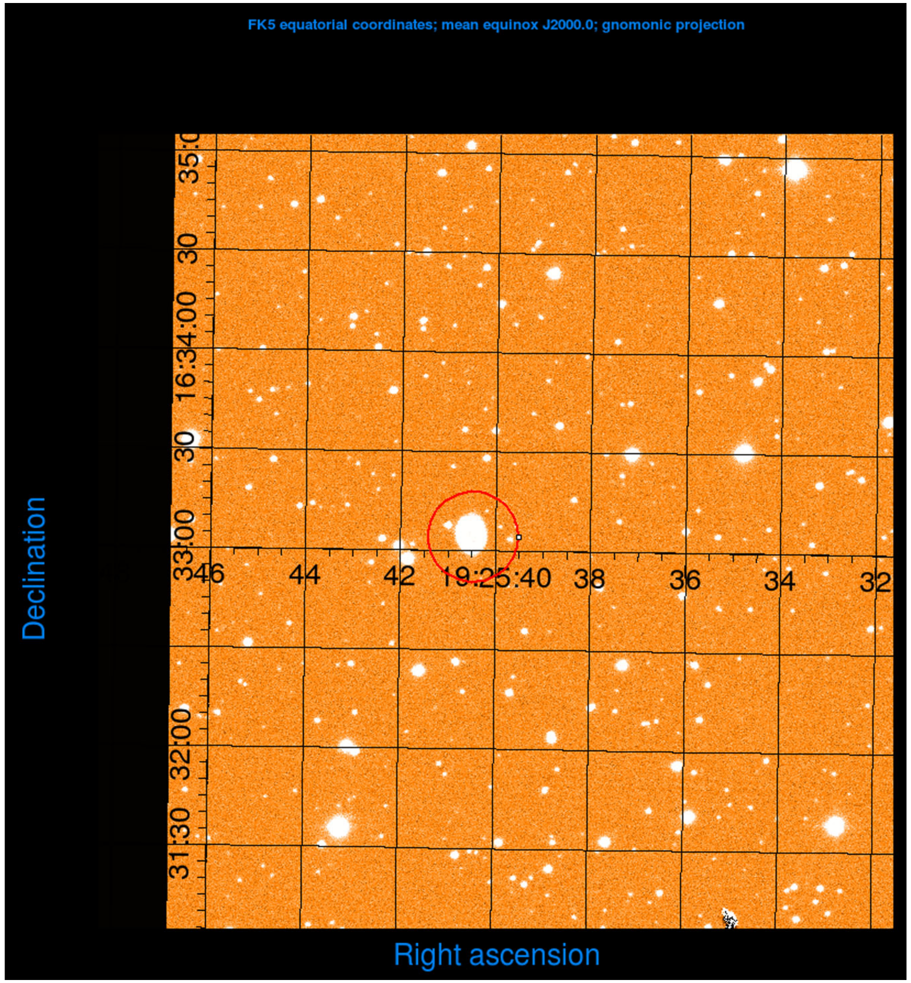

Comparison of IPHAS53, H_2 on the left, Hα on the right

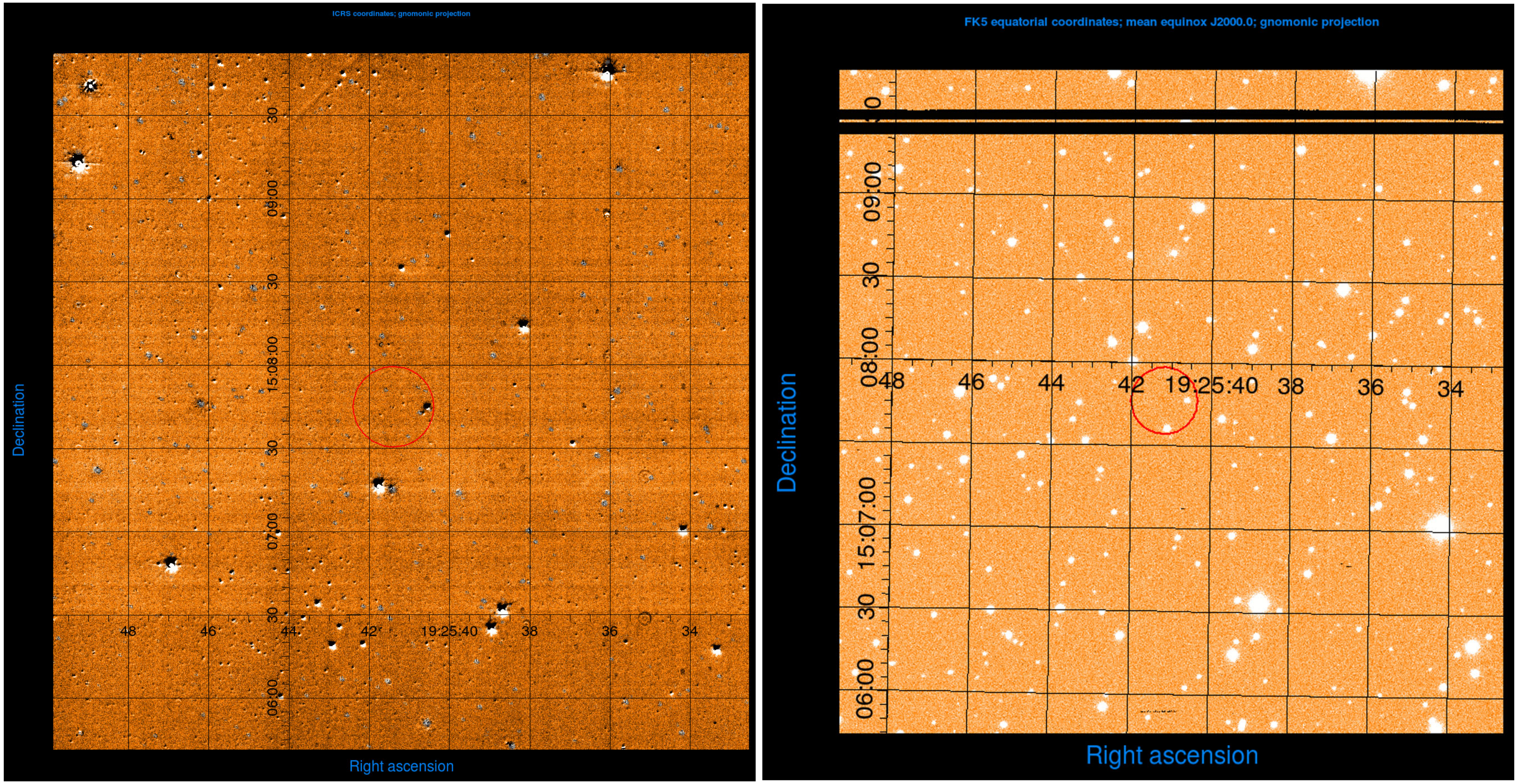

Comparison of IPHAS54, H_2 on the left, $H\alpha$ on the right

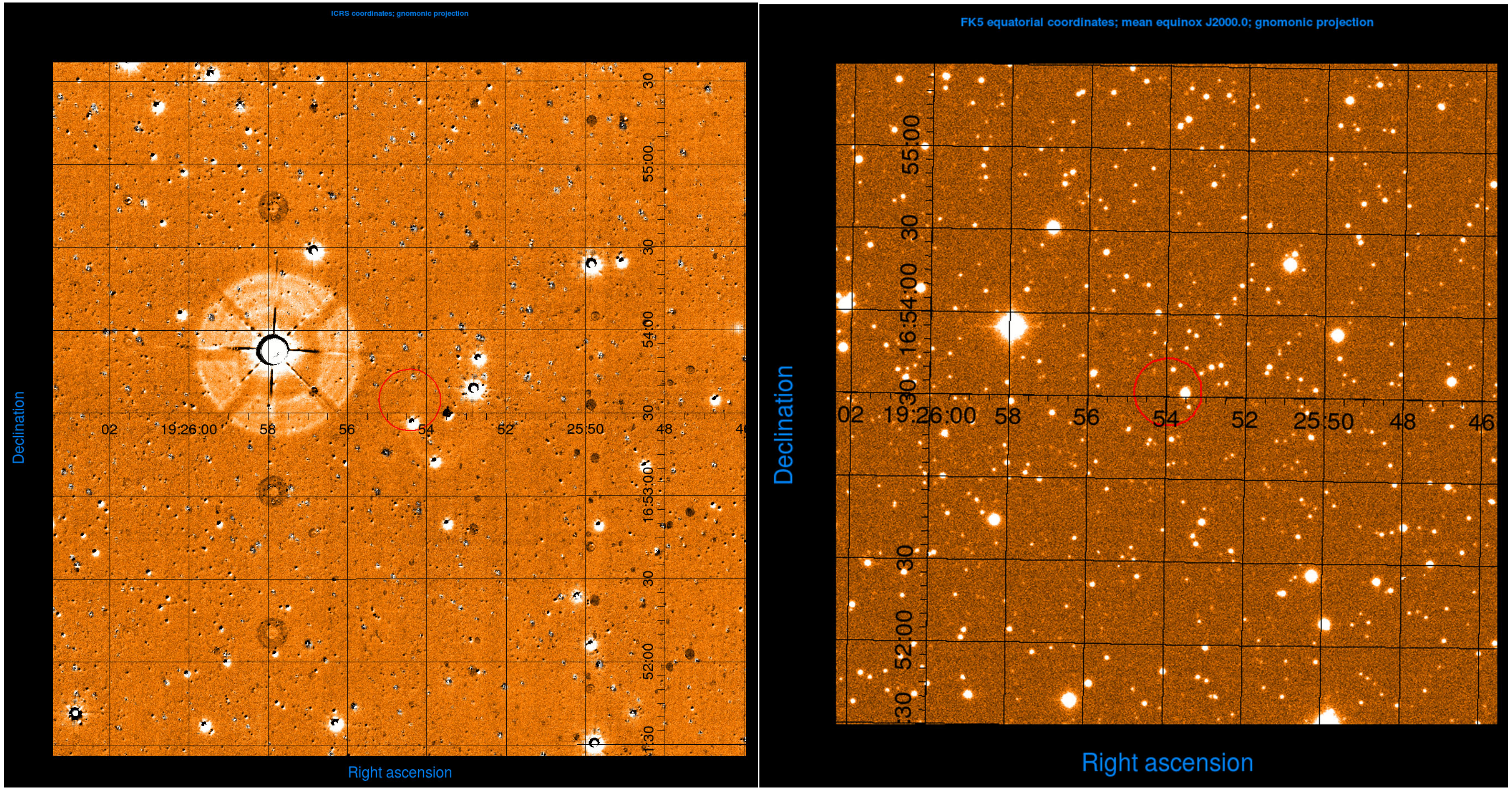

Comparison of IPHAS55, H_2 on the left, Hα on the right

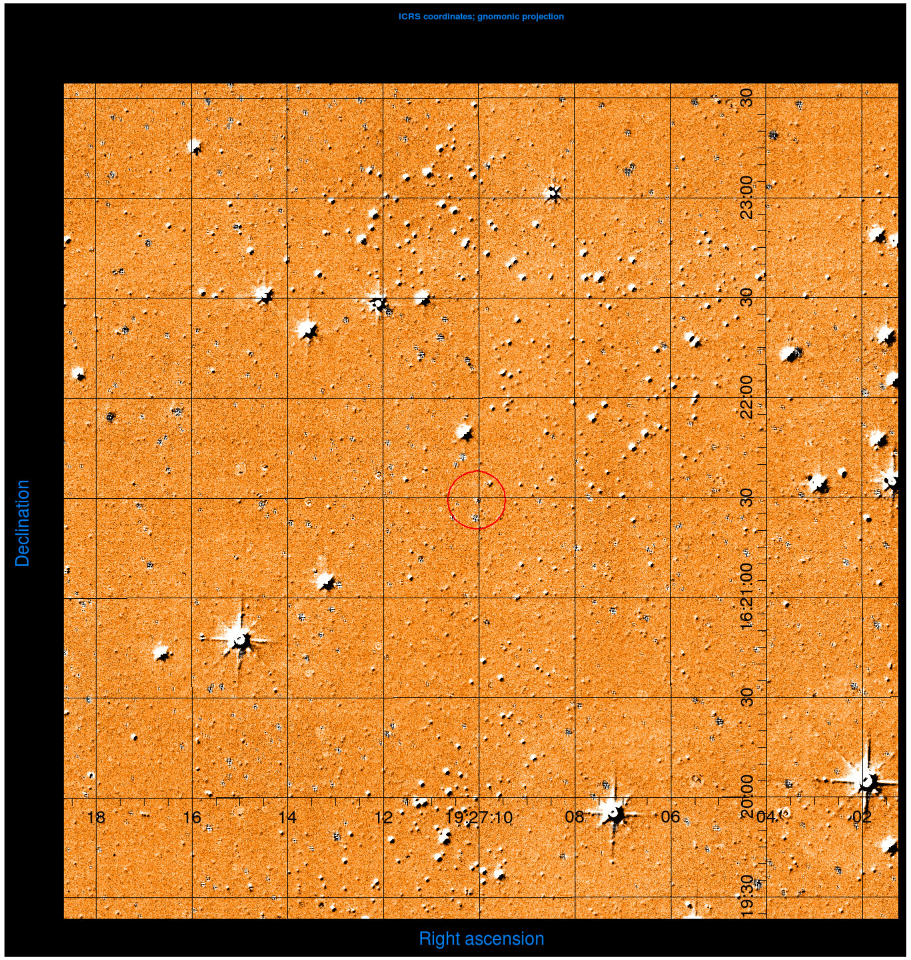

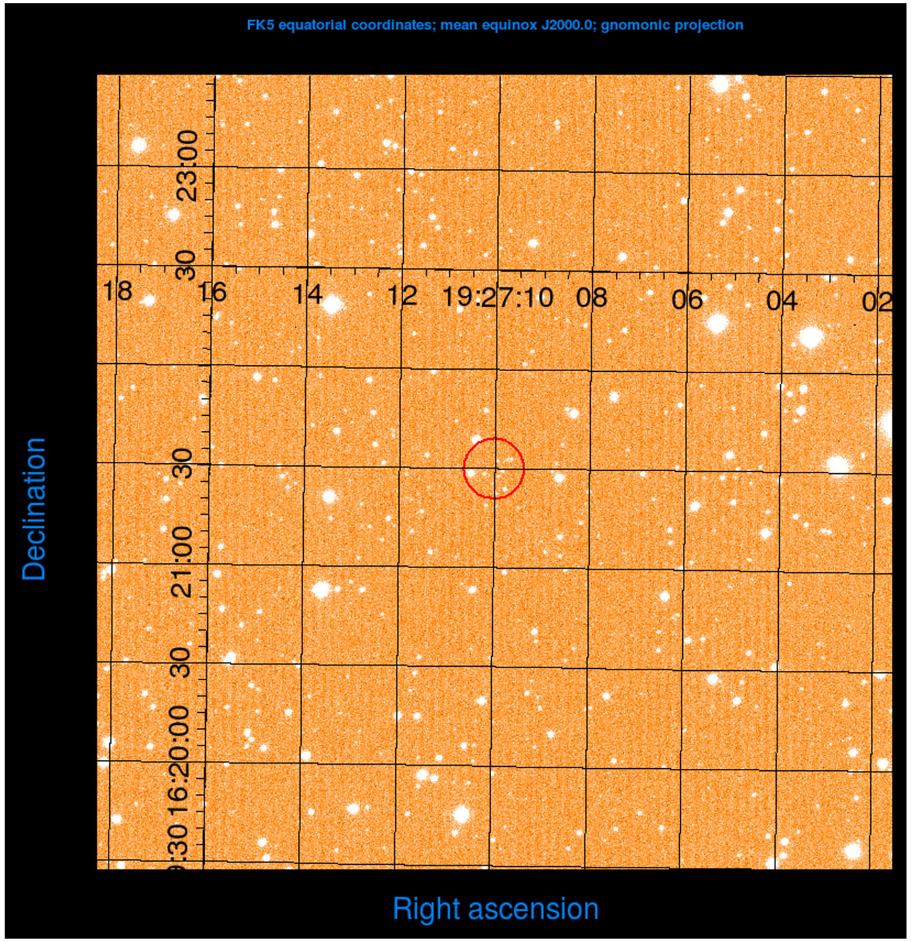

Comparison of IPHAS56, H_2 on the left, Hα on the right

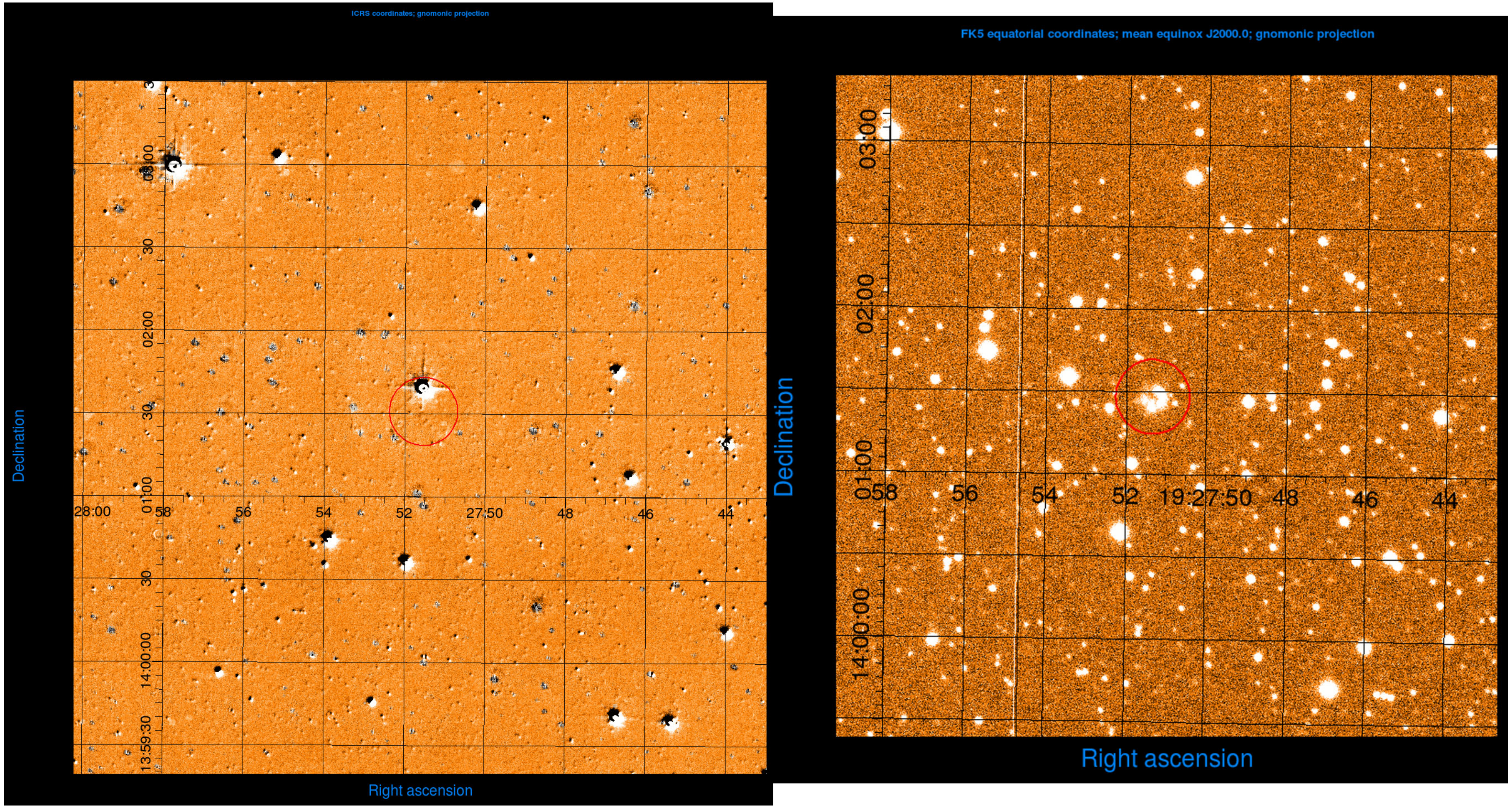

Comparison of IPHAS57, H_2 on the left, $H\alpha$ on the right

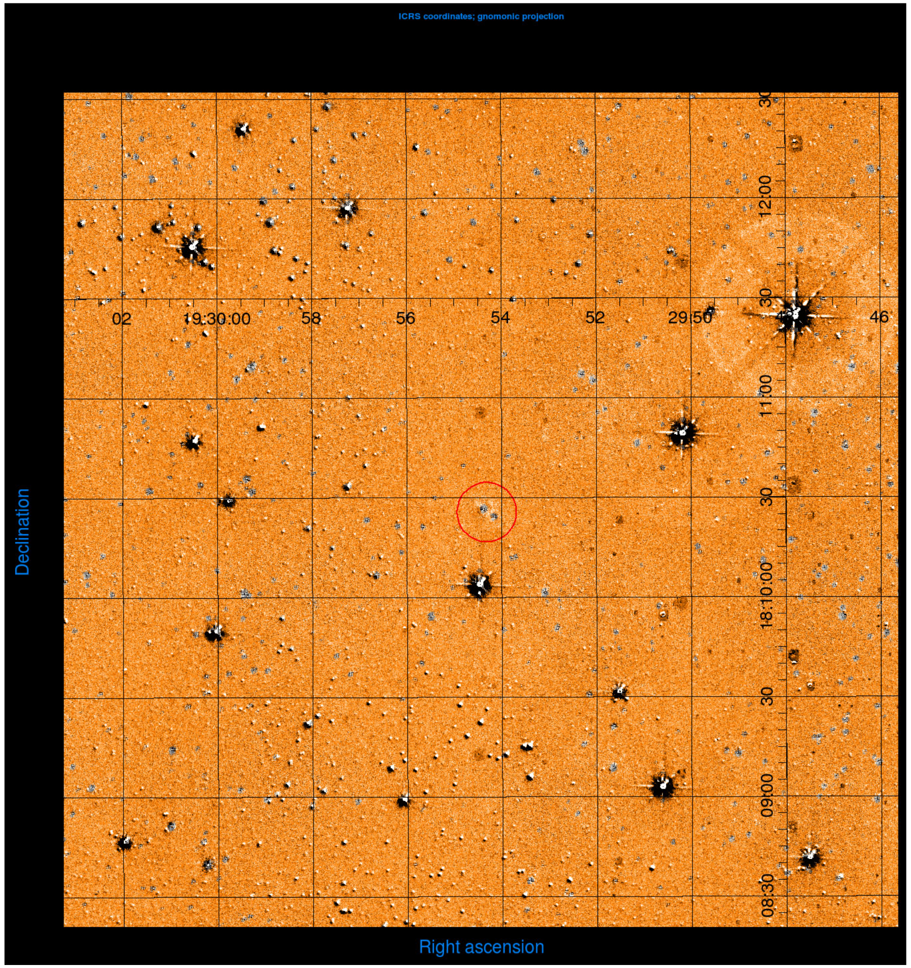

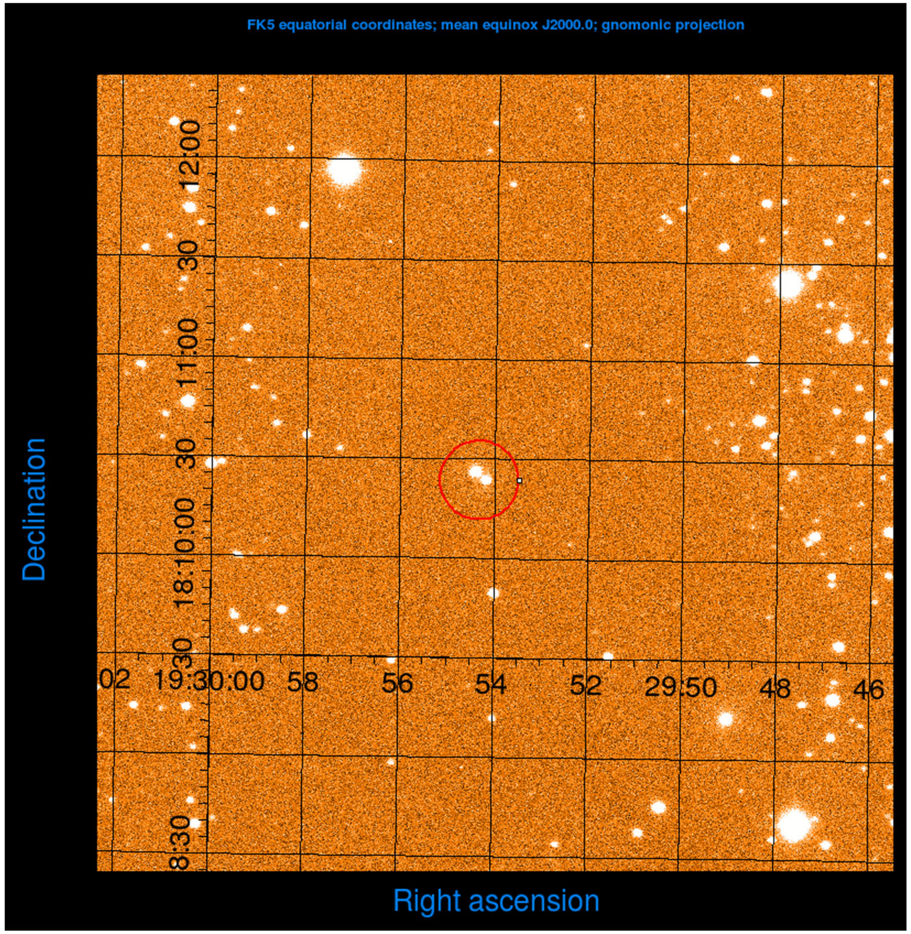

Comparison of IPHAS58, H_2 on the left, Hα on the right

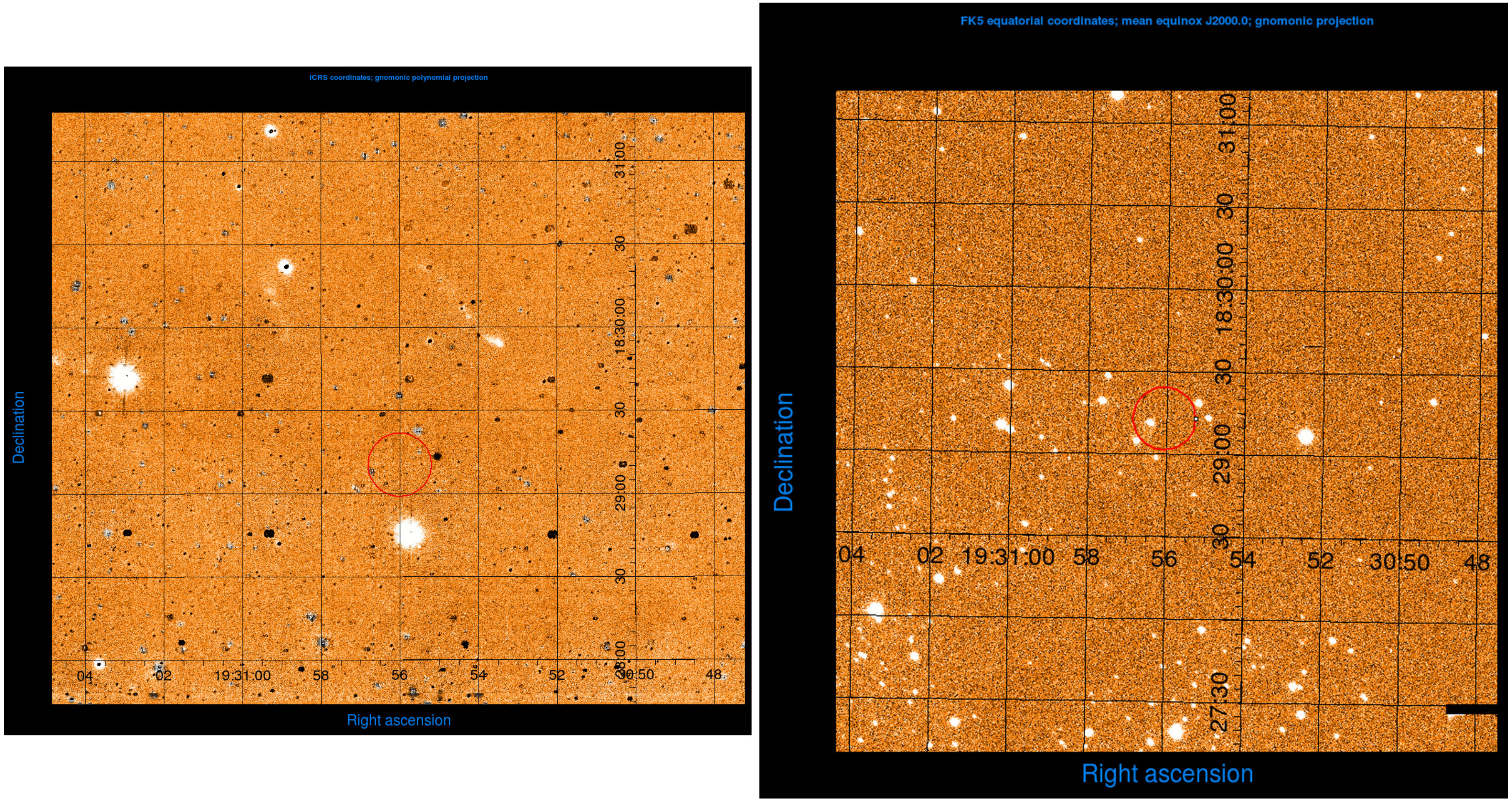

Comparison of IPHAS59, H_2 on the left, Hα on the right

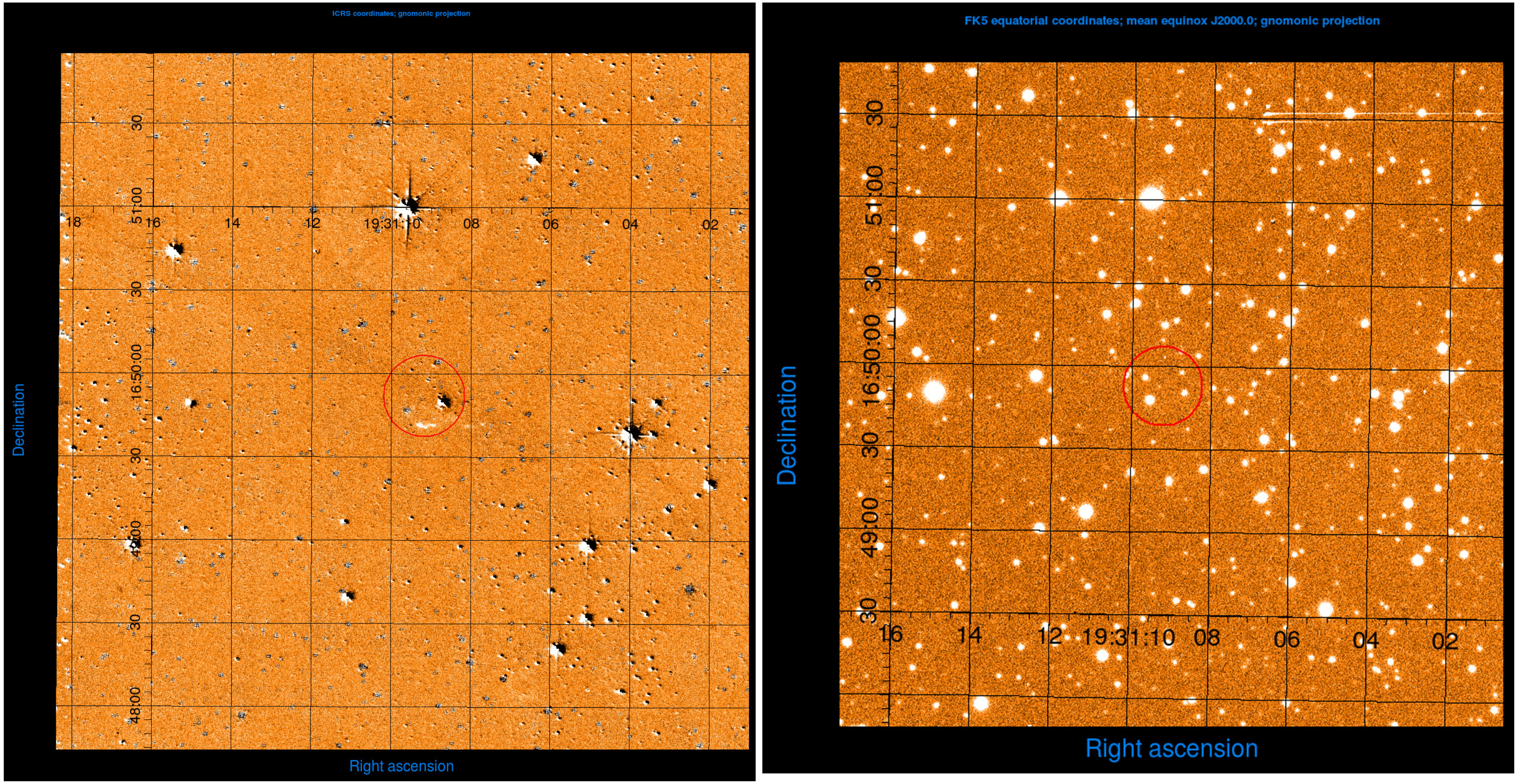

Comparison of IPHAS60, H_2 on the left, $H\alpha$ on the right

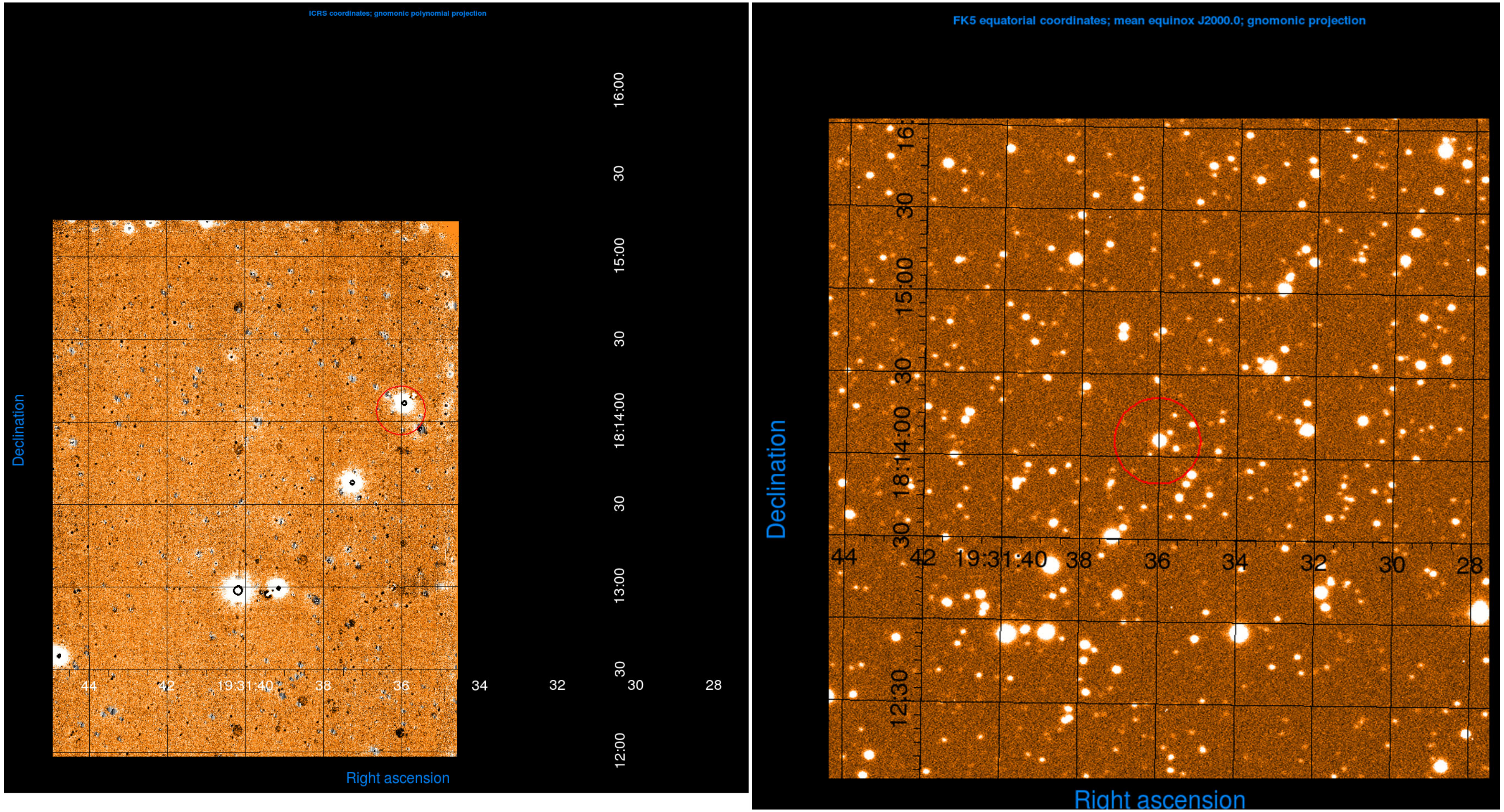

Comparison of IPHAS61, H_2 on the left, Hα on the right

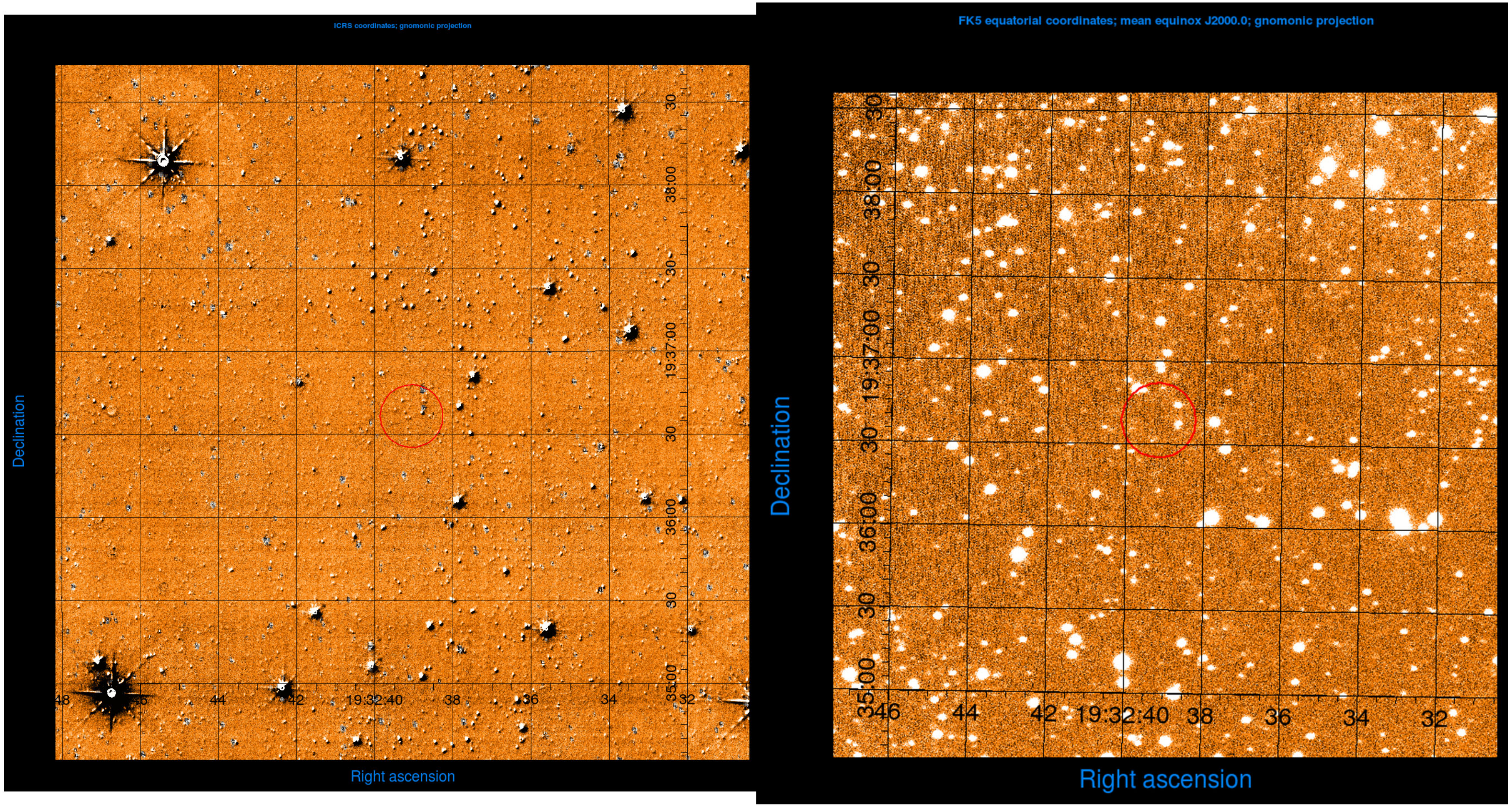

Comparison of IPHAS62, H_2 on the left, Hα on the right

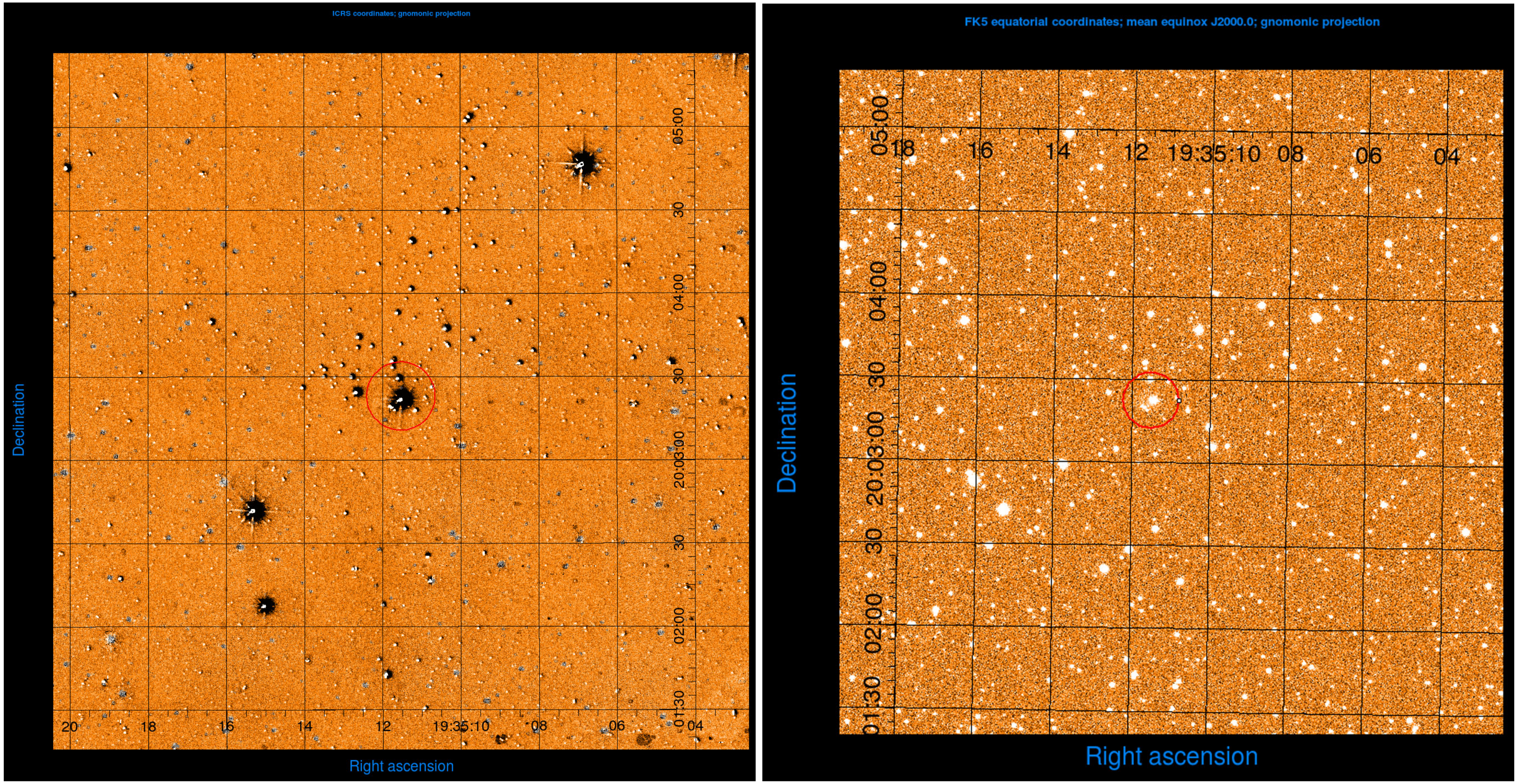

Comparison of IPHAS63, H_2 on the left, $H\alpha$ on the right

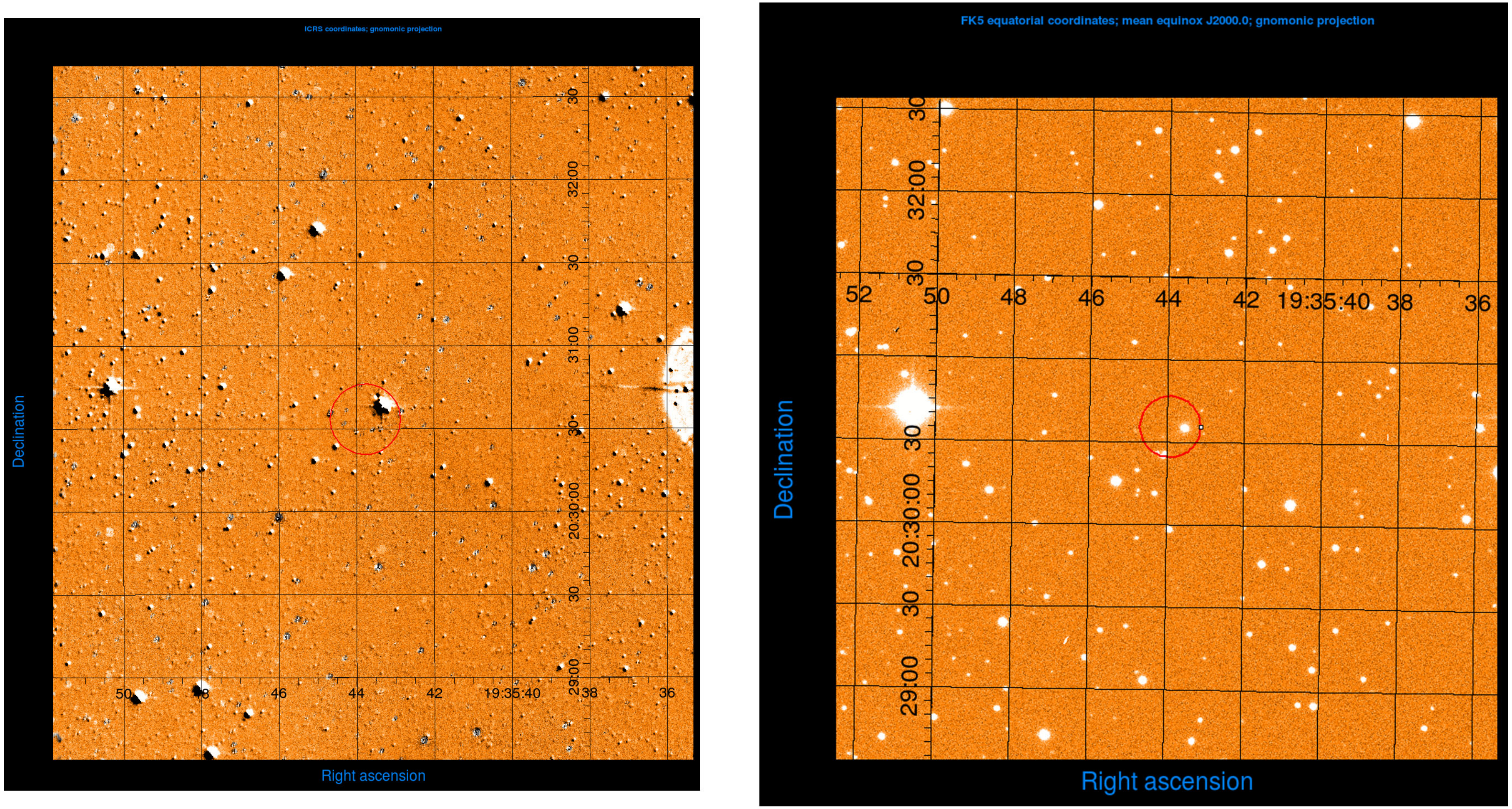

Comparison of IPHAS64, H_2 on the left, $H\alpha$ on the right

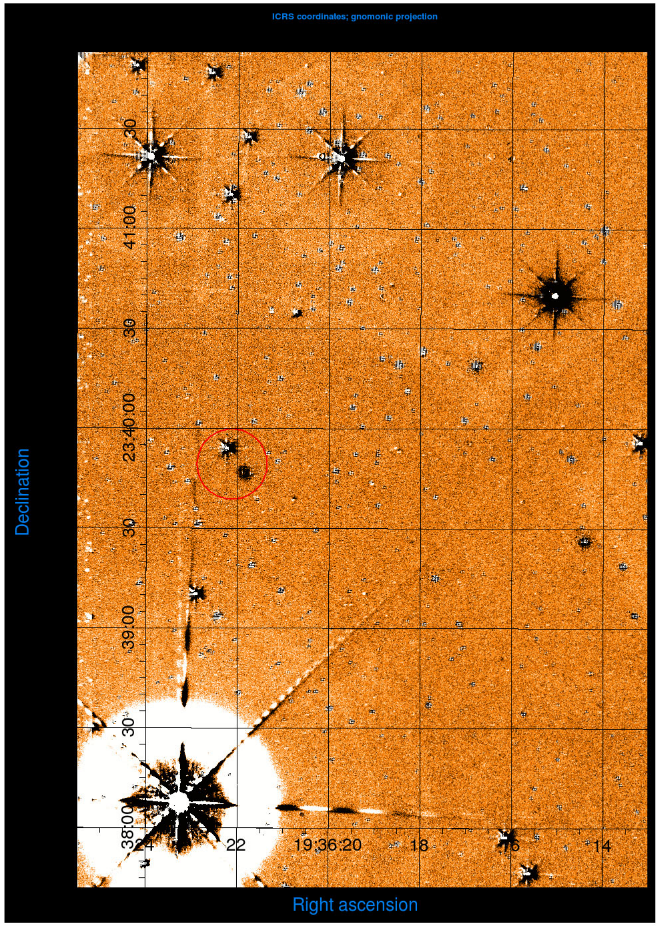

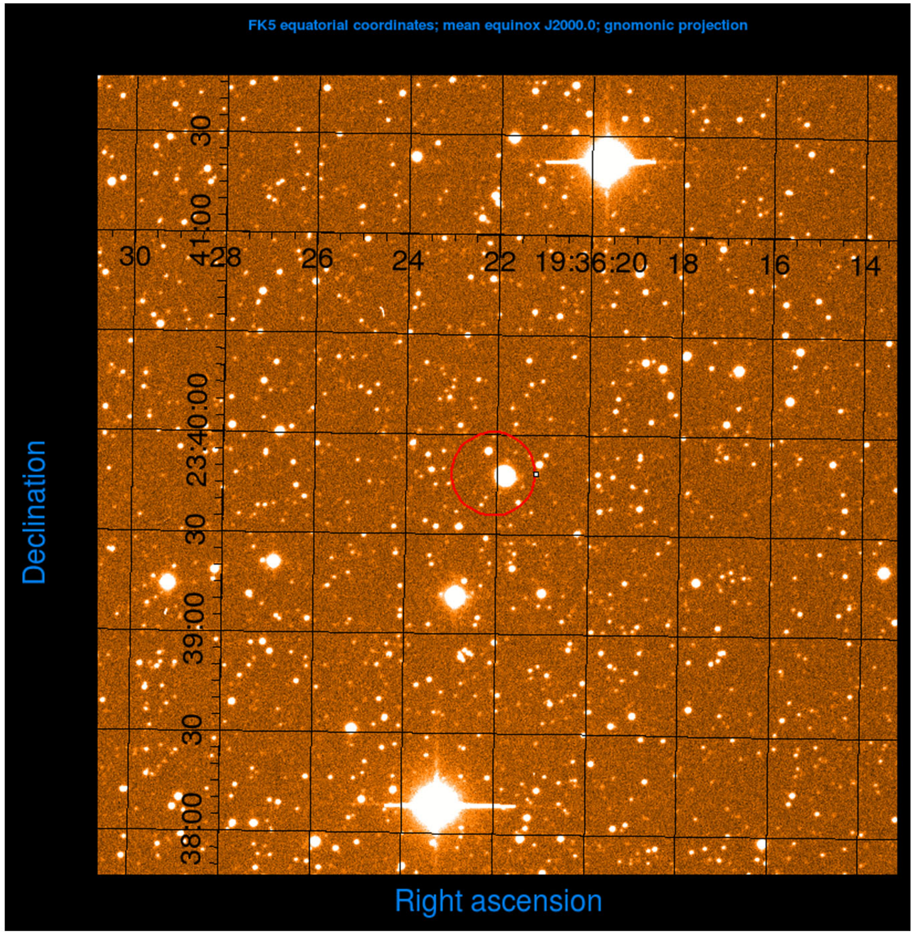

Comparison of IPHAS65, H_2 on the left, Hα on the right

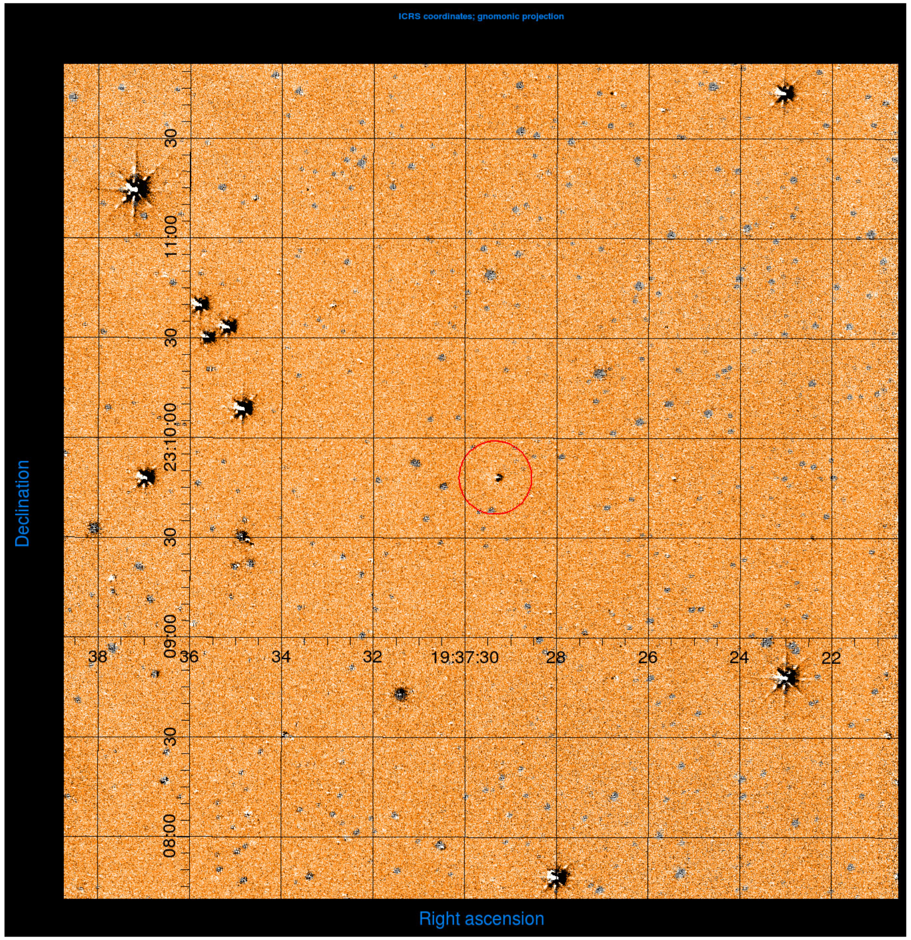

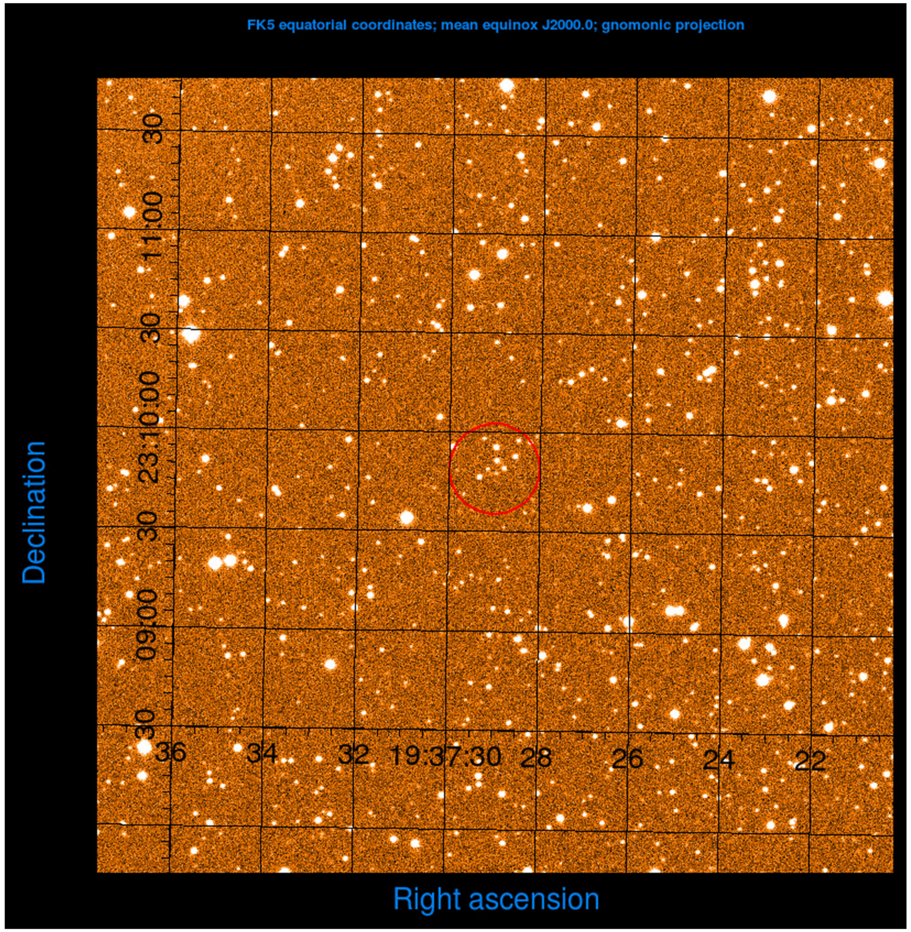

Comparison of IPHAS66, H_2 on the left, Hα on the right

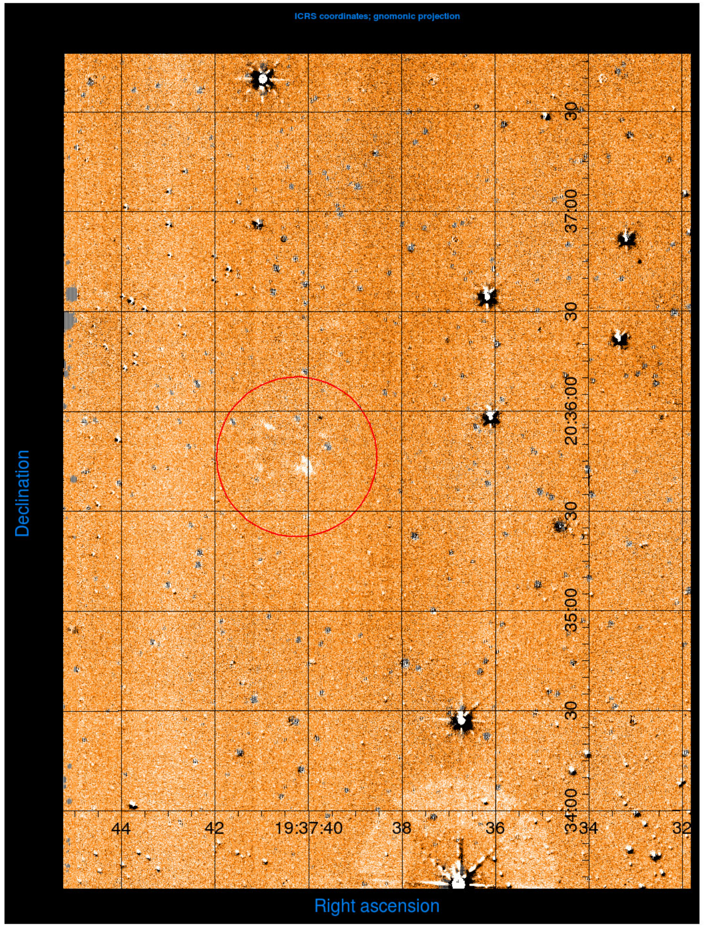

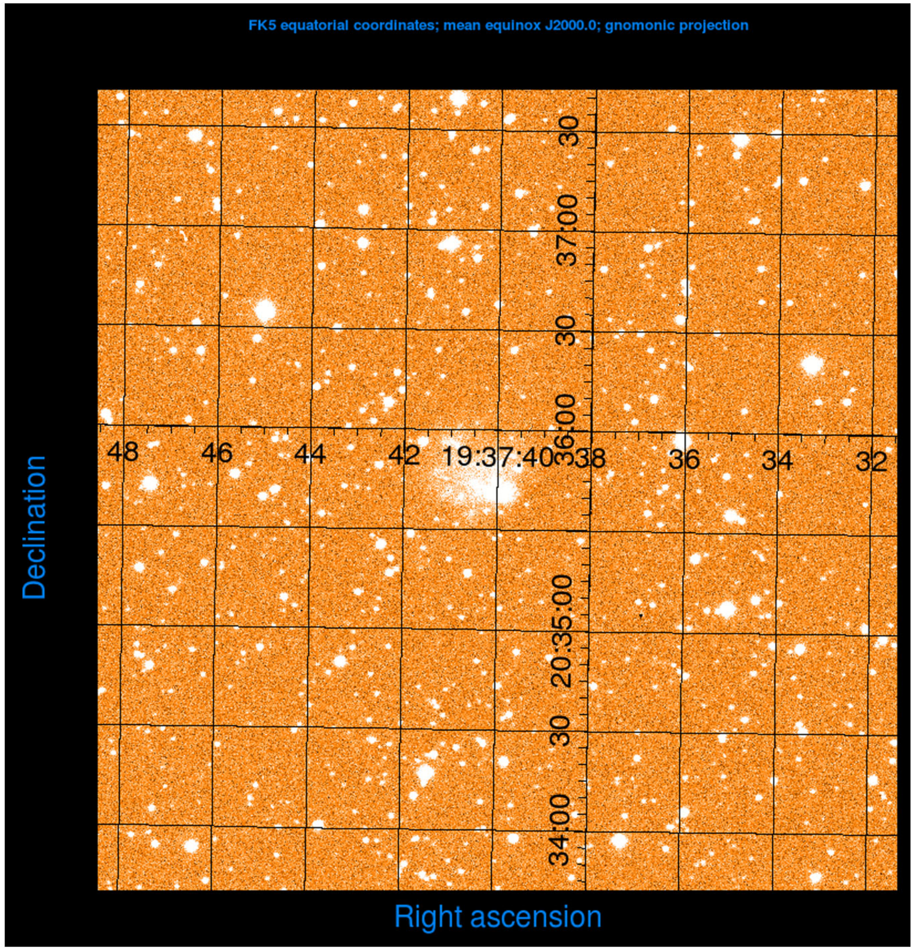

Comparison of IPHAS67, H_2 on the left, Hα on the right

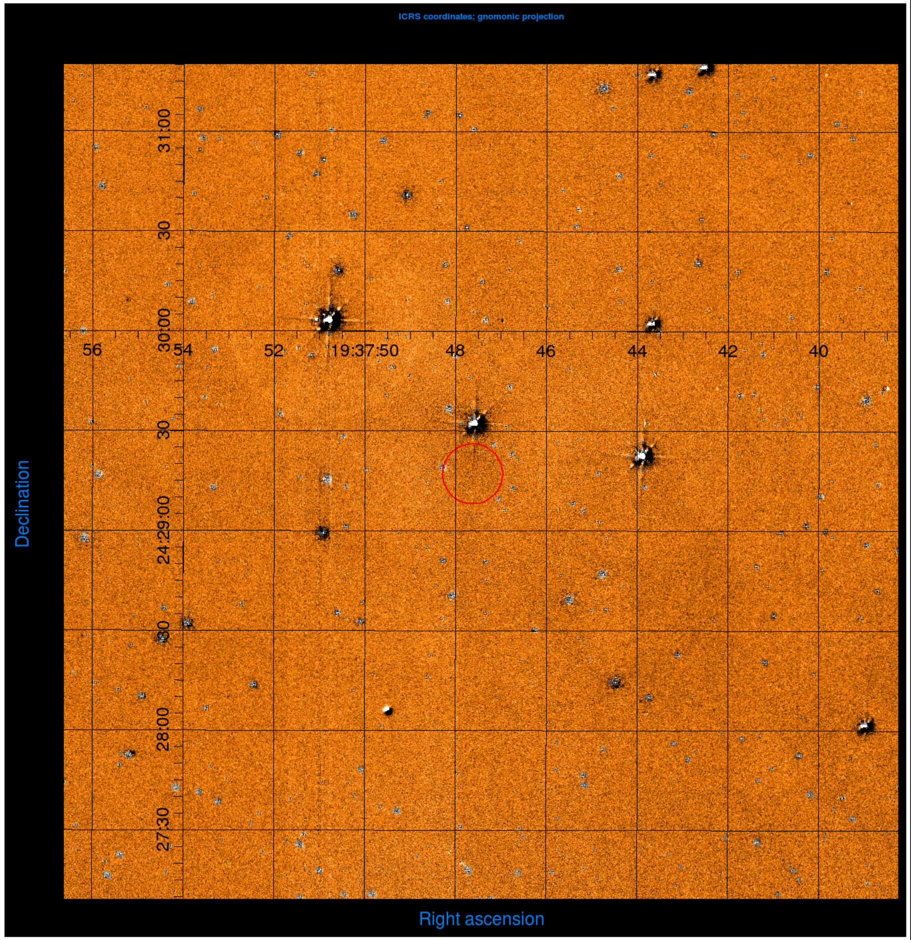

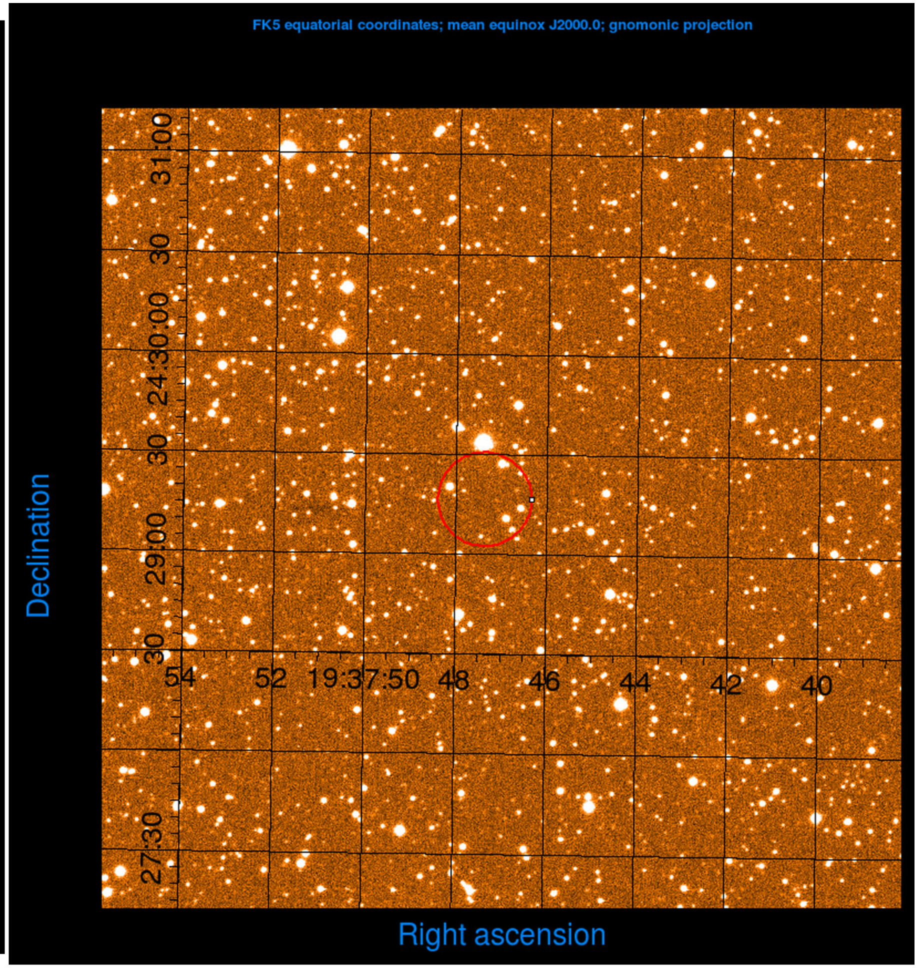

Comparison of IPHAS68, H_2 on the left, $H\alpha$ on the right

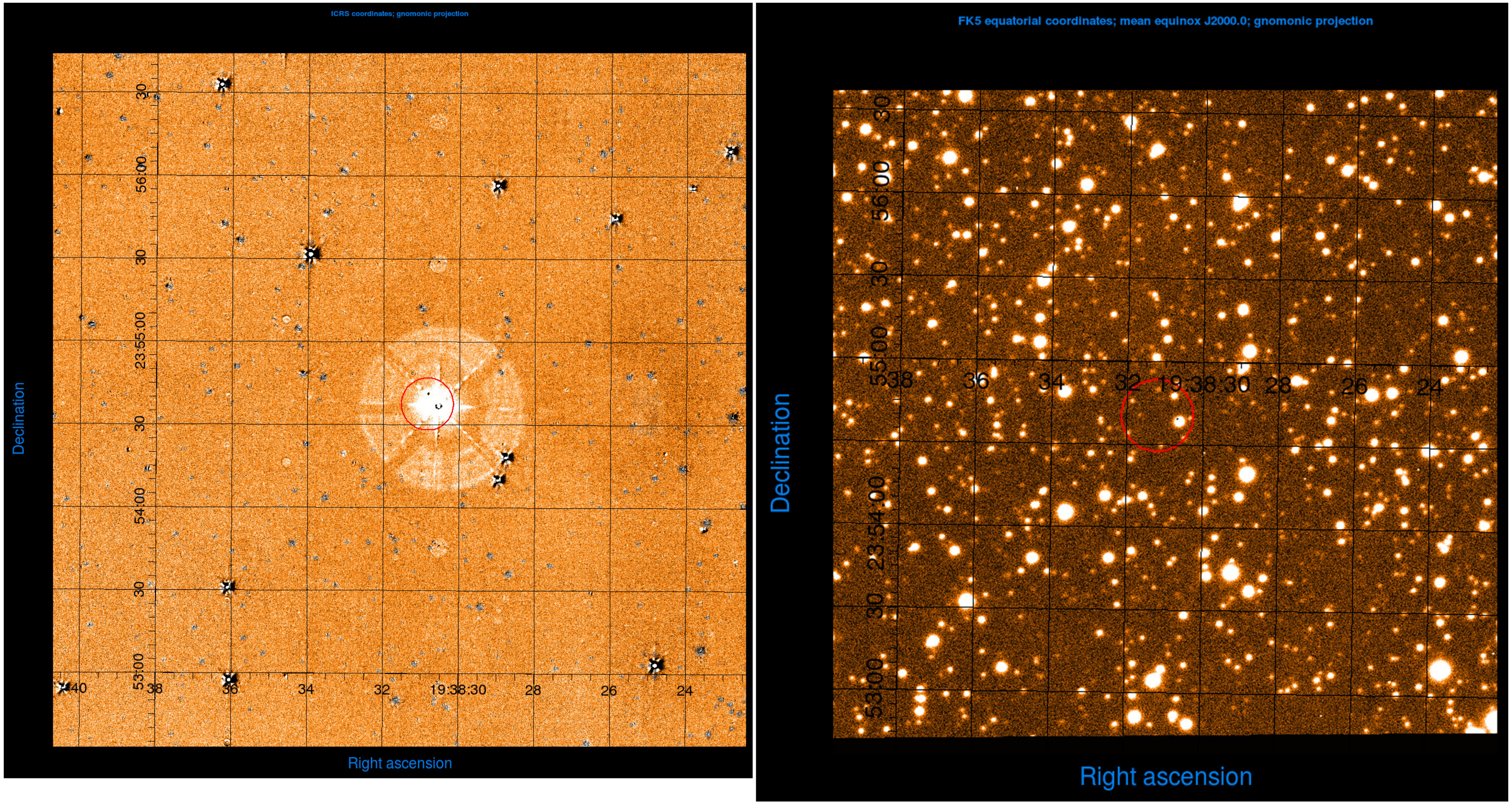

Comparison of IPHAS69, H_2 on the left, $H\alpha$ on the right

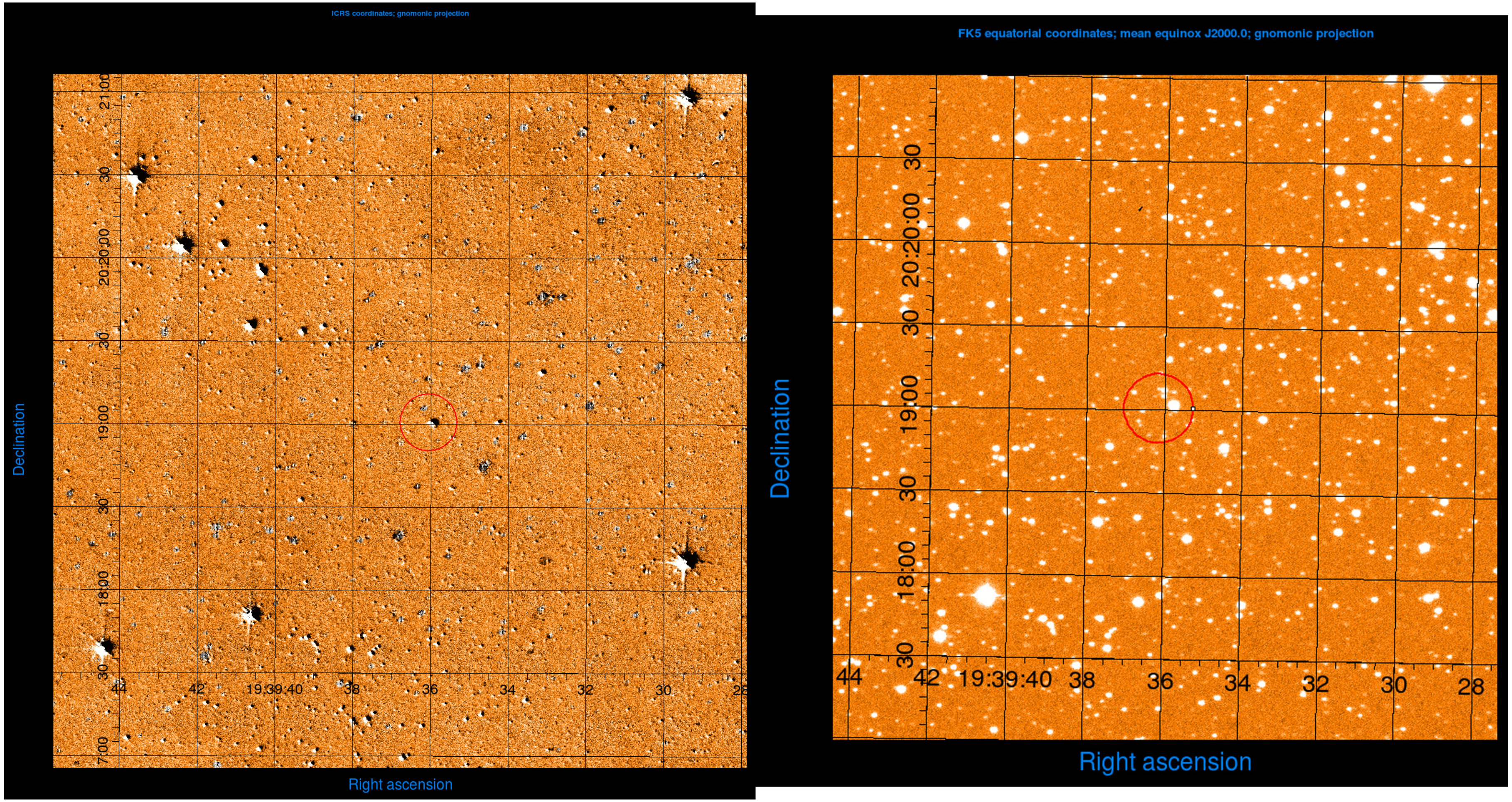

Comparison of IPHAS70, H_2 on the left, $H\alpha$ on the right

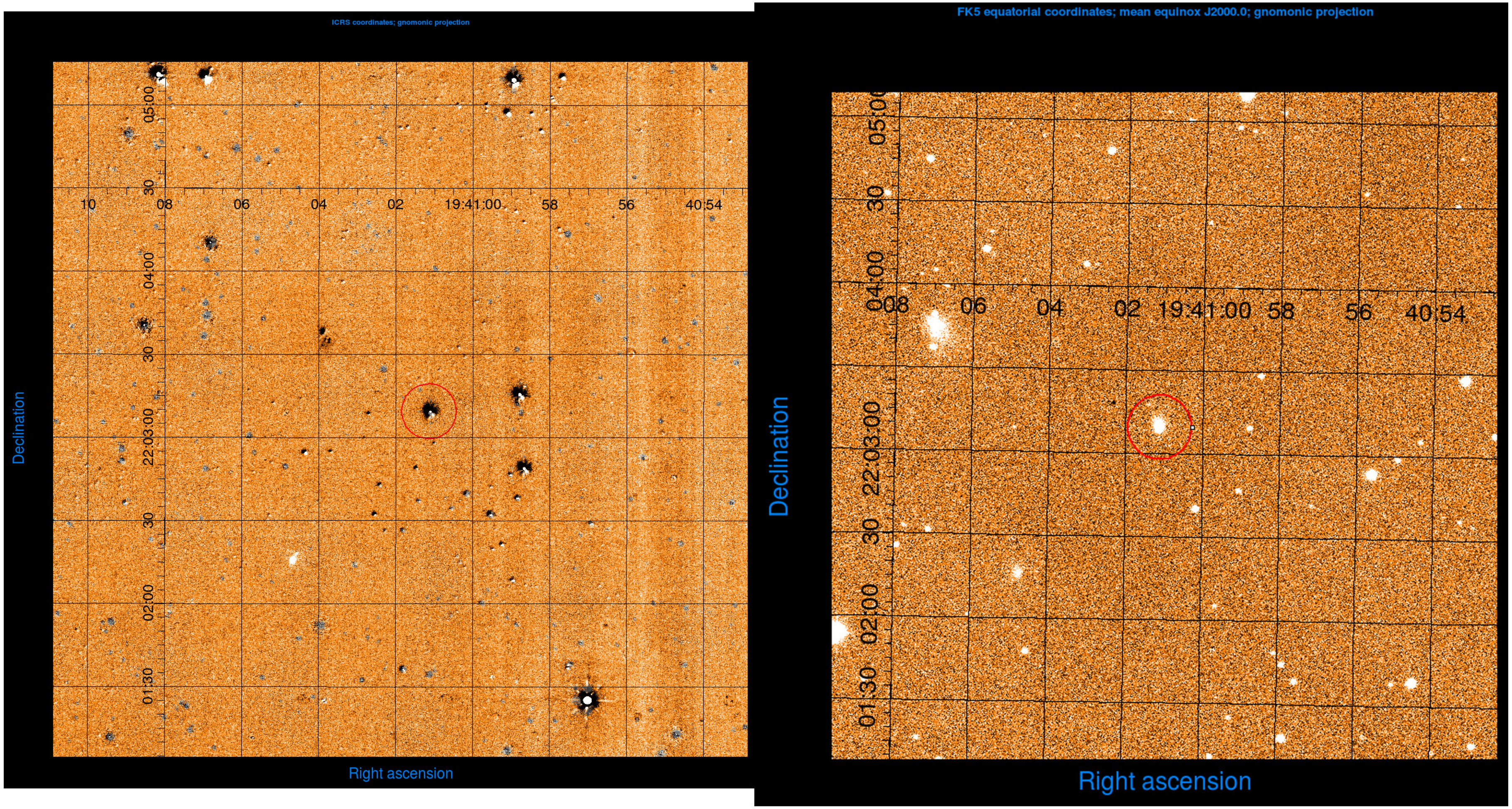

Comparison of IPHAS71, H_2 on the left, Hα on the right

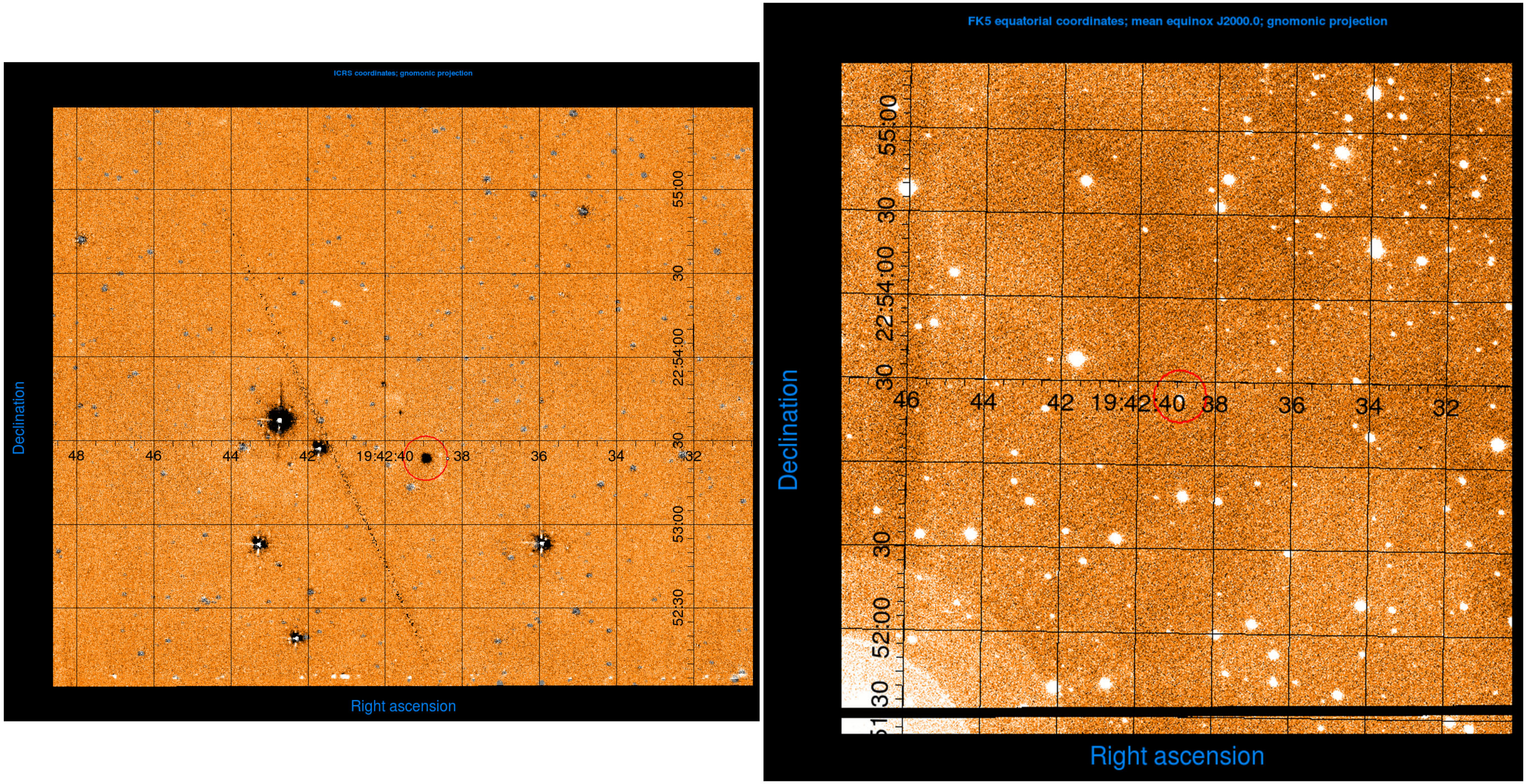

Comparison of IPHAS72, H_2 on the left, Hα on the right

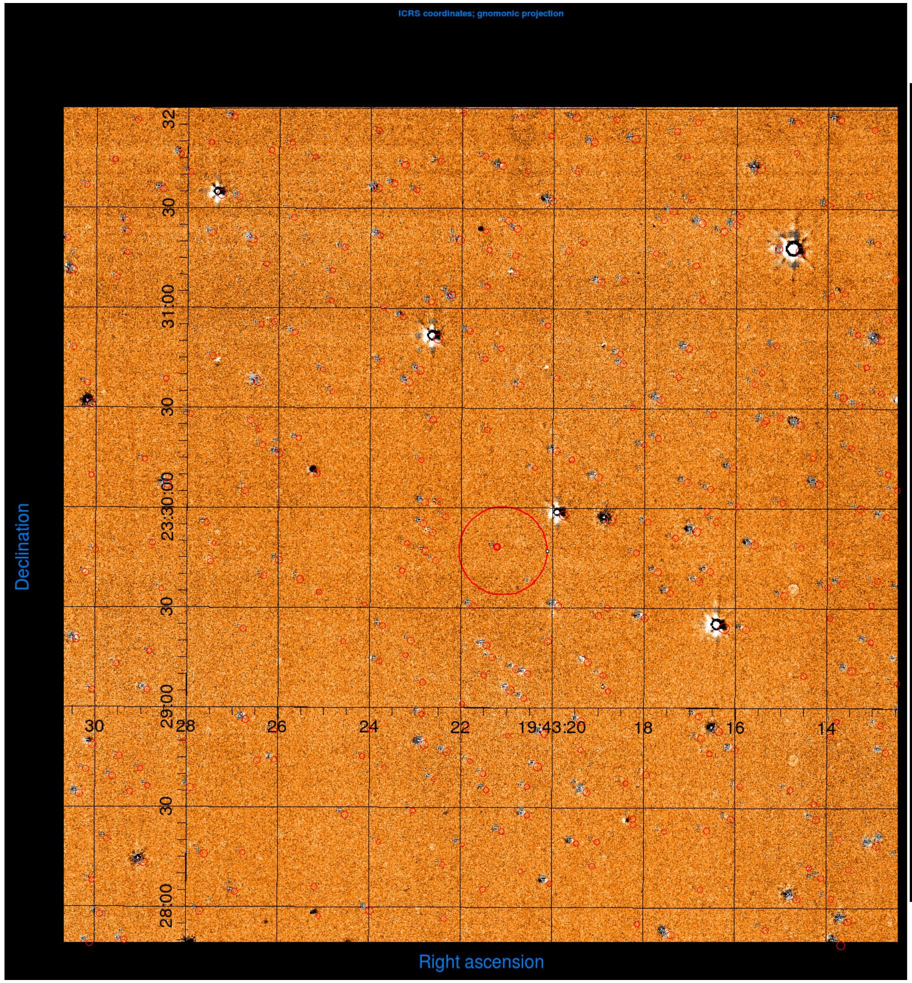

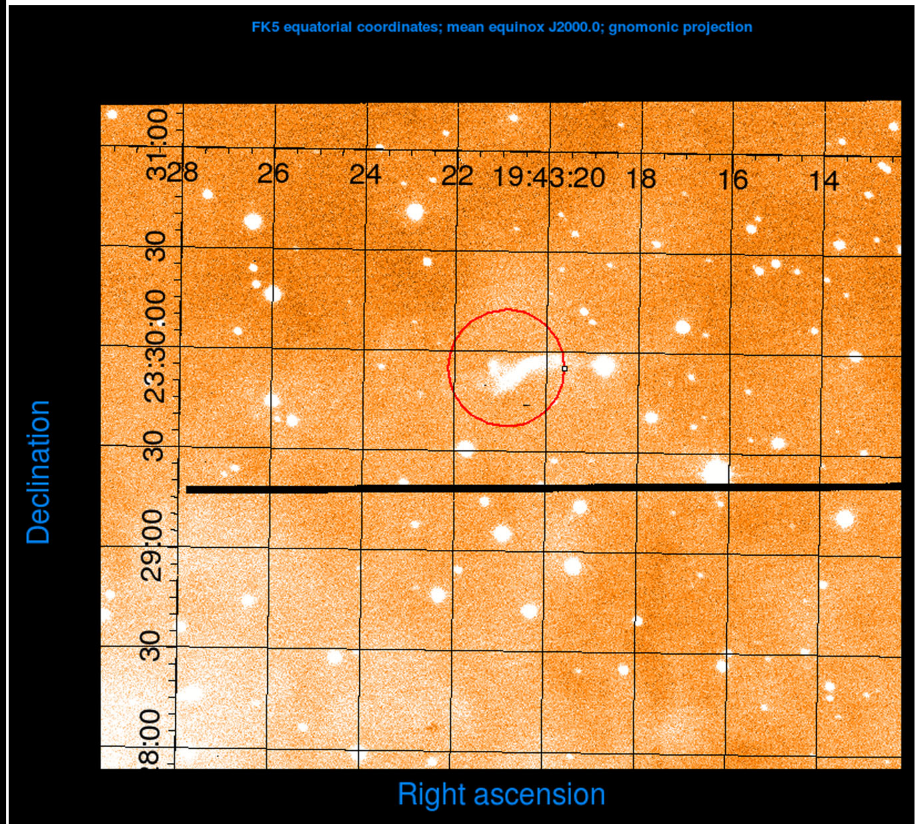

Comparison of IPHAS73, H_2 on the left, $H\alpha$ on the right

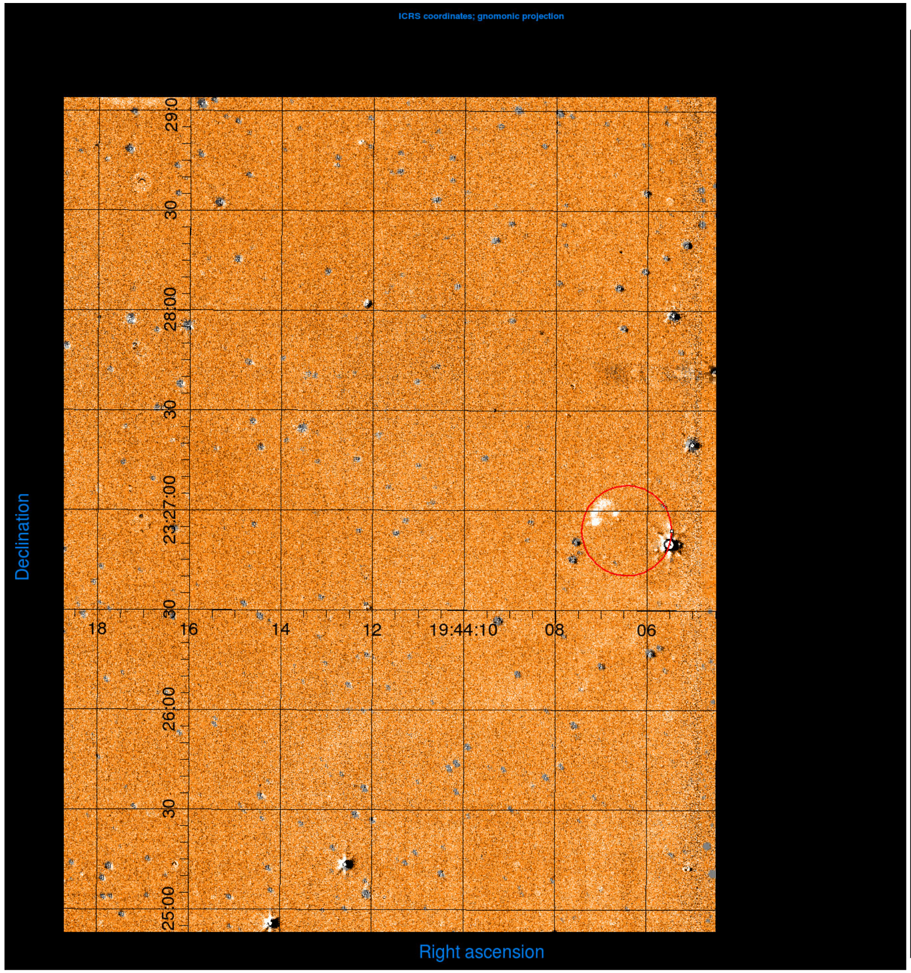

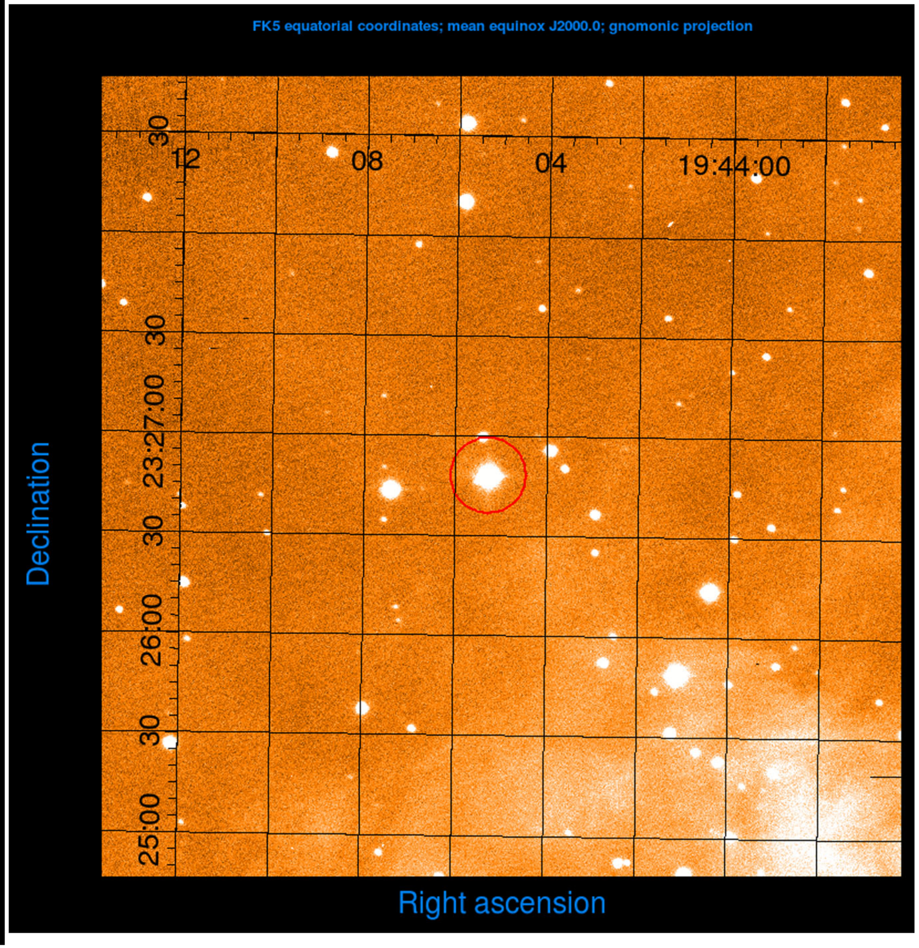

Comparison of IPHAS74, H_2 on the left, Hα on the right

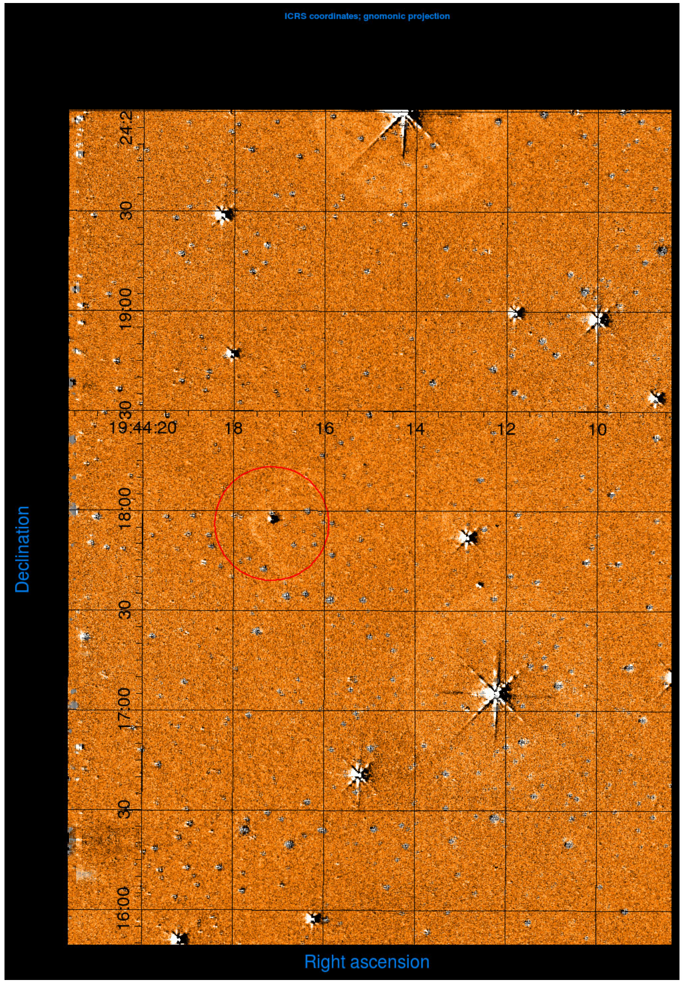

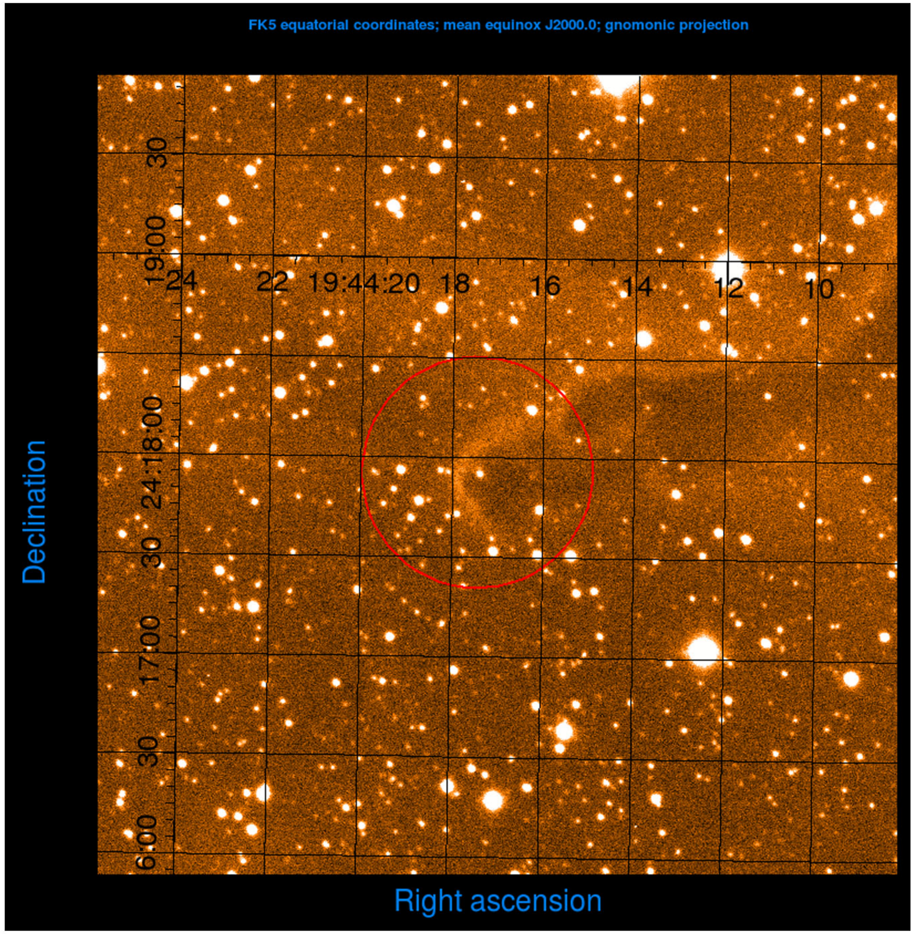

Comparison of IPHAS75, H_2 on the left, Hα on the right

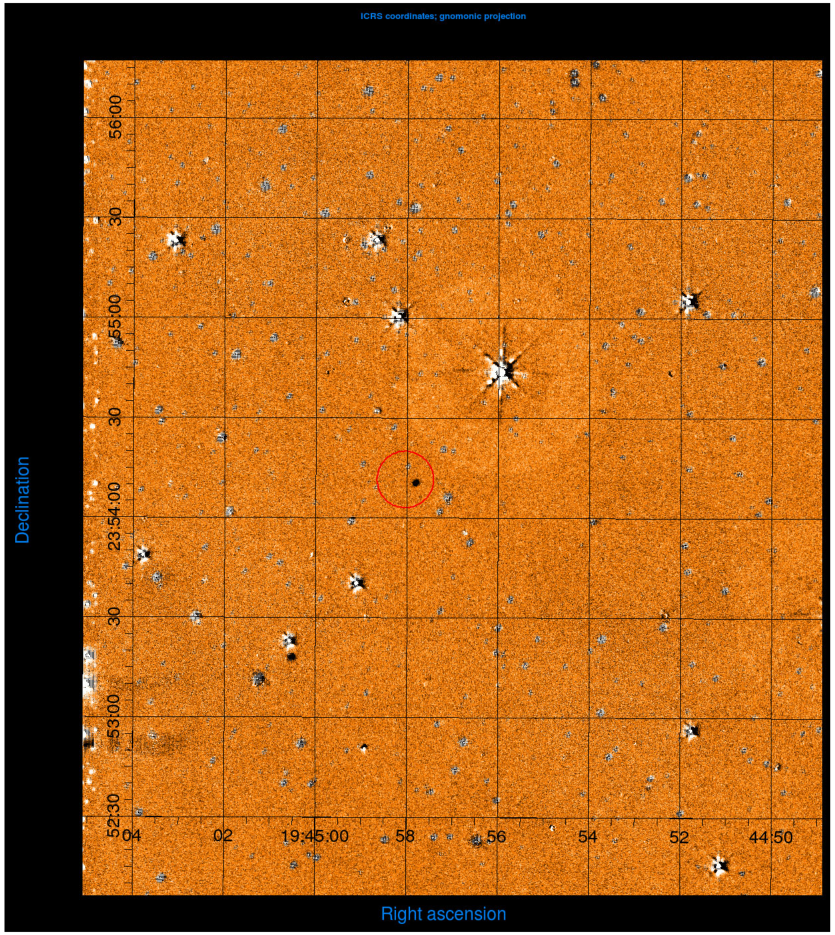

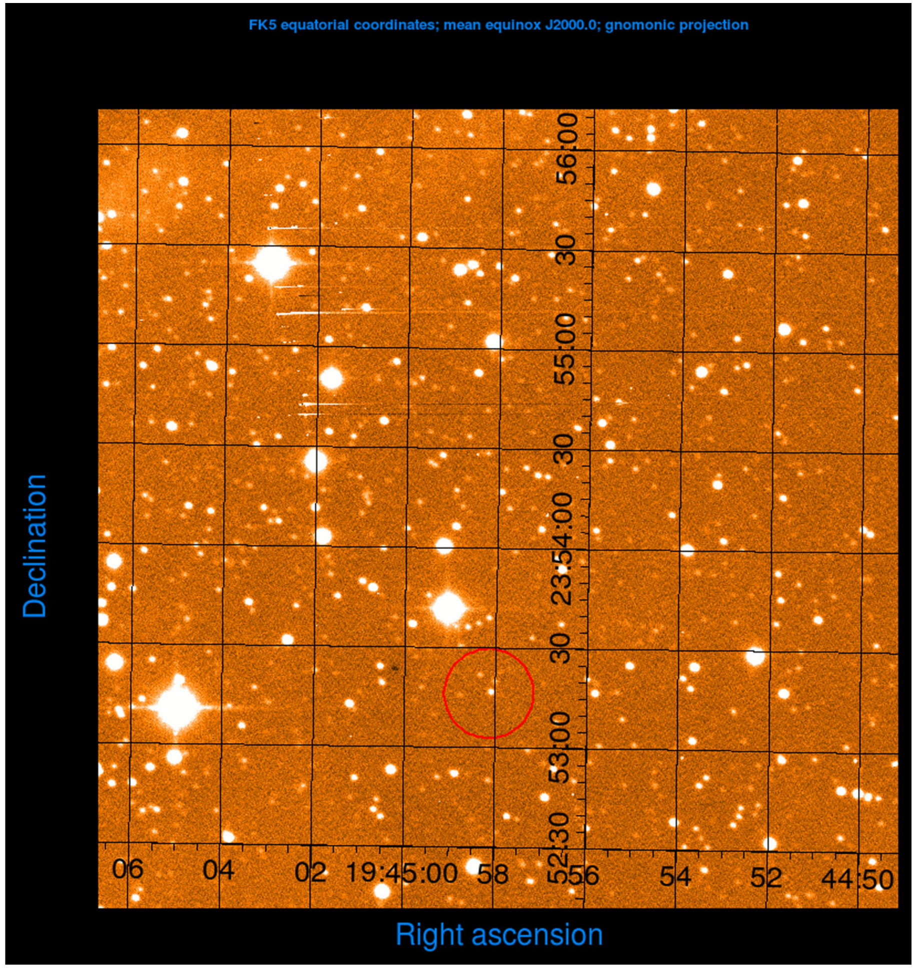

Comparison of IPHAS76, H_2 on the left, Hα on the right

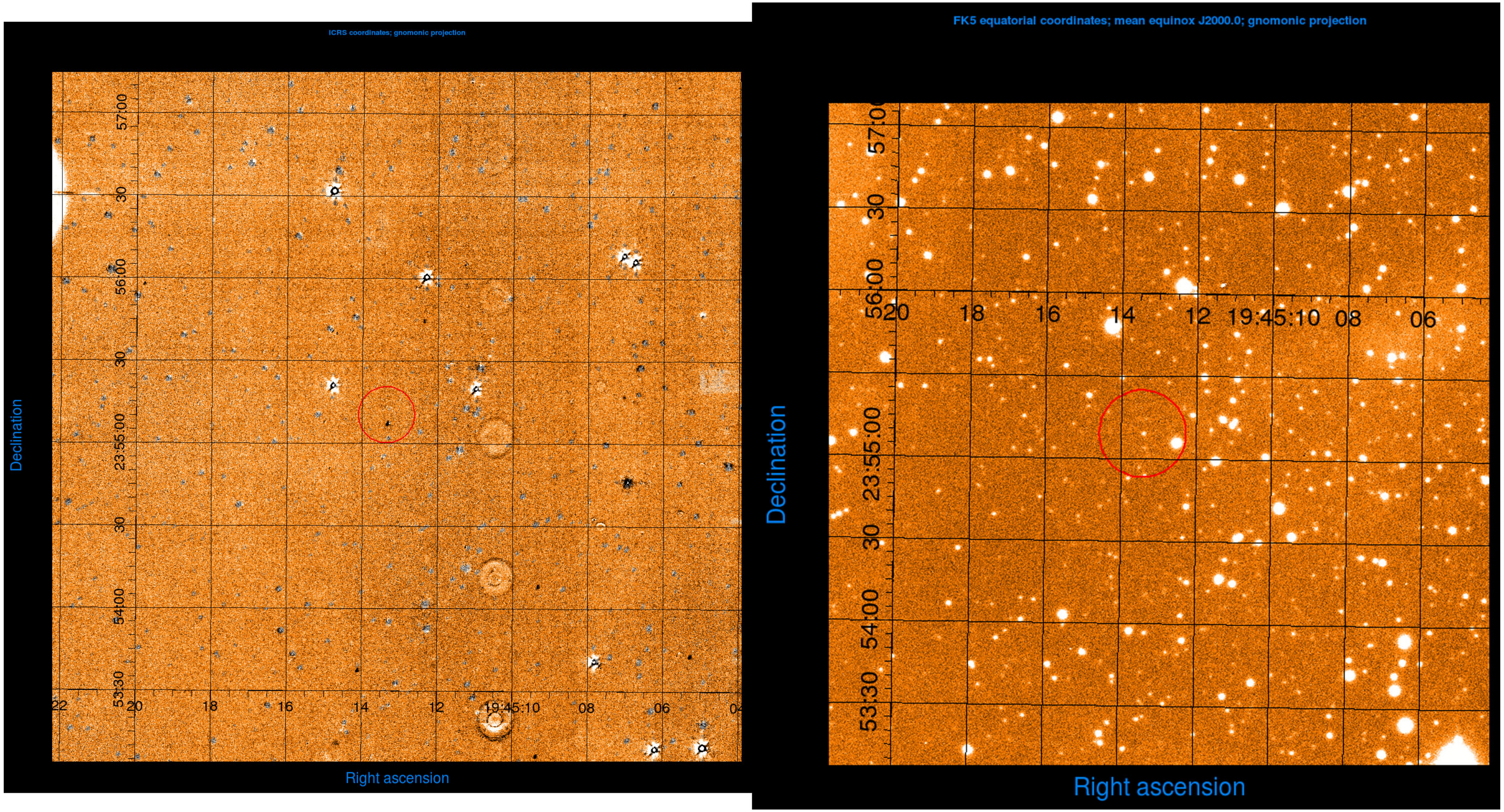

Comparison of IPHAS77, H_2 on the left, Hα on the right

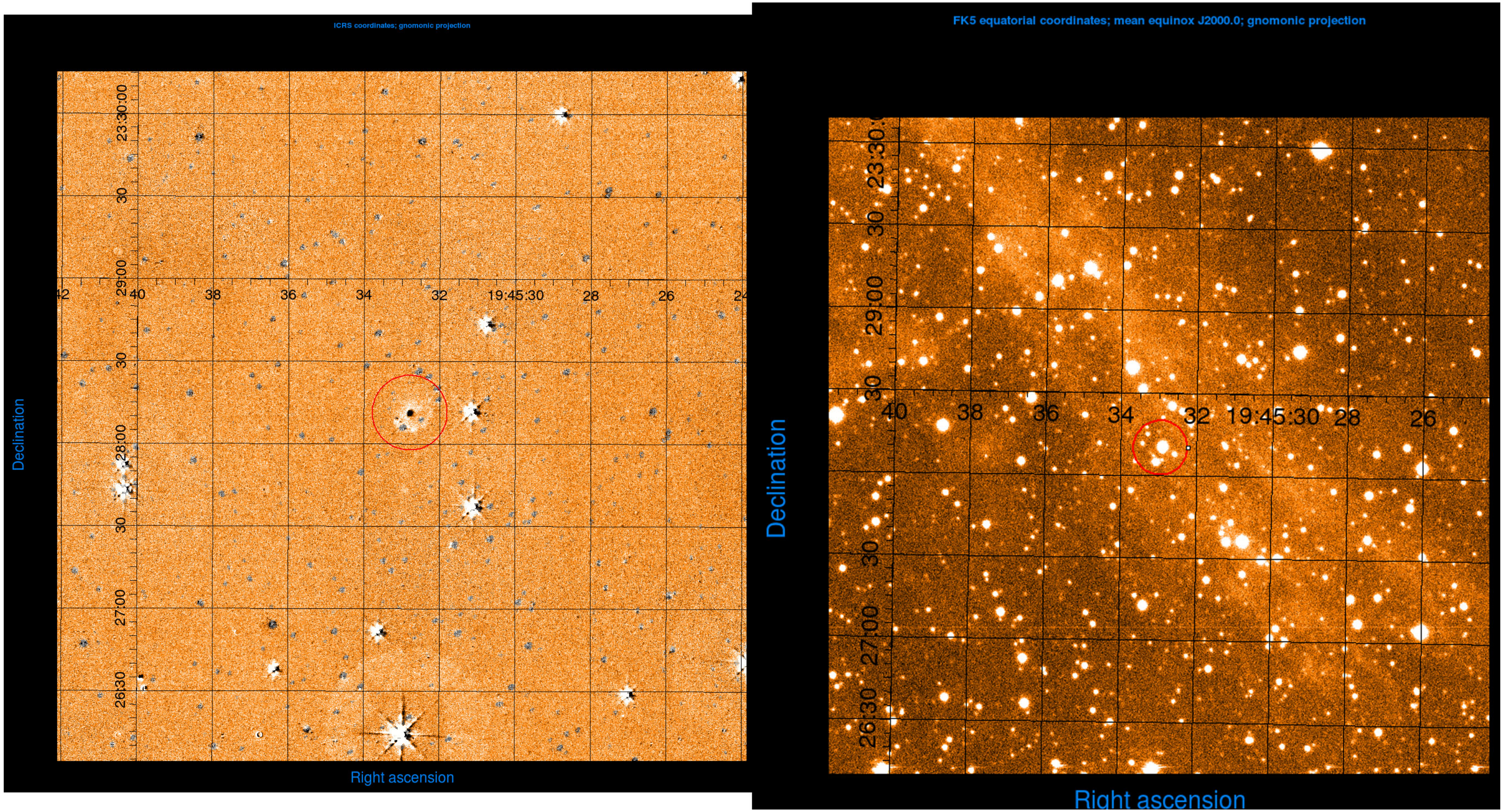

Comparison of IPHAS78, H_2 on the left, Hα on the right

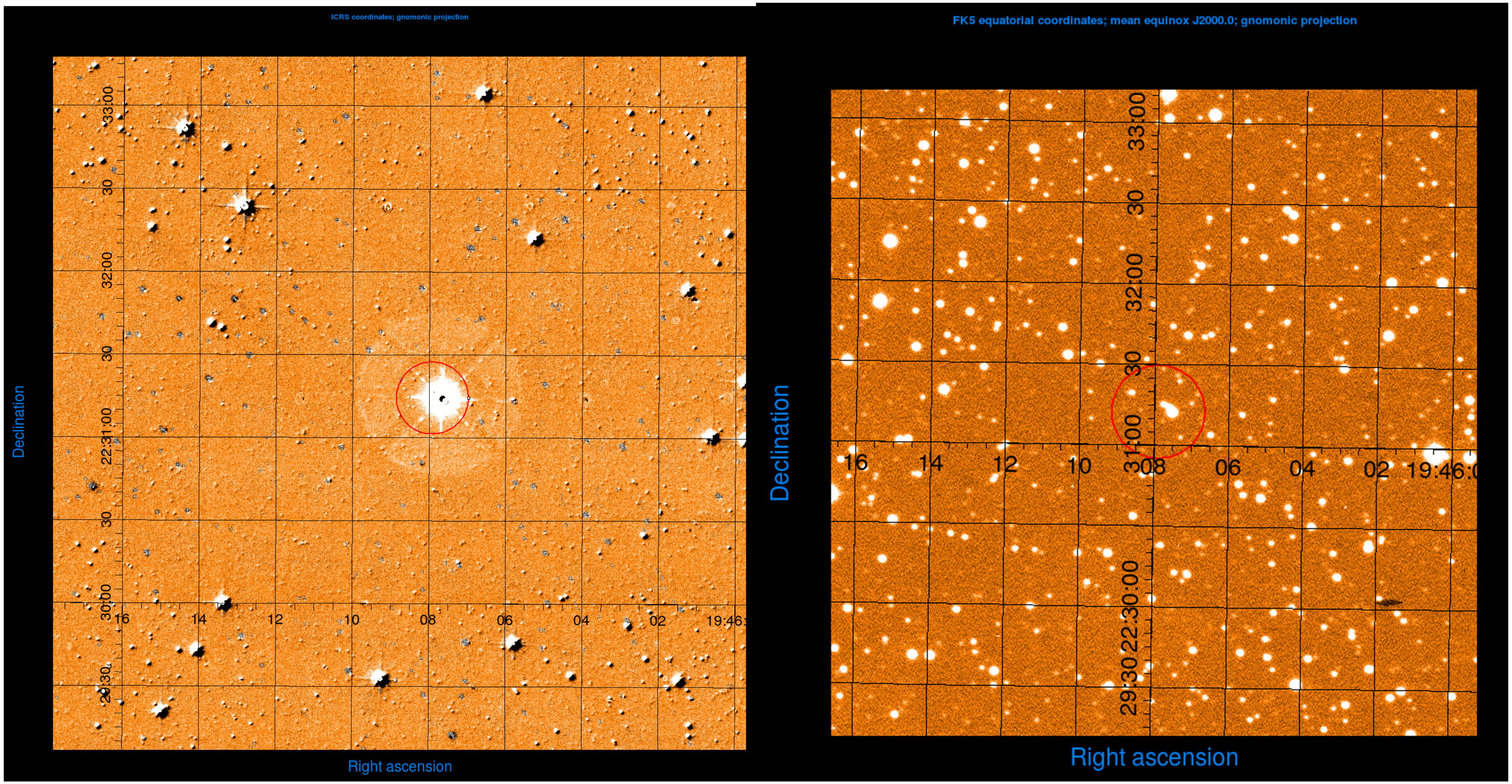

Comparison of IPHAS79, H_2 on the left, $H\alpha$ on the right

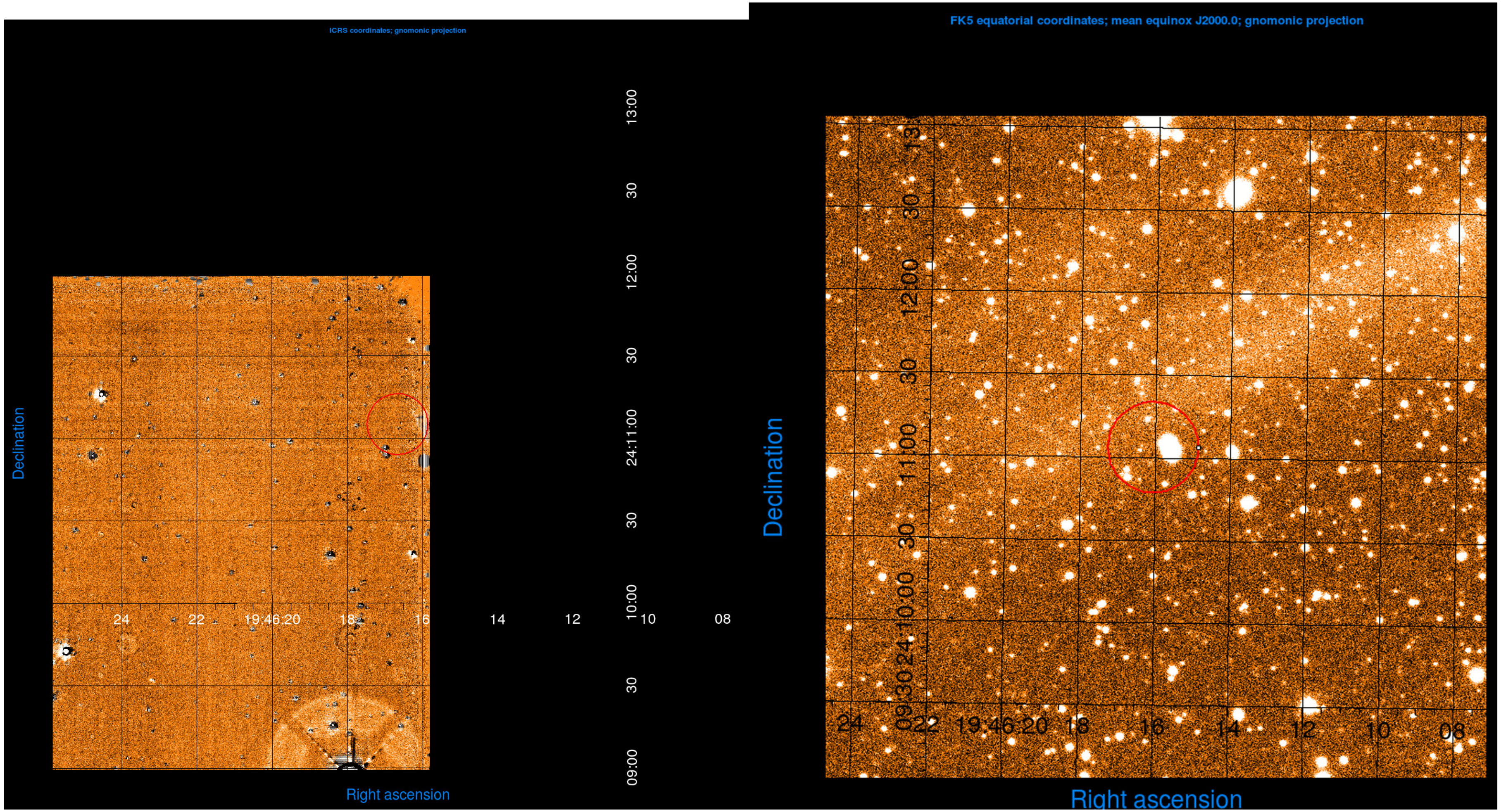

Comparison of IPHAS80, H_2 on the left, Hα on the right

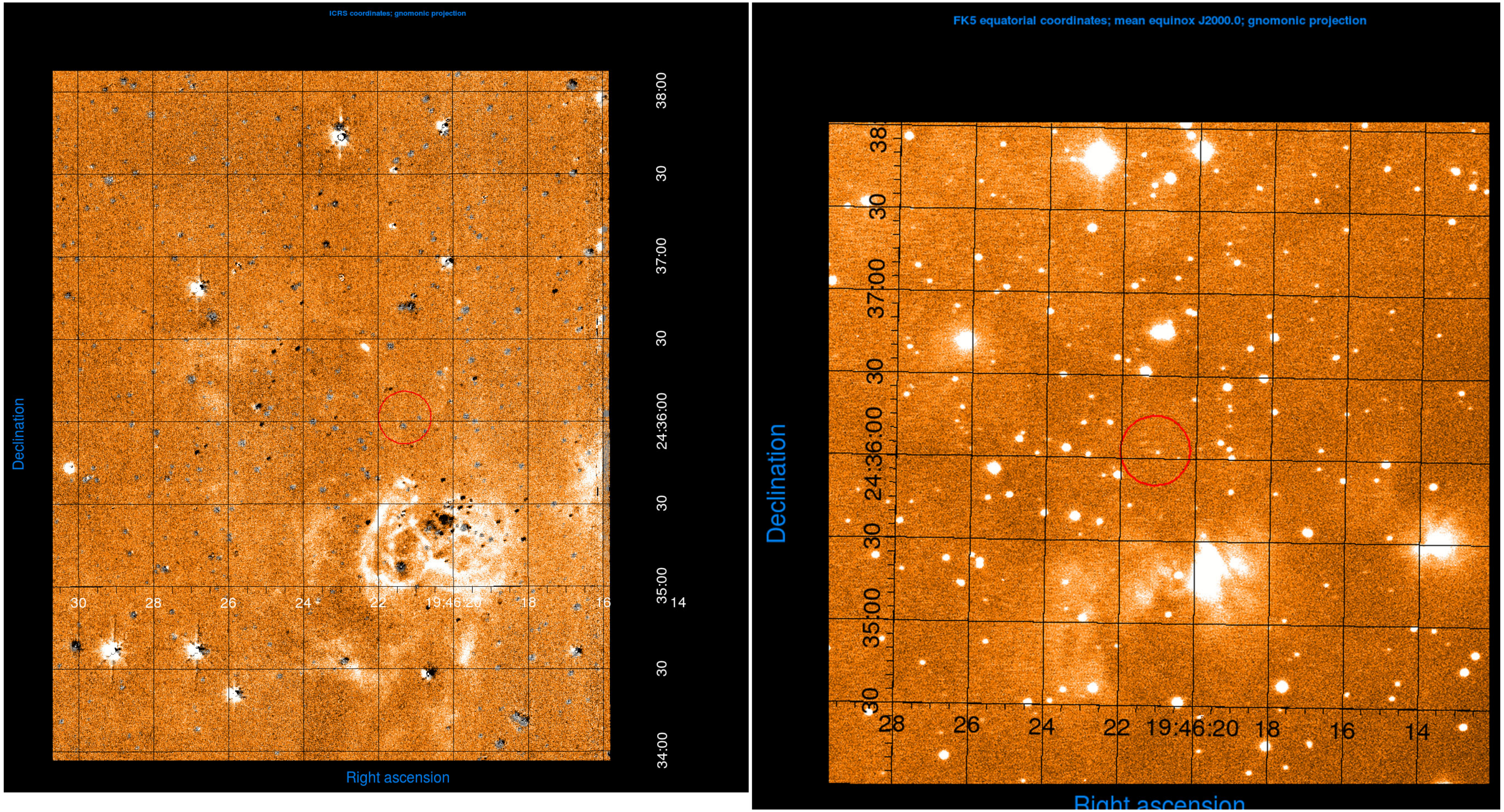

Comparison of IPHAS81, H_2 on the left, Hα on the right

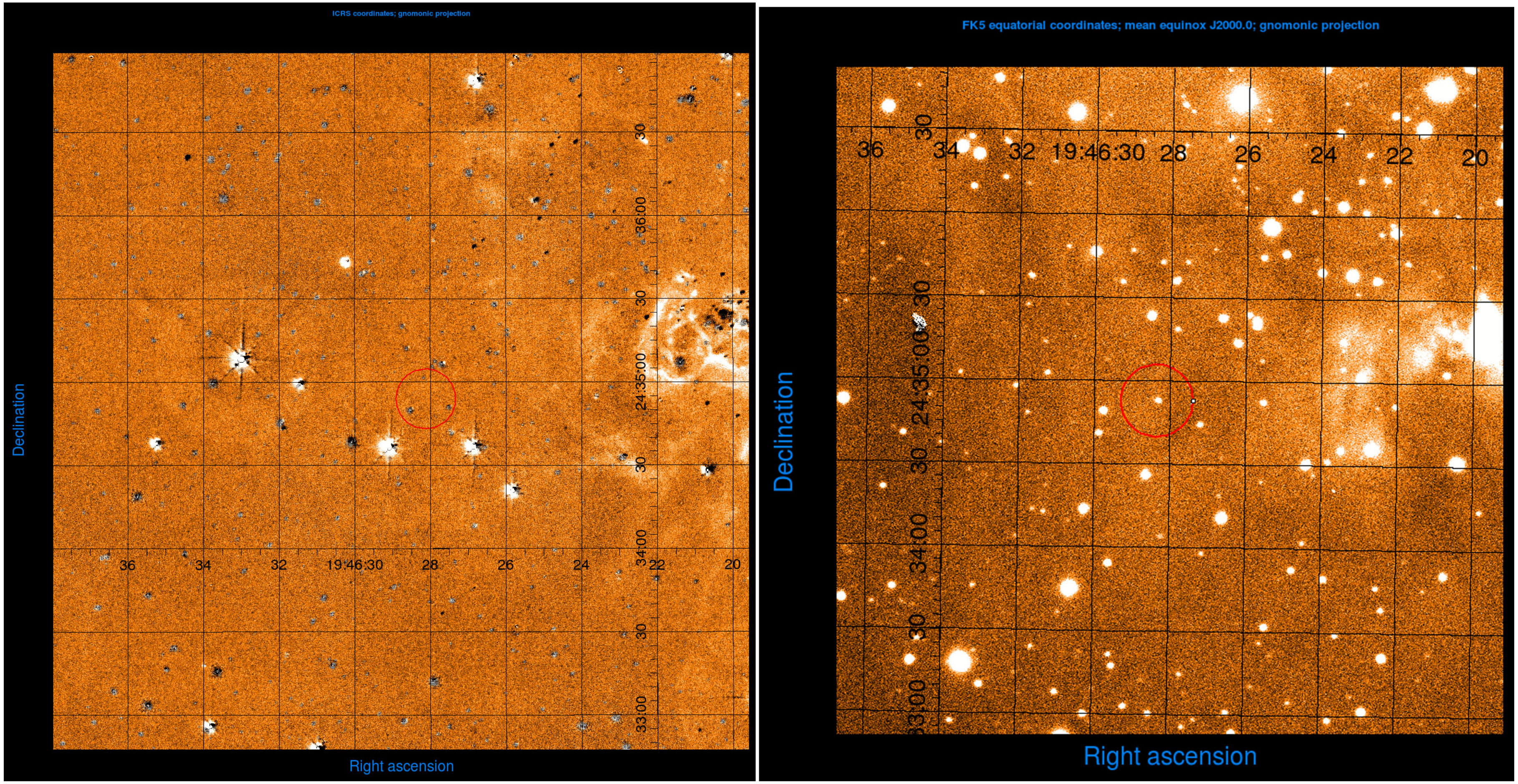

Comparison of IPHAS82, H_2 on the left, Hα on the right

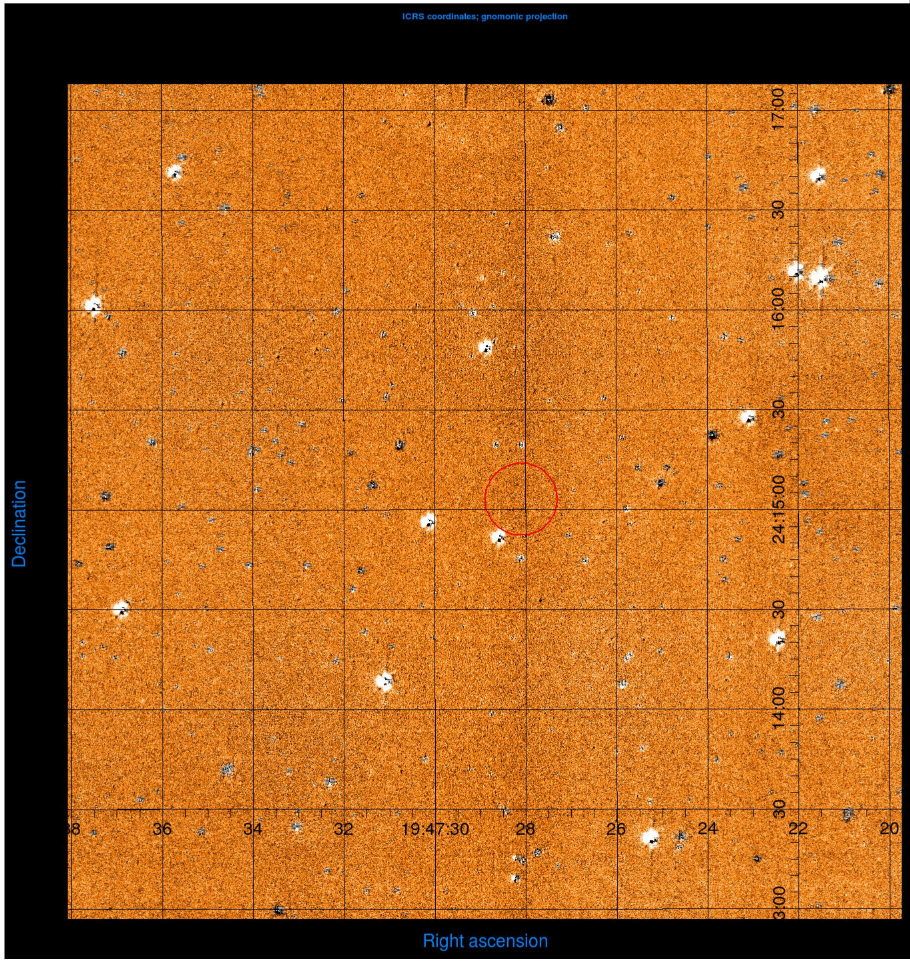

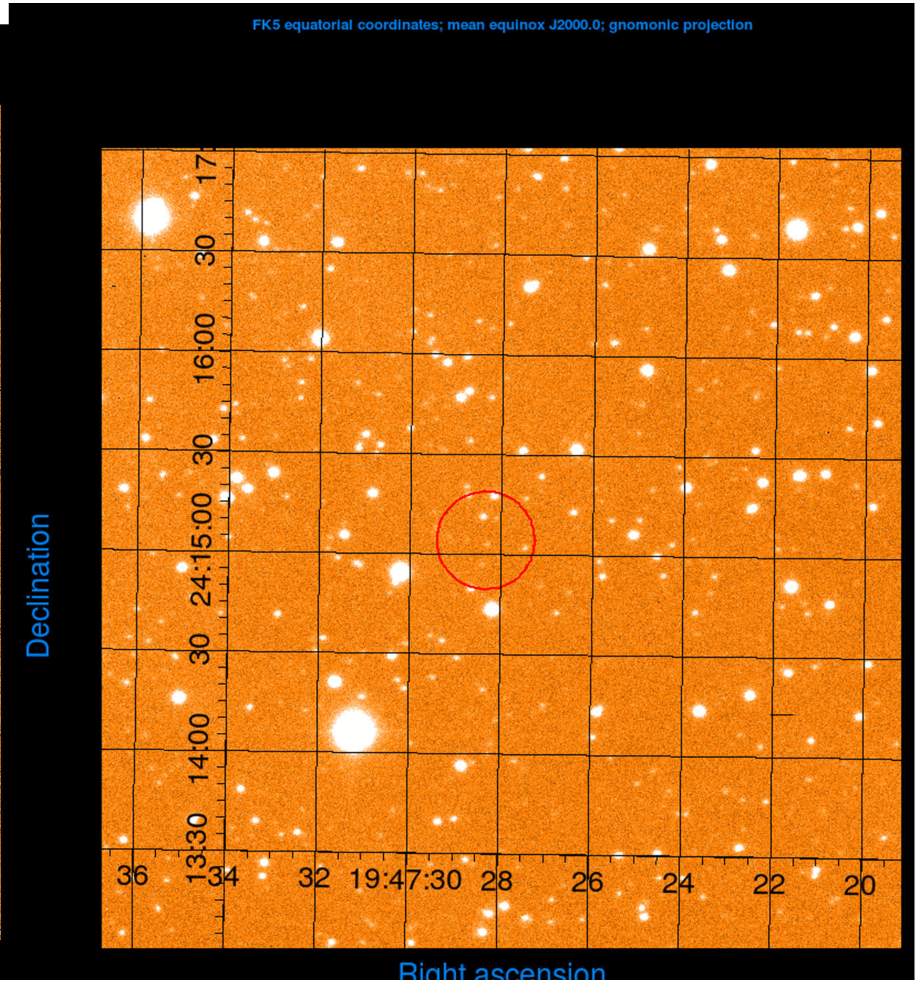

Comparison of IPHAS83, H_2 on the left, Hα on the right

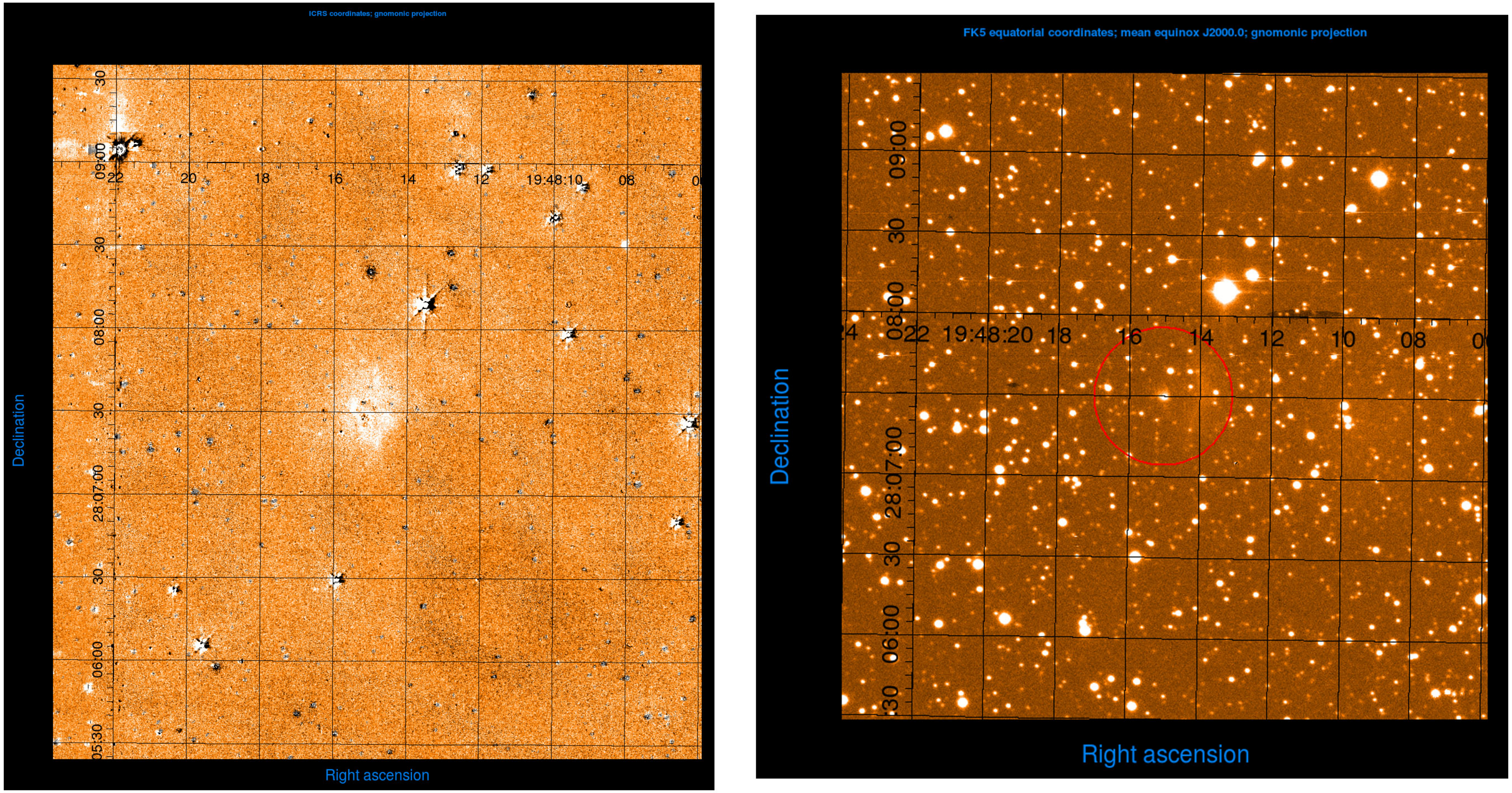

Comparison of IPHAS84, H_2 on the left, Hα on the right

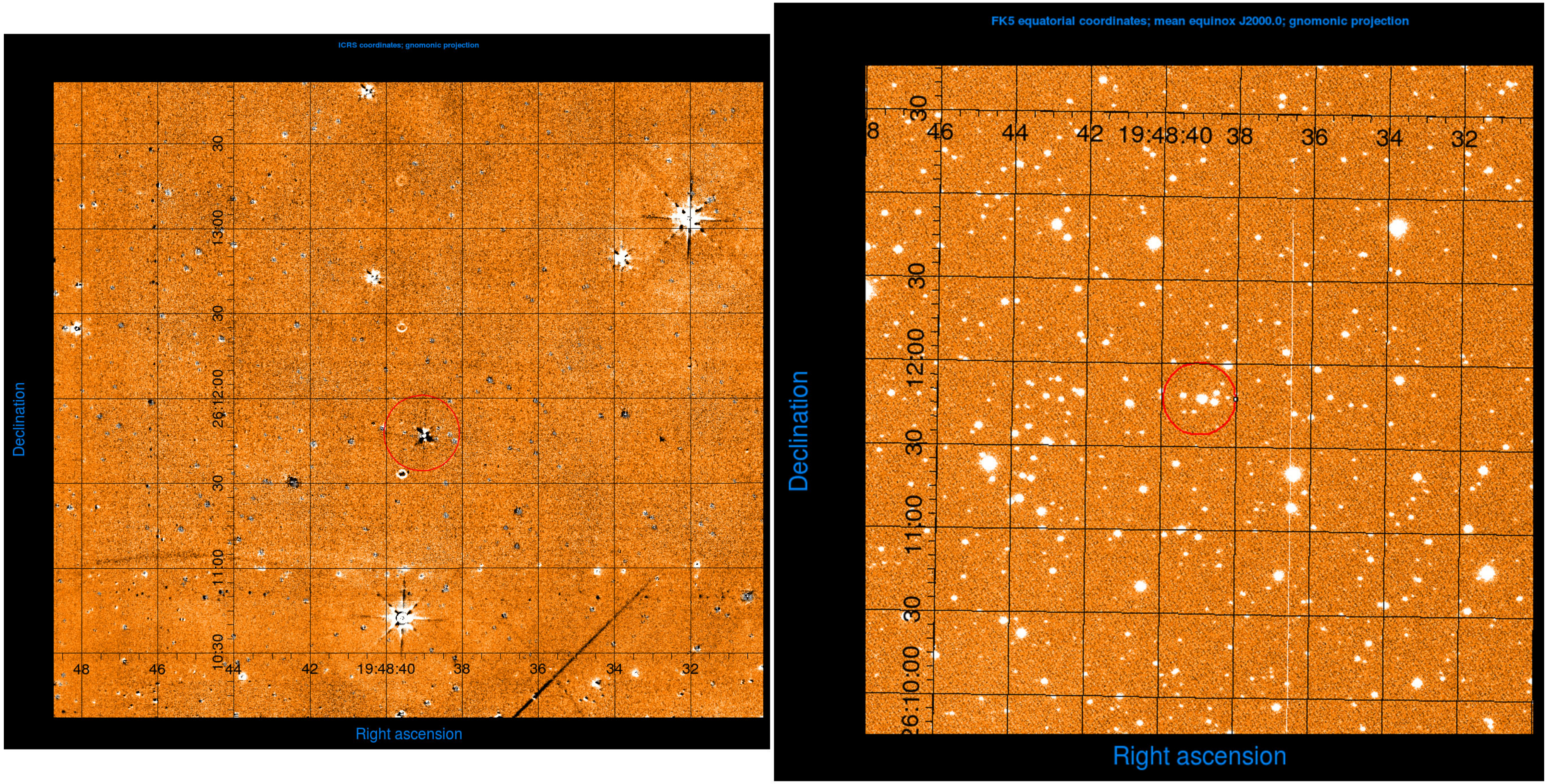

Comparison of IPHAS85, H_2 on the left, Hα on the right

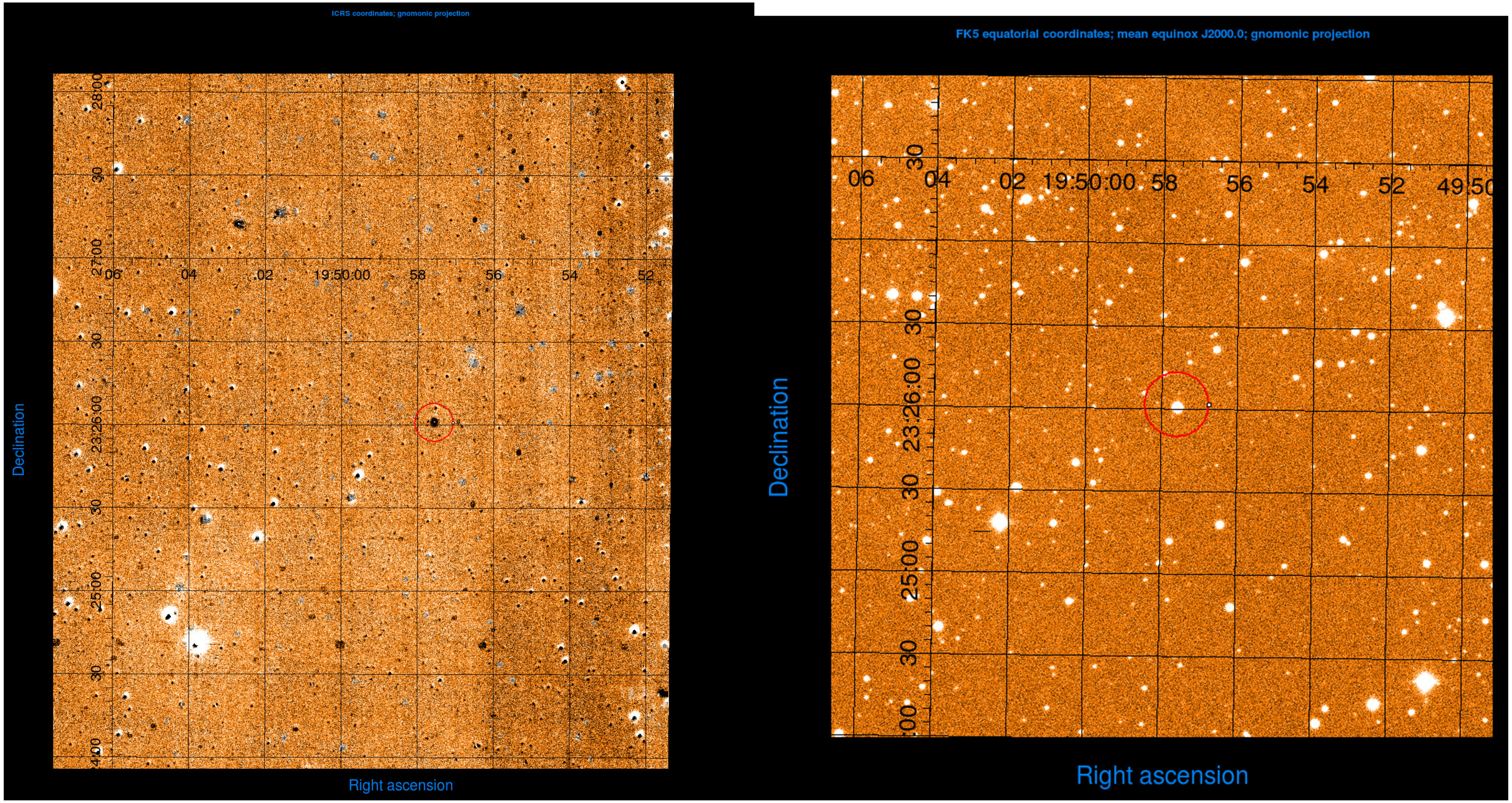

Comparison of IPHAS86, H_2 on the left, Hα on the right

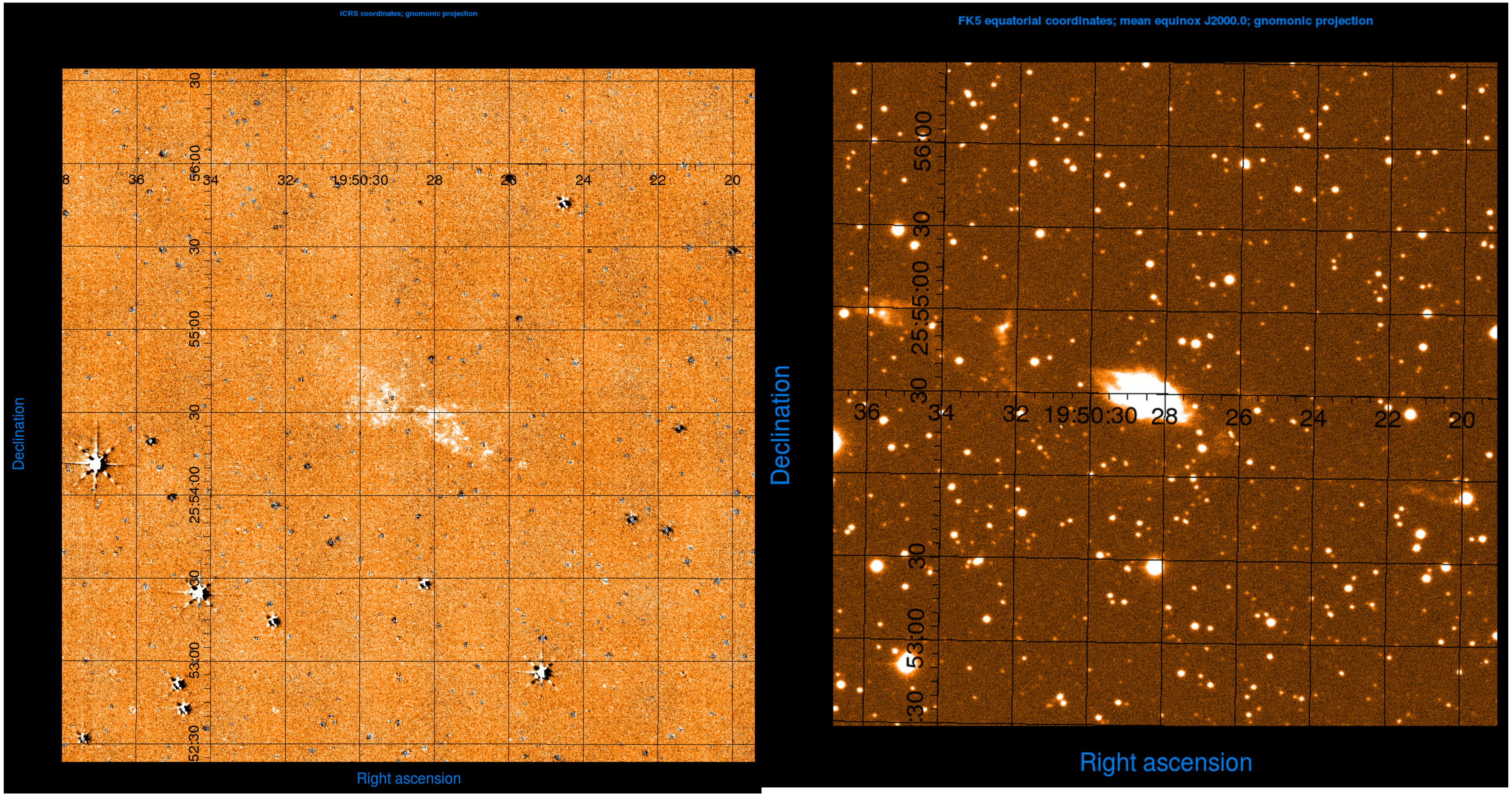

Comparison of IPHAS87, H_2 on the left, $H\alpha$ on the right

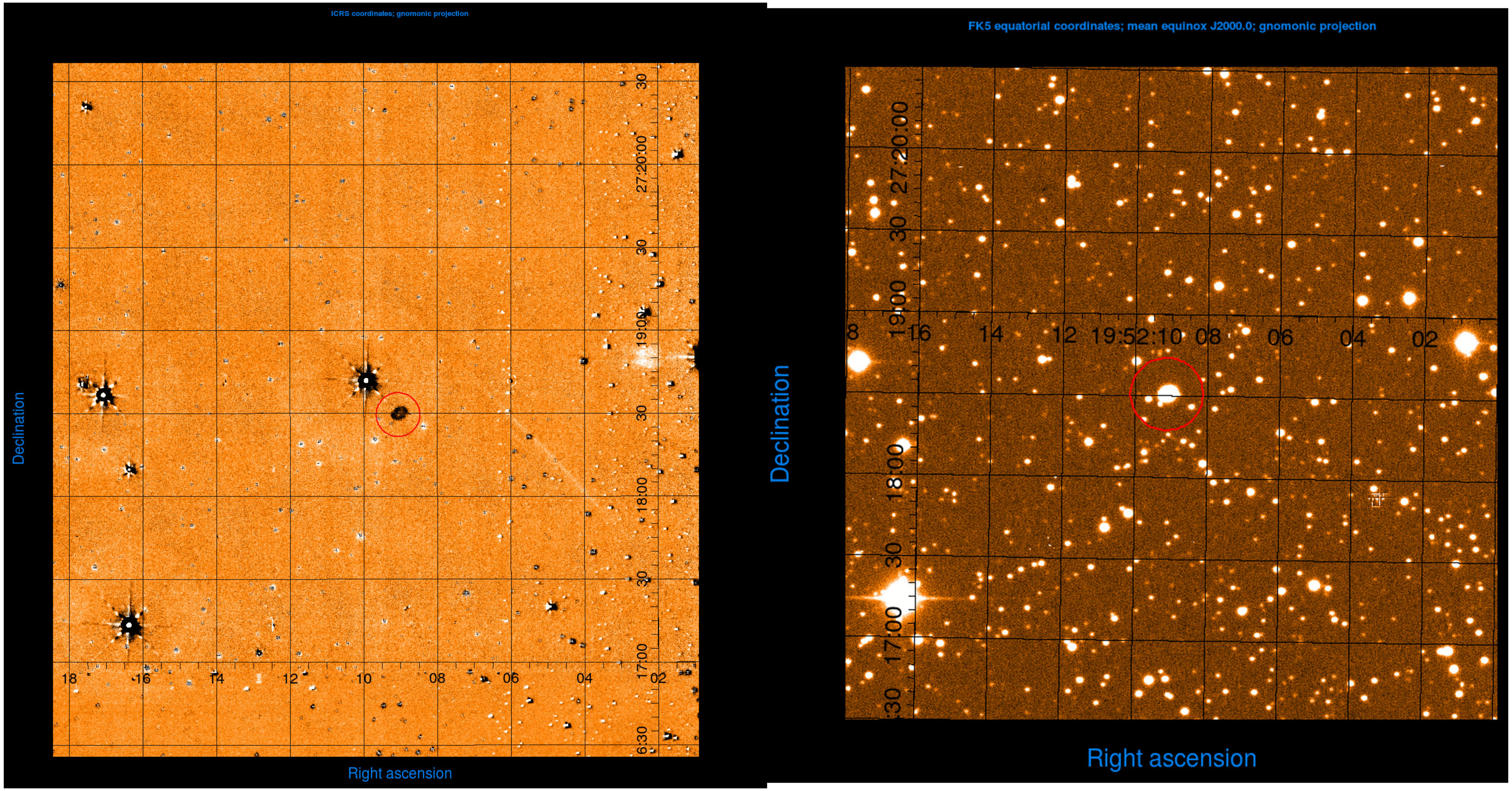

Comparison of IPHAS88, H_2 on the left, Hα on the right

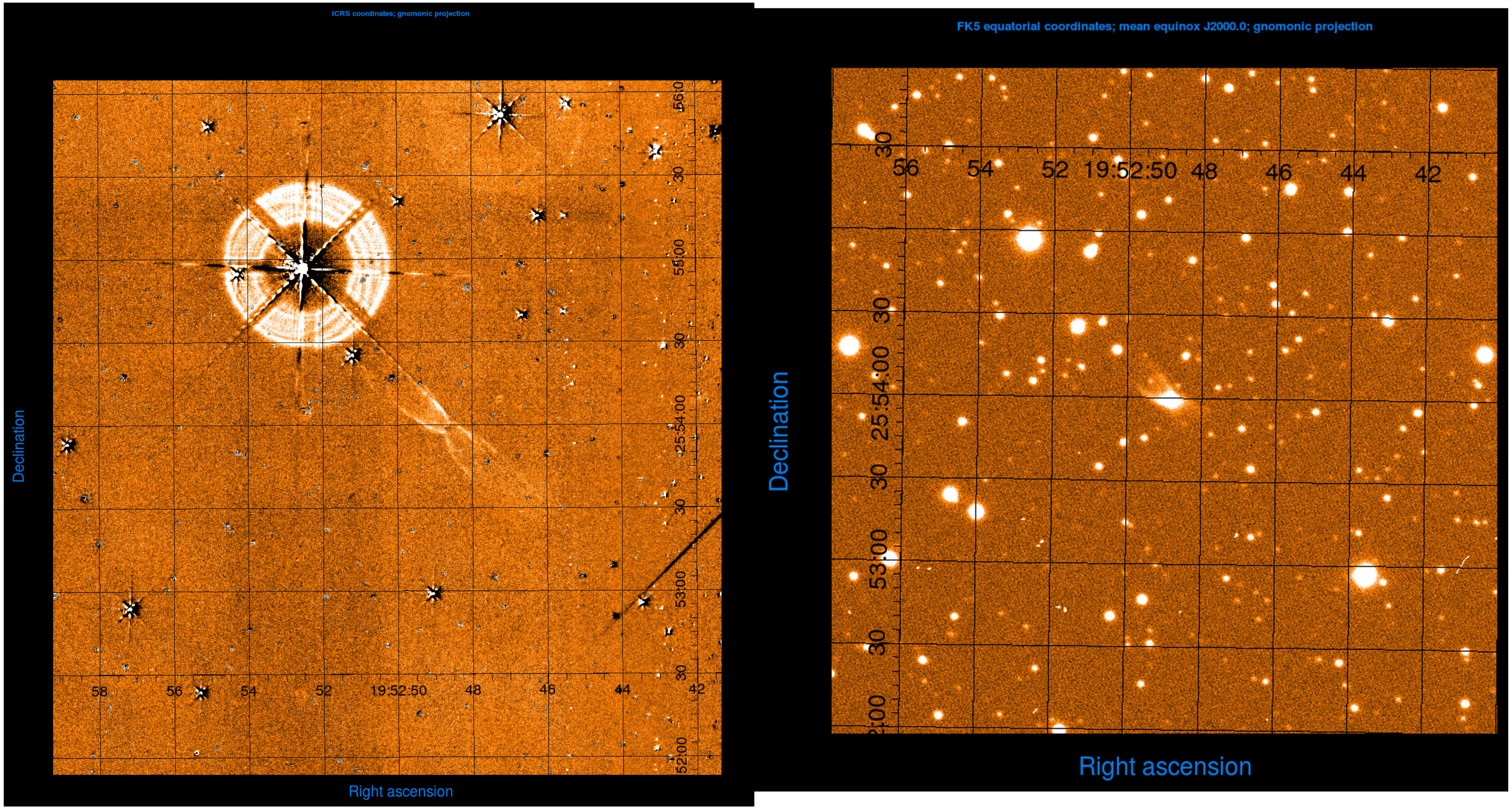

Comparison of IPHAS89, H_2 on the left, $H\alpha$ on the right

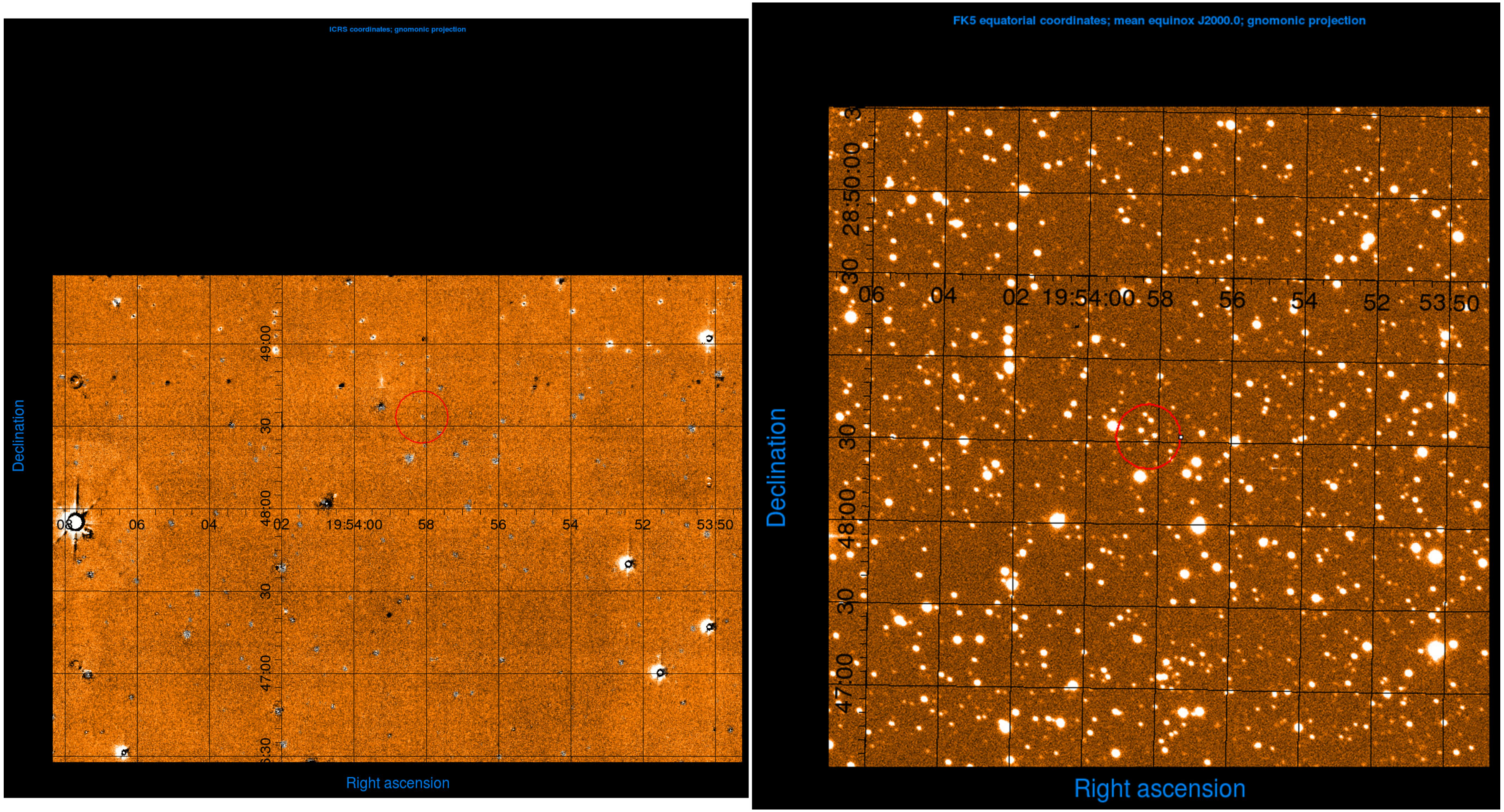

Comparison of IPHAS90, H_2 on the left, $H\alpha$ on the right

```
import os
import math
fm = open('IPHAS-Viironen-edit.txt','r')
fu = open('UWISH2_tiles.txt','r')
f = open('IPHAS-Results.txt','w')

fml = fm.readlines()

f.write(fm.name+' Lines: '+str(len(fml))+'\n\n')

ful = fu.readlines()

f.write(fu.name+' Lines: '+str(len(ful))+'\n\n')

# For each row of the IPHAS file
for ml in fml:
dx = 15*float(ml[14:16]) + float(ml[17:19])/4 + float(ml[21:23])/240
dy = float(ml[35:38]) + float (ml[39:41])/60 + float(ml[42:44])/3600
# f.write( str(dx)+'   '+str(dy)+'\n')
for ul in ful[3:]:
        ux = 15*float(ul[29:31]) + float(ul[32:34])/4 + float(ul[35:40])/240
        uy = float(ul[45:47]) + float(ul[48:50])/60 + float(ul[51:55])/3600
if ul[44] == '-':
uy = -1*uy
#    f.write(str(ux)+'   '+str(uy)+'\n')
# Dimensions for the tile from the point definition
blx = ux - (math.sqrt(0.75)*5/8)
bly = uy - (math.sqrt(0.75)*3/8)
brx = blx + math.sqrt(0.75)
bry = bly
```

```
tlx = blx
tly = bly + math.sqrt(0.75)
trx = brx
#          try = tly
if (dx > blx) and (dx < brx) and (dy > bly) and (dy < tly):
f.write(ml[0:24]+' '+ul[1:26]+'  '+ml[25:45]+'  /  '+ul[29:55]+'\n')


fm.close()
fu.close()
```

The code for the Python program mentioned in Section 2.2